Characterization of the dynamin family in the human intestinal parasite *Entamoeba histolytica*

Submitted by

Maria Anita Siegesmund

to the University of Exeter as a thesis for the degree of

Doctor of Philosophy by Research in Biological Sciences September 2011.

I certify that all material in this thesis which is not my own work has been identified and that no material has previously been submitted and approved for the award of a degree by this or any other University.

_____

Abstract

Entamoeba histolytica is an important human intestinal parasite that has a major impact on human health and is responsible for approximately 100,000 deaths each year. *Entamoeba histolytica* is one of several known eukaryotes that harbour strongly reduced mitochondria, called mitosomes, which have lost the vast majority of mitochondrial pathways as well as their organellar genome. While the occurrence and function of mitosomes have been well studied, little is known about their inheritance and division. Mitochondrial division in all studied eukaryotes relies on the participation of dynamin proteins for membrane scission. The central aim of this study was to characterize the dynamin protein family in *Entamoeba histolytica* and to analyze if they participate in mitosomal division. In relation to this work we studied the occurrence of mitosomes in the distantly related reptilian parasite *Entamoeba invadens* and revisited the phylogenetic relationships among mitosomal Hsp70, a protein we used for mitosomal localization experiments. Our studies revealed that *Entamoeba histolytica* contains two classical and two strongly derived members of the dynamin protein family, which we called Drp1, Drp2, Drp3 and Drp4. Drp1 and Drp2 exhibit the classical dynamin protein structure with a GTPase, middle and GTPase effector domain, while Drp3 and Drp4 only appear to contain the dynamin GTPase domain. Using phylogenetic reconstructions we could not identify closely, and thus functionally related, dynamins for Drp1 and Drp2 within the eukaryotic tree of life including the mitochondria-associated amoebozoan dynamins DymA and DymB. The structurally derived dynamins however, were closely related to amoebozoan and archaeplastidan proteins involved in cytokinesis and chloroplast division. All *Entamoeba* dynamins are differentially expressed in trophozoites with EhDrp2 appearing to be most abundant and Drp3 expressed the least. We conducted stage conversion experiments using *E. invadens* to understand the importance of dynamins during cyst formation. During encystation all dynamin expression levels increased. Interestingly, Drp3 expression is strongly upregulated in the mid cyst stages and Drp4 during the late phase of encystation. Thus, Drp3 and Drp4 appear not to be involved in cytokinesis and possibly evolved a novel function in the cyst formation process. We carried out Drp2 enzymatic characterization and localization experiments as well as

complementation studies using the related amoebozoan *Dictyostelium discoideum* in order to understand the role and function of *E. histolytica* Drp2 in the cell. We found that its kinetic characteristics are comparable to other members of the eukaryotic dynamin protein family by exhibiting low substrate specificity, the ability to oligomerize to higher structures and a substrate dependent cooperative enzyme activity. Drp2 localized to abundant punctate structures in the cytosol but did not co-localize with mitosomes. In addition, Drp2 was not able to complement *D. discoideum* DymA. Both findings suggest that Drp2 is not directly involved in mitosomal (or mitochondrial) division. We overexpressed Drp2 in *E. histolytica* and *D. discoideum* and found a significant effect on cytoskeletal organization. Both strains showed a strong impairment in amoeboid movement, cell-surface attachment and cell growth. Additionally, the number of nuclei was increased significantly. Our data imply that Drp2 plays an important role for cytoskeletal organization. Additionally in this study, we show that mitosomes are also abundantly present in *E. invadens* suggesting that mitosomes are characteristic for all *Entamoeba* spp.. Furthermore, we demonstrate that *E. invadens* cysts contain mitosomes in high abundance comparable to its vegetative life stage. Our studies verify that mitosomal Hsp70 is part of the amoebozoan protein family and of mitochondrial origin as shown by *in silico* characterization and localization experiments using the homologous Hsp70 antibody.

Acknowledgements

I would most importantly like to thank Dr. Mark van der Giezen for his guidance, encouragement and support throughout the last four years and for teaching me how to stay calm during the more challenging moments. Members of our lab, past and present, especially Dr. Karleigh Hamblin, Dr. Kailash Chand Pandey, Sheera Abdulla and Kim Payne for a great time in the lab and for being wonderful people. Thanks to Dr. Tom Richards and Dr. Bryony Williams for their input and support, and the latter for being a good friend. Everyone who helped contributing to this work by teaching me methods, giving advice and providing cultures, especially Dr. Graham Clark, Professor Adrian Hehl, Professor Egbert Tannich, Susann Ofori, Professor Dietmar Manstein and Dr. Amrita Rai. A special mention to Dr. Theresa Hudson for reading my thesis, providing helpful corrections and generally being great and Dr. Guy Leonard for bioinformatical advice.

I am grateful to the University of Exeter, which kindly funded me and thus gave me the opportunity to work in the exciting scientific field of eukaryotic evolution and biochemistry together with great and inspiring people.

I am especially grateful to my parents Helga und Ulrich Siegesmund for supporting me tremendously throughout University and during this PhD and to Henning, simply for being Henning.

Table of contents

Figures

Tables

Abbreviations

APS	[^{35}S]-labeled adenosine-5′-phosphosulfate
APSK	APS kinase
AS	ATP sulfurylase
BLAST	Basic local alignment search tool
Bp	Base pairs
BSA	Bovine serum albumin
cDNA	Complementary DNA
Cpn10	Chaperonin 10
Cpn60	Chaperonin 50
DAPI	Diamidino-2-phenylindole dihydrochloride
DNA	Deoxyribonucleic acid
dNTPs	Deoxynucleoside triphosphates
Drp	Dynamin related protein
DTT	Dithiothreitol
EDTA	Ethylenediaminetetraacetic
Fe-S	Iron sulphur cluster
GDP	Guanosine diphosphate
GTP	Guanosine triphosphate
HRP	Horseradish peroxidase
Hsp60	60 kDa heat shock protein
HSP70	70 kDa heat shock protein
IPP	Inorganic pyrophosphate
IPTG	Isopropyl-beta-D-thiogalactopyranoside
Kb	Kilobase
MCF	Mitochondrial carrier family
NaS	Sodium sulfate transporter
PAPS	3′-phosphoadenosine-5′-phosphosulfate
PAPST	3′-phosphoadenosine-5′-phosphosulfate transporter
PHT	Phosphate transporter
SDS	Sodium dodecyl sulfate
SULT	Sulfotransferase

1. General introduction

Entamoeba histolytica is an anaerobic parasitic protist which inhabits the intestines of humans. From a medical perspective, *E. histolytica* is best known for causing amoebiasis, a common intestinal infection connected to severe diarrhea. In the field of evolutionary biology *Entamoeba* takes a special place for containing highly reduced mitochondria, termed mitosomes (Tovar *et al.*, 1999) and interesting characteristics connected to its anaerobic parasitic life style (Dolezal *et al.*, 2010, Mi-ichi *et al.*, 2009, Loftus *et al.*, 2005).

1.1. Life cycle and morphology

Entamoeba spp. have a simple life cycle involving binary division of vegetative cells, called trophozoites, or changing between the trophozoites and the resistant cyst stage (Fig. 1.1). The human parasite *E. gingivalis* provides an exception, as it does not appear to form cysts (Dobell, 1919). All *Entamoeba* require an animal host, in which the trophozoites live, to multiply and form cysts. The cysts are released into the environment by the host's faeces. The life cycle is completed once a new host ingests the cysts from which new trophozoites emerge. After ingestion, the cysts pass through the stomach and enter the upper intestinal tract. Here, excystation of trophozoites from cysts is induced by bile salts and bicarbonate (Mitra *et al.*, 2010). Trophozoites multiply by binary fission and spread throughout the host's intestines. As they move down the bowel, they encyst again and are released into the environment with the host's faeces. In rare cases, trophozoites become invasive by destroying the intestinal tissue causing ulceration. The destruction of tissue can provide entry for trophozoites into the host's bloodstream and cause subsequent infection of other organs, especially the liver. Trophozoites are amoeboid cells and vary in cell size and shape. They show amoeboid movement and feed on the intestinal bacterial flora, partially digested host food and cell debris in the intestines (Pritt & Clark, 2008). Using light microscopy, the cytosol of *Entamoeba* appears granular and densely packed with glycogen particles, the main storage product, while the cyst cytoplasmic content appears unstructured (Fig. 1.2). The cysts are usually spherical to oval in appearance with a strong chitin

containing cyst wall (Chatterjee *et al.*, 2009). The sizes of the cysts and trophozoites as well as the amount of nuclei vary in different species and are used to differentiate taxa (Dobell, 1919, Stensvold *et al.*, 2011, Clark, 2000).

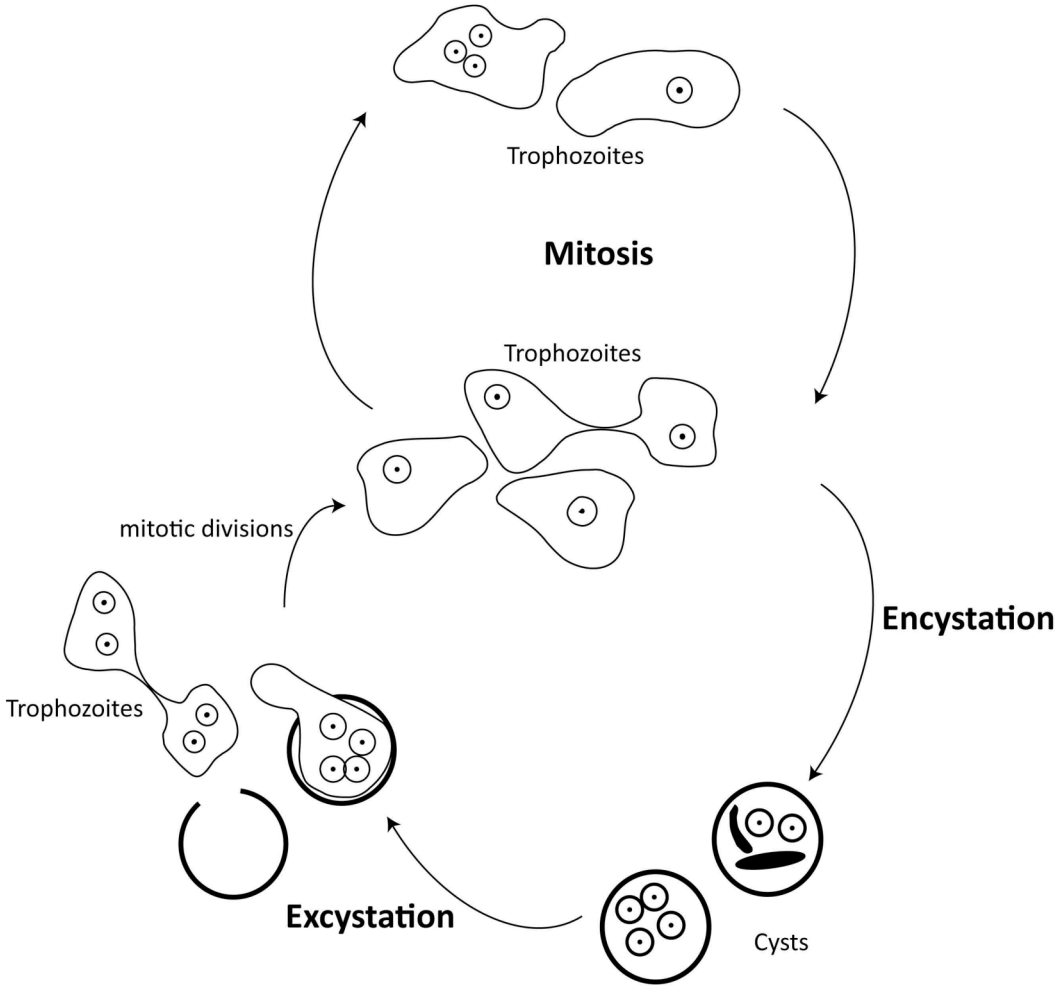

Figure 1.1 Schematic representation of the *Entamoeba* spp. life cycle. Vegetative amoeboid cells (=trophozoites) divide mitotically by binary fission in the host's intestines. Encystation of trophozoites occurs by formation of a rigid chitin containing cyst wall. The numbers of nuclei differ between species. Typical is the formation of chromatoid bodies, crystalline ribosomes (indicated by black structures in cysts) in immature cysts. Cysts are released by the host with faeces, where they can remain dormant in the environment. Once a new host takes the cysts up and ingests them, for example by drinking contaminated water, trophozoites emerge from the cysts (=excystation), settle in the intestines and multiply by binary fission.

Characteristic in cysts is the presence of chromatoid bodies, crystalline ribosomes that are formed during cyst formation (Morgan *et al.*, 1968, Lake & Slayter, 1972, Lake & Slayter, 1970). Chromatoid bars are characteristic for *Entamoeba* cysts and unknown in any free-living organism (Clark, 2000). The numbers of nuclei in the cysts is an important feature to morphologically differentiate *Entamoeba* taxa. While *Entamoeba coli* contains eight nuclei, *E. histolytica* exhibits four and *E. chattoni* only one nucleus. To date, various *Entamoeba* taxa are described from human, cattle, non-human primates, ostriches, reptiles and even unicellular eukaryotes such as the ciliate *Zelleriella* (Stensvold *et al.*, 2010, Stensvold *et al*., 2011, Stabler, 1936, Ponce Gordo *et al.*, 2004). Early taxonomic classifications were almost entirely based on morphological characteristics of the trophozoite and the cyst as well as the host from which they have been isolated (Dobell, 1919, Clark, 2000).

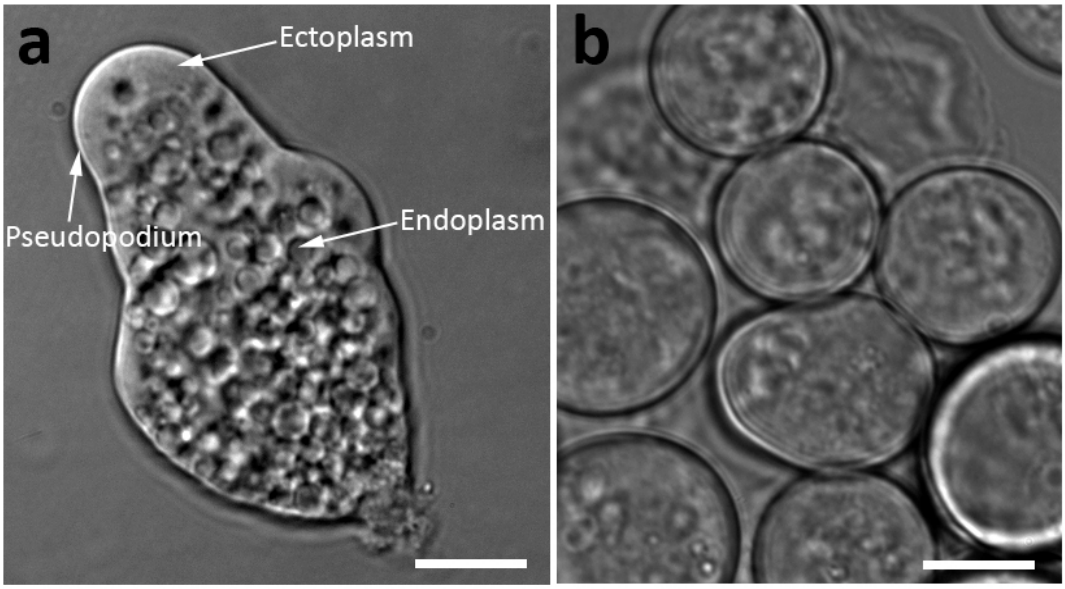

Figure 1.2 *Entamoeba invadens* vegetative cell and cysts. (a) Amoeboid trophozoite with granular contents. (b) Cysts with content that appears unstructured in comparison to the trophozoite cell. The trophozoite shows the differentiation between smooth ectoplasm and granular endoplasm. The pseudopodium at the anterior of the cell moves the cell forward. Scale bars=10 μm.

With the availability of molecular tools, formerly indistinguishable species could be clearly separated (Clark & Diamond, 1997a, Clark & Diamond, 1997b, Stensvold *et al*.,

2010, Stensvold *et al*., 2011). Famous examples are the human parasites *E. histolytica, E. dispar* and *E. moshkovskii*. While *E. histolytica* can cause severe amoebic dysentery and hepatic abscesses, *E. dispar* and *E. moshkovskii* do not. Because the three species are morphologically identical it was assumed that 1/10 (500 million to 600 million people) of the world population suffered from amoebiasis. However, it has since become apparent that several asymptomatic (*E. dispar*) or less virulent (*E. moshkovskii*) *Entamoeba* taxa are more common than *E. histolytica* infections reducing the *E. histolytica* infections to approximately 50 million cases annually (more detailed information in paragraph 1.2.2). Recent analyses using the small subunit ribosomal RNA genes suggest either a larger diversity among morphologically indistinguishable taxa or no differences between described species from different hosts (Stensvold *et al*. 2011).

1.2. *Entamoeba histolytica* Schaudinn, 1903 (Emended Walker, 1911) and the cause of amoebiasis

1.2.1. A brief history of discovery

Amoebiasis evidently caused by *Entamoeba* was first described by Fedor Alexandrovich Lösch in 1875 in St. Petersburg. He isolated trophozoites from a patient who died from pneumonia but additionally showed a severe intestinal disease. He infected dogs with the sample, and showed that *Entamoeba* was the causative agent of the intestinal disease. He named the organism '*Amoeba coli*' but failed to describe the organism according to the rules of zoological nomenclature (Dobell, 1919 and references therein). The earliest cases of infections causing intestinal ulcers and liver abscesses were described independently by Stephan Kartulis in 1887 in Egypt, Councilman and Lafleur, who first established the term 'amoebic dysentery', and Robert Koch *et al*. in 1887. The genus *Entamoeba* was established by Casagrandi and Barbagallo in 1895 according to the rules of zoological nomenclature. In the beginning to mid 1890s, it became increasingly clear that several *Entamoeba* species with the same morphology were present in the human intestines, some of which caused disease and some, which were non-pathogenic. Schaudinn reclassified Löschs pathogenic '*Amoeba coli*'

according to the rules of zoological nomenclature to *E. histolytica* in 1903 and used the name *Entamoeba coli* for the non-pathogenic *Entamoeba* form. He himself died of self-inflicted amoebiasis 3 years later. The occurrence of cysts were discovered by Quincke and Roos, 1893, refined by Huber in 1903 and the *Entamoeba* life cycle was finally correctly described by Walker in 1911 (Dobell, 1919 and references therein).

1.2.2. Amoebiasis today

E. histolytica is the causative agent of amoebiasis, a disease that infects approximately 50 million people per year (WHO 2009). Although globally distributed, it shows a higher prevalence in countries with poor socioeconomic and sanitary conditions especially in tropical and subtropical areas leading to 40,000 to 100,000 deaths annually (WHO, 1997, Walsh, 1986). Most infections are asymptomatic. Approximately 10 % of infected humans develop gastrointestinal complications, which range from mild diarrhea to dysentery (Gathiram & Jackson, 1987, Haque *et al.*, 2003, Haque *et al.*, 2006). Invasive infections with *E. histolytica* can cause the formation of flask shaped ulcers in the intestinal wall, by invading the colon tissue laterally (Pritt & Clark, 2008). In the most severe developments of this disease, patients suffer from acute necrotizing colitis, including severe diarrhea, ulceration and perforation of the colon and subsequent sepsis of the body, a development, which is often fatal (Shimada *et al.*, 2002, Gupta *et al.*, 2009). Invasive amoebiasis occurs in approximately 1 % of the clinical cases and affects mostly children and the elderly, malnourished patients and pregnant women (Haque *et al*., 2003, Petri *et al.*, 2009, Haque *et al*., 2006). Extraintestinal amoebiasis is rare and occurs by trophozoites, which enter the blood stream from the intestines and disperse throughout the rest of the body. Infections usually occur in the liver because trophozoites are carried from the intestines via the hepatic portal vein into the right lobe of the liver. Hepatic infections lead to the formation of multiple granulomes that join to form large abscesses and tissue destruction that may cause death (Chadee & Meerovitch, 1984). The disease can take place independently of amoebic colitis and often develops months or years after colon infection (Stanley, 2003). In extremely rare and often fatal cases, trophozoites spread to other regions of the body such as the brain, lungs, spleen and the genitourinary

system (Viriyavejakul & Riganti, 2009, Ohnishi *et al.*, 1994, Shamsuzzaman & Hashiguchi, 2002, Lawford & Sorrell, 1994, Kjaeldgaard *et al.*, 1985).

1.3. Treatment of amoebiasis

The World Health Organization (WHO) and the Pan American Health Organization (PAHO) recommend treating all cases of amoebiasis including patients who do not show symptoms. Asymptomatic amoebiasis is commonly treated with luminal amoebicides such as paromomycin and diloxanide furoate (Gupta *et al.*, 2004) and with tissue amoebicides such as metronidazole or trinidazole if infection is invasive and extraintestinal (Pritt & Clark, 2008, Haque *et al.*, 2003). An alternative for the treatment of both luminal and invasive amoebiasis is nitazoxanide (Rossignol *et al.*, 2007), a common anti-protozoal drug that is thought to interfere with the pyruvate: ferredoxin oxidoreductase (PFOR) by substracting a proton from its vitamin cofactor thiamine pyrophosphate and thus inhibiting the production of acetyl-CoA and CO_2 essential for the *E. histolytica* energy metabolism (Hoffman *et al.*, 2007, Ballard *et al.*, 2010).

1.4. Phylogenetic position and systematics of *Entamoeba*

Entamoeba was long considered to be 'primitive' because classical eukaryotic characteristics such as mitochondria, Golgi apparatus and continuous endoplasmic reticulum were not detected (Chavez-Munguia *et al.*, 2000). *Entamoeba* also uses glycolytic enzymes that depend on pyrophosphate rather than ATP (Reeves, 1968, Reeves *et al.*, 1968, Reeves *et al.*, 1974, Saavedra *et al.*, 2005). However, parasite genomes are often shaped by gene loss and high sequence divergence (Carlton *et al.*, 2007, Morrison *et al.*, 2007), which hampers the identification of closely related free living relatives and the correct positioning in the eukaryotic tree of life. The development of more complex molecular phylogenetic approaches allows the resolution of *Entamoeba* diversity and its relationship within the eukaryotic tree of life, despite the absence of defining morphological characteristics. *Entamoeba* belongs to the amoebozoa, which is sister to the Opisthokonta. Within the amoebozoan supergroup *Entamoeba* belongs to the subphylum Conosea (Fig. 1.3) (Bapteste *et al.*,

2002) and within the Conosea they are classified as Archamoebae (Fig. 1.4) (Pawlowski & Burki, 2009).

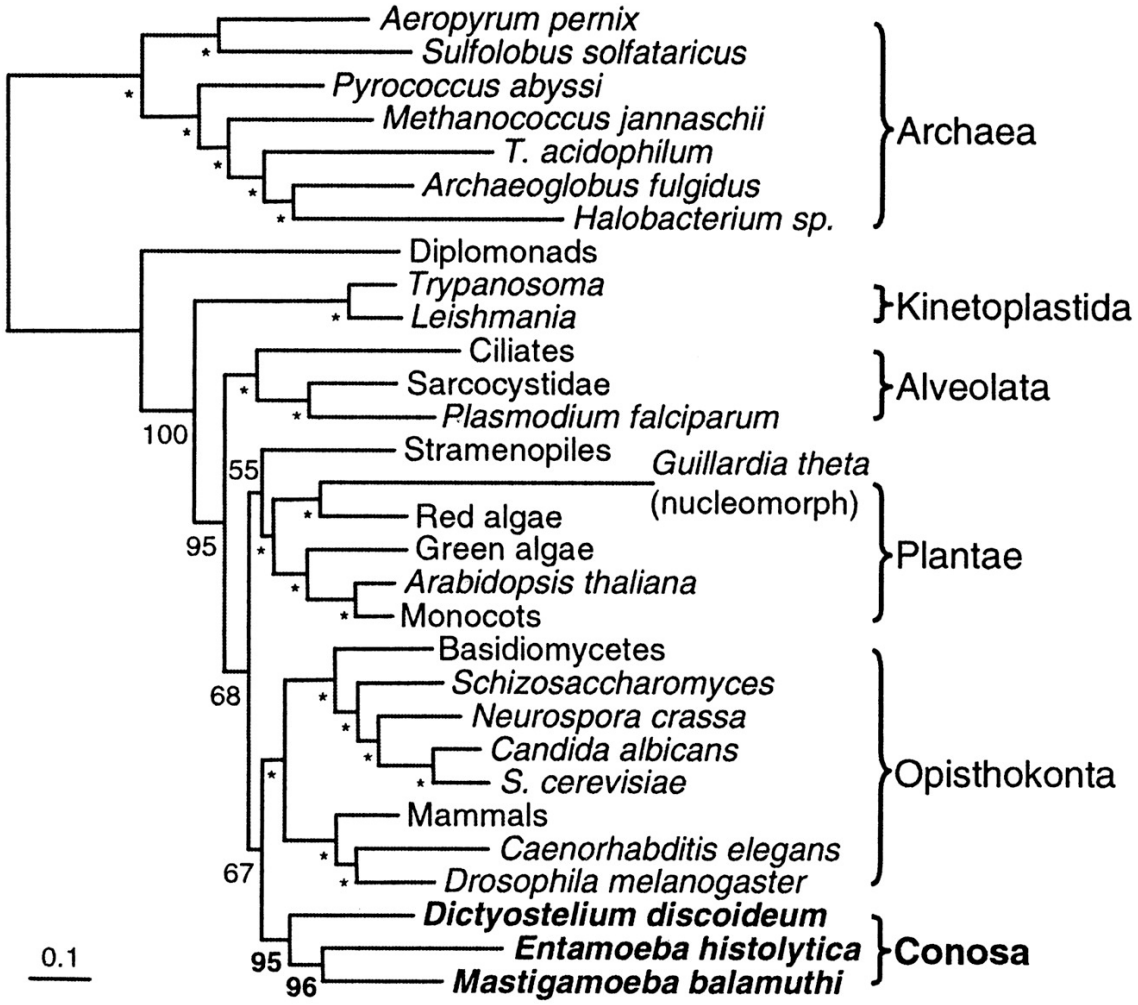

Figure 1.3 Maximum likelihood phylogenetic reconstruction showing the sister group relationship of the amoebozoa including *Entamoeba histolytica* to the Opisthokonta. Image taken from Bapteste *et al*. 2002. The analysis was based on 25,032 amino acid positions using 123 concatenated sequences.

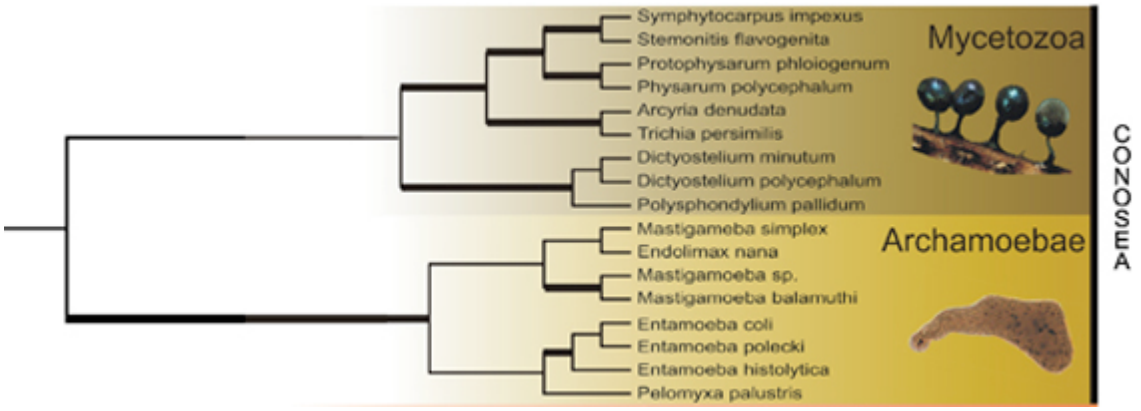

Figure 1.4 Detail from maximum likelihood small subunit rDNA tree taken from Pawlowski and Burki (2009) showing the evolutionary relationships within the Conosea. The tree was inferred from 1,298 aligned positions. Thick branches denote bootrap support higher than 90 %.

Various animal lineages are infected by *Entamoeba* species. Phenotypic characteristics are not always reliable due to morphological plasticity of trophozoites and cysts and differences in the specificity for the host(s) (Clark & Diamond, 1997a, Clark *et al.*, 2006, Stensvold *et al*., 2011). With the availability of molecular methods, new taxa and a large hidden diversity within morphospecies were recovered (Ponce Gordo *et al*., 2004, Clark *et al*., 2006, Kobayashi *et al.*, 2009, Stensvold *et al*., 2010, Levecke *et al.,* Ximenez *et al.,* Stensvold *et al*., 2011). However, due the absence of unique morphological characteristics and suitable methods to cultivate genetically distinct taxa, it is still impossible to either describe new species or to assess if new lineages can be assigned to already existing taxonomic species. Stensvold *et al*. (2011) propose the use of ribotypes in combination with morphological characteristics and host specificity to describe and classify *Entamoeba* diversity.

1.4.1. *Entamoeba* spp. with uninucleate cysts

Entamoeba species with only one nucleus in cysts have been discovered in cattle (Stensvold *et al*., 2010, Stensvold *et al*., 2011), humans (Verweij *et al.*, 2001), ostriches (Ponce Gordo *et al*., 2004), pigs and monkeys (Silberman *et al.*, 1999). Several new ribosomal lineages closely related to taxa with uninucleated cysts have been recently discovered (Stensvold *et al*., 2011). For most of them no morphological data are

available. Therefore, they are described as subtypes or ribosomal lineages. The number of nuclei is however not necessarily a marker for sistergroup relationship. The cattle parasite *E. bovis*, which exhibits uninucleated cysts is more closely related to the tetranucleated human parasites *E. histolytica* and *E. dispar* than to uninucleate and cattle infecting *E. suis* and *E. pollecki* (Stensvold *et al*., 2011).

1.4.2. *Entamoeba* spp. with tetranucleate cysts

Entamoeba spp. with tetranucleated cysts have been discovered in human, non-human primates and reptiles. *E. histolytica* and *E. invadens* are the most well studied parasites in this cluster. Both the human parasite *E. histolytica* and the reptilian parasite *E. invadens* exist as axenic cultures. Furthermore, *E. invadens* cyst formation can be readily induced *in vitro*, which makes it an important model organism. However, similar to uninucleate cyst forming *Entamoebae*, the presence of 4 nuclei in the cysts is not a characteristic of sistergroup relationship and it appears that the uninucleated species *E. bovis* is more closely related to the *E. histolytica*/ *E. dispar*/*E. moshkovskii*/*E. nutalli* species group than to the tetranucleate *E. invadens* (Stensvold *et al*., 2011).

1.4.3. *Entamoeba* spp. with octonucleate cysts

Entamoeba with octonucleated cysts have been found in mice, non-human primates, human and gorilla. Unlike the uni- and tetranucleate cyst formers, this group appears to be monophyletic (Stensvold *et al*., 2011). The most famous representative is *Entamoeba coli*. Furthermore, this clade appears to be more diverse than previously thought due to the presence of morphologically indistinguishable taxa (Stensvold *et al*., 2010).

1.5. Unique ultrastructural characteristics of *Entamoeba* spp.

Entamoeba has long been considered ‘primitive’ due to the lack of eukaryotic characteristics, such as mitochondria, the Golgi apparatus and a continuous

endoplasmic reticulum (ER). Furthermore, some enzymes of its glycolytic pathway use pyrophosphate instead of ATP (Reeves *et al.*, 1974, Reeves, 1968, Reeves *et al.*, 1968, Saavedra *et al.*, 2005). With the advances in molecular methods and the use of gene phylogenies, the derived rather than primitive nature of *Entamoeba* became apparent (Tovar *et al*., 1999, Sogin & Silberman, 1998, Clark & Roger, 1995, Bakatselou *et al.*, 2003, León-Avila & Tovar, 2004, Tovar *et al.*, 2007). Additionally, recent studies suggest the innermembrane system to be continuous and similar to other eukaryotes rather than vesicular (Teixeira & Huston, 2008, Vaithilingam *et al.*, 2008). The discovery of mitochondrial proteins and subsequently minute mitochondrial organelles, called mitosomes, showed that *Entamoeba*'s morphological simplicity is an adaptation to its parasitic life style rather than evidence for its basal positioning in the eukaryotic tree of life (Fig. 1.5).

1.6. Mitosomes

Mitosomes are evolutionary highly reduced mitochondria, from which the genome, most metabolic pathways and ATP production are absent. Mitosomes do not show the same morphology as textbook mitochondria (Fig. 1.5). They are much smaller than mitochondria and do not exhibit the classical cristae structure known from aerobic mitochondria (Fig. 1.5A). Mitosomes represent the far end of mitochondrial diversity being the most reduced form to date. They are present in various lineages across the eukaryotic tree of life, such as *Giardia* (Tovar *et al*., 2003), several microsporidia (Vavra, 2005, Burri *et al.*, 2006, Goldberg *et al.*, 2008, Williams *et al.*, 2002), *Cryptosporidium* (Riordan *et al.*, 2003) and *Entamoeba histolytica* (Tovar *et al.*, 1999, Mai *et al.*, 1999). This indicates that reduction of mitochondria to mitosomes happened several times independently during eukaryotic evolution. There are several characteristics, which are still shared by *Entamoeba* mitosomes and mitochondria.

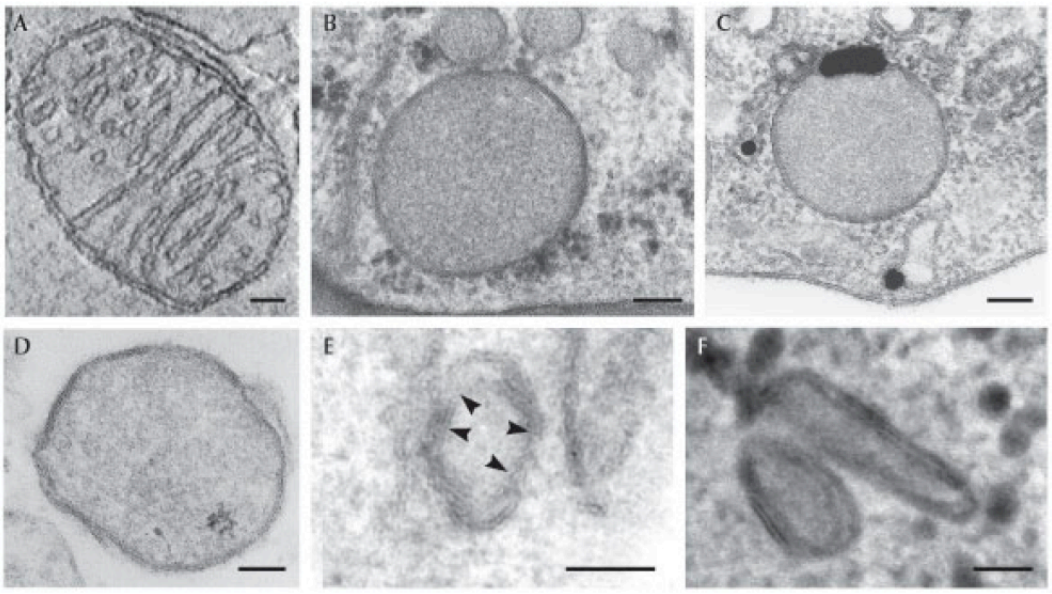

Figure 1.5 Electron microscopy photographs of various mitochondrial organelles taken from (van der Giezen & Tovar, 2005). (A) Classical textbook mitochondrion from chicken cerebrellum. (B) Hydrogenosome from the fungus *Neocallimastix patriciarum*. (C) Hydrogenosome from *Tritrichomonas foetus*. (D) Mitosome from *E. histolytica*. (E) Mitosome from *Giardia intestinalis*. (F) Mitosome from *Trachipleistophora hominis*. (A)-(C) Scale bars=100 nm. (D)-(F) scale bar=50 nm.

Both contain a double membrane and share various proteins, namely mitochondrial Hsp70 (Bakatselou & Clark, 2000, Bakatselou *et al.*, 2000, Tovar *et al.*, 2007), Hsp10 (van der Giezen *et al.*, 2005), Hsp60 (Clark & Roger, 1995, Mai *et al.*, 1999, León-Avila & Tovar, 2004, Tovar *et al.*, 1999) and the ADP/ATP transporter mitochondria carrier family (Chan *et al.*, 2005). Unique to *Entamoeba histolytica* mitosomes is the presence of a complete sulfate activation pathway (Mi-ichi *et al.*, 2009).

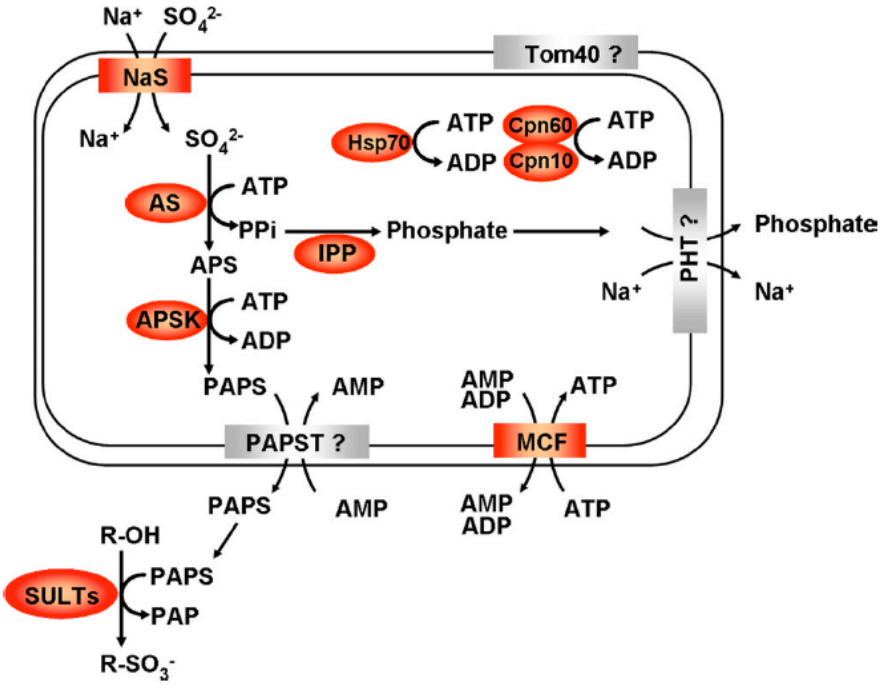

Figure 1.6 *E. histolytica* mitosomal functions taken from Mi-Ichi *et al*. (2009). All orange proteins were shown to be present in the organelle by localization. Grey proteins were predicted to be present. The complete sulphate activation pathway is shown, including the last step outside the mitosome.

Using mass spectroscopy on isolated mitosomes, Mi-Ichi *et al*. (2009) showed the presence of a total of 95 putative mitosomal proteins increasing the functional complexity of the organelle. Mitosomes are very abundant in *Entamoeba histolytica* (León-Avila & Tovar, 2004, Mi-ichi *et al*., 2009). León-Avila and Tovar (2004) measured 256 mitosomes in the *Entamoeba* cell. While confocal imaging by Mi-Ichi *et al*. and work from this thesis suggest an abundance of several thousand organelles. However, it is still unknown how these organelles divide and are distributed to the daughter cells during cell division. Studies on *Giardia* and microsporidia show the association of their mitosomes with the microtubular cytoskeleton, suggesting its involvement in mitosomal division and segregation during cell division (Vavra, 2005, Regoes *et al.*, 2005). Regoes *et al*. found a single centrally positioned mitosome in *Giardia* that was tightly associated with the basal bodies during interphase and were regularly able to observe the division of the single mitosome prior to karyokinesis. Furthermore, they could show the involvement of microtubules, but not actin, in mitosomal division. They

conclude that the single centrally positioned mitosome is tightly associated with the cell cycle and that peripheral mitosomes are distributed stochastically during cell division (Regoes *et al.*, 2005). However, there are many unanswered questions concerning the exact procedure of organelle division, especially about the involvement of associated proteins. Mitochondrial division in mammalian and yeast cells is facilitated by dynamin related proteins, mechanochemical GTPases, which assemble to form a ring around the organelle and divide it by constriction. In this study, we attempted to clarify whether dynamin related proteins are involved in mitosomal division (chapter 5).

1.7. The dynamin protein family

In the following section the terms dynamin protein family, dynamins, dynamin like proteins and dynamin related proteins are being used interchangeably. This also reflects the various terms used in the literature. The differences between the dynamins are being indicated by their function or specific names. Originally, the term dynamin referred only to proteins with the metazoan dynamin-1 structure (GTPase domain, middle domain, PH domain, GED domain and PRD domain, see Fig. 1.7 for explanation of abbreviations) involved in clathrin-mediated endocytosis. All other proteins in the dynamin family were called dynamin related or dynamin like proteins. However, Dynamin-1 is not likely to be the most basal member of the protein family and this separation is arbitrary. Dynamins are universally conserved large GTPases, which are involved in mechanochemical scission of membranes in organelle and cell division, vesicle scission as well as cytoskeleton organization (Praefcke & McMahon, 2004). Protein architecture and functionality has been studied extensively in model systems such as mammalian cells and yeast. To date, all studied eukaryotic organisms have been shown to contain at least one member of this important protein family. Recently, a protein with a similar function and architecture but low sequence similarity has been found in prokaryotic cells (Low & Löwe, 2006). Traditionally, the common overall architecture considered for the eukaryotic dynamin protein family includes the GTPase domain (~300 amino acids), the middle domain (~200 amino acids) and the GTPase effector domain (GED) (~100 amino acids). Additional domains, such as

organelle targeting sequences, membrane spanning, protein interaction or membrane interaction domains, were found to be associated with the specific role of the protein in the cell (Ferguson *et al.*, 1994, Misaka *et al.*, 2002, Mears *et al.*, 2010, Pelloquin *et al.*, 1999, Jin *et al.*, 2001).

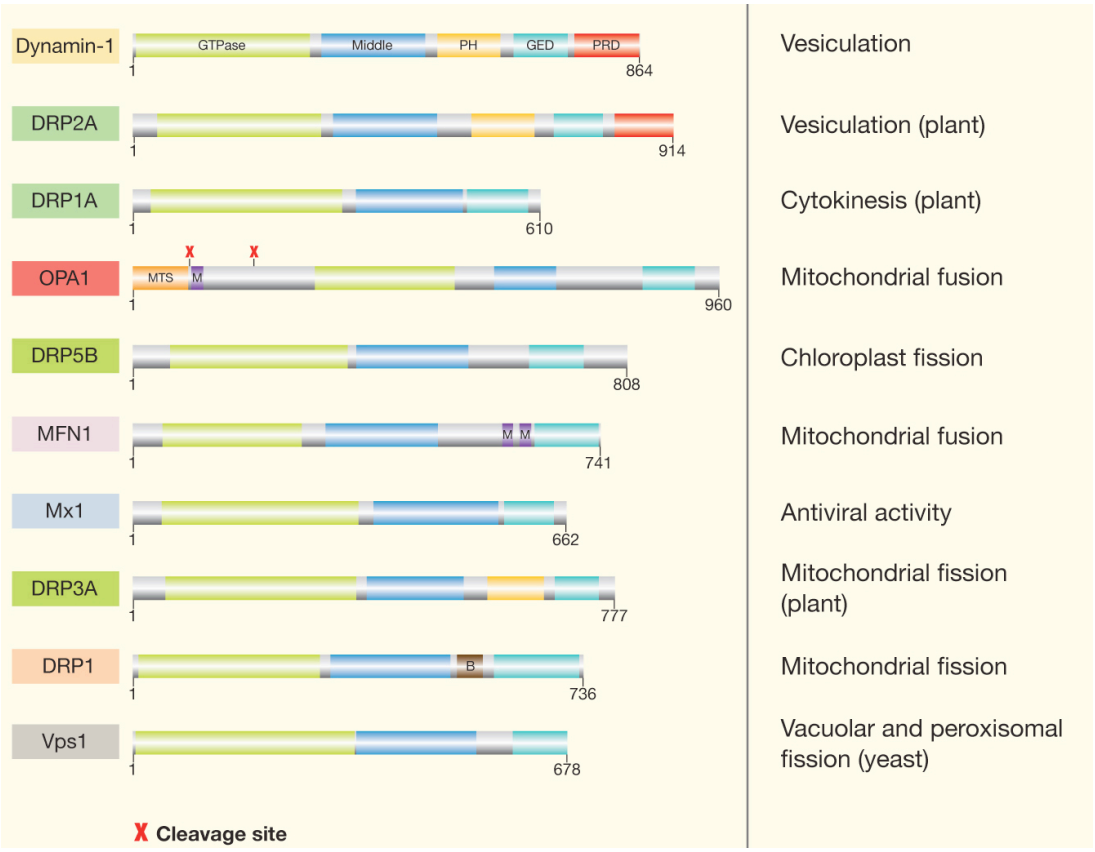

Figure 1.7 Domains of various dynamins taken from Heymann and Hinshaw (2009). Green=large GTPase domain, blue=middle domain, yellow=Pleckstrin homology domain (PH), light blue=GTPase effector domain (GED), red=proline rich domain, orange=mitochondrial targeting signal, grey=other protein sequence, purple=transmembrane domains, brown=yeast specific insert B. The number of amino acids for each protein is indicated by the number at the end of the sequence. Protein functions are written on the side.

Recent structural analyses of dynamin related proteins do not support the traditional separation into the three main domains and rather suggest a similar conserved protein fold across the tree of life (Low & Löwe, 2006, Low & Löwe, 2010).

1.7.1. The structural characteristics in the dynamin protein family

Structural data of complete dynamin proteins are accumulating. To date, three complete structures have been solved, namely the human guanylate-binding protein (GBP1) (Prakash *et al.*, 2000), human dynamin-1 (Chappie *et al.*, 2010) and the bacterial dynamin like protein (BDLP1) from *Nostoc punctiforme* (Low & Löwe, 2006). GBP1 and BDLP1 are quite divergent in their sequence from other members of the dynamin protein family. Additionally, independent domains have been structurally solved by crystallisation, namely the large GTPase domain of rat Dynamin-1 (Reubold *et al.*, 2005), the GTPase region of *Dictyostelium discoideum* DymA (Niemann *et al.*, 2001) and the stalk region, including the middle and the GTPase effector domain of the human Mx protein (Gao *et al.*, 2010). From the structures a general model for dynamin like proteins has been proposed (Fig. 1.8) (Gao *et al*., 2010).

Figure 1.8 Structural hybrid model for dynamin related proteins taken from Gao *et al*. (2010). The model includes the rat dynamin-1 GTPase region, the Mx-stalk region and the human dynamin-1 PH domain. The left panel shows a dynamin dimer with the globular GTPase head region and the stalk region. The PH domain forms the bottom of the stalk. The right panel shows the dynamin dimers in the oligomerized state assembled to a ring structure. The GTPase head regions point outside, the region between the middle and the GED domain inside the ring. This region is potentially involved in protein-protein interactions or membrane-protein interactions.

The model of a dynamin monomer includes a globular head region, which is composed of the large C-terminal GTPase region and a stalk, which contains the middle and the C-terminal GED domain folded to a four-helix bundle (Fig. 1.8). The tip of the stalk exhibits a lipid interaction region, for example the PH domain in metazoan dynamin-1. The proteins oligomerize to form rings or spirals by self-assembly (Fig. 1.8). Information about protein assembly has been gathered in many functional and structural studies and oligomerization appears to be a common characteristic of all known dynamin proteins and a prerequisite to membrane scission (Low & Löwe, 2010, Praefcke & McMahon, 2004, Osteryoung & Nunnari, 2003, Ramachandran, 2011).

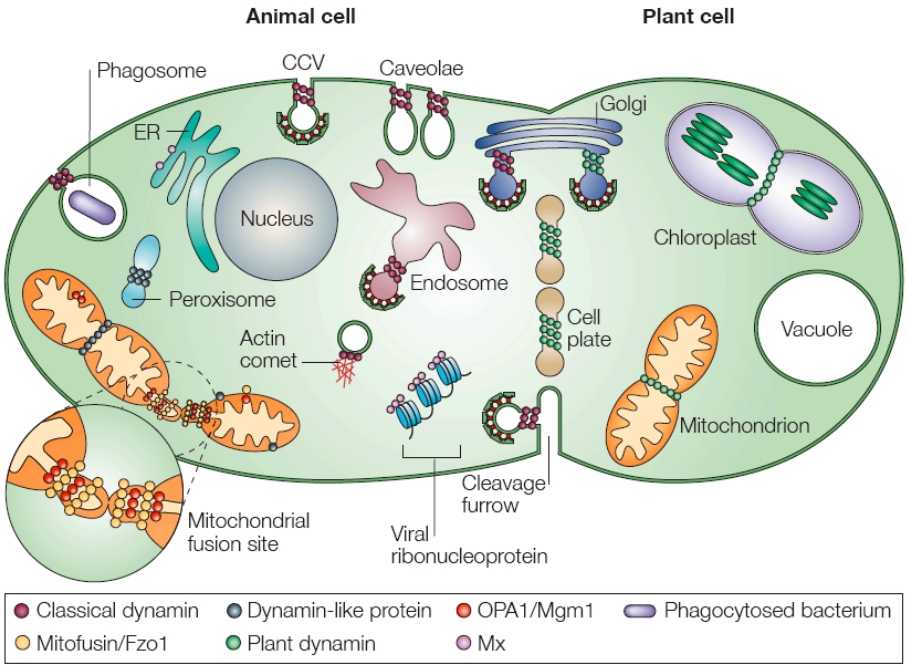

Figure 1.9 Various functions of dynamins in the animal and the plant cell. The image was taken from Praefcke and McMahon (2004).

1.7.2. Self-assembly of dynamin proteins

Dynamin self-assembly is required to remodel membranes *in vivo*. First, protein monomers homodimerize across their nucleotide-binding pockets (Ghosh *et al.*, 2006, Low & Löwe, 2006). Then, they assemble in their stalk region (middle and the GED domain) to higher order of rings or spirals around lipids (Figs. 1.9-1.11) (Mears *et al.*, 2010, Gao *et al.*, 2010). The large GTPase domain is hereby positioned to the outside of the structure, while the substrate binding region (in the example below it is the lipid

binding PH domain of metazoan dynamin-1) is facing to the inside of the spiral (Gao *et al.*, 2010). Protein assembly appears to be independent from GTP hydrolysis (Stowell *et al.*, 1999).

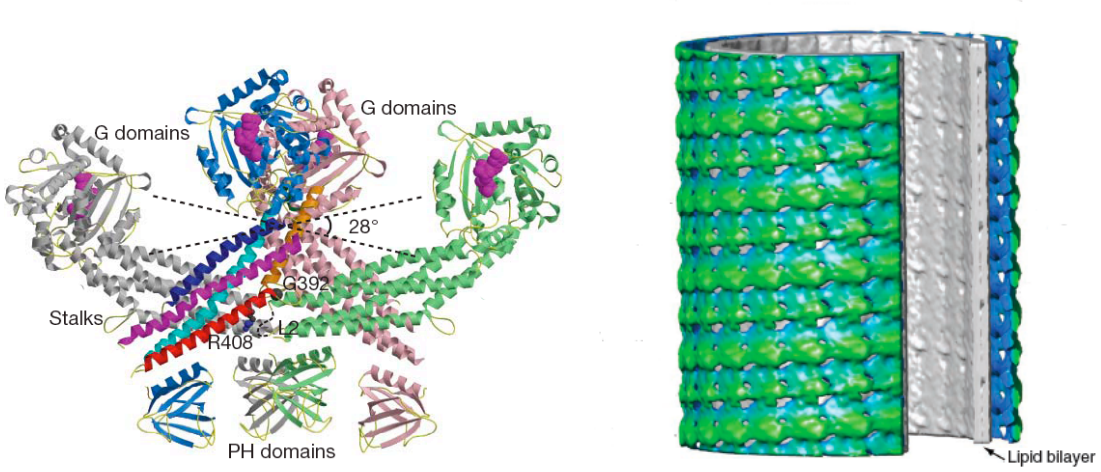

Figure 1.10 Self-assembly of dynamins. The left image was taken from Gao *et al*. (2010). It shows a tetramer to illustrate the mode of dynamin protein assembly. Two GTPase domains, also called G domains, form the head region. The stalk regions assemble in a criss-cross fashion. The conserved Ph domains are specific for mammalian dynamin-1 and differ in sequence composition and length to other members of the dynamin protein family. Nevertheless, this region is usually positioned at the same place in the assembled protein structure as the Ph domain in mammalian dynamins. The right image was taken from Mears *et al*. (2010) and shows a three-dimension reconstruction of yeast Dnm1 to illustrate spiral assembly around a lipid bilayer. Each node resembles the GTPase head region. The stalk is facing inwards towards the lipid bilayer (grey tube).

Upon GTP hydrolysis, the spiral constricts and shears the membrane (Fig. 1.11) (Danino & Hinshaw, 2001, Danino *et al.*, 2004, Roux *et al.*, 2006), followed by dissociation of the protein from the lipids (Mears *et al.*, 2010, Low *et al.*, 2009).

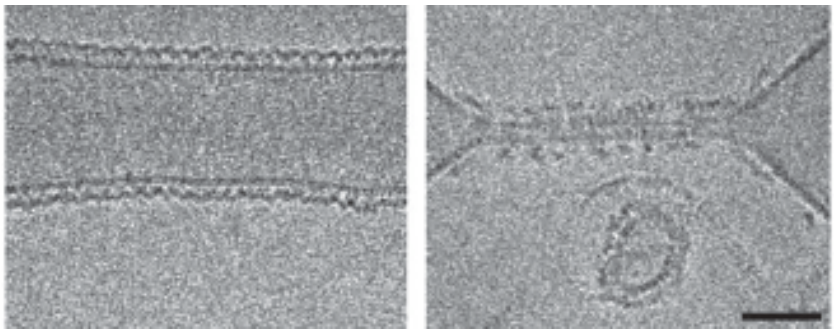

Figure 1.11 *In vitro* mitochondrial yeast Dnm1 lipid tube contriction upon GTP hydrolysis taken from Mears *et al*. (2010). The left image shows the assembly of Dnm1 into a spiral around a lipid tube. The right image shows the constriction of the dynamin spiral upon GTP hydrolysis.

The presence of lipids appears to stimulate dynamins to oligomerize (Ingerman *et al.*, 2005, Stowell *et al*., 1999, Chappie *et al*., 2010, Song *et al.*, 2004a). A direct physical link to the lipid bilayer does not seem to be essential for all dynamins (Mears *et al*., 2010). While metazoan and plant dynamin-1 like proteins bind to the membrane with their PH domain (Zheng *et al.*, 1996, Lee *et al.*, 2002), no direct interaction for yeast Dnm1 was found (Mears *et al*., 2010).

1.7.3. GTPase activity

Dimerization of protein monomers prior to oligomerization appears to play an important role for GTPase activity stimulation. In this process the GTPase monomers homodimerize upon nucleotide binding across the nucleotide binding pockets and subsequently activate the GTPase reaction (Fig. 1.12) (Gasper *et al.*, 2009, Low & Löwe, 2010). Increase in GTPase activity upon protein self-assembly has been observed frequently (Shpetner & Vallee, 1992, Maeda *et al.*, 1992, Danino *et al*., 2004, Song *et al*., 2004a, Ingerman *et al*., 2005, Ghosh *et al*., 2006, Meglei & McQuibban, 2009, Chappie *et al*., 2010).

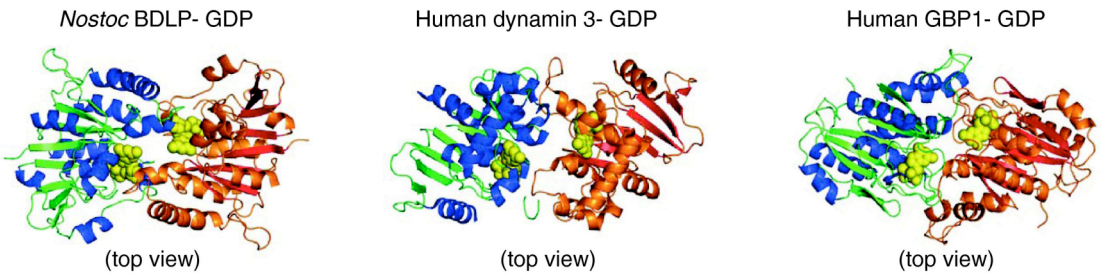

Figure 1.12 Two-fold symmetry of GTPase domains in different dynamins showing the homodimerization across nucleotide binding pockets. Image was taken from Low and Löwe, 2010.

The active site in dynamin proteins resembles closely the one found in Ras GTPases with similar conserved GTP binding sites and fold (Pai *et al.*, 1990, Niemann *et al.*, 2001). Four conserved binding sites, which are present in all GTPases, are responsible for GTP binding and hydrolysis (Bourne *et al.*, 1991) (Fig. 4.2). Characteristic for the dynamin protein family are the low basal substrate affinities, with Michaelis-Menten constants between 65 and 310 μM and basal turnover numbers between 0.5 and 27 min^{-1}, which increase cooperatively upon protein assembly (Richter *et al.*, 1995, Song *et al.*, 2004a, Meglei & McQuibban, 2009, Chappie *et al.*, 2010).

1.7.4. The process of constriction

Several mechanisms of membrane fission have been suggested, including vesicle separation by spiral extension in a “spring-like” manner (Stowell *et al.*, 1999), spiral constriction (Sweitzer & Hinshaw, 1998, Danino *et al.*, 2004), torsion between the rungs of a dynamin protein spiral (Roux *et al.*, 2006) or passive spontaneous fission based on dynamin induced membrane curvature (Bashkirov *et al.*, 2008, Pucadyil & Schmid, 2008, Low *et al.*, 2009).

1.7.5. The various functions in the dynamin protein family

Dynamins are a protein family of great cellular importance and involved in many membrane-altering processes. Their roles involve for example endocytosis, cytokinesis, organelle division and fusion, antiviral defence and vesicle scission (see Fig. 1.9).

1.7.6. Endocytosis

There are several ways of entry into the cell (Fig. 1.13). Particle uptake is facilitated by phagocytosis. There is evidence, mostly from mammalian macrophages, that dynamin plays a crucial role in the formation of intracellular vesicles needed for the formation of the phagocytic cup (Di *et al.*, 2003). Wiejak *et al*. (2003) showed an up-regulation of dynamin in *Paramecium* during phagocytosis and its localization to the phagocytic compartment indicating that dynamins involved in the phagocytosis process are conserved beyond the metazoan clade (Wiejak *et al.*, 2003). However, data on dynamin related proteins involved in phagocytosis in non-human cells are sparse and more research is needed to understand the role of this protein family in such an important process.

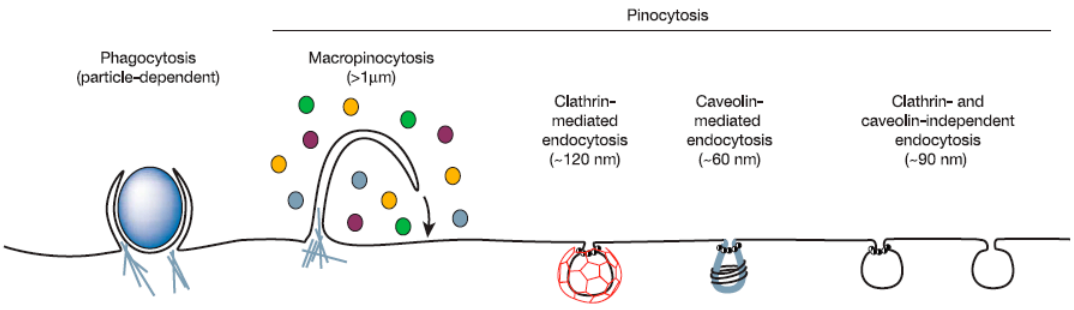

Figure 1.13 Multiple ways of entry into the cell taken from (Conner & Schmid, 2003). The processes are based on the mammalian cell system and show the two main ways of uptake: phagocytosis for particle/food uptake and pinocytosis, which involves fluid uptake. Phagocytosis and Macropinocytosis involve actin-assembly (blue lines). Dynamins are involved in Chlathrin and Caveolin-mediated endocytosis as well as endocytosis independent of both proteins. However, cellular intake through phagocytosis and several processes of pinocytosis have been found to be dynamin independent.

Pinocytosis circumvents several processes of endocytosis for fluid uptake, of which at least two mechanisms involve the dynamin protein family in eukaryotes. These are clathrin mediated endocytosis (CME) and clathrin-independent endocytosis (Fig. 1.13). Both processes are well described in metazoan cells (Merrifield *et al.*, 2002, Schmid & Frolov, 2011, Sandvig *et al.*, 2011, Doherty & McMahon, 2009), but information is sparse for protist lineages. Dynamin-1 from metazoan cells is important in clathrin-mediated endocytosis. Dynamin-1 is a large protein with 5 domains (Fig. 1.7): the N-terminal GTPase domain, the middle domain, a PH domain, the GED domain and a C-terminal proline rich (PR) domain. The PH domain was shown to be essential for lipid binding and thus membrane curvature and fission (Zheng *et al*., 1996, Liu *et al.,* Roux *et al.*, 2010), while the proline rich tail is responsible for interacting with protein partners such as Amphiphysin, which is responsible for recruiting dynamin-1 to the endocytotic vesicle (David *et al.*, 1996, Shupliakov *et al.*, 1997). The protein forms a collar around the neck of the vesicle and is responsible for the separation from the cellular membrane by mechanochemical fission (Fig. 1.13) (Mettlen *et al.*, 2009). Clathrin mediated endocytosis (CME) with the involvement of dynamin appears to be largely an adaptation found in metazoans. However, CME has been studied little outside the metazoan clade. An example for another dynamin related protein involved in CME was recently discovered in the alveolate ciliate *Tetrahymena thermophila* (Elde *et al*., 2005). The protein differs in domain structure and sequence composition to metazoan dynamin-1 suggesting the acquisition of a dynamin related protein not closely related to metazoan dynamin-1 by convergent evolution (Elde *et al*., 2005). The presence of dynamins involved in CME outside the metazoan clade was also reported from *Saccharomyces cerevisiae* (Nannapaneni *et al.*, 2010, Smaczynska-de *et al.*, 2010). Vps1, a dynamin related protein functioning in several vacuolar fusion and fission events in the Golgi, endosomal and peroxisomal systems (Vater *et al.*, 1992, Nothwehr *et al.*, 1996, Hoepfner *et al.*, 2001, Peters *et al.*, 2004), has been found to be important during endocytosis (Nannapaneni *et al*., 2010, Smaczynska-de *et al.*, 2010). However, its actual role (as a regulator or a mechanochemical enzyme) has not been revealed yet. The most studied clathrin independent endocytic process involving the dynamin protein family is the caveolae-mediated endocytosis (Fig. 1.13) (Henley *et al.*, 1998, Oh

et al., 1998, Magalhaes *et al.*, 2002). Similar to CME, dynamins (in mammalian cells dynamin-2) are responsible for vesicle fission from the plasma membrane (Fig. 1.14).

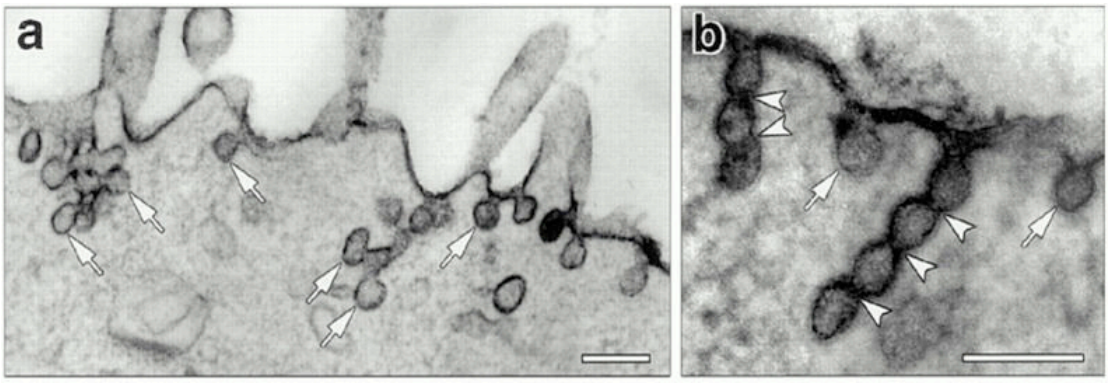

Figure 1.14 Electron micrographs showing endocytic caveolae in hepatic cells stained with anti-dynamin-2 antibody. The images were taken from Henley *et al.*, 1998. Bars=0.15 μm. The arrows point at various budding profiles. The arrowheads show "chains" of vesicles separated by constrictions.

However, at present there appear to be no information about caveolae-mediated endocytosis involving the dynamin protein family in other than metazoan cells and information about the participation of the dynamin protein family in any endocytic processes in protists is sparse.

The involvement of dynamin related proteins in different endocytic events in protists have been observed in *Trypanosoma brucei* (Chanez *et al.*, 2006), *Giardia intestinalis* (Gaechter *et al.*, 2008), *Dictyostelium discoideum* (Wienke *et al.*, 1999), *Paramecium aurelia* (Wiejak *et al.*, 2003) and *Tetrahymena thermophila* (Elde *et al.*, 2005). However, the actual mechanisms are often poorly understood and more research is needed to clarify the importance of dynamins for endocytosis across the eukaryotic tree of life.

1.7.7. Dynamins and mitochondrial division

Mitochondria are dynamic, double membrane bound organelles that are descended from a marine planktonic α-proteobacterium approximately 1.5 billion years ago (Gray *et al.*, 1999, Thrash *et al.*, 2011). The dynamin protein family plays an essential role in mitochondrial fusion and division (Hoppins *et al.*, 2007, Hoppins & Nunnari, 2009),

processes often uncoupled from cell division (Bleazard *et al.*, 1999). To date all eukaryotic organisms studied exhibit at least one dynamin that is involved in mitochondrial division (Smirnova *et al.*, 1998, Arimura & Tsutsumi, 2002, Nishida *et al.*, 2003, Bleazard *et al*., 1999, Wienke *et al*., 1999, Morgan *et al.*, 2004). The division of each organelle is orchestrated by multi-component protein complexes, which drive the synchronized constriction of inner and outer membranes and the separation of both daughter organelles (Osteryoung, 2001, Shaw & Nunnari, 2002, Heymann & Hinshaw, 2009). Interestingly, hydrogenosomes of two *Trichomonas* species and *Tritrichomonas suis* show a similar division pattern of inner and outer mitochondrial membrane as mitochondria in yeast (Ingerman *et al*., 2005) suggesting the involvement of dynamin as a mechanochemical enzyme in this process (Benchimol *et al.*, 1996). The involvement of dynamins in mitochondrial division has been especially well studied in human cells and yeast. In both organisms, Drp1 (Yoon & McNiven, 2001) and Dnm1 (Ingerman *et al*., 2005, Mears *et al.*, 2010) respectively, are responsible for the constriction of the outer mitochondrial membrane. They assemble to helical structures around the organelle in a similar fashion as dynamins involved in endocytosis and fission occurs upon GTP hydrolysis (Ingerman *et al*., 2005, Mears *et al*., 2010). Additionally to the constriction of the outer mitochondrial membrane, the inner membrane divides in an orchestrated fashion (Wong *et al.*, 2000, Wong *et al.*, 2003, Meeusen *et al.*, 2006). Interestingly, the proteins involved appear to differ across the tree of life. The rhodophyte *Cyanidioschyzon merolae* as well as and the amoebozoan *Dictyostelium*, various stramenopiles and possibly the Glaucocystophytes rely on the bacterial cell division protein FtsZ for inner mitochondrial membrane fission (Kiefel *et al.*, 2004, Gilson *et al.*, 2003, Beech *et al.*, 2000, Takahara *et al.*, 2000). These organisms contain a hybrid system between the bacterial descendent FtsZ at the inner mitochondrial membrane and the eukaryotic dynamin at the outside of the mitochondrion. This curious combination could be explained by the event leading to the formation of mitochondria from free-living α-proteobacteria. While FtsZ may have been responsible for the bacterial endosymbiont cell division, in accordance with extant bacterial cell division, the early dynamin host protein may have adapted to controlling the division of the newly acquired endosymbiont and would place the

dynamin involved in mitochondrial division at the base of the eukaryotic dynamin protein family (Osteryoung & Nunnari, 2003, Kuroiwa, 2010).

1.7.8. Dynamins in prokaryotes

Prokaryotic homologues of eukaryotic dynamin protein family were found in various bacterial lineages (van der Bliek, 1999) and recently, the dynamin related protein of *Nostoc punctiforme* BDLP1 was shown to be structurally and functionally comparable to its eukaryotic counterparts albeit with a low sequence similarity (Low & Löwe, 2006, Low *et al*., 2009). Sequences related to BDLP1 were also found in other prokaryotic lineages including archea. Dynamins in archea have not been studied and their relationship to bacterial and eukaryotic members of this family as well as their function is unknown. However, the ubiquitous presence of this protein family in the tree of life indicates that dynamins are ancient and of fundamental importance for cellular functionality. Since all known dynamins appear to function in a similar fashion as mechanochemical enzymes interacting with membranes, they might have played this role early on. The presence of dynamins in archeae as well as bacteria might have implications for the evolution of dynamins in eukaryotes. Eukaryotes evolved from a symbiosis between an archaebacterium and a eubacterium (Martin & Müller, 1998). The dynamin protein family in eukaryotes might therefore stem from either one of these groups or even from both. This, however, is purely speculative and research on dynamins in prokaryotes and especially on archeae is needed to elucidate dynamins' evolutionary and functional importance.

1.7.9. The dynamin protein family in the Amoebozoa

The free-living amoebozoan *Dictyostelium discoideum* contains five well-characterized dynamin related proteins: DymA, DymB, DLPA, DLPB and DLPC. The DymA GTPase region has been structurally solved (Niemann *et al*., 2001) and is involved in mitochondrial division (Wienke *et al*., 1999). DymB appears to be involved with cytoskeletal and organellar structures and its depletion affects various processes in the cell indicating a wider spectrum of functions (Rai *et al.*, 2010). DLPA, DLPB and DLPC participate in cell division processes and are closely related to the plant chloroplast

and cell division dynamins DRP5A and DRP5B (Miyagishima *et al.*, 2008) (chapter 4). This relationship is very interesting because plants and amoebozoa are not closely related. It indicates that they share a common evolutionary history of dynamins involved in cytokinesis, which reaches back to before the endocytic event, which led to the acquisition of chloroplasts in plants (Miyagishima *et al.,* 2008). Information on the dynamin protein family in *Entamoeba* is sparse. However, while conducting this project, (Jain *et al.*, 2010) discovered that Drp1 is nuclear associated. In this study, we show that *Entamoeba histolytica* contains a total of four dynamin related proteins. Aim of this project was the characterization of the remaining three proteins.

1.8. Aims of this study

Little is known about the division and inheritance of mitosomes in *Entamoeba histolytica*. The aim of this study is to analyze if dynamin related proteins are involved in mitosomal division similar to their involvement in mitochondrial division. In addition to molecular and cell biological methods, the *Entamoeba* dynamin protein family was also assessed using bioinformatics.

Specific thesis objectives:

1. Are dynamins present within the *Entamoeba* genus and if yes, what role do they play for cellular integrity?
2. Are dynamins involved in mitosomal division?
3. Do *Entamoeba histolytica* dynamins differ from previously characterized eukaryotic dynamins?
4. Are *Entamoeba* dynamins involved in the conversion from trophozoites to cysts?
5. Are mitosomes also present in other *Entamoeba* species?
6. What happens to mitosomes in *Entamoeba* cysts?

2. Material and Methods

2.1. Material

2.1.1. Bacterial strains

Bacterial strains used in this study are detailed in table 2.1.

Table 2.1 *Escherichia coli* and protist strains used in this study including names of the strains, their molecular characteristics, the sources and the experiments in which the strains were used.

Name of strain	Strain information	Source	Experiment
***Escherichia coli* strains**			
One shot Mach1-T1	lacZΔM15 hsdR lacX74 recA endA tonA	Invitrogen	Complementation of Drp2
One Shot® ccdB Survival™ T1 Phage Resistant Cells	F- mcrA (mrr-hsdRMS-mcrBC) 80lacZM15 lacX74 recA1 ara139 D(ara-leu)7697 galU galK rpsL (StrR) endA1 nupG tonA::Ptrc-ccdA	Invitrogen	Complementation of Drp2
α select silver efficiency	deoR endA1 recA1 relA1 gyrA96	Bioline	All cloning experiments
BL21 pLysY	F^- *ompT* $hsdS_B(r_B^-m_B^-)$ *gal dcm* (DE3) pLysE (Cam^R)	Bioline	Drp2 recombinant gene expression
Rosetta 2 (DE3) pLysS	F– *ompT hsdS*B (rB–mB–) *gal dcm* (DE3) pLacIRARE2 (Cam^R)	Novagen	Drp2 recombinant gene expression
Protist strains			
Entamoeba histolytica strain HM-1:IMSS	Axenic culture	Dr. Graham Clark, London School of Hygiene and Tropical Medicine, UK	All chapters
Entamoeba invadens strains IP-1	Axenic culture	Dr. Graham Clark, London School of Hygiene and Tropical Medicine, UK	Expression profile of dynamin protein family, localization experiments
Dictyostelium discoideum AX2	Axenic culture	Prof. Dietmar Manstein, Hannover Medical School, Germany	Complementation and overexpression of Drp2

2.1.2. Plasmids

The plasmids used in this study are detailed in table 2.2.

Table 2.2 List of plasmids used in this study including plasmid names, their characteristics, plasmid sizes and sources.

Name of plasmid	Description	Size [kb]	Source
pGEM-T-Easy	TA cloning vector	3.015	Promega
pCR8/GW/TOPO	Gateway entry vector	2.817	Invitrogen
pAH-DEST	Gateway destination vector	10.5	Dr. Carol Gilchrist, School of Medicine, University of Virginia, USA
pDXA-3H	*Dictyostelium discoideum* expression vector	6.1	Prof. Dietmar Manstein, Hannover Medical School, Germany
Drp2/pDXA-3H	*Dictyostelium discoideum* expression vector with Drp2	8.092	This study
pET-14b	Expression vector adds His-tag to N- or C-terminus of protein to be expressed	4.7	Novagen
EhDrp2pET-14b	Cloned full length Drp2 into pET-14b vector	6.689	This study
pET-3c	Expression vector without His-tag	4.6	Novagen
Hsp70/pET-3c	Expression vector with codon optimized Hsp70 sequence and His-tag	6.444	This study
EhDrp1/pGEM-T-Easy	Drp1 PCR product cloned into pGEM-T-Easy vector	5.064	This study
EhDrp2/pGEM-T easy	Drp2 PCR product cloned into pGEM-T-Easy vector	5.007	This study
EhDrp3/pGEM-T-Easy	Drp3 PCR product cloned into pGEM-T-Easy vector	5.388	This study
EhDrp4/pGEM-T-Easy	Drp4 PCR product cloned into pGEM-T-Easy vector	5.370	This study
EhDrp1Flag/pAHDEST	Drp1 gene with C-terminal Flag-tag in pAH-DEST vector	12.573	This study
EhDrp2Flag/pAHDEST	Drp2 gene with C-terminal Flag-tag in pAH-DEST vector	12.716	This study

2.1.3. Primers

The primers used in this study are described in table 2.3. The primer pairs EhDrp1_Flag-F and EhDrp1_Flag-R, EhDrp1_544F and EhDrp1_2912R and EhDrp2_731F and EhDrp2_2884R were designed by Dr. Mark van der Giezen. The other primers were designed by Maria A. Siegesmund. Primers amplifying fragments for gene expression were taken from the beginning and the end of the DNA sequence. In addition restriction sites and/or sequence tags were added manually. From DNA fragments that were cloned into the expression vector pET-14b the stop codon was removed to allow the addition of the C-terminal His-tag. Primers were tested for secondary structure formation using the program Netprimer (Premier Biosoft). RT-PCR primers were designed using the Primer 3 {Rozen, 2000 #1035}.

Table 2.3 List of primers with their assigned names, primer sequences and purposes in this study.

Name of primer	Primer sequence (5' to 3')	Purpose
General gene amplification and sequencing		
EhDrp1_544F	CACTGCAATTTTATTTGAGCTTCAAGG	PCR Drp1 amplification forward primer
EhDrp1_2912R	GGGGATATGCTGCAGAGCAA	PCR Drp1 amplification reverse primer
EhDrp1_752F	CACGTGAAGTTGACCCAGAT	Sequencing Drp1 forward primer
EhDrp1_1914R	TTCAACTTTAGGTTCTGGTTGGA	Sequencing Drp1 reverse primer
EhDrp2_731F	AAGCAGAATGACATTTCCAAACA	PCR Drp2 amplification forward primer
EhDrp2_2884R	TTTGGGATTGAACAGAATTCCTTG	PCR Drp2 amplification reverse primer
EhDrp1_1941F	TGAAAGTCCAGCAATTACAACAA	Sequencing end of Drp1 and Gateway vector to gain C-terminal vector sequence
EhDrp2_middleF	GGTTCTTTTGCTGCTGCATT	Sequencing Drp2 forward primer, middle region of gene
EhDrp2_middle	CGAGTTCCACTTGCGTTTTT	Sequencing Drp2 forward primer, middle region of gene
EhDrp3_146F	GGAGAGAGTGAATGATGGGAAG	PCR Drp3 amplification forward primer
EhDrp3_2482R	TCTTCCAAATGGTCAACGTG	PCR Drp3 amplification reverse primer
EhDrp4_61F	TTGAGGAAAGGGGATGAAAA	PCR Drp4 amplification forward primer
EhDrp4_2484R	TTTATGAATGTTTCCGCAAATTA	PCR Drp4 amplification reverse primer

pAHDEST_fdx_F	ACTTAATTGAGAAGATATTACACT AAC	Sequencing insert in pAH-DEST Gateway vector forward primer
Flag-tag primers for Drp2 over-expression in *E. histolytica*		
EhDrp2_Flag-F	ATGCAAAGATTAATTCCTGT	PCR Drp2 amplification with Flag-tag forward primer
EhDrp2_Flag-R	TTA*TTTATCATCATCATCTTTATAAT* CGAAGCATTGATCTCTTACTTGAT	PCR Drp2 amplification for addition of Flag-tag on C-terminus reverse primer, Flag-tag italicized
Amplification of Drp2 for *D. discoideum* expression vector		
EhDrp2_pDXA3H_F	agaagaGGTACCATGCAAAGATTAA TTCCTG	Amplification of Drp2 for the *D. discoideum* expression vector pDXA-3H, including restriction site *Kpn*I (underlined); small letters indicate nonsense sequence to simplify restriction digest of PCR product
EhDrp2_pDXA3H_ R	agaagaGGTACCGAAGCATTGATCT CTTACT	Amplification of Drp2 for the *D. discoideum* expression vector pDXA-3H, including restriction site *Kpn*I (underlined); small letters indicate nonsense sequence to simplify restriction digest of PCR product
Recombinant gene expression		
EhDrp2pET-14b_F	agaagaCCATGGAAAGATTAATTC CTGTAATTAATAG	PCR Drp2 amplification for addition of restriction site *Nco*I (underlined) to beginning of the Drp2 gene
EhDrp2pET-14b_R	tcttctCCATGGGGAAGCATTGATC TCTTACTTG	PCR Drp2 amplification for addition of restriction site *Nco*I (underlined) to end of the Drp2 gene
Hsp70_imp_NcoI_ F	agaagaCCATGGTTGTTTCTCAGCC GGCT	Amplification from storage vector pUC57 for the addition of restriction sites *Nco*I (underlined) for pET-3c expression vector; small letters indicate nonsense sequence to simplify restriction digest of PCR product
Hsp70_imp_NcoI_ R	agaagaGGATCCTTAGTGGTGGTG GTGGTGGTGAG	Amplification from storage vector pUC57 for the addition of restriction sites *Nco*I (underlined) for pET-3c expression vector; small letters indicate nonsense sequence to simplify restriction digest of PCR product
RT-PCR primer		
EhDrp1RTPCR_F	TGAAGTTGACCCAGATGGAG	*E. histolytica* Drp1 specific RT-PCR primer
EhDrp1RTPCR_R	AATGCCAAGTCTGTCTGCAA	*E. histolytica* Drp1 specific RT-PCR

		primer
EhDrp2RTPCR_F	CCACAACAACAACACGTTCC	*E. histolytica* Drp2 specific RT-PCR primer
EhDrp2RTPCR_R	GCAGGATTTTCTGCAAGAAGG	*E. histolytica* Drp2 specific RT-PCR primer
EhDrp3RTPCR_F	AGGATTTCCACGAGCAAAAA	*E. histolytica* Drp3 specific RT-PCR primer
EhDrp3RTPCR_R	TCTTCTTGGGCTGTTTGTCC	*E. histolytica* Drp3 specific RT-PCR primer
EhDrp4RTPCR_F	ATGTGAAAAATGGCCTGGAG	*E. histolytica* Drp4 specific RT-PCR primer
EhDrp4RTPCR_R	CACGTGATGCCTTCGTTTTA	*E. histolytica* Drp4 specific RT-PCR primer
EhActinRTPCR_F	TGCACCAGAAGAACATCCAG	*E. histolytica* actin specific RT-PCR primer
EhActinRTPCR_R	TCACGTCCTGCAAGATCAAG	*E. histolytica* actin specific RT-PCR primer
EiDrp1RTPCR_F	TACGGGAAAATTGCGGATAG	*E. invadens* Drp1 specific RT-PCR primer
EiDrp1RTPCR_R	CCTCCAATCAGCTCGTGTTT	*E. invadens* Drp1 specific RT-PCR primer
EiDrp2RTPCR_F	GACGAAATTAAACCGGACGA	*E. invadens* Drp2 specific RT-PCR primer
EiDrp2RTPCR_R	AAACATGGTCGTGTCCCACT	*E. invadens* Drp2 specific RT-PCR primer
EiDrp2aRTPCR_F	TCCGAATGTCGTTGATTTGA	*E. invadens* Drp2a specific RT-PCR primer
EiDrp2aRTPCR_R	TCGAGTTGGTTCCTTTGTCC	*E. invadens* Drp2a specific RT-PCR primer
EiDrp3RTPCR_F	GAGCCTTTCGACCAGTCTTG	*E. invadens* Drp3 specific RT-PCR primer
EiDrp3RTPCR_R	TATTTCGCGGCTCAGGTACT	*E. invadens* Drp3 specific RT-PCR primer
EiDrp4RTPCR_F	AATTATCGAGGCGATTGTCG	*E. invadens* Drp4 specific RT-PCR primer
EiDrp4RTPCR_R	GTCGATCAAACACGATGGAA	*E. invadens* Drp4 specific RT-PCR primer
EiActinRTPCR_F	CGAGCTGTCTTCCCATCAAT	*E. invadens* actin specific RT-PCR primer
EiActinRTPCR_R	TTAGCCTTTGGGTTCATTGG	*E. invadens* actin specific RT-PCR primer
qPCR primer		
Ei ssRNA_F	CGCCCGTCGCTCCTACCG	*E. invadens* ssRNA quantitative PCR primer
Ei ssRNA_R	ATGATCCTTCCGCAGG	*E. invadens* ssRNA quantitative PCR primer
EiActq_F	CGGTTTTGCTGGTGATGA	*E. invadens* actin quantitative PCR primer
EiActq_R	GGTGTCCTTGTTGCCCATA	*E. invadens* actin quantitative PCR primer

EiSKIPdomain_F	TGCCAGAACAACCCACAA	*E. invadens* SKIP domain quantitative PCR primer
EiSKIPdomain_R	TCAAACACGGGAGAACCAA	*E. invadens* SKIP domain quantitative PCR primer
EiDrp3q_F	CAGAGCGACGGCAAAAGT	*E. invadens* Drp3 quantitative PCR primer
EiDrp3q_R	GCAGAATCAACGGACGAC	*E. invadens* Drp3 quantitative PCR primer
EiDrp4q_F	CGAAAGCAGCACAAGCAC	*E. invadens* Drp4 quantitative PCR primer
EiDrp4q_R	TCCATCGCACCAATAGCA	*E. invadens* Drp4 quantitative PCR primer

2.1.4. Bacterial media and solutions

The following media and solutions were used in this study.

Luria-Bertani (LB) broth, 1000 ml
- 10 g Bacto-tryptone
- 5 g yeast extract
- 10 g NaCl
- H_2O up to 1000 ml

LB-agar, pH 7.2, 1000 ml
- 10 g Bacto-tryptone
- 5 g yeast extract
- 10 g NaCl
- 10 g Agar
- H_2O up to 1000 ml

2YT, 1000 ml
- 5 g NaCl
- 10 g yeast extract
- 16 g Bacto-peptone
- H_2O up to 1000 ml

SOC, 1000 ml
- 20 g Bacto-tryptone
- 5 g yeast extract
- 2 ml of 5 M NaCl
- 2.5 ml of 1 M KCl
- 10 ml of 1 M $MgCl_2$

- 10 ml of 1 M $MgSO_4$
- 20 ml of 1 M glucose
- H_2O up to 1000 ml

Ampicillin (100 mg/ ml)

- Ampicillin sodium salt was dissolved in millipure water and filter-sterilized through a 0.2 μm filter. The final concentration used was 100 μg/ml.

Hygromycin (50 mg/ ml)

- A 400 mg/ml hygromycin B stock solution was diluted in millipure water to 50 mg/ml, filtersterilized through a 0.2 μm filter and aliquoted into 1.5 ml sterile reaction tubes.

Chloramphenicol (34 mg/ ml)

- Chloramphenicol was dissolved in ethanol. The final concentration used was 34 μg/ml.

X-Gal (20 mg/ml)

- X-Gal (5-bromo-4-chloro-3-indolyl-beta-D-galactopyranoside) was dissolved in dimethylformamide and was used at a final concentration of 80 μg/ml.

Phosphate buffered saline (PBS), 1000 ml

- 0.454 g Na_2HPO_4
- 0.068 g KH_2PO_4
- 0.097 g KCl
- 7.89 g NaCl
- H_2O up to 1000 ml
- The pH was adjusted to 7.4.

Isopropyl-beta-D-thioglactopyranoside (IPTG) (1 M)

- IPTG was dissolved in millipure water and filter sterilised. The final concentration used was 1 mM.

2.1.5. Protist media and solutions

LYI-S Medium, pH 6.8 for culturing *Entamoeba histolytica* and *Entamoeba invadens*

Base

- 1 g K_2HPO_4
- 0.6 g KH_2PO_4
- 2 g NaCl
- 25 g yeast extract
- 5 g liver digest neutralized
- 10 g glucose
- 1 g cysteine
- 0.2 g ascorbic Acid
- 2 ml ferric ammonium citrate (brown) (22.8 mg/ml)
- 1M sodium hydroxide to adjust pH to 6.8
- H_2O up to 880 ml

The medium base was aliquoted into 10 x 88 ml, autoclaved at 121 °C for 15 min and stored at -20 °C.

Vitamin mixture #18 (Diamond and Cunnick 1991)

Solution 1

- 45 mg niacinamide
- 4 mg pyridoxal hydrochloride
- 23 mg pantothenic acid
- 5 mg thiamine hydrochloride
- 1.2 mg Vitamin B12
- H_2O up to 25 ml

Solution 2

- 7 mg riboflavin was dissolved in a minimum amount of 0.1 M NaOH. H_2O was added to a final volume of 45 ml.

Solution 3

- 5.5 mg folic acid was dissolved in a minimum amount of 0.1 M NaOH. H_2O was added to a final volume of 45 ml.

Solution 4

- 2 mg D-biotin was dissolved in 45 ml of H_2O.

The solutions 1-4 were combined.

Solution 5

- 1 mg DL-6-8-thioctic acid (oxidized form)
- 5 ml 95 % ethanol
- 500 mg Tween-80
- H_2O up to 30 ml

Solution 5 was added to the combined solutions 1-4. The final volume was adjusted to 200 ml with distilled H_2O and autoclaved at 121 °C for 15 min.
Adult bovine serum was heat inactivated at 56 °C to remove complement.
88 ml of medium were completed by the addition of 2 ml Vitamin mixture and 15 ml of adult bovine serum.

50 % LY-G Encystation medium for *E. invadens* (LYI without glucose)

Recipe for 400 ml

- 0.2 g potassium diphosphate
- 0.12 g potassium monophosphate
- 0.4 g NaCl
- 0.2 g cysteine
- 0.04 g ascorbic acid
- 1 g liver extract
- 5 g yeast extract

- 0.4 ml ferric ammonium citrate (22.8 mg/ml)
- H_2O to 380 ml
- The pH was adjusted to 6.8 with 1 M NaOH.

The medium was aliquoted into 4 x 95 ml and autoclaved for 15 min at 121 °C.
95 ml of medium were completed by adding 5 ml of adult bovine serum and 2 ml of vitamin mix per bottle.

Cytomix for *E. histolytica* electroporation, 1000 ml

- 8.95 g KCl
- 0.02 g $CaCl_2$
- 5.96 g HEPES
- 0.76 g EGTA
- 0.48 g $MgCl_2$

All chemicals were dissolved in 1000 ml of 10 mM K_2HPO_4/KH_2PO_4 buffer (pH 7.6). The pH was adjusted to 7.8-7.9 with KOH. The buffer was filtersterilized. Just before the electroporation, 8 ml cytomix were completed by adding 20 mg ATP to a final concentration of 4 mM and 24 mg reduced gluthathione to a final concentration of 10 mM.

2.1.6. Solutions for DNA work

Tris / Borate / EDTA (TBE) electrophoresis buffer, 1000 ml

- 10.78 g Tris
- 5.5 g boric acid
- 0.58 g EDTA
- The pH was adjusted to 8.3.

Tris / Acetic acid / EDTA (TAE) electrophoresis buffer 1000 ml

- 4.84 g Tris base [tris(hydroxymethyl)aminomethane]
- 1.14 ml of glacial acetic acid
- 0.29 g EDTA
- The pH did not have to be adjusted and should be approximately 8.5.

DNA Marker

The Bioline hyperladder I was used for DNA fragment sizes larger than 400 bp. Fig. 2.1 shows the bands produced by this marker.

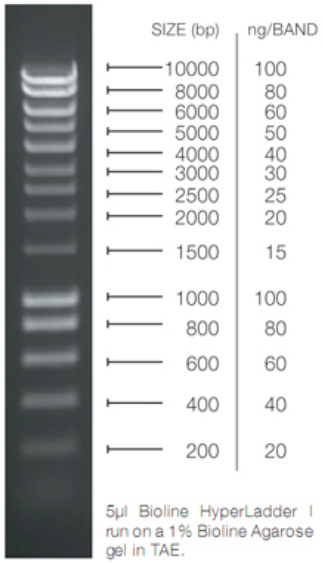

Figure 2.1 Bioline Hyperladder I was the DNA ladder used in this study. The sizes of the bands correspond to the amount of DNA in a 1 % agarose gel when 5 µl marker are loaded. (The figure was taken from the Bioline website).

The NEB 100 bp DNA ladder was used for DNA fragment sizes between 50 and 400 bp (Fig. 2.2).

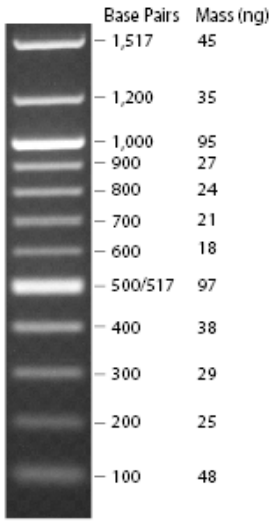

Figure 2.2 NEB 100 bp ladder. The sizes of the bands correspond to the amount of DNA in a 1 % agarose gel when 5 µl marker are loaded. The figure was taken from the NEB website.

2.1.7. Solutions for Protein work

SDS Polyacrylamide gel electrophoresis (SDS-PAGE)

12% SDS-gels were used for all protein experiments. Table 2.4 details the composition of the stacking and resolving gel.

Table 2.4 Composition of the 12 % SDS polyacrylamide gel used in this study.

	5 % Stacking gel	12 % Resolving gel
Water	5.825 ml	7.15 ml
40 % Acrylamide	0.975 ml	3.75 ml
1.5 M Tris-HCl, pH 8.8	-	3.8 ml
0.5 M Tris-HCl, pH 6.8	1 ml	-
10 % SDS	0.08 ml	0.15 ml
10 % APS	0.08 ml	0.15 ml
TEMED	0.008 ml	0.006 ml

Protein Marker

The NEB ColorPlus prestained protein marker was used. See Fig. 2.3.

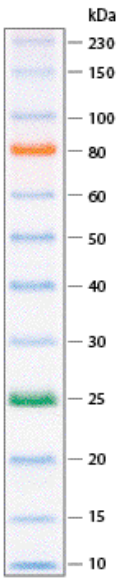

Figure 2.3 NEB ColorPlus prestained protein marker was used in this study. The figure shows the sizes of the bands produced by the protein marker. The figure was taken from the NEB homepage.

4 x SDS loading buffer 100 ml

- 2.42 g Tris base
- 6.17 g DTT
- 8 g SDS
- 0.4 g bromphenol blue
- 40 ml glycerol
- The pH was adjusted to 6.8.
- H_2O up to 100 ml

SDS running buffer 1000 ml

- 30.29 g Tris Base
- 150 g glycine
- 100 g SDS

Coomassie Blue stain 1000 ml

- 0.25 g Coomassie Brilliant Blue
- 400 ml methanol
- 140 ml acetic acid
- H_2O up to 1000 ml

Destaining solution I 1000 ml

- 400 ml methanol
- 70 ml acetic acid
- H_2O up to 1000 ml

Destaining solution II 1000 ml

- 50 ml methanol
- 70 ml acetic acid
- H_2O up to 1000 ml

2.1.7.1. Solutions for immobilized metal ion affinity chromatography

Column cellulose charging buffer, 1000 ml

- 15.48 g $NiSO_4$

Wash buffer 1 for insoluble recombinant protein, 1000 ml

- 120 g Urea
- 2.4 g Tris base
- 0.1 ml Triton
- The pH was adjusted to 8.5 with HCl.

Binding buffer for insoluble recombinant protein, 1000 ml

- 480.48 g Urea
- 2.4 g Tris base
- 1.36 g Imidazole
- The pH was adjusted to 8.5 with HCl.

Wash buffer 2 for insoluble recombinant protein, 1000 ml

- 480.48 g Urea
- 2.4 g Tris base
- 3.4 g Imidazole
- The pH was adjusted to 8.5 with HCl.

Elution buffer for insoluble recombinant protein, 1000 ml

- 480.48 g Urea
- 2.4 g Tris base
- 6.8 g Imidazole (100 mM)
- 13.6 g Imidazole (200 mM)
- 27.2 g Imidazole (400 mM)
- The pH was adjusted to 8.5 with HCl.

Binding buffer for soluble recombinant protein, 1000 ml

- 2.4 g Tris base
- 1.36 g Imidazole
- The pH was adjusted to 8.5 with HCl.

Wash buffer for soluble recombinant protein

- 2.4 g Tris base
- 3.4 g Imidazole
- The pH was adjusted to 8.5 with HCl

Elution buffer for soluble recombinant protein

- 2.4 g Tris base
- 6.8 g Imidazole (100 mM)
- 13.6 g Imidazole (200 mM)
- 27.2 g Imidazole (400 mM)
- The pH was adjusted to 8.5 with HCl.

Column cellulose strip buffer, 1000 ml

- 2.84 g Na_2HPO_4
- 29.2 g NaCl
- 29.2 g EDTA
- The pH was adjusted to 7.4.

2.1.7.2. Refolding of recombinant insoluble protein

Refolding buffer for denatured recombinant protein, 1000 ml

- 12.1 g Tris base
- 100 ml Glycerol
- 5.84 g $NaCl_2$
- The pH was adjusted to 8.0 with HCl.

2.1.7.3. Solutions for Western blotting

Towbin transfer buffer, 1000 ml

- 3.028 g Tris base
- 15.14 g glycine
- 100 ml methanol
- H_2O up to 1000 ml.
- The pH did not have to be adjusted.

5 x TBST, 1000 ml

- 12.112 g Tris base
- 12.86 g NaCl
- 50 ml Tween 20
- H_2O up to 1000 ml.
- The pH was adjusted to 7.6 with HCl.

1 x TBST + 5 % milk, 500 ml

- 100 ml 5 x TBST
- 25 g fat free dried milk powder
- H_2O up to 500 ml.
- The pH did not have to be adjusted.

Ponceau S, 100 ml

- 0.1 g Ponceau S
- 5 ml acetic acid
- H_2O up to 100 ml.

2.1.8. Solutions for fluorescence microscopy

10 x PBS, 1000 ml

- 4.56 g NaH_2PO_4
- 23 g Na_2HPO_4
- 87.66 g NaCl
- H_2O up to 1000 ml.
- The pH was adjusted to 7.4 with HCl.

1 x PBS + Tween 20, 1000 ml

- 100 ml 10 x PBS, 5 ml Tween 20

McIlvaine's buffer, 1000 ml

- 23.3 g Na_2HPO_4
- 3.46 g Citric acid
- H_2O up to 1000 ml.
- The pH was adjusted to 7.0 with HCl.

DAPI (4', 6-diamidino-2-phenylindole) (100 µg/ml)

- DAPI was dissolved in millipure water to a stock concentration of 100 µg/ml and subsequently diluted in McIlvaine's buffer to a working concentration of 2 µg/ml.

Calcofluor white stain (0.5 μg/ml)

- Calcofluor white stain was dissolved in millipure water to a final concentration of 0.05%.

2.1.9. Enzyme assay solutions

2.1.9.1. Colorimetric GTPase assay

Malachite Green reagent

- 50 mg malachite green
- 500 mg ammonium molybdate tetrahydrate
- 50 ml of 1 M hydrochloric acid

The solution was filtered through a 0.45 μm filter and stored at room temperature in the dark for a maximum of 8 weeks.

10 x GTPase assay buffer, 1000 ml

- 12.1 g Tris base
- 5.84 g NaCl
- 4.07 g MgCl•6 H_2O
- 5 ml Tween 80
- H_2O up to 1000 ml
- The pH was adjusted to pH 7.4 with HCl.

5 x Dynamin dilution buffer, 1000 ml

- 3.63 Tris-HCl
- 5.84 g NaCl
- 1 ml Tween 80
- H_2O up to 1000 ml
- The pH was adjusted to pH 7.4 with HCl.

100 x Guanosine 5' Triphosphate (GTP), 1 ml

- 17 mg GTP
- 100 mM Tris base to 0.8 ml.

The pH was measured by transferring small amounts of GTP solution onto pH strips and adjusted to 7.0 with 100 mM HCl. The final volume of 1 ml was acquired by adding 100 mM Tris-HCl, pH 7.0. Stock solutions were prepared every two months.

10 x GTP working solution
- 100 µl 100 x GTP stock solution
- 900 µl 20 mM Tris-HCl, pH 7.4.

The working solution was made fresh from the stock solution for every assay.

10 x Leupeptin
- 10 µg / ml in H_2O

100 x PMSF, 10 ml
- 0.174 g in Ethanol

10 x PMSF working solution, 10 ml
- 1 ml of 100 x stock solution
- 9 ml H_2O were added just before use.

Stop buffer, 10 ml
- 1.46 g EDTA
- H_2O up to 10 ml
- The pH was adjusted to 8.5 using NaOH.

2.2. Methods

2.2.1. Bioinformatics techniques

2.2.1.1. Sequence alignment and phylogenetic analyses.

Three sets of dynamin sequence data were constructed. The first set comprised a large sample of protein sequences (133) that included dynamin protein sequences from all supergroups, namely the Plantae *Arabidopsis thaliana*, *Oryza sativa*, *Physcomitrella patens*, *Chlamydomonas reinhardtii*, *Cyanidioschyzon merolae*, the Opisthokonta *Homo sapiens*, *Drosophila melanogaster*, *Gallus gallus*, *Monosiga brevicollis*, *Saccharomyces cerevisiae*, *Cryptococcus neoformans*, *Batrachochytrium dendrobatidis*, *Phycomyces blakesleeanus*, *Encephalitozoon cuniculi*, the Alveolata *Cryptosporidium*

parvum, *Plasmodium falciparum*, *Tetrahymena thermophila*, *Toxoplasma gondii*, *Theileria parva*, the Chromista *Thalassiosira pseudonana*, *Emiliania huxleyi*, *Phytophthora ramorum*; the Excavata *Naegleria gruberi*, *Trichomonas vaginalis*, *Leishmania major*, *Giardia intestinalis* and the Amoebozoa *Entamoeba histolytica*, *E. invadens*, *E. moshkovskii*, *Polysphodylium pallidum* and *Dictyostelium discoideum*. A list with all accession numbers can be found in the appendix. Excluded from the analyses were the highly divergent Fzl like dynamin family proteins in plants, because they did not align confidently within the dataset. The data set contained 229 distinct alignment patterns. It represented a compromise between having the largest taxon sampling possible and reasonably long sequences with sufficient phylogenetic informative sites. The smaller data sets had longer sequences, but a reduced number of sequences. The Drp1 and 2 dataset contained 67 sequences with 299 informative sites out of 307 amino acid positions. The Drp3 and 4 dataset had 25 sequences with 485 informative sites out of 492 amino acids. The protein sequences were aligned using ClustalW in Seaview (Gouy *et al.*, 2010) and manually refined by eye. Regions not clearly alignable for all sequences were excluded from the phylogenetic analyses by masking the alignment in the program Seaview. The dynamin phylogenies were calculated using the maximum likelihood (ML) approaches with the programmes PhyML v2.4.4 (Guindon *et al.*, 2010) and rAXML (Stamatakis *et al.*, 2008). The Drp3 and Drp4 phylogeny was additionally analysed using the Bayesian analysis program MrBayes (Ronquist & Huelsenbeck, 2003). For the model-based approach ML, a likelihood ratio test using Modelgenerator version 0.85 (Keane *et al.*, 2006) was performed to determine the available model that fits the observed data best. For all datasets the LG substitution model (Le & Gascuel, 2008) was found to be most suitable. For the large dataset the model LG+G (= LG + discrete Gamma; number of rate categories = 4, gamma distribution parameter α = 0.9), for the reduced dataset Drp1 and 2 the model LG+I+G (LG + Invariable sites + discrete Gamma; proportion of invariable sites = 0.11, gamma distribution parameter α = 0.94) and for the reduced dataset Drp3 and 4 the model LG + G (gamma distribution parameter α = 1.36, number of rate categories = 4) was applied according to the modelgenerator calculations. Bootstrap resampling was performed on ML trees with 100 replications for all data sets. Phylogenetic reconstruction of Drp3 and Drp4 using MrBayes were run using a mixed amino acid

model accommodating 4 rate+inv categories containing 4 chains each. One million generations were calculated and trees sampled every 1,000 generations. The model stabilised rapidly and 200 trees were discarded as burn-in.

The mitochondrial Hsp70 phylogenetic relationships were analysed using a dataset of 39 protein sequences with 25 eukaryotic and 14 prokaryotic taxa, namely the Amoebozoa *Dictyostelium purpureum*, *D. discoideum*, *Polysphondylium pallidum*, *Hartmannella vermiformis*, *Entamoeba histolytica*, *E. invadens*, *E. dispar*, the Opisthokonta *Caenorhabditis elegans*, *Homo sapiens*, *Monosiga brevicollis*, *Schizosaccharomyces pombe*, *Cryptococcus neoformans*, *Blastocladiella emersonii*, the Excavata *Trypanosoma cruzi*, *Leishmania major*, *Trichomonas vaginalis*, the Alveolata *Toxoplasma gondii*, *Eimeria tenella*, *Plasmodium falciparum*, the Archaeplastida *Pisum sativum*, *Arabidopsis thaliana*, *Chlamydomonas reinhardtii*, the Stramenopiles *Thalassiosira pseudonana*, *Phytophthora ramorum*, *Blastocystis* sp., the alpha-proteobacteria *Ochrobactrum anthropi*, *Agrobacterium tumefaciens*, *Rhodopseudomonas* sp., *Methylobacterium populi*, *Rhodobacter capsulatus*, *Rickettsia prowazekii*, *Neorickettsia sennetsu*, the beta-proteobacteria *Nitrosomonas europaea*, *Burkholderia cepacia*, the gamma-proteobacteria *Haemophilus influenzae*, *Escherichia coli*, *Legionella pneumophila*, the Spirochaeta *Borrelia burgdorferi* and the Chlamydia *Chlamydia trachomatis*. The accession numbers are found in chapter 3, figure 3.6. Protein sequences were aligned using ClustalW in SeaView version 4.2.12. The dataset contained 620 informative patterns from a total of 704 sites. Sequences were tested for their sequence composition homogeneity with a 5 % level chi-square-test using Tree-Puzzle (Schmidt *et al.*, 2002). Here, the base composition of each sequence was compared to the average base composition of all sequences in an alignment. Sequences, which failed the chi-square-test and thus showed high divergence in comparison to the majority of the sequences in the aligment, were removed.

Phylogenies were calculated using ML with the program PhyML and the Bayesian inference approach using MrBayes. For ML analyses, modelgenerator v.0.85 suggested the model LG+G+F, with 8 rate categories and alpha shape parameter of 0.48 to fit the observed data best. Additionally, four Bayesian analyses were run using a mixed amino acid model accommodating 4 rate+inv categories containing 4 chains

each. One million generations were calculated and trees sampled every 1,000 generations. The model stabilised rapidly and 250 trees were discarded as burn-in.

2.2.2. PCR reactions

A Techne TC-312 PCR machine was used to perform standard PCR reactions. To gain correct annealing temperatures for primers the Biorad Gradient PCR cycler was used for Gradient PCR reactions. Two different PCR polymerases were used together in a PCR reaction mix, a *Pfu Taq* polymerase (Promega) and the non-proofreading Go*Taq* polymerase (Promega). The combination of both *Taq* polymerases allowed the addition of adenosine triphosphate overhangs for TA cloning by the regular *Taq* polymerase and the 5'- 3' proofreading activity by the *Pfu Taq* polymerase. DNA was isolated from *Entamoeba histolytica* strain HM1:IMSS cells. The GoTaq© polymerase in a ready mixed, ready to use format was used for gradient PCR, colony PCR and semi-quantitative RT-PCR.

Pfu Taq / regular _Taq_ reaction

- 5 µl GoTaq buffer
- 2.5 µl $MgCl_2$
- 0.5 µl 10 mM dNTPs
- 1 µl 20 pM forward primer
- 1 µl 20 pM reverse primer
- 1 µl template DNA
- 0.3 µl *Pfu Taq* polymerase
- 0.2 µl *Taq* polymerase
- 13.5 µl millipure water

GoTaq© Green Master Mix

- 12.5 µl Green Master mix
- 0.5 µl 20 pM forward primer
- 0.5 µl 20 pM reverse primer
- 1 µl template DNA
- 10.5 µl millipure water

2.2.2.1. PCR cycling instructions

The PCR cycling conditions used in this study are outlined in Table 2.5 below. Gradient PCR was used to determine the optimal annealing temperature.

Table 2.5 PCR cycling conditions for the *Pfu*/regular *Taq* mix and the GoTaq© Green Master Mix

Cycle step	Number of cycles	Temperature	Time
PCR cycling conditions for the *Pfu Taq* / regular *Taq* mix			
Initial denaturation	1	95 °C	2 minutes
Denaturation Annealing Extension	33	95 °C 50-65 °C [1] 72 °C	45 seconds 45 seconds x minutes [2]
Final extension	1	72 °C	5 minutes
PCR cycling conditions for the GoTaq Green Master mix			
Initial denaturation	1	95 °C	1 minute
Denaturation Annealing Extension	30	95 °C 50-65 °C [1] 72 °C	45 seconds 45 seconds x minutes [2]
Final extension	1	72 °C	5 minutes

[1] Annealing temperature varied depending on the gene. They were determined by gradient PCR.

[2] Extension time was 1.3 minutes per 1000 bp and varied for different genes.

2.2.3. cDNA synthesis

Cells were harvested and washed in PBS. *E. histolytica* trophozoites and *E. invadens* trophozoites and cysts were resuspended in Tripure (Roche) and freeze-thawed three times to break the cells. Afterwards, RNA was isolated following the manufacturers instructions. The RNA concentrations were measured spectrophotometrically using the Nanodrop ND-1000 (Thermo Fisher). To remove genomic DNA, the RNA samples were treated with the Turbo DNA free kit (Ambion) following the manufacturers instructions. To test for successful DNA removal, the RNA sample was subjected to PCR using gene specific primers. If PCR product was detectable, DNAse treatment was

repeated. DNA free RNA was used to synthesise cDNA. The DNA free RNA concentration was analysed spectrophotometrically using the Nanodrop ND-1000. To synthesise first strand cDNA 2μg of RNA, random primers and the M-MLV reverse transcriptase (Promega) were used following the manufacturers instructions.

2.2.4. Real-time quantitative PCR

Real-time quantitative PCR was used to monitor expression levels of dynamin related proteins in *E. histolytica* and *E. invadens* trophozoites and cysts. The experiments were carried out using a Stratagene Mx3005P real-time PCR system, the Brilliant II Sybr Green qPCR Master Mix (Agilent) and cDNA prepared as described in paragraph 2.2.3. Primer specificities and PCR amplification efficiencies were analysed by melt curve and standard curve experiments. The melt curve was established for each primer pair by increasing temperatures at the end of the PCR reaction from 55 to 94 °C, and monitoring the fluorescence. The standard curve for each primer pair was conducted by using serial diluted cDNA templates for PCR. The concentrations used were: concentrated cDNA and cDNA, diluted 1:8, 1:16, 1:64 and 1:256. QPCR experiments were conducted in technical triplicates and with two biological replicates. Actin, the SKI-interacting protein (SKIP) and the 18S rDNA were used as normalizer genes. Actin and the 18S ribosomal RNA gene are housekeeping genes that are traditionally used for pPCR analyses. SKIP was shown to be stably expressed during stage conversion in *Entamoeba invadens* (Ehrenkaufer *et al.*, 2007). The trophozoite sample was used as the internal calibrator and set as 1 in comparison to the various cyst time points. The qPCR included 40 cycles with the conditions outlined in table 2.6.

Table 2.6 PCR conditions for quantitative real-time PCR using Brilliant II Sybr Green QPCR Master mix (Agilent).

Cycle step	Number of cycles	Temperature	Time
Initial denaturation	1	95 °C	10 minutes
Denaturation Annealing Extension	40	95 °C 58 °C 72 °C	30 seconds 30 seconds 30 seconds
For the dissociation curve			
Initial denaturation	1	95 °C	1 minute
Denaturation Annealing	30	95 °C 50-95 °C [1]	45 seconds 30 seconds steps

[1] Fluorescence was measured at each temperature step.

Relative mRNA quantities were calculated with the MxPro QPCR software.

2.2.5. DNA electrophoresis

DNA electrophoresis was used to separate DNA fragments by size for identification and isolation of PCR products. A 1 % agarose gel was used for PCR fragments larger than 500 bp during electrophoresis. Smaller PCR products were separated on a 2 % agarose gel. The agarose was dissolved in either TBE or TAE buffer by boiling it for several minutes until the solution appeared clear. The nucleic acid stain ethidium bromide was added to a working concentration of 0.5 µg/ml. DNA samples containing 20 % of loading buffer, either already provided in the PCR buffer or added, were transferred to the agarose gel wells and separated by electrophoresis at 100 Volts for 1-2 hours. The DNA was visualised on a UV light box and photographs were taken.

2.2.6. Isolation and purification of DNA fragments

DNA fragments were separated on an agarose gel as described under 2.2.3 and excised from the gel with a clean scalpel. The DNA was extracted using either the QIAquick Gel Extraction Kit (Qiagen) or the Wizard® PCR Preps DNA Purification System (Promega)

following the manufacturers instructions. Alternatively, PCR products were purified directly without the electrophoresis step using the same kits.

2.2.7. Cloning of PCR products

PCR products were cloned using the T-vector system pGEM-T-Easy (Promega). The adenosine triphosphate overhang was added during the PCR reaction by the GoTaq polymerase. The vector pGEM-T-Easy is linear and contains the complementary thymidine triphosphate overhang, which allows the hybridization of the PCR product and the vector. Before cloning, the PCR product was purified using either the Wizard® SV Gel and PCR Clean-Up System (Promega) or the QIAquick PCR Purification Kit (Qiagen) following the manufacturers instructions.

2.2.8. Isolation of plasmid DNA

Plasmid DNA from up to 4 ml *E. coli* cell sample was isolated with either the QIAprep Spin Miniprep Kit (Qiagen) or the Wizard® *Plus* Minipreps DNA Purification System (Promega). Larger volumes of plasmid DNA from up to 100 ml of *E. coli* cell sample were isolated using the PureYield™ Plasmid Midiprep System (Promega). A detailed description of the protocols is available in the manufacturer's instructions.

2.2.9. Restriction enzyme digestion of DNA

DNA was digested using New England Biolab or Promega restriction enzymes. The samples were incubated for 3 to 4 hours at 37 °C. If only one restriction enzyme was used, the digested vectors were dephosphorylated with alkaline phosphatase (NEB) to prevent religation of the ends.

Restriction digest

- 2 µg DNA
- 2 µl restriction enzyme
- 3 µl restriction enzyme buffer
- 0.5 µl 10 mg / ml BSA
- millipure water added to a total reaction volume of 30 µl

2.2.10. Ligation of DNA fragments into expression vectors

The PCR products and the vectors were digested with the relevant restriction enzyme and subsequently purified with the Wizard® SV Gel and PCR Clean-Up System (Promega) or the QIAquick PCR Purification Kit (Qiagen) following the manufacturers instructions. The DNA concentration was determined using the Nanodrop ND-1000 Spectrophotometer. The vector and PCR product were joined together using the Takara Mighty DNA ligation kit with an insert to vector ratio of 3:1. The cloning was tested by colony PCR, restriction digest and sequencing (MWG).

2.2.11. Sequence optimization of gene sequences

To avoid codon usage bias during recombinant gene expression the *E. histolytica* Hsp70 gene sequence was changed to the *E. coli* codon usage to correspond to its more abundant tRNA species using the codon adaptation tool JCat (Grote *et al.*, 2005). Additionally, a C-terminal His-tag and the restriction site *Nco*I was added to both ends to transfer the gene from the pUC57 storage vector into the gene expression vector pET-3c.

2.2.12. Cloning into expression vectors

The two expression vectors pET-14b and pET-3c were used in this study. PET-14b contains a Histidine tag sequence unlike pET-3c. EhDrp2 was cloned into pET14b and the codon optimized EhHsp70 sequence was cloned into pET-3c. The stop codon was deleted from EhDrp2 to allow amplification of a C-terminal His-tag.

2.2.12.1. pET-14b

The 5' and 3' end of the Drp2 gene sequence that was cloned into pET-14b had the start codon ATG and stop codon TAA nucleotides replaced with the *Nco*I restriction site CCATGG. The stop codon was removed to allow a continuous transcription of the gene with the C-terminal His-tag. A T7 promoter drives the expression of the inserted gene. The ampicillin resistance allowed selection for positive clones.

2.2.12.2. pET-3c

The codon optimized Hsp70 sequence with His-tag was cloned into this vector using the *BamH*I restriction sites at both ends of the gene. The stop codon was present behind the his-tag to allow transcription termination at the end of the amplicon. A T7 promoter drives the expression of the inserted gene. The ampicillin resistance allowed selection for positive clones.

2.2.12.3. pAH-DEST

The pAH-DEST expression vector is a non-commercial *E. histolytica* specific vector developed by (Abhyankar *et al.*, 2009) (Fig. 2.4). It was a kind gift from Dr. William A. Petri, University of Virginia, School of Medicine, USA. The vector was constructed based on the Invitrogen Gateway vector system, which uses recombination to rapidly transfer inserts from vector to vector. PAH-DEST was designed to be a Gateway destination vector, which receives ligants by recombination from an entry vector. The recombination sites (*attR*) in pAH-DEST are placed at both ends of the cloning site (Fig. 2.4). They correspond to recombination sites (*attL*) in the entry vector pCR8/GW/TOPO. The gene expression in pAH-DEST was driven by the *E. histolytica* ferredoxin promoter (Fig. 2.4). The unligated vector carries a ccdB death gene, which requires the use of ccdB resistant *E. coli* cells for storage (Table 2.1). For positive bacterial clone selection an ampicillin resistance cassette was present. Positively transfected *E. histolytica* cells were selected with the antibiotic hygromycin.

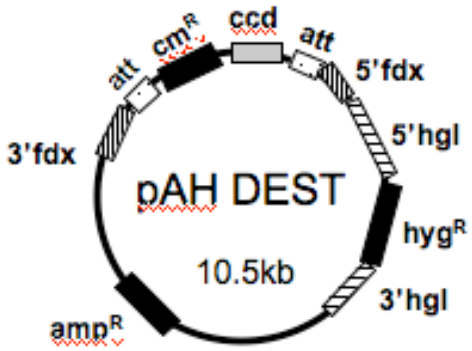

Figure 2.4 pAH-DEST *E. histolytica* specific Gateway expression vector. Image taken from (Abhyankar et al., 2009). The vector exhibits the recombination sites 'att', the *Entamoeba histolytica* ferredoxin promoter (fdx), a hygromycin resistance cassette (hyg^R), the ccdB death gene cassette for positive clone selection (ccd) and an ampicillin resistance gene (amp^R).

2.2.12.4. pDXA-3H

pDXA-3H (Fig. 2.5) is a *Dictyostelium discoideum* specific expression vector with an actin promoter that drives gene expression and neomycin as a selectable marker for transformed *E. coli* clones and a hygromycin resistance for selecting transfected *D. discoideum* cells. The vector was a kind gift from Prof. Dietmar Manstein, Hannover Medical School, Institute for Biophysical Chemistry, Germany.

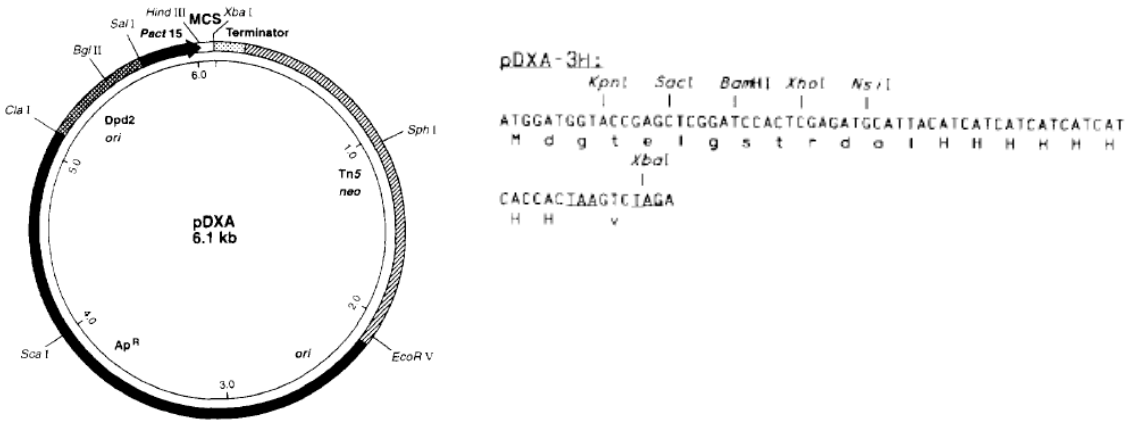

Figure 2.5 pDXA-3H vector map and cloning site. The image was taken from Manstein *et al.*, 1995.

*Kpn*I in the multiple cloning site (MCS) was the restriction site used to insert Drp2 into the vector.

2.3. Microbiological methods

2.3.1. Making competent Ros2 expression cells

A 2.5 ml starter culture of Ros2 *E. coli* was grown overnight in LB supplemented with 1 mM ampicillin at 37 °C under constant shaking. 25 ml of LB_{Amp} was inoculated with the starter culture the next morning and grown to an OD_{600} of 0.4. The cells were collected by centrifugation for 10 min at 6,000 x g at 4 °C. The pellet was resuspended in 12.5 ml of cold and sterile 50 mM $CaCl_2$ and incubated on ice for 30 min. The cells were pelleted and than resuspended again in ice cold 2.5 ml of 50 mM $CaCl_2$. 50-200 µl were used for each transformation. The cells were stored by adding glycerol to a final concentration of 10 % and than frozen at -80 °C.

2.3.2. Transformation of competent cells with plasmid DNA

The competent *E. coli* cells for cloning were defrosted on ice. For each transformation between 1 and 5 µl plasmid DNA was added to the cells and then left on ice for another 20 minutes. The cells were heat-shocked at 42 °C for 45 seconds and then returned onto ice for 2 minutes. 500 µl of SOC medium was added and the suspension incubated at 37 °C under constant shaking for 45 min. 50 µl and 100 µl of the cell suspension were spread onto LB agar plates containing 1 mM ampicillin.

2.3.3. Long term storage of clones

Important bacterial clones were grown over night in LB_{Amp} and than mixed with an equal volume of sterile glycerol. The clones were stored at -80 °C.

2.3.4. Recombinant protein production

E. coli BL21 pLysY and Rosetta 2 (DE3) pLyS were used to overexpress recombinant *E. histolytica* Drp2 and Hsp70. The transformed cells were grown in LB medium containing 1 mM ampicillin at 37 °C shaking vigorously until they reached an OD600 of 0.4 to 0.6. IPTG was added to a final concentration of 1 mM. The cells were then grown at either 37 °C for 4 hours or 18 °C overnight. The cells were harvested by centrifugation at 6,000 x g for 10 minutes at 4 °C. The supernatant was discarded and the pellet suspended in 20 mM Tris-HCl, pH 8.5 for sonication (section 2.3.5).

2.3.5. Sonication

For the purification of protein the harvested cells were suspended in 100 ml of cold 20 mM Tris-HCl, pH 8.5 (see 2.3.4) and sonicated on ice with a low vibration frequency of 25 kHz and a 60 % amplitude for 5 minutes by pulsing in a 10 sec on/off cycle. For protein purification, the crude lysate was centrifuged at 15,000 x g to separate the cell debris from the lysate.

2.4. *Entamoeba* culturing methods

2.4.1. Subculturing procedure

Entamoeba histolytica strain HM-1:IMSS and *E. invadens* strain IP-1 were grown axenically in borosilicate tubes in LIY-S medium supplemented with 15 % adult bovine serum and 2 % Diamond vitamin mixture (section 2.1.5 or purchased from Sigma Aldrich). *E. histolytica* was grown at 37 °C, whereas *E. invadens* was kept at 20 °C. *E. histolytica* was subcultured twice weekly and *E. invadens* once fortnightly.

For culturing *E. histolytica*, the medium was pre-warmed to 37 °C. The cell culture was kept on ice for 5-10 min to detach the cells from the borosilicate tube surface. After cooling the tube was inverted carefully several times and approx. 100 µl were transferred into a new tube with 12.9 ml of fresh LIY-S medium. The amount of transferred cell suspension varied depending on the density of the 'parent' culture. Two tubes were inoculated each time. The culture tubes were kept at an angle of

approximately 35°. *E. invadens* was cultured similarly with the exception that the medium was pre-warmed to room temperature and the 'parent' culture was not cooled on ice. Instead the tube was turned several times. This was sufficient to detach the cells from the surface of the borosilicate tubes. The cultures were cultured upright. When larger volumes were required cells were grown in 50 ml culture flasks and unvented lids with the culture medium filled up to the neck of the bottle to limit the amount of headspace.

2.4.2. *Entamoeba* protein isolation

Entamoeba cells were collected by centrifugation at 800 x g and 4 °C for 5 min. The cell pellet was washed 2 times in cold PBS and finally suspended in TriPure isolation reagent (Roche). The sample was freeze-thawed 3 times by submerging it in liquid nitrogen and thawing it in a 45 °C water bath. The protein was isolated following the manufacturers protocol.

2.4.3. *Entamoeba histolytica* transfection

Transfections were performed by electroporation on logarithmic-phase trophozoites. 2.5 x 10^6 trophozoites were transfected with 100 µg of plasmid DNA per 4 mm cuvette. Drug selection was started 48 hr after transfection, using hygromycin at a start concentration of 8 µg/ml hygromycin and a final concentration of 50 µg/ml. Briefly, culture flasks were shaken gently four times to detach cells from the flask surface. Cells were centrifuged at 1,300 rpm at 4 °C for 4 min to separate the cells from their culture medium. Cells were washed two times in PBS buffer and once in incomplete cytomix buffer (120 mM KCI/0.15 mM $CaCl_2$/10 mM K_2HPO_4/ KH_2PO_4, pH 7.5/25 mM Hepes/2 mM EGTA/5 mM $MgC1_2$, final pH 7.8-7.9). The cells were electroporated in cytomix buffer completed with 5 mM reduced glutathione and 2 mM ATP. Two pulses were applied, each with an exponential discharge of 1200 V at a capacitance of 25 µF and a time constant of 0.4-0.8 ms with the Bio-Rad Gene Pulser Xcell Electroporation System.

2.5. Biochemical methods

2.5.1. Protein purification procedures

2.5.1.1. Immobilized metal ion affinity chromatography

This method was used to purify recombinant polyhistidine-tagged protein over a chelating resin charged with nickel. The nickel binds the polyhistidine tag of the recombinant protein. Varying concentrations of imidazole ranging from 20 mM to 400 mM were used to wash and elute the bound protein by competing for the nickel ions.

2.5.1.2. Isolating and purifying recombinant protein from the insoluble fraction

Drp2p and Hsp70 were produced in *E. coli* BL21 pYLys cells. The proteins were isolated from the cell pellet, *i.e.* the insoluble fraction after sonication by washing it twice for one hour with Wash buffer 1 for insoluble recombinant protein followed by dissolving in Binding buffer for insoluble recombinant protein (section 2.1.7). The mixture was incubated for 1 h at room temperature under gentle rocking and subsequently centrifuged at 20,000 x g for 30 min. The supernatant was transferred onto a glass column (Bio-rad, cross-sectional area 19.63 cm^2) with approx. 3-4 ml of equilibrated Ni-NTA cellulose matrix (Bioline) and incubated at room temperature under constant shaking at 100 rpm for at least 1 h to allow the protein to bind to the Ni-NTA matrix. Bound recombinant Drp2 protein was washed with Wash buffer 2 for insoluble recombinant protein (section 2.1.7) and eluted from the column using Elution buffer for insoluble recombinant protein with 100 mM, 200 mM and 400 mM imidazole concentrations. The elutants were collected in 6 ml fractions and analyzed by SDS-PAGE. The fractions containing the highest protein contents were pooled and concentrated at 20 °C in centrifugal filter units (Millipore, 50 kDa cut-off).

2.5.1.3. Isolating and purifying recombinant protein from the soluble fraction

Soluble recombinant Drp2 protein and Hsp70 protein was produced in *E. coli* Rosetta 2 cells. The cells were centrifuged at 6000 x g for 15 min at 4 °C to remove the culture medium. The cell pellet was resuspended in Binding buffer for soluble recombinant protein and sonicated as described in section 2.3.5. After sonication and centrifugation the cell lysate was transferred onto a glass column (Bio-rad, cross-sectional area 19.63 cm^2) with approx. 3-4 ml of equilibrated Ni-NTA cellulose matrix (Bioline) and incubated at 4 °C under constant turning overnight to allow protein to bind. Bound recombinant protein was washed with Wash buffer for soluble recombinant protein (see 2.1.7) and eluted from the column using Elution buffer with 100 mM, 200 mM and 400 mM imidazole concentrations. The elutants were collected in 20 ml fractions and analyzed by SDS-PAGE. The most promising fractions were pooled and concentrated in centrifugal filter units (Millipore, 50 kDa cut-off). The elution buffer was exchanged to refolding buffer (section 2.1.7), to remove the imidazole and transfer the recombinant protein into a stabilizing buffer system.

2.5.1.4. Protein concentration determination

Concentration of protein samples without detergent such as Urea, Triton X-100 and SDS were measured spectrophotometrically with the Bradford assay (Bradford, 1976) at a wavelength of 595 nm against a bovine serum albumin (BSA) standard curve. These samples included recombinant soluble Drp2 protein in refolding buffer and recombinant refolded protein. Additionally, protein was quantified against a known BSA standard using SDS-PAGE (Sodium dodecyl sulphate polyacrylamide gel electrophoresis).

Protein samples that contained a detergent were quantified against known BSA concentrations using SDS-PAGE. Additionally, protein was quantified spectrophotometrically at 280 nm using the Nanodrop ND-1000 (Thermo Scientific).

2.5.2. SDS-PAGE

SDS-PAGE was used to separate proteins according to their apparent molecular weight. 12 % SDS polacrylamide gels were prepared and run according to (Laemmli, 1970) using the solutions described in section 2.1.7. Samples were mixed with 4 x SDS sample buffer, boiled for 5 min to denature the proteins and centrifuged for 10 minutes at 12,000 x g to remove aggregates and debris. A prestained protein ladder was loaded alongside the samples on the gel to allow determination of the protein size (see Figure 2.3). The mini-PROTEAN II system (Bio-Rad) was used for SDS-PAGE. Protein was separated at 180 V and 25 mA using a PowerPac Basic power supply (Bio-Rad). The gels were stained with Coomassie Blue stain and destained with destaining solution I and II (section 2.1.7).

2.5.3. Electroelution of protein

To gain pure protein for antibody production concentrated Ni-NTA elutants were separated on a large 12 % SDS gel using a Protean II gel electrophoresis system. The samples were separated at 10 mA and overnight, subsequently stained with Coomassie blue and destained with ddH_2O. The band of interest was excised from the gel and electroeluted for 4 hours with the Electro-Eluter Model 422 (Bio-Rad) following the manufacturers protocol.

2.5.4. Antibodies

His-tagged *E. histolytica* Drp2 protein was isolated and purified by immobilized metal ion affinity chromatography and electroelution. A total of 480 μg of Drp2 protein in electroelution buffer was sent to Eurogentec (Belgium) for antibody production in two rats.

The recombinant Hsp70 protein was isolated and purified similar to the recombinant Drp2 protein. A total of 900 μg of protein in electroelution buffer was sent to Eurogentec for antibody production in two rabbits. Before the start of each antibody production program, 5 animals were pre-screened. The Hsp70 antibody was raised in the Eurogentec 28-day speedy program. The *E. histolytica* Hsp60 antibody was kindly

donated by Dr. Graham Clark (London School of Hygiene and Tropical Medicine, UK). This antibody was raised in rabbit against *E. histolytica* Hsp60. Monoclonal Anti-Flag antibody was purchased from Sigma Aldrich (F1804).

2.5.5. Enzyme Assays

2.5.5.1. NADH – coupled assay

This GTPase assay is based on the regeneration of GTP from GDP by a coupled series of reactions and concomitant depletion of NADH, which was measured in the assay. The reaction is outlined in Fig. 2.6. The GTPase assay was performed in 1 ml quartz-cuvettes. Depletion of NADH was measured over a time period of 60 minutes at 340 nm in 5-second intervals. The first 30 minutes autodegradation of the substrate GTP was measured, then Drp2p was added to initiate the enzymatic reaction.

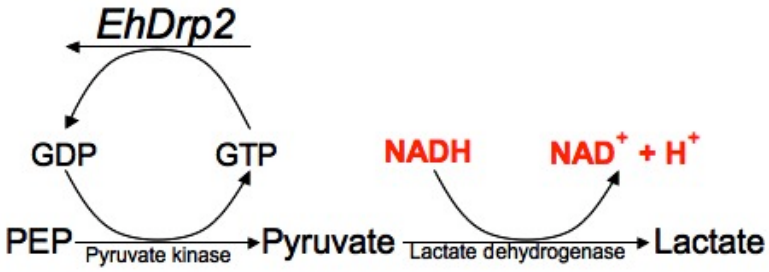

Figure 2.6 Schematic representation of the coupled GTPase assay in which one molecule NADH oxidised into NAD^+ corresponds to the conversion of one molecule of GTP into GDP by the GTPase domain of the EhDrp2p. The enzyme pyruvate kinase converts phosphoenol pyruvate to pyruvate under regeneration of GTP from GDP. Pyruvate is reduced to lactate by the lactate dehydrogenase and depletion of NADH is monitored at an absorbance of 340 nm (based on Ingerman & Nunnari, 2005).

2.5.5.2. Colorimetric GTPase assay

Enzyme activity of EhDrp2p was analyzed using the nonradioactive malachite green assay following the protocol of (Quan & Robinson, 2005). The malachite green colorimetric GTPase assay was performed in triplicates in 96-well polystyrene plates in

a final volume of 40 µl GTPase buffer and protein concentrations between 0.2 µg and 1.2 µg per reaction.

2.5.5.3. Drp2 sedimentation assay

To test if EhDrp2 oligomerizes to higher order structures, a sedimentation assay was performed. Drp2 in refolding buffer was centrifuged at 20,000 x g for 10 min at 4 °C to remove aggregates. The solution was incubated at room temperature for 1 hour and subsequently centrifuged for 20 minutes at 100,000 x g. The supernatant was carefully removed and the pellet dissolved in PBS. To both fractions, SDS loading buffer was added and the solutions separated on a 12 % SDS gel.

2.5.6. Western Blot

Entamoeba histolytica whole cell protein lysate was separated by SDS-PAGE and the gel was equilibrated in Towbin buffer (section 2.1.7) for 10 minutes at room temperature. Proteins were transferred to a nitrocellulose membrane (Biorad) in a wet blotter, using Towbin buffer, for 1.15 hour at 100 V and 400 mA. The transfer was checked by staining the membrane for 5 minutes in Ponceau S stain. Additionally, the polyacrylamide gel was stained with Coomassie Blue stain. The membrane was blocked in 1 x TBST with 5 % milk for a minimum of 1 hour on a rocker at room temperature. Each antibody (Drp2, Hsp60 or Hsp70; 1 in 1,000 dilution in fresh TBST with 5 % milk) was incubated with the membrane for at least 1 hour on a shaker at room temperature. The membrane was washed four times (1 x short, 3 x 5 min) in TBST with 5 % milk. The secondary HRP conjugate antibody (anti-rat or anti-rabbit; Pierce) was added to the membrane in a 1 in 5,000 dilution in TBST with 5 % milk and incubated for 1 hour on a shaker at room temperature. The membrane was washed 4 times (1 x short, 3 x 5 min) in TBST. The signal was detected using the DAB Substrate (Pierce) in the presence of hydrogen peroxide.

2.5.7. Fluorescence microscopy

Localization experiments were conducted by Prof. Adrian Hehl, Institute for Parasitology, University Zürich, Switzerland. The protocol below describes the experimental procedures, which were applied for localization experiments in his laboratory. *E. invadens* trophozoites and cysts were fixed in Exeter as described below and subsequently sent to Prof. Hehl for further analysis. *E. histolytica* and *E. invadens* trophozoites were fixed with 3% formaldehyde in PBS for 45 min. Mature *E. invadens* cysts were fixed using 3 % formaldehyde in PBS overnight at 4 °C. The dehydrated specimens were rehydrated with PBS for 30 minutes, permeabilized with 0.2 % Triton X-100 in PBS for 20 minutes at room temperature and blocked for 2 hours with 2 % BSA in PBS. The *E. invadens* cell preparations were incubated with titrated *Entamoeba* Hsp60 (1:300) and mHsp70 (1:100) antibodies in PBS with 2 % BSA and 0.2 % Triton X-100 for 1 hour at room temperature in a humid chamber. Secondary antibodies coupled to Alexa Fluor® 594 and 488 (Invitrogen), respectively, were used to detect bound antibodies. *E. histolytica* cells were incubated with titrated Drp2 (1:100) and Hsp70 (1:100) antibodies accordingly. Secondary antibodies coupled to Alexa Fluor® 488 and Alexa Fluor® 594, respectively, were applied in a similar way to the *E. invadens* samples. Specimens were thoroughly washed in PBS with 0.5 % BSA and 0.05 % Triton X-100 between incubations and finally mounted with Vectashield (Vector Labs) or Glycergel (Dako) medium. Nuclear DNA was detected with the intercalating agent 4',6-diamidino-2-phenylindole (DAPI). Immunofluorescence image data collection was performed on a Leica SP2 AOBS confocal laser-scanning microscope (Leica Microsystems, Wetzlar, Germany) with an oil immersion objective (Leica, HCX PL APO 63x 1.4) and a pinhole setting of Airy 1 with twofold oversampling. Image stacks were further processed using the Huygens deconvolution software package version 2.7 (Scientific Volume Imaging, Hilversum, Netherlands). Three-dimensional reconstruction, volume rendering and colocalization analysis were done with the Imaris software suite, version 7.2 (Bitplane, Zurich, Switzerland).

2.5.8. Calcofluor staining

Cysts were centrifuged at 800 x g for 3 minutes, resuspended in PBS and transferred onto microscope slides. Two drops of 0.05 % Calcofluor solution were added and incubated for 5 minutes at room temperature before applying the coverslip. The cysts were observed under UV using a fluorescent microscope. Spores from the ascomycete fungus *Magnaporthe grisea* were used as a positive control. For a negative control, *E. invadens* mature cysts were not treated with Calcofluor.

2.5.9. *Entamoeba invadens* encystation and excystation

Entamoeba invadens trophozoites were grown in 50 ml unvented culture flasks for 3 days until the culture formed a dense monolayer at the flask bottom. The culture medium was replaced by encystation medium (chapter 2.1.5) and the cultures were incubated for 72 h at room temperature. Seven time points, 24 h, 28 h, 32 h, 36 h, 40 h, 44 h and 72 h after cyst induction, were taken, to monitor the encystation progress. For each time point two cultures were set up and subsequently harvested. The 72 h time point sample was additionally treated with 0.05 % Sarkosyl to remove trophozoites. The cysts from each time point were stained with Calcofluor (section 2.6.1) and total RNA was isolated for cDNA synthesis (section 2.2.3).

3. Immunolocalization of mitosomes in *E. histolytica* and *E. invadens* trophozoites using Hsp70 and Hsp60 antibodies

Mitochondria are double membrane bound eukaryotic organelles that are thought to have evolved from the planktonic marine Sar11 group within the α-proteobacteria 1.5 to 2 billion years ago (Gray *et al*., 1999, Thrash *et al*., 2011, Lane, 2011). They have played a fundamental role for the evolution of eukaryotes by enabling the prokaryotic host cell to expand in cell and genome size, as well as acquiring sexuality and enabling the development of multi-cellular life (Lane, 2011). Although information on the origin of mitochondria is well studied, less is known about its host (van der Giezen, 2011). It was long hypothesised that simple protomitochondrial eukaryotes capable of endocytosis function as the last eukaryotic common ancestor to all extant eukaryotes. Extant organisms resembling the protomitochondrial state contained metamonads, microsporidia, parabasalids and archamoebae. They were named Archezoa in reference to their primitive appearance. The existance of amitochondriate organisms fitted the concept of the evolution of mitochondria from bacterial ancestors by phagocytosis well (Keeling, 1998). However, the detection of genes encoding mitochondrial proteins and the subsequent discovery of minute mitochondrial organelles in archezoan taxa led to a reassessment of the eukaryotic origin and evolution (Martin & Müller, 1998, Lane, 2011, Embley & Martin, 2006). Morphologically, mitochondria range from large tubular branched to small round systems and the inner mitochondrial membrane is often folded in a complex fashion. The organelles are especially well known for harbouring various essential metabolic pathways such as the citric acid cycle, the electron transport chain for ATP production or beta-oxidation. However the metabolic set up can vary in different organisms depending on the metabolic needs (Embley *et al.*, 2003, Boxma *et al.*, 2005, Stechmann *et al.*, 2008). Mitosomes stand at the far end of organellar reductive evolution. They are tiny ovoid mitochondria found in parasites from oxygen poor environments. They were first discovered in *Entamoeba histolytica* by using homologous antibodies against the mitochondrial chaperonin Hsp60 (Tovar *et al*.,

1999, Mai *et al.*, 1999) that was previously discovered in the *E. histolytica* genome (Clark & Roger, 1995). Additionally, mitochondrial Hsp70 was identified by sequence comparison and phylogenetic analyses (Bakatselou *et al.*, 2000, Bakatselou & Clark, 2000, Arisue *et al.*, 2002). Density gradient fractionation experiments supported the mitosomal origin of the mitochondrial type Hsp70 from *E. histolytica* (Tovar *et al.*, 2007). While the presence of mitosomes is well established in *E. histolytica* trophozoites, they have never been shown in other *Entamoeba* species. Most *Entamoeba* species form cysts, which represent the infectious stage during the parasites life cycle. A well-established *Entamoeba* cyst model organism is *E. invadens*, a reptilian parasite. This study aims to show mitosomes in *Entamoeba invadens* trophozoites and cysts in comparison to *E. histolytica* trophozoites using specific polyclonal antibodies of Hsp60 and Hsp70. Additionally to localization experiments, we characterized the mitochondrial Hsp70 protein family in the amoebozoa using all available mitochondrial Hsp70 sequences to date. This work was conducted in collaboration with Prof. Adrian Hehl from the University of Zürich. While the Hsp70 antibody was raised by Maria A. Siegesmund, the localization experiments were conducted by Prof. Adrian Hehl. The Hsp60 antibody was a kind gift from Dr. C. Graham Clark from the London School of Hygiene and Tropical Medicine, UK.

3.1 Cloning and amplification of Hsp70

3.1.1 Sequence optimization

In order to maximize recombinant protein production, codon usage was converted from *E. histolytica* to *Escherichia coli* using JCat (Grote *et al.*, 2005). Subsequently, a synthetic gene was constructed, which included a C-terminal histidine tag for protein purification and the restriction site *Bam*HI at both termini to enable cloning into the *Bam*HI site of the pET-3c expression vector. Hsp70 gene was successfully transferred from the storage vector pUC57 into the expression vector pET-3c for recombinant gene expression using the restriction enzyme *Bam*HI (Fig. 3.1).

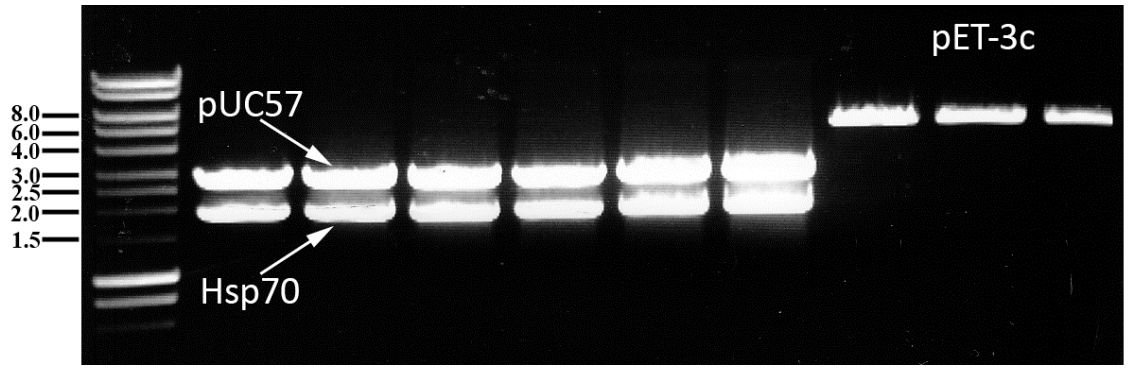

Figure 3.1 Restriction digest of Hsp70 out of the pUC57 vector and digestion of pET-3c to linearity using the restriction enzyme *Bam*HI. The molecular weight marker is shown on the left in kb.

3.2 Expression of recombinant Hsp70

The Hsp70/pET-3c construct was cloned into E. *coli* BL21(DE3)pLysY cells. Recombinant protein was produced overnight at 18 °C and purified from the soluble fraction by immobilized metal ion affinity chromatography with Ni-NTA using different concentrations of imidazole (20 mM, 50 mM, 100 mM, 200 mM and 400 mM imidazole in Tris, pH 8.5). Hsp70 enriched fractions were concentrated in 50 kDa centrifugation units (Millipore) and separated on 12 % SDS polyacrylamide gels. Hsp70 was purified and concentrated from SDS gels by electroelution (Fig. 3.2).

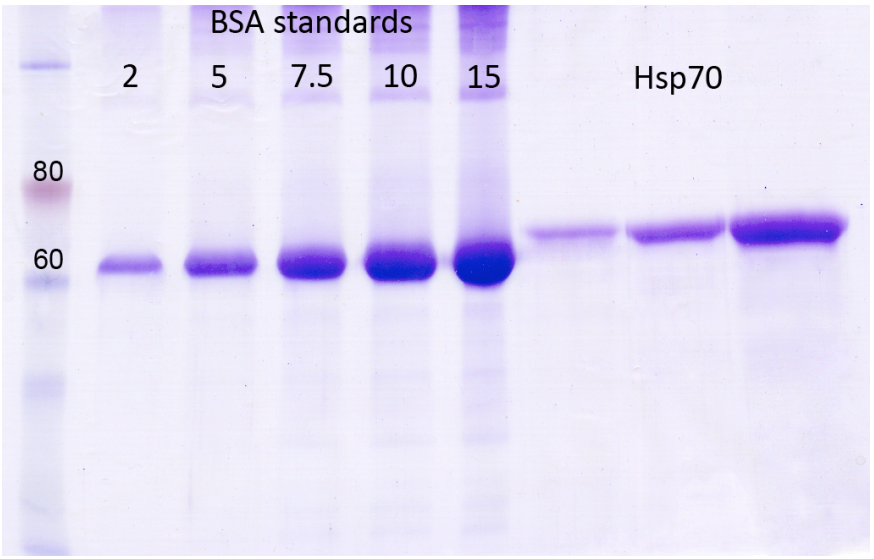

Figure 3.2 Purification and quantification of recombinant Hsp70. The concentration of three electroeluted Hsp70 fractions were compared to known BSA standards. The numbers indicate concentrations in μg. The molecular weight marker is shown on the left. Relevant marker bands are indicated in kDa.

Correct protein identity was verified by mass spectrometry analysis (Fig. 3.3). 0.9 mg Hsp70 protein was subsequently used to generate polyclonal immune serum in rabbit.

The matched peptides cover **71%** (433/607 AA's) of the protein.
Protein Name: **HSP70**
Species: **Entamoeba histolytica**
Masses are:
pI of Protein: **9.24**
Protein MW: **66704.3** Da

1 MVVSQPARST CIGIDLGTTNSCM CVFDKTTPRILE NAEGKRTTPSCVS FTILVGEAAKRM
61 EALHPTTTVS GVKRMIGCQYKNV EQQRKPYKIVEG KNGEGWIYINGKT YSPSEISSFILK
122 KLKKDAEAKL GKRVDEAVITCPA YFNDAQRQATKD AGTLAGLKVKRII NEPTAAALAYGI
183 DTRKENEGKN IAVYDLGRGTFDI SILNINKGIFQV KATNGDTMLGGED FDKAICQYIEKE
244 FERKYKRNLQ RNKKGISRIKEAA EKVKCELSSSEE SVISLPYLDRQDS LEITISRRKIEQ
305 LCKGICKRTE YPCLQCMKDAKLR KKDISDVVLVGG MTRMPLIQTLSRI FGKKPSKNVNPD
366 EAVAIGAAIQ ASIIEGKKKDIIL VDVTPLTLGIET YGGVMTPLINRNT TIPTSVSKEFTT
427 SMDNQQEVDI KVFQGERRVTRKN KKLGEFKLVGIP PAKKGVAKIEVTF DIDVNGIVKVSA
488 LDKGTGKKTG IQVKSNGGLNEEE INRLVKEGEEHA AEDKRKEQLLLHR QRLKEMIESAED
549 IQKELLKKKI ETRELERVINQSK KVITSEDENEIK RLIDQLGEETSNS SAKLYNGSS

Figure 3.3 Identification of recombinant Hsp70 protein by mass spectrometry. Detail from the protein identification Mascot search engine using the mass spectrometry data from putative recombinant Hsp70p. Matched peptides are shown in red.

3.3 Hsp70 characterization, pre-sequences and signature motifs in the Amoebozoa

Putative mitochondrial Hsp70 proteins from the amoebozoan group were identified by BLAST searches (Altschul *et al.*, 1990) and subsequently analysed for mitochondrial targeting signals using the localization prediction tools WoLF PSORT (Horton *et al.*, 2007) and mitoprot (Claros & Vincens, 1996). Additionally, sequences were searched for mitochondrial Hsp70 signature motifs and analysed by phylogenetic reconstructions. The previously identified *E. histolytica* mitochondrial Hsp70 (Bakatselou *et al*., 2000, Bakatselou & Clark, 2000) and its *E. dispar* and *E.invadens* homologues exhibit the same lengths of 598 amino acids and theoretical molecular weights between 65.8 and 66.5 kDa (Table 3.1). This is in accordance with experimentally determined *E. histolytica* Hsp70 molecular weight of 66.7 kDa including the poly-his tag (Fig. 3.2). *E. histolytica* and *E. dispar* show an elevated AT content of 68.5 % and 70.4 % in comparison to the human mitochondrial Hsp70 sequence of 54 % and the free-living amoebozoan Hsp70 sequences.

Table 3.1 Mitochondrial Hsp70 sequence length, molecular weight and AT content from amoebozoa and human.

Species	Number of aa	Molecular weight [kDa]	AT gene content
D. discoideum	658	71.37	62.3
D. purpureum	656	71.49	62.1
P. pallidum	662	72.03	53.4
E. histolytica	598	66.53	68.5
E. dispar	598	66.49	70.4
E. invadens	598	65.82	56.6
H. sapiens	679	73.68	53.7

The Hsp70 sequences from the free-living Amoebozoa *D. discoideum* and *D. purpureum*, *P. pallidum* and *H. vermiformis* were predicted to be of mitochondrial

origin with either both, WOLF PSORT and Mitoprot, or one of the prediction tools (Table 3.2). Mitochondrial Hsp70 sequences from *Entamoeba terrapinae, E. moshkovskii* and *Mastigamoeba balamuthi* could not be identified on their respective genome projects and were therefore not included in the analyses. Mitosomal proteins contain very short mitochondrial targeting signals (Fig. 3.4) that cannot be identified with present prediction tools such as WoLF PSORT and Mitoprot (Table 3.2). Additionally, predictions can be ambiguous as in the case of *P. pallidum* Hsp70. While Mitoprot identified the mitochondrial origin, WoLF PSORT did not (Table 3.2). For *D. discoideum*, both prediction programs were able to identify the mitochondrial origin of Hsp70, but not its presequence cleavage site. The N-terminus of the *Acanthamoeba* and *Hartmannella* Hsp70 sequences could not be completely extracted from their respective genome projects. However, both putative Hsp70 presequences were of sufficient length to include them into the targeting prediction analysis. In order to analyse their putative localization, methionine was added artificially to the incomplete N-terminus to simulate the beginning of the sequence. Localization predictions for amoebozoan Hsp60 sequences were comparable to Hsp70. The free-living Amoebozoa showed high support for mitochondrial origin, while *Entamoeba* Hsp60 did not (Table 3.2). *A. castellani* and *H. vermiformis* Hsp60 sequences could not be identified from their genomes and were therefore not included into the analysis. *E. terrapineae* and *E. moshkovskii* Hsp60 sequences were found. However, both sequences lacked the N-terminus and could therefore not be incorporated into the analysis.

The *in silico* analyses show that localization prediction data based on sequence composition alone should be analysed critically, especially for taxa that exhibit very short mitochondrial targeting signals (Fig. 3.4).

Table 3.2 Localization predictions using Mitoprot and WoLF PSORT for amoebozoan Hsp60 and Hsp70 sequences. (*) indicate incomplete sequences at the N-terminus as extracted from genome projects. Abbreviations for localization predictions: mito=mitochondria, cyto=cytosol, cyto_nucl=cytosol and nucleus, nucl=nucleus, E.R.=endoplasmic reticulum, pero=peroxisome. Mitochondrial predictions were emphasized in bold.

Taxon	Mitoprot	WoLF PSORT
Amoebozoan Hsp60		
D. discoideum	0.9355	**mito:** 18.0, cyto: 7.5, cyto_nucl: 5.5, nucl: 2.5
D. purpureum	0.9937	**mito:** 18.0, cyto: 7.0, nucl: 2.0, E.R.: 2.0
P. pallidum	0.8632	**mito:** 31.0
E. histolytica	0.0864	cyto: 24.0, nucl: 4.0, pero: 2.0
E. dispar	0.0306	cyto: 24.0, nucl: 5.0
E. invadens	0.3744	cyto: 20.0, nucl: 3.0, **mito**: 3.0, pero: 3.0
Amoebozoan Hsp70		
D. discoideum	0.8818	**mito:** 23.0, nucl: 5.5, cyto_nucl: 4.5
D. purpureum	0.8648	**mito:** 20.0, cyto: 6.5, cyto_nucl: 6.0, nucl: 4.5
P. pallidum	0.8575	nucl: 17.0, cyto: 6.0, **mito:** 6.0
*H. vermiformis**	0.4419	**mito:** 21.0, cyto: 11.0
*A. castellani**	0.5926	**mito:** 26.0, nucl: 2.0, cyto: 2.0
E. histolytica	0.4227	cyto: 26.0, nucl: 3.0
E. dispar	0.3996	cyto: 26.0, **mito:** 3.0
E. invadens	0.0276	cyto: 23.0, cyto_nucl: 17.0, nucl: 7.0

In contrast to localization prediction tools, the alignment of the N-termini of Hsp60 and Hsp70 clearly indicates the presence of presequences (Fig. 3.4), which have been shown to be targeting signals in *E. histolytica* (Fig. 3.4) (Bakatselou *et al*., 2000, Tovar *et al*., 1999). *Entamoeba* presequences are very short in comparison to their free-living amoebozoan relatives and do not exhibit recognizable cleavage sites (Fig. 3.4).

A

```
Entamoeba histolytica                          MLSSSSHYNGKLLSLNI
Entamoeba dispar                               MLSSSNHYNGKLLSLNV
Entamoeba invadens                             MMSNTPSFNGKALSTGV
Dictyostelium discoideum                 MFRQIANKSTKFGLRNY-STGKDIKFGA
Dictyostelium purpureum                  MFRQVLRKSSSQFVRNY-SSGKDIKFGA
Polysphondylium pallidum            MLRYSLAKTTSQLVGRRAY-STGKDIKFGA
Rickettsia prowazekii                                  MTTKLIKHGS
```

B

```
Entamoeba histolytica                                  MFVSQPARSTCIGIDLG
Entamoeba dispar                                       MFISQPTRSTCIGIDLG
Entamoeba invadens                                     MLSHHPEFHTTIGIDLG
Dictyostelium discoideum MLRSLKALKLNSLNAQKGIRQFCSDSKISGQVIGIDLG
Dictyostelium purpureum  MLRSFSKVLKSN-NSANGIRSFCSESKVSGHVIGIDLG
Polysphondylium pallidum MLKQFTKVNKNSLYNGLRSY-STQNSKVSGPVIGIDLG
Acanthamoeba castellanii *ALSRCRRATLLSRADCRDPPHFNSAKSGDHIIGIDLG
Hartmannella vermiformis       *KKAVTQQSLFALGTRQY-ATDRSPTIGIDLG
Rickettsia prowazekii                                  MGKVIGIDLG
```

Figure 3.4 Analyses of the amino-terminal regions of the mitochondrial chaperones Hsp60 (A) and mHsp70 (B) from the Amoebozoa. The bacterial homologue from *Rickettsia prowazekii* is shown for comparison. *A. castellanii* Hsp60 is not shown due to being incomplete at the N-terminus. Predicted or confirmed cleavage sites are indicated by a dash while the asterisk denotes an incomplete N-terminus. The underlined residues for *E. histolytica* Hsp60 have been shown to be required for mitosomal targeting (Tovar *et al.*, 1999).

In addition to identifying targeting signals, the presence of signature sequences was used to recognize putative mitochondrial Hsp70 proteins (Fig. 3.5). Mitochondrial Hsp70 contains two specific signature sequences, 'GDAW[V/I]' and 'YSPSQI', that are present in all amoebozoan sequences with a non-conservative difference (missense mutation) in amino acid composition (Fig. 3.5) (Germot *et al.*, 1996, Arisue *et al.*, 2002). Sequence comparison among the lineages including amoebozoan taxa show variation within these motifs (Fig. 3.5) and the Amoebozoa differ slightly in motif sequence composition from the Opisthokonta and Excavata. All analyzed Amoebozoa, except for *E. invadens*, show the composition 'YSPS*E*I', which is also present in the excavate *Giardia intestinalis*. Additionally, *E. dispar* and *E. histolytica* show an alteration in the consensus sequence 'GDAW[V/I] to 'G*EG*WI'. However, variations in the signature sequence amino acid composition are also found in other eukaryotes such as the Stramenopiles (Fig. 3.5).

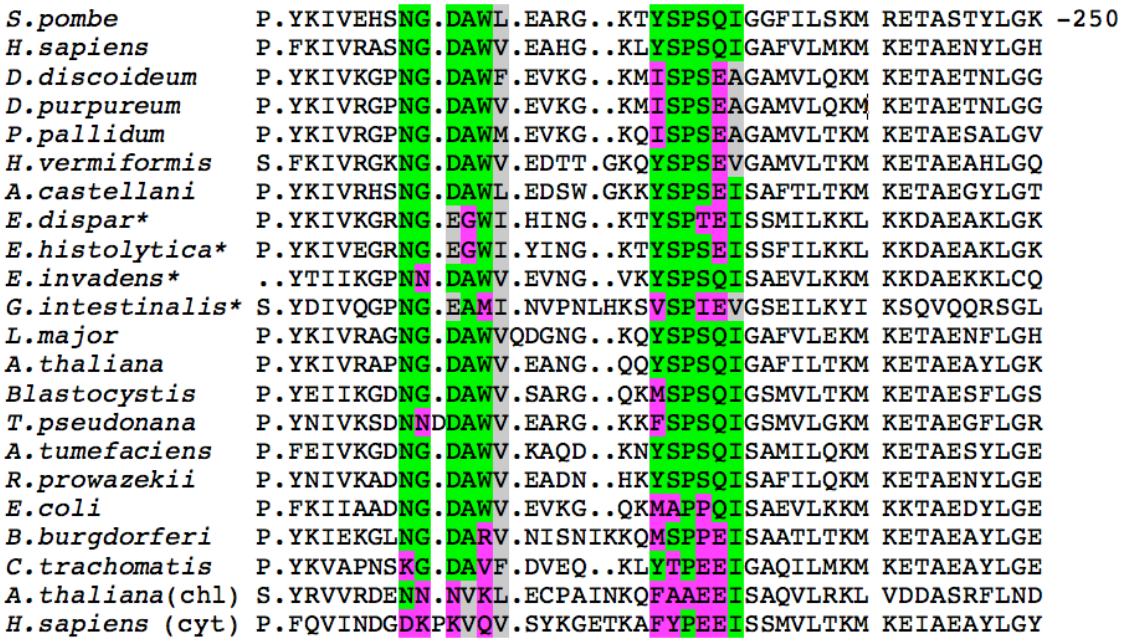

Figure 3.5 Two putative signature motifs (=green) from mitochondrial Hsp70 of eukaryotes and homologous sequences in proteobacterial taxa as well as one spirochaete and one chlamydia species. Grey color indicates conservative amino acid replacements. Purple colour indicates non-conservative amino acid replacements. Sequences from top to bottom: Opisthokonta: *Saccharomyces cerevisiae*, *Homo sapiens*. Amoebozoa: *Dictyostelium discoideum, D. purpureum, Hartmannella vermiformis, Acanthamoeba castellani, Entamoeba dispar, E. histolytica, E. invadens, Polysphondylium pallidum*. Excavata: *Giardia intestinalis, Leishmania major*. Archaeplastida: *Arabidopsis thaliana*. Stramenopiles: *Blastocystis* sp., *Thalassiosira pseudonana*. α-proteobacteria: *Agrobacterium tumefaciens, Rickettsia prowazekii*. γ-proteobacteria *Escherichia coli*. Spirochaeta: *Borrelia burgdorferi*. Chlamydiae: *Chlamydia trachomatis*. *A. thaliana* chloroplast Hsp70, *H. sapiens* cytosolic Hsp70. The asterix marks mitosome-containing taxa. X= non-mitochondrial Hsp70 sequences from *A. thaliana* and *H. sapiens*.

Furthermore, the sequence comparison reveals that the signature motifs appear to be more conserved across lineages than previously thought, because they were also present in the spirochaete *B. burgdorferi* and *Chlamydia trachomatis* (Fig. 3.5), which are not closely related to the mitochondrial α-proteobacterial sistergroup. However, the described conserved motifs are not present in the chloroplast and cytosolic Hsp70 sequences, which allowed the clear separation of the mitochondrial from the other Hsp70 sequences, especially in *Entamoeba* spp. (Fig. 3.5).

3.4 Phylogenetic analysis of mitochondrial Hsp70 proteins

In order to confirm the mitochondrial nature of the identified putative mHsp70 phylogenetic analyses including extended amoebozoan sampling were conducted (Fig. 3.6). Initially, database searches (BLASTp and tBLASTn) over a wide taxonomic spectrum were searched using known mitochondrial Hsp70 and prokaryotic homolog DnaK sequences. The methodological approaches are outlined in chapter 2, section 2.2.1. The phylogenetic analyses clearly confirm the mitochondrial ancestry and monophyly of amoebozoan mHsp70s. Although the sister group relationship with the Opisthokonta was recovered, this node was only weakly supported. As shown in previous studies (Bakatselou *et al*., 2000, Bakatselou & Clark, 2000), our phylogeny recovers the sistergroup relationship between eukaryotic mitochondrial Hsp70 and their α-proteobacterial homologs. *E. histolytica* and *E. dispar* form a clade and are sister to *E. invadens.* Their monophyly is highly supported, as is their sistergroup relationship with the free-living amoebozoa *Dictyostelium*, *Hartmannella* and *Polysphondylium* (Fig. 3.6). Although the *Entamoeba* taxa form a long branch, all amobozoan species cluster together with 100 % bootstrap support. *Acanthamoeba* Hsp70 was originally included into the phylogenetic analysis but did not fall within the amoebozoan clade. Instead it clustered unsupported within the γ-proteobacteria and was therefore omitted from the final analysis (data not shown).

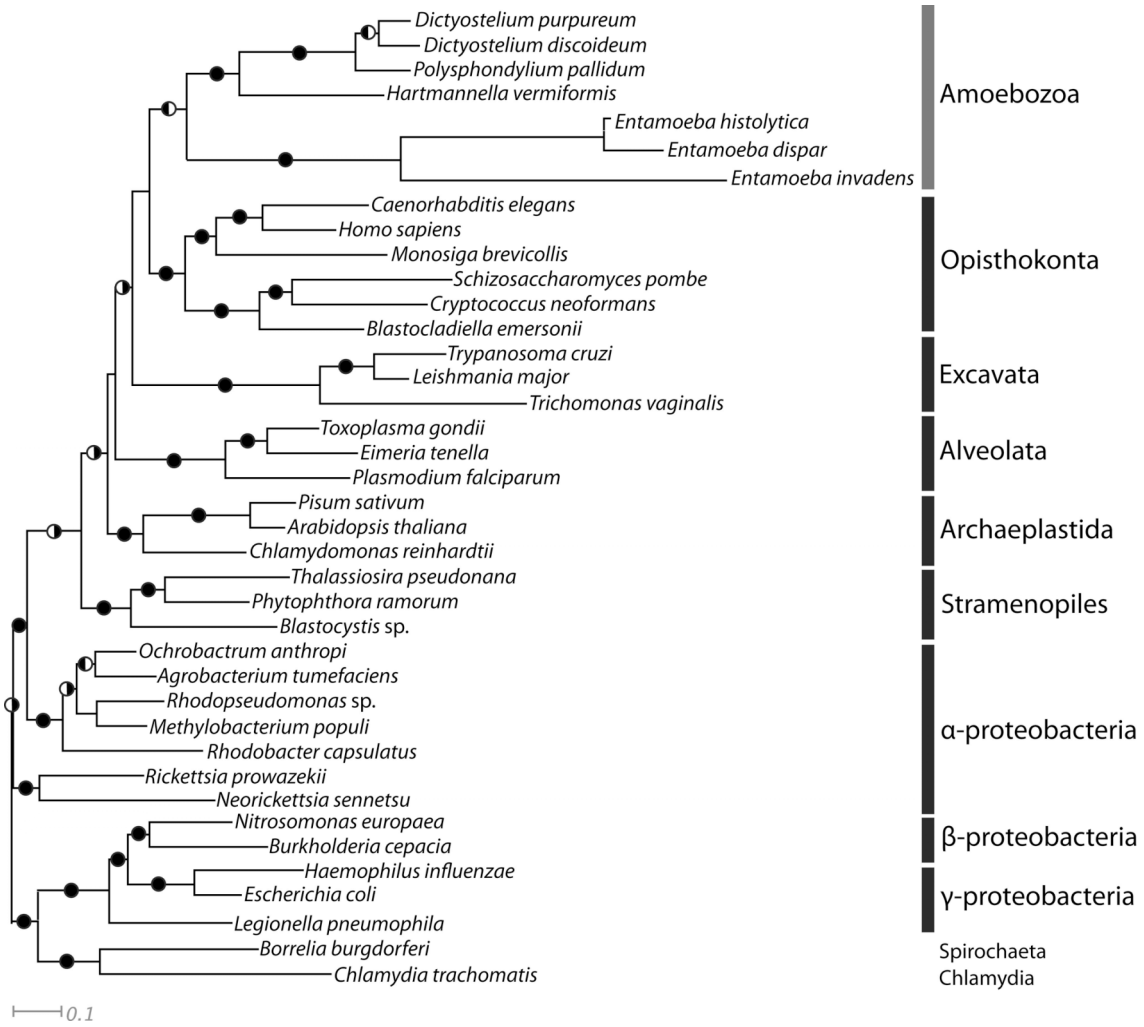

Figure 3.6 Phylogenetic relationships of eukaryotic mHsp70 and prokaryotic DnaK homologues. An unrooted maximum likelihood tree produced by PhyML is shown. Circles at the nodes represent bootstrap values as determined using PhyML and posterior probabilities (pp) as determined by MrBayes (black circle: bootstrap > 60% and pp > 0.9; half circle black on the left: bootstrap > 60 % and pp < 0.9; half circle black on the right: bootstrap < 60% and pp > 0.9). The long branch leading to the *Entamoeba* spp. has been shortened by 50%. The *Acanthamoeba castellanii* mHsp70 was removed from the analyses due to its erratic placement in the analyses in addition to it failing the compositional chi-square-test in PUZZLE. Accession numbers of sequences used: Amoebozoa: *D. discoideum* AAN23118, *D. purpureum* EGC39496, *P. pallidum* EFA85858, *H. vermiformis* *, *E. histolytica* BAB69030, *E. dispar* XP001736890, *E. invadens* EIN_161450; Metazoa: *C. elegans* P11141, *H. sapiens* P38646, *M. brevicollis* XP001750629; Fungi: *S. pombe* P22774, *C. neoformans* XP567978, *B. emersonii* ABE28014; Excavatae: *T. cruzi* P20583, *L. major* XP001684852, *T. vaginalis* XP_001582674; Alveolatae: *T. gondii* XP002367417, *E. tenella* CAA87086, *P. falciparum* XP001348022; Viridiplantae: *P. sativum* P37900, *A. thaliana* NP196521, *C. reinhardtii*

XP001694468; Heterokontophyta: *T. pseudonana* XP002295809, *P. ramorum* XP002898043, *Blastocystis* sp. CBK19749; α-proteobacteria: *O. anthropi* YP001369341, *A. tumefaciens* CAA60592, *Rhodopseudomonas* sp. BAA19796, *M. populi* YP001925829, *R. capsulatus* Q52701, *R. prowazekii* Q9ZDX9, *N. sennetsu* AAC27487; β-proteobacteria: *N. europaea* O06430, *B. cepacia* P42373; γ-proteobacteria: *H. influenzae* P43736, *E. coli* NP285706, *L. pseumophila* BAA22783; Spirochaetae: *B. burgdorferi* CAA47888, Chlamydiae: *C. trachomatis* CAA36423. The *H. vermiformis* sequence is incomplete and was retrieved from the TBEST EST database (http://amoebidia.bcm.umontreal.ca/pepdb/searches/welcome.php).

3.5 Protein targeting into the *E. histolytica* and *E. invadens* mitosome

In order to verify the *in silico* mitochondrial prediction for *E. histolytica* and *E. invadens*, localization studies with the homologous *E. histolytica* mHsp70 antibody were conducted (Fig. 3.7). In addition, the well-characterized mitochondrial Hsp60 antibody (Tovar et al. 1999) was employed for co-localization experiments. The data show that Hsp60 and Hsp70 co-localize to punctate structures in both species (Fig. 3.7). *E. histolytica* Hsp60 has previously been shown to localize to mitosomes (Tovar *et al*. 1999). Co-localization of both antibodies verify the mitosomal origin of mHsp70 and support the *in silico* mitochondrial targeting data. *E. histolytica* exhibits a high density of mitosomes dispersed throughout the vegetative cell. In contrast, mitosomes in *E. invadens* trophozoites appear to be much less abundant (Fig. 3.7). The analyses clearly suggest that *Entamoeba invadens* contains mitosomes like *E. histolytica*. Because *E. histolytica* and *E. invadens* are distantly related *Entamoeba* species, this observation allows the conclusion that all species in the genus contain this organelle.

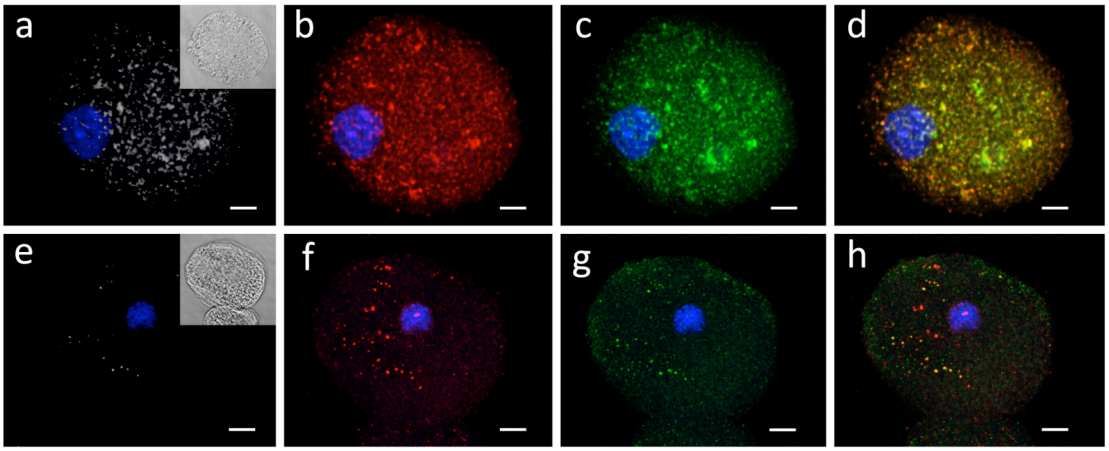

Figure 3.7 Localization of *E. histolytica* and *E. invadens* mitosomes using mHsp70 and Hsp60 antibodies. (a-d) *E. histolytica* trophozoites labelled with (a) DAPI DNA stain (blue), (b) Hsp60 (red) and (c) Hsp70 (green), (d) merged Hsp60 and Hsp70 localization. The corresponding bright field image is included into panel a. (e-h) *E. invadens* trophozoites with (e) DAPI DNA stain (blue), (f) Hsp70 (green) and (g) Hsp60 (red), (h) merged Cpn60 and Hsp70 localization. The corresponding bright field image is included into panel (e). Scale bar = 3 μm.

Additionally, to examining the mitosomal presence and distribution in *Entamoeba* trophozoites, the abundance of these organelles in *E. invadens* cysts was analyzed (Fig. 3.8). As no information about mitosomes in cysts exists for any species localization experiments using the Hsp60 and Hsp70 antibodies were carried out on mature 72-hour-old *E. invadens* cysts. The distribution and abundance of mitosomes resembles that found in *E. invadens* trophozoites (Fig. 3.8). Unlike in dividing *Giardia* cells, no mitosome-organising centre (Regoes *et al*., 2005) could be identified in the cysts suggesting that the inheritance of these organelles in *Entamoeba* is stochastic.

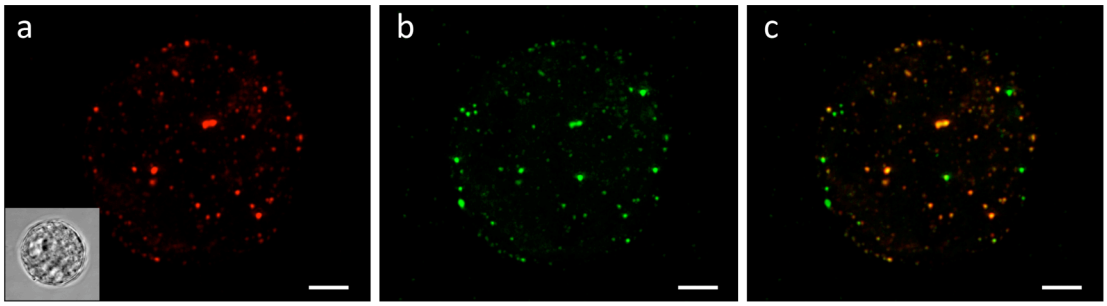

Figure 3.8 Targeting of *E. invadens* mitosomes in mature cysts using *E. histolytica* Hsp60 and Hsp70 homologous antibodies. (a) Hsp60 labelling (red). The corresponding bright field image is included into this panel; (b) Hsp70 labelling (green); (c) merged Hsp60 and Hsp70 signals. Scale bar=3 μm.

In conclusion, the work clearly demonstrates the presence of mitosomes in the reptilian parasite *E. invadens*, which is distantly related to *E. histolytica*. The presence of these organelles in both *E. histolytica* and *E. invadens* suggests that all *Entamoeba* spp. contain this organelle. Furthermore, mitosomes are abundant in the infectious cysts suggesting that these enigmatic organelles seem to play a role in this important life-cycle stage as well. Additionally, phylogenetic analyses clearly show *Entamoeba* mHsp70 to be homologous to eukaryotic mitochondrial Hsp70 and α-proteobacterial DnaK. As previously observed for Hsp70 phylogenies (Karlin & Brocchieri, 1998, Bakatselou *et al*., 2000, Slapeta & Keithly, 2004), the backbone of the phylogenetic tree is largely unsupported. However, the positioning of *Entamoeba* within the amoebozoan is well supported and unambiguous. In addition, mitochondrial targeting signals and sequence signature motifs clearly show the mitochondrial origin of the amoebozoan Hsp60 and Hsp70 proteins.

4 *In silico* characterization of *Entamoeba* Dynamin family proteins

The dynamin protein family is a diverse and important group of mechanochemical enzymes involved in various membrane altering processes. They are fundamentally important for example in endocytosis, organelle division and fusion, cytokinesis and viral resistance (Low & Löwe, 2010, Osteryoung & Nunnari, 2003, Praefcke & McMahon, 2004). To date no eukaryotic organism is known without at least one member of the dynamin protein family. Most research has been conducted on the eukaryotic dynamin protein family, especially the proteins involved in endocytosis and mitochondrial division in human and yeast. Recently, a prokaryotic homolog was described in the cyanobacterium *Nostoc punctiforme* (Low and Löwe, 2006). Subsequently, by sequence comparison, dynamin related proteins appear to be more widespread and deep branching in the tree of life than previously assumed (van der Bliek, 1999, Low & Löwe, 2006). Characteristic for the eukaryotic dynamin protein family is the three-partite domain structure (Praefcke & McMahon, 2004). Classically, they contain a large GTPase domain at the C-terminus (Obar *et al.*, 1990), followed by a middle domain (Smirnova *et al.*, 1998) and an N-terminal GTPase effector domain (Muhlberg *et al.*, 1997). Another feature of the dynamin protein family is the ability to oligomerize to rings and spirals (Hinshaw & Schmid, 1995, Ghosh *et al.*, 2006, Low *et al.*, 2009, Vopel *et al.*, 2010, Chappie *et al.*, 2010). Most research on the dynamin protein family was conducted on the classical mammalian dynamin-1 involved in clathrin mediated endocytosis (Praefcke & McMahon, 2004) and yeast mitochondrial division protein Dnm1 (Osteryoung & Nunnari, 2003). Less is known about the dynamin protein family in protists. This chapter aims to identify and analyse *in silico* dynamin related proteins in the amoebozoan *Entamoeba* spp..

To gain insight into presence and function of the dynamin protein family in *Entamoeba* species, all available *Entamoeba* genomes were searched for dynamin protein sequences. The acquired sequences were characterized using several web-based bioinformatics tools. Phylogenetic analyses were conducted to analyse the evolutionary relationships within the dynamin protein family.

4.1 Acquisition of dynamin protein sequences from *Entamoeba* spp.

The *Entamoeba histolytica* genome (Loftus *et al*., 2005) was queried using BLAST at http://www.ncbi.nlm.nih.gov/, www.sanger.ac.uk/ and http://pathema.jcvi.org with various dynamin protein family amino acid sequences. In order to maximise the taxonomic spread the following members of the dynamin protein family were included: human: dynamin-1 (endocytosis), OPA1 (mitochondrial fusion inner membrane), Drp1 (mitochondrial division), Mx1 (antiviral activity), IF3 (mitochondrial/peroxisomal division); *Saccharomyces*: Dnm1 (mitochondrial division), Mgm1 (mitochondrial fusion inner membrane), Vps1 (vacuolar and peroxisomal division), Fzo1 (mitochondrial fusion outer membrane); *Arabidopsis*: ADL2B (mitochondrial division), ADL4 (cell plate formation), Drp4C (Mx-like), Drp5A (cytokinesis), Drp5B (chloroplast division); *Cyanidioschyzon*: CmDnm1 (mitochondrial division), CmDnm2 (chloroplast division); *Dictyostelium*: DymA (mitochondrial division) and DymB (various interactions including the cytoskeleton, contractile vacuole, peroxisomes and cell adhesion sites), DLPA-C (cytokinesis); *Giardia intestinalis*: GIDRP (encystation specific vesicles); *Trypanosoma brucei*-TbDLP (mitochondrial division); *Trichomonas vaginalis*-TvDlp1 (no assigned function); *Tetrahymena thermophila*-Drp1 (endocytosis) and Drp6p (macronuclear development). This resulted in the identification of four sequences with similarities to members of the dynamin protein family on the *E. histolytica* genome, which have been termed EhDrp1, EhDrp2, EhDrp3 and EhDrp4. EhDrp1 and EhDrp2 had been previously annotated in the *E. histolytica* genome project as dynamin-1 like (= EhDrp1) and dynamin like protein (= EhDrp2). EhDrp3 and EhDrp4 were annotated as hypothetical proteins but identified as dynamin related proteins in this study. In order to assess the distribution of all four dynamin like proteins among the *Entamoebae*, the genomes of *E. invadens*, *E. moshkovskii*, *E. dispar* and *E. terrapineae* were searched for homologues using EhDrp1-4. In addition, the dynamin like proteins DymA, DymB and DLPA, B and C of the closely related amoebozoan *Dictyostelium discoideum* were used to query these other *Entamoebae* genomes. BLAST searches reveal the presence of four full-length dynamin like proteins on the *E. dispar* genome and five dynamin like proteins in the *E. invadens* genome. As there is limited genome information for *E. moshkovskii* and *E. terrapineae*, it was not

possible to gain full length sequences and a definite amount of dynamin related proteins. However, the BLAST searches suggest the presence of three dynamin like proteins on the *E. moshkovskii* and four dynamin like proteins in the *E. terrapinae* genome (Table 4.1).

4.2 Sequence analysis of *Entamoeba* spp. dynamin related proteins

Entamoeba spp. Drp1-4 are comparable in length and molecular weight to other members of the dynamin protein family (van der Bliek *et al.*, 1993, Bleazard et al., 1999, Wienke et al., 1999, Obar et al., 1990, van der Bliek & Meyerowitz, 1991, Guan *et al.*, 1993) such as the classical human dynamin-1 protein (864 residues and 97.4kDa), *Saccharomyces cerevisae* Dnm1 (757 residues and 85kDa) or *D. discoideum* DymA (853 residues and 96.1kDa). *Entamoeba* spp. Drp3 and Drp4 have a higher molecular weight and are longer compared to Drp1 and Drp2 (Table 4.1).

Table 4.1 Dynamin protein family in *Entamoeba* spp. listing the length, theoretical molecular weight, isoelectric points and number of proteins in each taxon acquired in BLAST searches. *E. moshkovskii* and *E. terrapineae* putative dynamin like sequences found are incomplete. Therefore the number of amino acid residues, molecular weights and isoelectric points could not be analysed.

Taxon	Number of dynamin like proteins	Putative name in this study	Number of amino acid residues	Theoretical molecular weight [kDa]	Isoelectric point
E. histolytica	4	EhDLP1/EhDrp1	682	76.8	6.07
		EhDrp2	663	74.6	6.4
		EhDrp3	790	90.9	5.37
		EhDrp4	784	90.4	5.4
E. invadens	5	EiDrp1	675	76.2	5.45
		EiDrp2	666	74.85	6.2
		EiDrp2a	670	75.5	6.73
		EiDrp3	841	95.3	7.87

		EiDrp4	776	88.58	5.45
E. dispar	4	EdDrp1	681	76.74	6.2
		EdDrp2	664	74.86	6.91
		EdDrp3	789	91.16	5.29
		EdDrp3a	783	90.14	5.44
E. moshkovskii	3	EmDrp1-3	Incomplete	Incomplete	Incomplete
E. terrapineae	4	EtDrp1-4	Incomplete	Incomplete	Incomplete

The members of the *Entamoeba* dynamin protein family have isoelectric points between 5.40 and 7.87 but with the majority being negative to neutral (Table 4.1). The high sequence similarity of *Entamoeba* dynamin related proteins to other members of the dynamin protein family is mainly confined to the N-terminal GTPase region (Fig. 4.2), whereas the C-terminal region shows a higher level of sequence divergence. For example, the first 310 amino acids of EhDrp2 are 55 % identical to human dynamin-1, 49 % to *D. discoideum* DymA and 45 % to *S. cerevisiae* Dnm1. The remaining sequence of EhDrp2 only shows a 31 % identity to dynamin-1, 25 % to DymA and 35 % to Dnm1. A more drastic example is the difference between EhDrp3 and human dynamin-1. Whereas the GTPase regions show a 34 % identity, the comparison of the C-terminal sequences do not lead to a significant alignment. *Entamoeba* dynamin like protein orthologs are more similar to each other than paralogs. For example, EhDrp2 and EhDrp3 are 14.2 % identical (Table 4.2), whereas EhDrp2 and EiDrp2 share a sequence identity of 77.5 % (Table 4.5).

Table 4.2 *E. histolytica* protein sequence identities

	EhDrp2	EhDrp3	EhDrp4
EhDrp1	46 %	14.2 %	13.0 %
EhDrp2	--	14 %	10.6 %
EhDrp3	--	--	14.4 %

Table 4.3 *E. dispar* protein sequence identities

	EdDrp2	EdDrp3	EdDrp4
EdDrp1	44.1 %	14.4 %	10.4 %
EdDrp2	--	14.1 %	10 %
EdDrp3	--	--	17.1 %

Table 4.4 *E. invadens* protein sequence identities

	EiDrp2	EiDrp2a	EiDrp3	EiDrp4
EiDrp1	43 %	45 %	10.3 %	8.4 %
EiDrp2	--	83.8 %	9.1 %	8.4 %
EiDrp2a	--	--	8.8 %	8.4 %
EiDrp3	--	--	--	9.7 %

Table 4.5 Protein sequence identity comparison of *E. invadens* and *E. dispar* to *E. histolytica* dynamin related proteins. Green shading of cells highlights the dynamin protein in *E. histolytica* compared to the same dynamin related protein in *E. dispar* and *E. invadens*, *e. g.* EdDrp1 compared to EhDrp1.

	EhDrp1	EhDrp2	EhDrp3	EhDrp4
EdDrp1	91.6	43.6	14	8.6
EdDrp2	44.2	94.2	14.9	8.4
EdDrp3	12.9	13.9	91.2	15.2
EdDrp4	8.6	8.6	15.9	92.6
EiDrp1	76.6	44.4	13.8	8.2
EiDrp2	44.2	77.5	13.6	8.1
EiDrp2a	45.1	76.8	13.9	8.5
EiDrp3	12.1	12.8	56.6	12.2
EiDrp4	9.5	8.5	12	47.4

4.3 Targeting predictions of dynamin proteins in *Entamoeba*

All *Entamoeba* sequences except for EhDrp3, EhDrp4 and EiDrp3 were predicted to be cytosolic using WOLF PSORT, a version of PSORTII for the targeting of eukaryotic sequences (Horton *et al.*, 2007). EhDrp3 and EhDrp4 were predicted to be nuclear. For EiDrp3 a dual localization of cytosol and nucleus was predicted. These sequences were further analysed by Nucleo (Hawkins *et al.*, 2007) and NucPred (Brameier *et al.*, 2007), both nuclear targeting prediction tools. EhDrp3 was predicted again to have nuclear localization (Nucleo: 0.6 nuclear leading sequence (NLS)/ 0.4 nonNLS; NucPred: 0.99) (Fig. 4.1). A previous study by Jain *et al*. 2010 shows an association of EhDrp1 with the outer side of the nuclear membrane but no internalization of the protein indicating that EhDrp1 plays a role at the outer membrane of the nucleus. This is in agreement with the absence of a detectable nuclear localization signal.

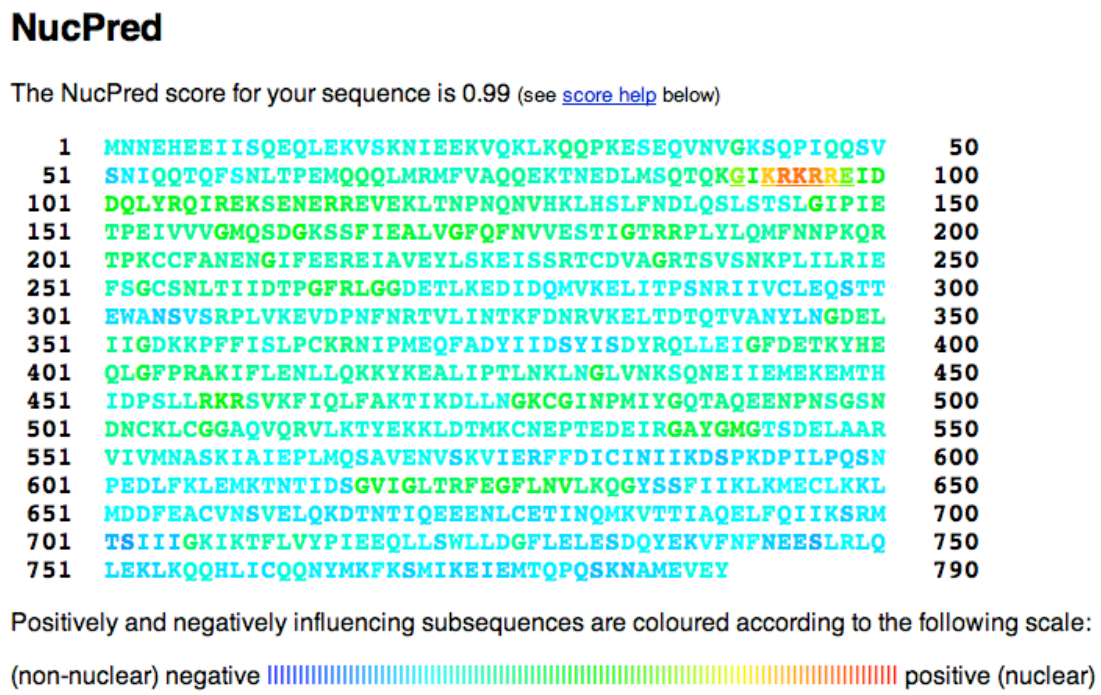

Figure 4.1 Nuclear prediction for EhDrp3 using NucPred. Sequences that show a NucPred score equal or higher than 0.8 and are predicted by PredictNLS to contain a nuclear leader signal are considered to be 93 % correct (Brameier *et al.*, 2007).

However, a nuclear localization signal was not detected using PredictNLS. EhDrp4 (Nucleo: 0.33/0.67, NucPred: 0.37) and EiDrp3 (Nucleo: 0.25/0.75; NucPred: 0.73) were not recognized as being nuclear targeted with neither Nucleo nor NucPred.

4.4 The *Entamoeba* dynamin protein family domain structure and sequence characterization

The domain structures of the dynamin related proteins in *Entamoeba* were analysed using the NCBI Conserved Domains database (http://www.ncbi.nlm.nih.gov/Structure/cdd/cdd.shtml), the SMART server (http://smart.embl-heidelberg.de/) and Pfam (http://pfam.sanger.ac.uk/). The domain structures of Drp1, Drp2 and EiDrp2a differ from Drp3 and Drp4. Whereas Drp1, Drp2 and Drp2a show the classical domain pattern of dynamin like proteins, Drp3 and 4 only exhibit the large GTPase domain (Fig. 4.3).

4.4.1 *Entamoeba* Drp1 and Drp2

Entamoeba Drp1 and Drp2 show the characteristic dynamin protein family domain architecture composed of the N-terminal large GTPase domain (Fig. 4.2), the middle domain and the C-terminal GTPase effector domain (Fig. 4.3). These two dynamin like proteins contain the dynamin signature sequence 'LPRGSG[M/I]VTR' at the positions 51-61 (section 4.5) and the consensus elements for GTP binding: G1=GSQSAGKS, G2=T, G3=DLPG and G4=TK[M/L]D which are conserved throughout GTP binding proteins (Fig. 4.2), (Bourne *et al*., 1991, Niemann *et al*., 2001, Chappie *et al.*, 2010).

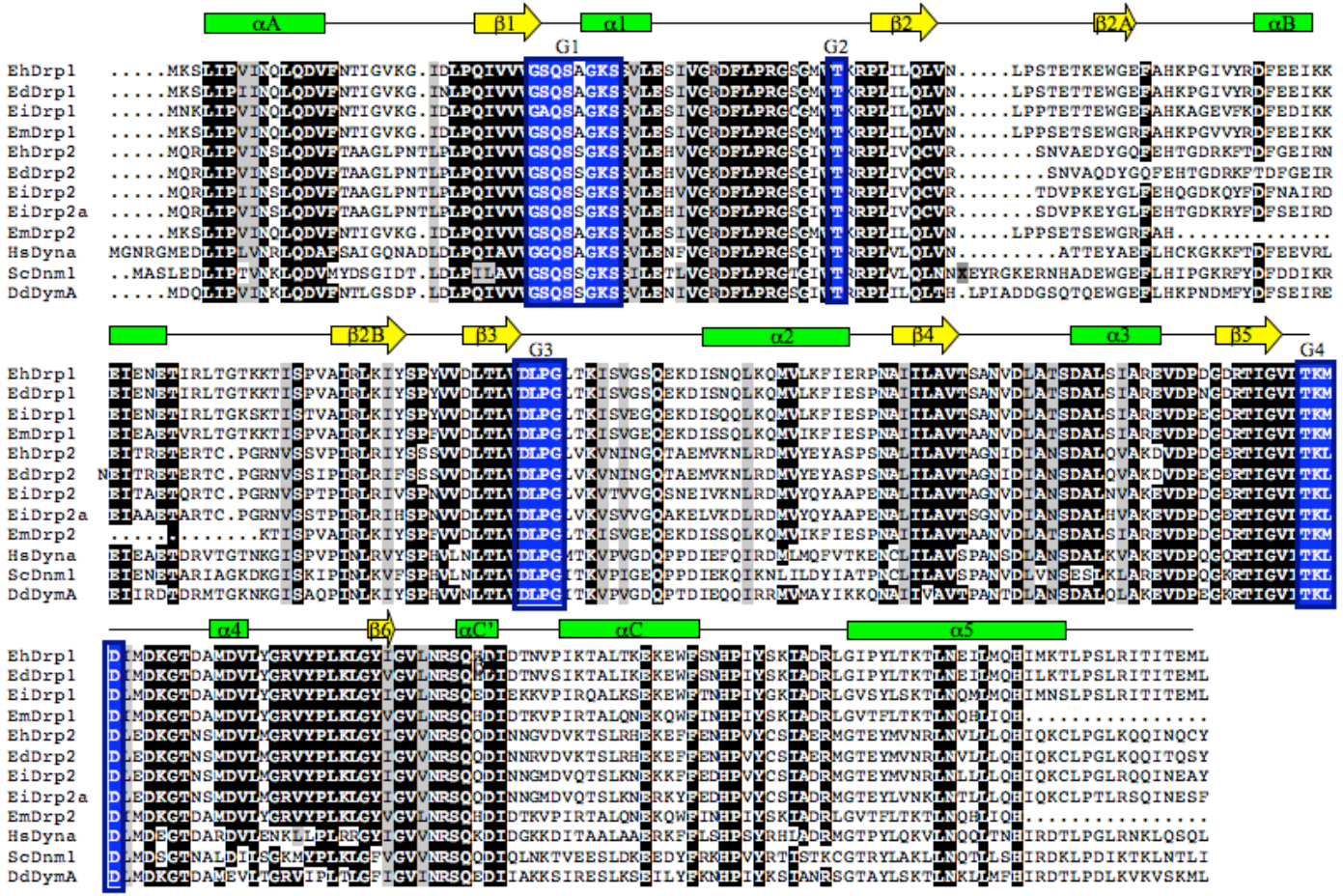

Figure 4.2 Sequence alignment of the N-terminal GTPase domains from *E. histolytica* (Eh), *E. dispar* (Ed), *E. invadens* (Ei) and *E. moshkovskii* (Em) Drp1 and Drp2, Drp2a, human dynamin-1 (= HsDyna), *S. cerevisiae* Dnm1 (= ScDnm1) and *D. discoideum* DymA (= DdDymA). The secondary structure is based on the crystal structure from the *D. discoideum* DymA GTPase domain (Niemann *et al*. 2001). Rectangles indicate helices and arrows indicate β-sheets. The conserved GTP binding sites are boxed in blue and labelled G1-G4. Residues that are identical are boxed in black, conservative substitutions are boxed in grey. x-sequence insertion in ScDnm1 that was omitted from the alignment.

In between the middle and the GTPase effector domain stretches a non-conserved segment of 63 to 79 amino acids (Table 4.6). This stretch will be referred to as V-segment (**V**ariable segment). The V-segment is not similar to the conserved Pleckstrin homology domain (PH, 120 aa) from human dynamin-1 (Fig. 4.3a), plant DRP2A or plant mitochondrial fission or the B-insert in *S. cerevisae* Dnm1, 114 aa (Mears *et al.*, 2010). The V-segment is approx. 50 amino acids shorter and only present in *Entamoeba* taxa.

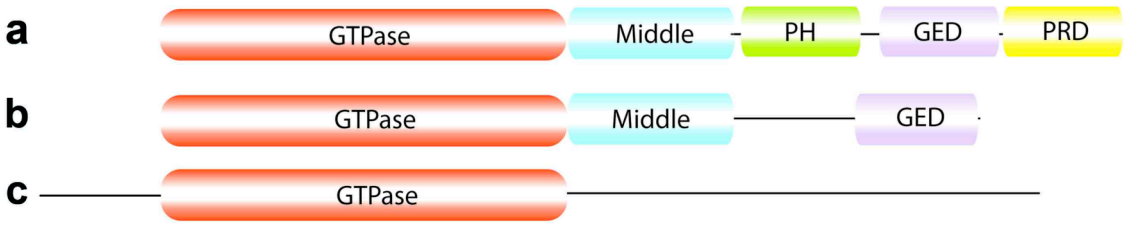

Figure 4.3 Predicted domain structures of *Entamoeba* Drp1-Drp4 in comparison to human dynamin-1. (a) Classical dynamin domain structure of human dynamin-1, (b) Drp1 and Drp2 of all *Entamoeba* taxa and Drp2a from *E. invadens*, (c) Drp3 and Drp4. Segment: red=large GTPase domain, blue=middle domain, green=pleckstrin homology domain (PH), purple=GTPase effector domain (GED), yellow=Proline rich domain (PRD).

Entamoeba Drp1 exhibits a proline enriched V-segment compared to Drp2 (Fig. 4.4) and both, Drp1 and Drp2 show a higher amount of glutamine compared to the rest of the sequence. Proline and glutamine form low complexity segments within the V-segment (Fig. 4.4). Generally, enrichment in the amino acids proline (P), glutamic acid (E), serine (S) and threonine (T) may indicate the presence of a PEST region, that act as proteolytic recognition sites. Therefore, *Entamoeba* Drp1 and Drp2 were analysed using the program 'epestfind' (http://emboss.bioinformatics.nl/cgi-bin/emboss/epestfind) but no significant sites were detected. Alternatively, glutamine rich sites can form unstructured flexible regions within protein tertiary structure. Intrinsic disorder can have many functions but is often found in linkers between two domains that allow them to twist or rotate. These regions are often rich in polar neutral amino acids such as glutamine, serine or threonine. Beside glutamine, which is highly abundant in all *Entamoeba* Drp1 and Drp2 V-stretches, threonine is

accumulated in EhDrp2 and EiDrp2a, whereas serine is increased in EiDrp2. When analysed with 'Disopred' (Ward *et al.*, 2004), a tool to analyse sequences for residue disorder prediction, all V-segments were significantly disordered (Fig. 4.5).

Table 4.6 Domain residue dimensions in dynamin like proteins from *Entamoeba* spp. for the N-terminal GTPase domain, the Middle domain, the GTPase effector domain and the low complexity region in between the Middle and the GTPase effector domain.

	GTPase domain residues	Middle domain residues	Variable region residues	GTPase effector domain residues
EhDrp1	1 – 314	314 – 496	497 – 576 (79)	586 – 674
EhDrp2	1 – 312	312 – 494	495 – 558 (63)	567 – 658
EiDrp1	1 – 312	314 – 496	497 – 569 (72)	578 – 669
EiDrp2	1 – 312	312 – 494	495 – 561 (66)	570 – 661
EiDrp2a	1 – 312	312 – 494	495 – 565 (70)	574 – 665
EdDrp1	1 – 314	314 – 496	497 – 575 (78)	584 – 675
EdDrp2	1 – 312	3 12 – 494	495 – 558 (63)	568 – 659

The amino acid proline plays an important role in protein-protein interactions (Kay *et al.*, 2000). For example, Src homology 3 (SH) modules, present predominantly in signalling and cytoskeletal proteins in eukaryotes (Koch *et al.*, 1991), rely on the binding to short proline rich segments (Mayer & Eck, 1995). Jain *et al*. (2010) previously characterized EhDrp1 and acknowledge the presence of the proline motif PxxP within the V-segment where 'x' stands for any amino acid (Fig. 4.4). They speculate that these sites might be involved in protein protein interaction by binding SH3 domains from other proteins. The PxxP motif is restricted to *E. histolytica* Drp1 and not conserved in the proline rich stretches of EiDrp1 and EdDrp1 (Fig. 4.4). However, two other proline rich motifs were found within the V-segment, which are conserved in all *Entamoeba* Drp1 sequences. These are 'PPKP' (positions 517) and KPPKK/KPKPKK in EhDrp1 (position 528), EdDrp1 (positions and 517 and 527) and EiDrp1 (positions 514 and 524) respectively (Fig. 4.4). Whether these specific motifs or

the general increase of proline in the V-segment are important for protein-protein interaction is however speculative.

Figure 4.4 ***Entamoeba*** **Drp1 and Drp2 alignment showing the V-segment between the middle domain and the GTPase effector domain (black box). Conserved proline rich sites in Drp1 are 'PPKP' and 'KPPKK'. Amino acid color scheme: Blue=leucine (I), isoleucine (I), valine (V), methionine (M), alanine (A), phenylalanine (F), tryptophan (W); orange=glycine; purple=aspartic acid (D), glutamic acid (E); red=lysine (K); green=threonine (T), asparagine (N), glutamine (Q), serine (S); yellow=proline (P); light blue=histidine (H).**

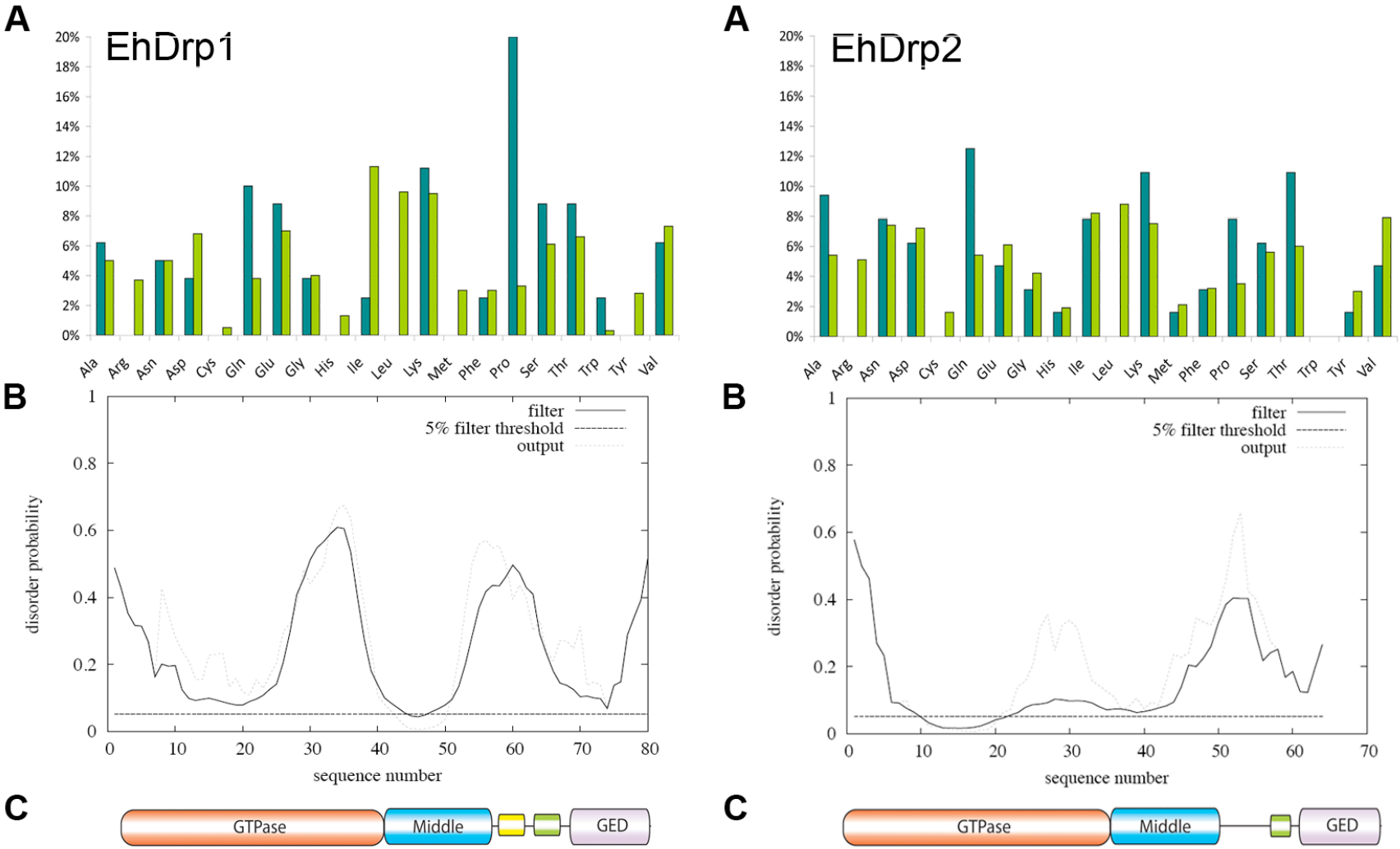
A
EhDrp1
20%
18%
16%
14%
12%
10%
8%
6%
4%
2%
0%
Ala Arg Asn Asp Cys Gln Glu Gly His Ile Leu Lys Met Phe Pro Ser Thr Trp Tyr Val
B
filter
5% filter threshold
output
disorder probability
sequence number
C
GTPase
Middle
GED
A
EhDrp2
B
filter
5% filter threshold
output
disorder probability
sequence number
C
GTPase
Middle
GED

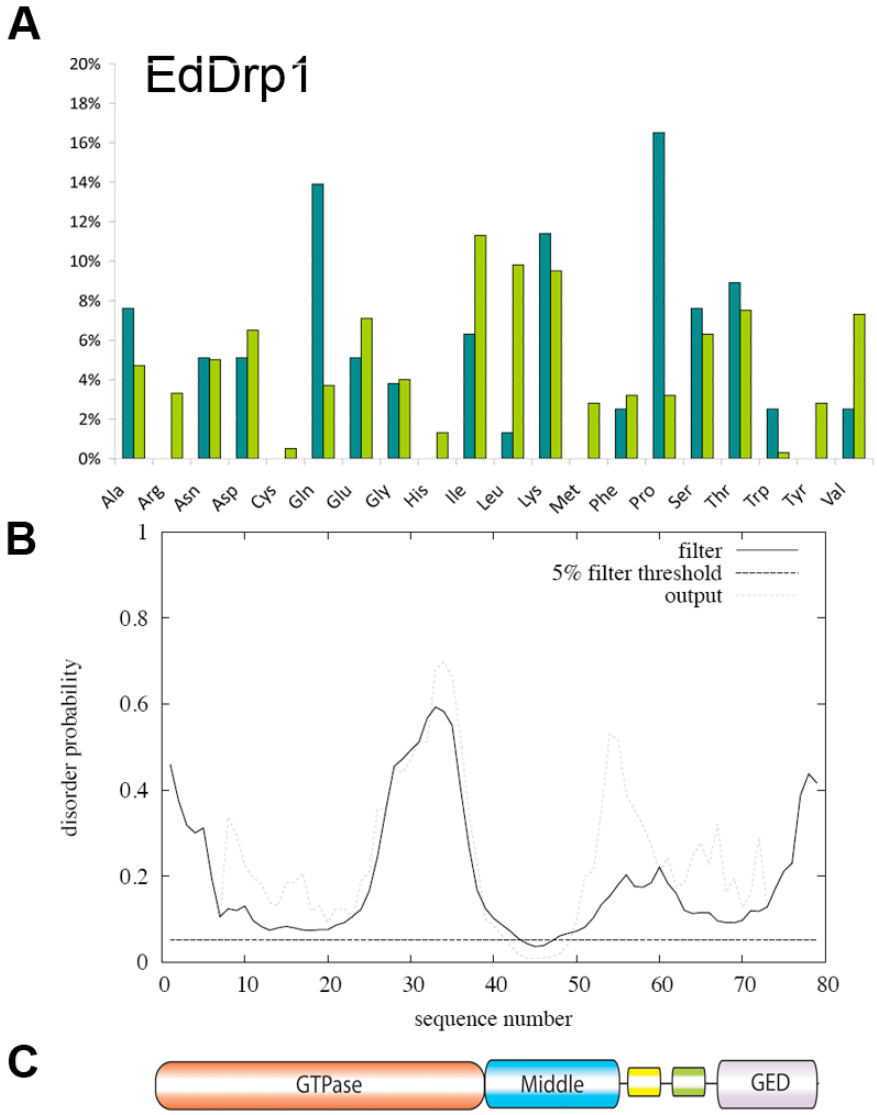
A
EdDrp1
20%
18%
16%
14%
12%
10%
8%
6%
4%
2%
0%
Ala Arg Asn Asp Cys Gln Glu Gly His Ile Leu Lys Met Phe Pro Ser Thr Trp Tyr Val
B
filter
5% filter threshold
output
disorder probability
sequence number
C
GTPase
Middle
GED

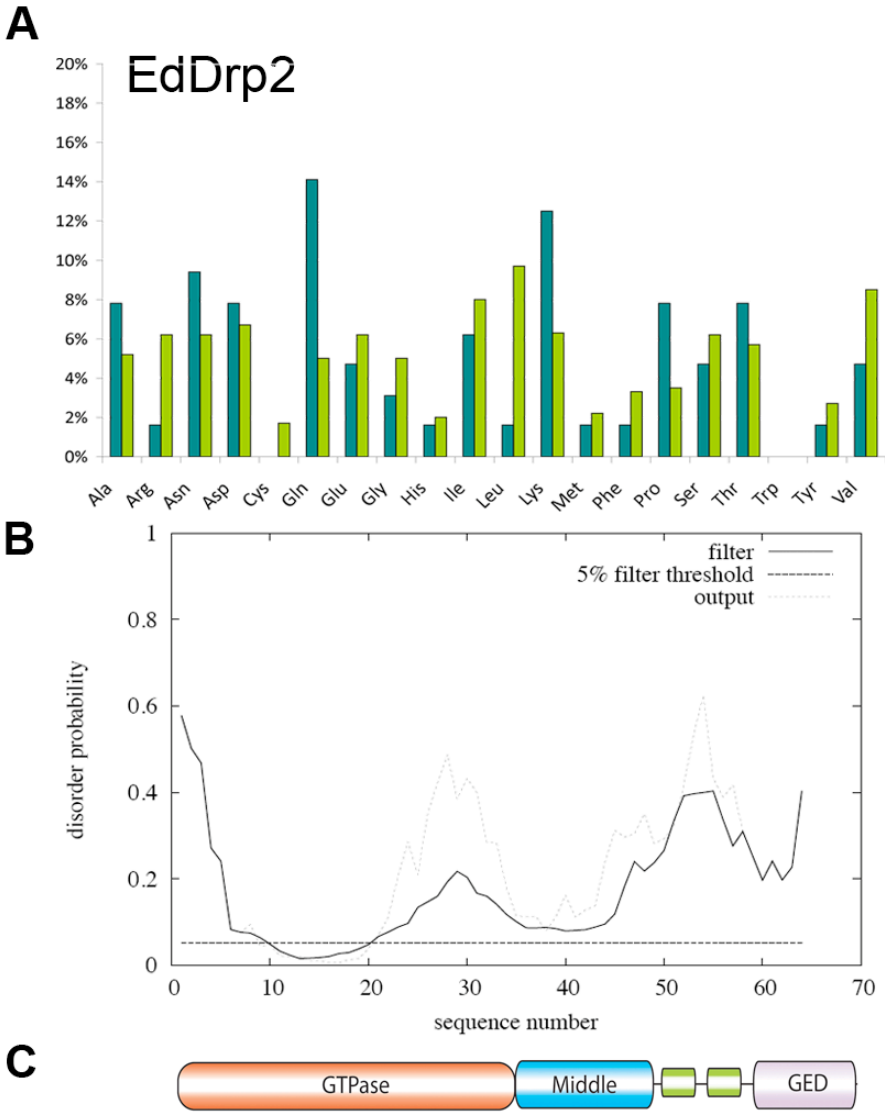
A
EdDrp2
20%
18%
16%
14%
12%
10%
8%
6%
4%
2%
0%
Ala Arg Asn Asp Cys Gln Glu Gly His Ile Leu Lys Met Phe Pro Ser Thr Trp Tyr Val
B
filter
5% filter threshold
output
disorder probability
sequence number
C
GTPase
Middle
GED

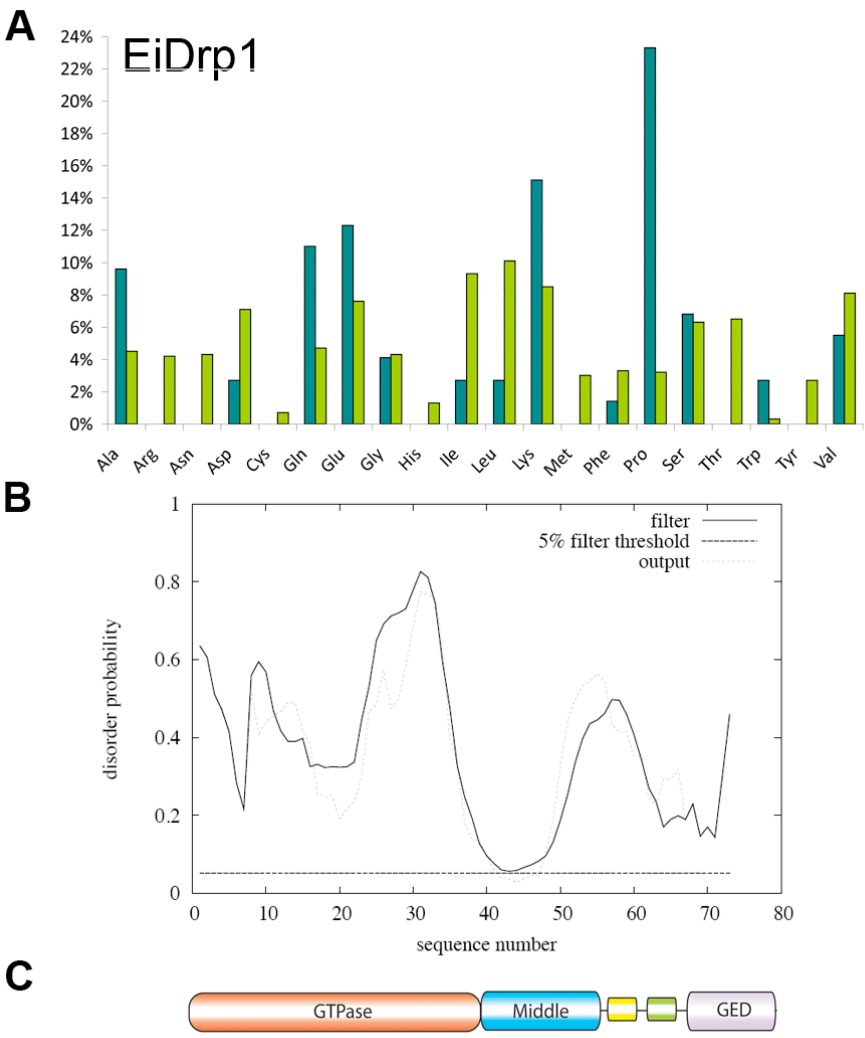
A
EiDrp1
24%
22%
20%
18%
16%
14%
12%
10%
8%
6%
4%
2%
0%
Ala Arg Asn Asp Cys Gln Glu Gly His Ile Leu Lys Met Phe Pro Ser Thr Trp Tyr Val
B
filter
5% filter threshold
output
disorder probability
sequence number
C
GTPase
Middle
GED

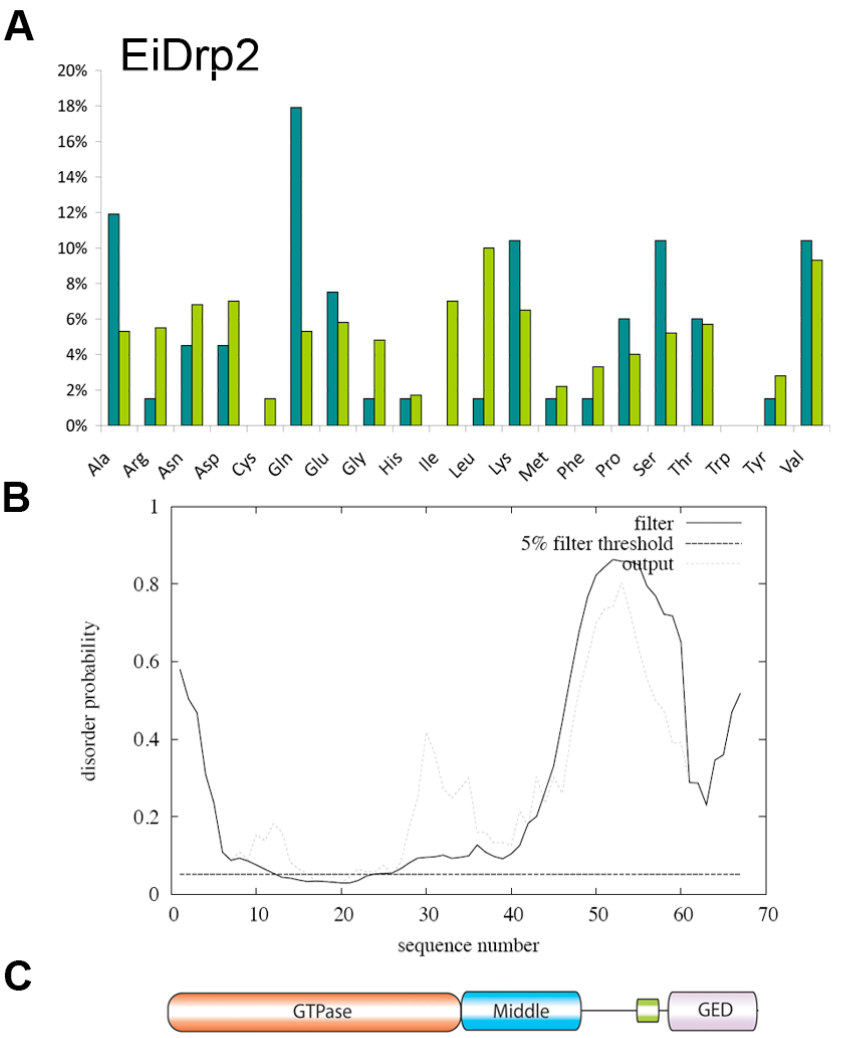
A
EiDrp2
20%
18%
16%
14%
12%
10%
8%
6%
4%
2%
0%
Ala Arg Asn Asp Cys Gln Glu Gly His Ile Leu Lys Met Phe Pro Ser Thr Trp Tyr Val
B
filter
5% filter threshold
output
disorder probability
sequence number
C
GTPase
Middle
GED

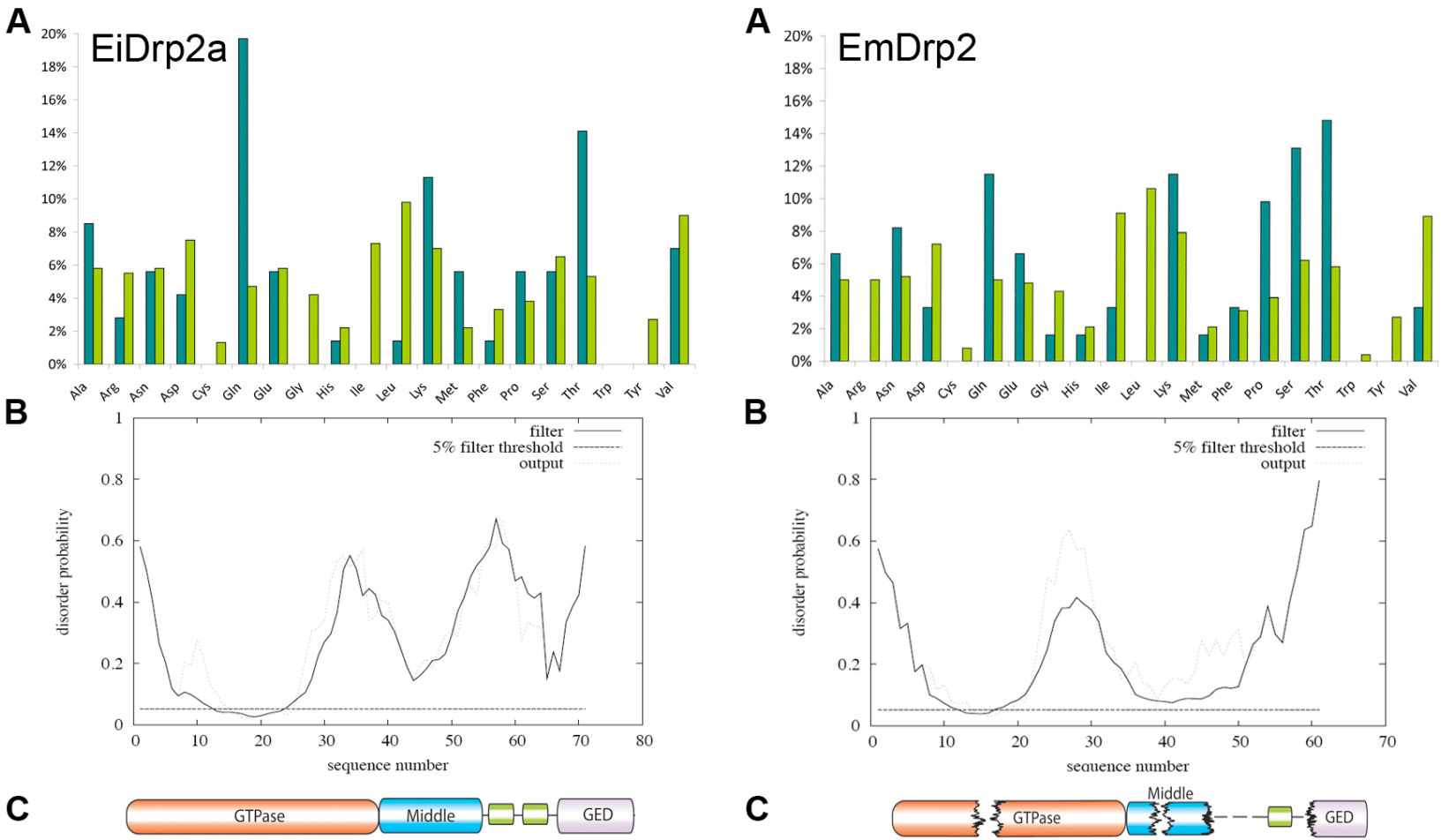

Figure 4.5 Amino acid composition of *Entamoeba* Drp1 and Drp2 comparing the V-segment with the remaining protein and disordered regions in V-segments. A: Amino acid composition; light green: protein excluding the V-segment; dark green: V- segment only. B: corresponding disordered sequence plot in V-segment. C: corresponding domain structure of the complete protein including low complex regions within V-segment; green-glutamine rich; yellow-proline rich. The EmDrp2 sequence is incomplete. Missing domain parts are indicated by broken lines. The dashed line represents the missing sequence not defined as part of domains.

4.4.2 *Entamoeba* Drp3 and Drp4

The Drp3 and Drp4 sequences seem different compared to the more classic dynamin like proteins such as Drp1 and Drp2. For Drp3 and 4 only the large GTPase domain was detected by the domain prediction tools Pfam (Finn *et al.*, 2010), SMART (Schultz *et al.*, 2000) and NCBI Conserved Domains database (Fig. 4.3c, Fig. 4.6). Furthermore, there is an additional sequence at the N-terminus in front of the GTPase domain of 128 to 190 residues in *Entamoeba* Drp3 and 90 residues in *Entamoeba* Drp4. *D. discoideum* DLPA, B and C also exhibit this pre-GTPase sequence of approximately 171 residues in DLPA, 23 in DLPB and 99 in DLPC (Fig. 4.6). According to TargetP (Emanuelsson *et al.*, 2007) and WoLFPSORT the segments found in *Entamoeba* do not contain a recognizable targeting signal. This is in agreement with the plant dynamin related proteins Drp5A and Drp5B, and the *Dictyostelium discoideum* DLPA, B and C, which also do not exhibit a detectable middle and GED domain and recognizable targeting signals (Fig. 4.6). Coiled coil regions were detected using the SMART domain prediction server in all but the plant DRP5A and DRP5B (Fig. 4.6). The predicted regions were confirmed by the prediction tool COILS (Lupas *et al.*, 1991). Coiled-coil regions contain repeated patterns of hydrophobic, polar and charged amino acid residues and are common structural motifs in proteins (Mason & Arndt, 2004) also found in the dynamin protein family (Wienke *et al*., 1999, Okamoto *et al.*, 1999, Pitts *et al.*, 2004). These regions have previously shown to be of major importance in the self-assembly of dynamin (Okamoto *et al*. 1999) and the targeting of human DLP1 to mitochondria (Pitts *et al*., 2004). The *Entamoeba* Drp3 and Drp4 sequences do not seem to contain the typical middle and GED domains normally found in the dynamin protein family. They have this lack of domain structure in common with the *D. discoideum* DLPA, B and C and plant DRP5A and DRP5B homologues. However, the middle and GTPase effector domains in Drp3 and Drp4 as well as DLPA, B and C and plant DRP5A and DRP5B might be too divergent to be detected through sequence comparison. High sequence divergence of the C-terminal region in the dynamin protein family especially in the helical parts is very common (Low and Löwe 2010). An example of low sequence similarity, but domain and functional similarity, is the BDLP

in *Nostoc punctiforme*, the first bacterial dynamin family member that was structurally solved (Low and Löwe 2006).

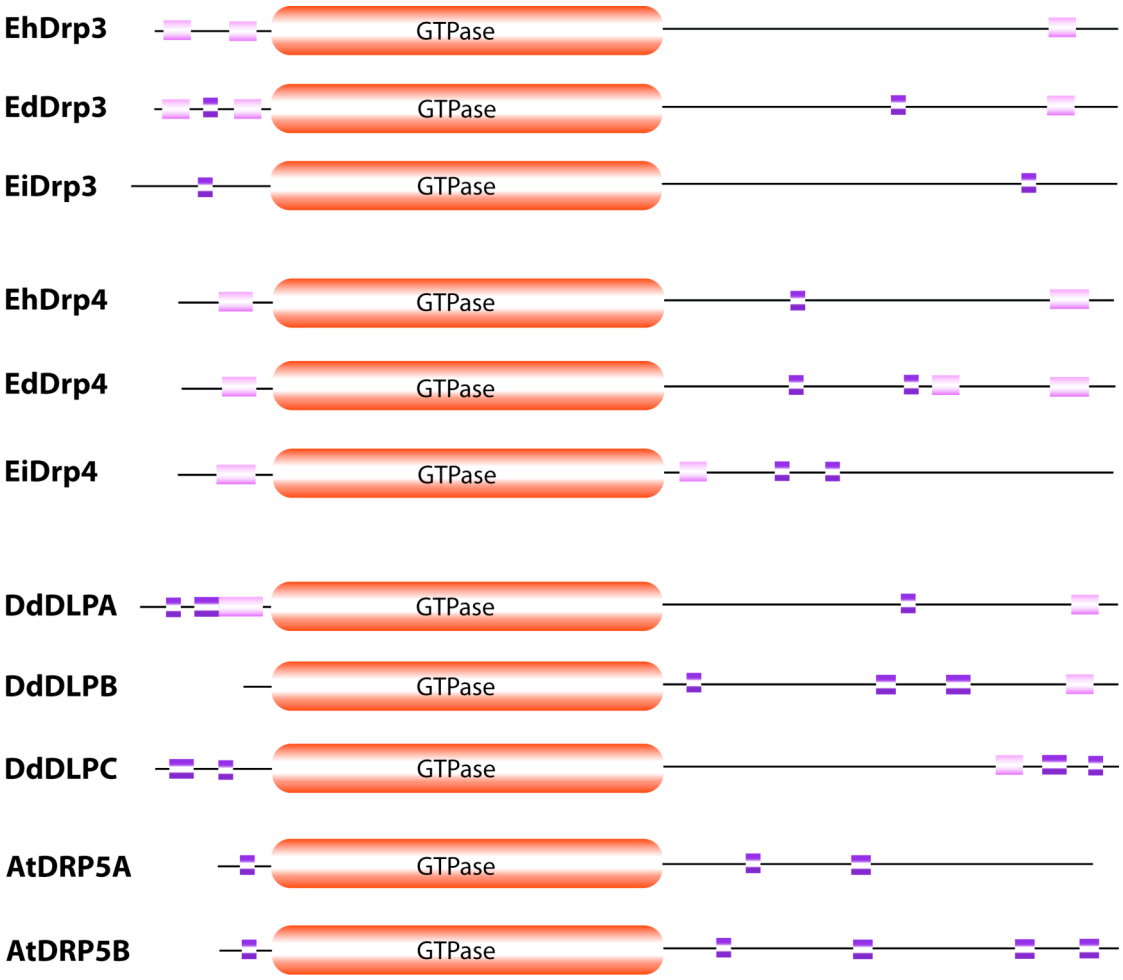

Figure 4.6 Domain structures from *Entamoeba* Drp3 and Drp4, *D. discoideum* DLPA-C and *A. thaliana* DRP5A and DRP5B. a: EhDrp3, b: EdDrp3, c: EiDrp3, d: EhDrp4, e: EdDrp4, f: EiDrp4; g: DdDLPA, h: DdDLPB, i: DdDLPC; j: AtDRP5A, k: AtDRP5B. Light purple segments indicate coiled-coil regions, dark purple segments low complexity regions. Domains were annotated using the SMART domain prediction tool and manually refined in alignment. *E. moshkovskii* and *E. terrapineae* sequences were not shown because complete sequences are not available.

4.4.3 Justification for classifying Drp3 and Drp4 as dynamin related proteins

Although Drp3 and Drp4 do not exhibit the middle and GTPase effector domain, several factors suggest they can be considered part of the dynamin protein family.

1. BLAST results always return dynamin related proteins (Fig. 4.7) as top hits when using Drp3 and Drp4. The domain analysis tools Pfam, SMART and the NCBI conserved domains database support this by identifying the large GTPase domain as dynamin like.

Sequences producing significant alignments:

Accession	Description	Max score	Total score	Query coverage	E value	Links
XP_645576.2	dynamin like protein [Dictyostelium discoideum AX4] >sp|Q55	457	457	84%	3e-126	U G
EFA76188.1	dynamin like protein [Polysphondylium pallidum PN500]	449	449	81%	1e-123	
EGC35126.1	hypothetical protein DICPUDRAFT_33855 [Dictyostelium purpur	447	447	84%	4e-123	
XP_002683545.1	dynamin family GTPase [Naegleria gruberi] >gb|EFC50801.1|	341	341	88%	2e-91	G
NP_001130364.1	hypothetical protein LOC100191459 [Zea mays] >gb|ACF7855	268	268	64%	2e-69	U G
XP_002317496.1	predicted protein [Populus trichocarpa] >gb|EEE98108.1| predi	268	268	64%	3e-69	U G
XP_002458482.1	hypothetical protein SORBIDRAFT_03g034500 [Sorghum bicolo	267	267	64%	6e-69	U G
XP_002891730.1	dynamin family protein [Arabidopsis lyrata subsp. lyrata] >gb	265	265	64%	2e-68	G
XP_002533903.1	ATP binding protein, putative [Ricinus communis] >gb|EEF284	264	264	66%	4e-68	G
NP_175722.1	dynamin family protein [Arabidopsis thaliana]	262	262	64%	2e-67	U G
EEC71470.1	hypothetical protein OsI_03724 [Oryza sativa Indica Group]	262	262	64%	2e-67	
BAD86966.1	dynamin-like [Oryza sativa Japonica Group]	260	260	64%	5e-67	
NP_001044237.2	Os01g0748000 [Oryza sativa Japonica Group] >dbj|BAF06151.	260	260	64%	6e-67	U G
EEE55376.1	hypothetical protein OsJ_03445 [Oryza sativa Japonica Group]	260	260	64%	6e-67	
XP_002961391.1	hypothetical protein SELMODRAFT_76041 [Selaginella moellenc	259	259	67%	1e-66	U G
AAF87857.1	Hypothetical protein [Arabidopsis thaliana]	258	258	64%	2e-66	
XP_001696853.1	dynamin-related GTPase [Chlamydomonas reinhardtii] >gb|ED	258	258	57%	3e-66	U G
XP_002980879.1	hypothetical protein SELMODRAFT_113285 [Selaginella moeller	257	257	67%	5e-66	G
EFN52892.1	hypothetical protein CHLNCDRAFT_26491 [Chlorella variabilis]	257	257	67%	6e-66	

Figure 4.7 NCBI protein BLAST result using EhDrp3 as query. Equally significant results were obtained with Drp4. *Entamoeba* proteins were excluded from the subject search to find the most similar matches outside *Entamoeba* spp.

2. Drp3 and Drp4 are similar in structure to the previously characterized *D. discoideum* dynamin related proteins DdDLPA, B and C and the *A. thaliana* AtDRP5A and AtDRP5B (Fig. 4.6; (Miyagishima *et al.*, 2008).
3. Drp3 and Drp4 are phylogenetically closely related to DdDLPA, B and C and AtDRP5A and AtDrp5B (Section 4.6.1.1).

4.5 The dynamin consensus sequence in *Entamoeba*

The dynamin consensus sequence 'LPRGSGIVTR' is a common feature in the dynamin protein family (Nakayama *et al.*, 1993, Wienke *et al.*, 1999, Alexander *et al.*, 2000). It is situated downstream of the G1 loop and includes the G2 loop within the N-terminal large GTPase domain (Fig. 4.2). *Entamoeba* Drp1 and Drp2 exhibit this conserved stretch of amino acid residues, which has been shown to be involved in self-assembly in mammalian Mx-protein (Nakayama *et al.*, 1993). However, this supposedly consensus sequence is not universally conserved within the dynamin

protein family. For example, the mitochondrial fusion dynamin like proteins such as Fzo1 in human and yeast (Fig. 4.8) and various protist dynamin like proteins without assigned functions, *e.g. Toxoplasma gondii* DrpB, *Naegleria gruberi* dlp (59684) and *Phytophthora ramorum* dlp (86760) do not exhibit the consensus sequence.

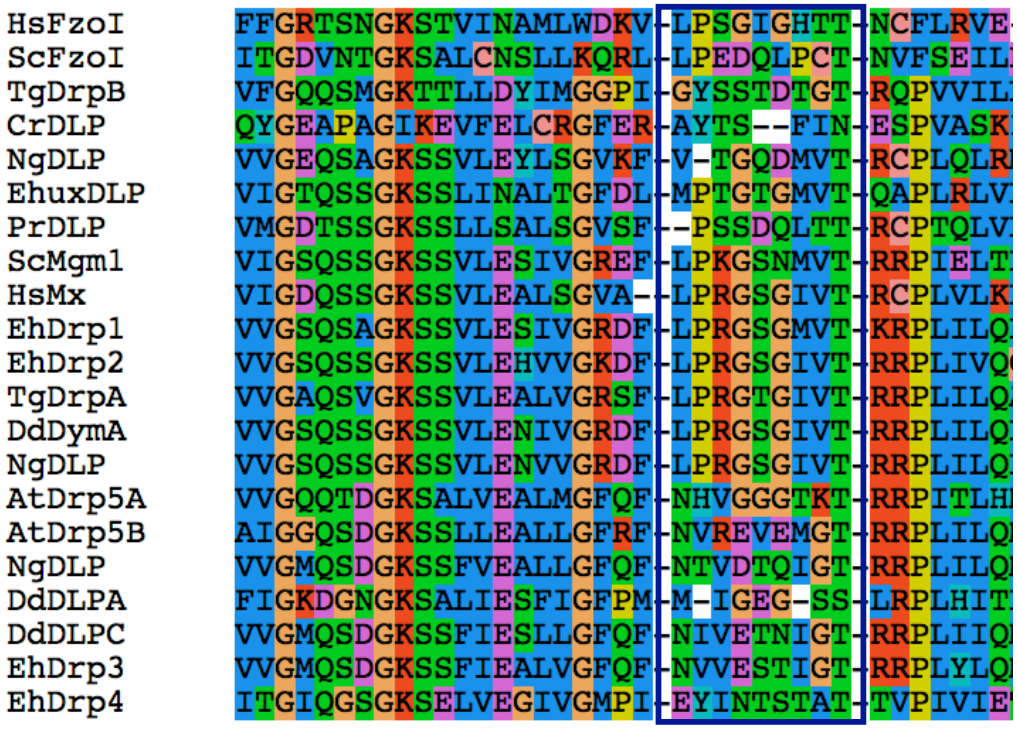

Figure 4.8 Dynamin protein sequence alignment showing presence and absence of the dynamin consensus sequence (LPRGSGIVTR) in different taxa. Boxed in is the region of the dynamin consensus sequence. Hs: *Homo sapiens*, Sc: *Saccharomyces cerevisiae*, Tg: *Toxoplasma gondii*, Cr: *Chlamydomonas reinhardtii*, Ng: *Naegleria gruberi*, Ehux: *Emiliana huxleyi*, Eh: *Entamoeba histolytica*, Pr: *Phytophthora ramorum*, Dd: *Dictyostelium discoideum*, At: *Arabidopsis thaliana*. 'DLP' stands for dynamin like protein and was assigned to proteins without known function.

4.6 Phylogenetic relationships of *Entamoeba* dynamin-like proteins

Dynamins and dynamin related proteins are a large protein family and genome projects keep adding new ones. However, it not clear how dynamin related proteins with the same function in different phylogenetic groups are related to each other. To this point no phylogeny including members of all eukaryotic supergroups and a large

variety of dynamin related proteins has been published. So, to understand the evolutionary relationship within the dynamin protein family and in particular those from *Entamoeba* spp., phylogenetic reconstruction were conducted in this study.

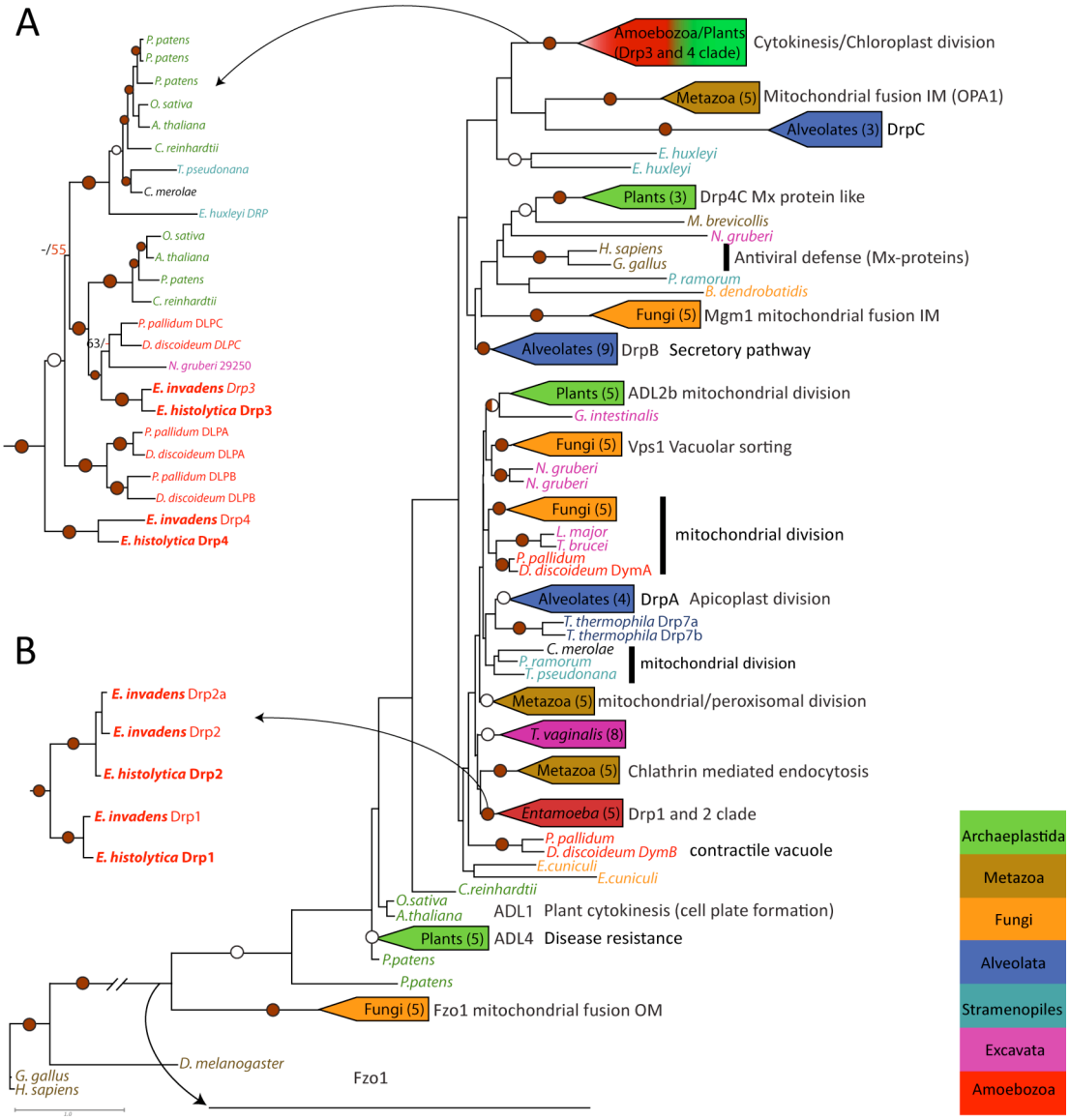

Figure 4.9 Phylogenetic reconstruction of the relationships between dynamin family proteins. The figure shown is a maximum-likelihood tree constructed using PhyML and based on an alignment of 133 sequences containing 229 distinct alignment patterns. The red circles and blue stars indicate local bootstrap values above 80 % and 60 % respectively. They were calculated using PhyML and RaxML, respectively. The tree contains dynamin family protein sequences of taxa from all supergroups including Archaeplastida (in green), Opisthokonta (Metazoa-in brown, fungi-in orange), Alveolata (in blue), Stramenopiles (in light blue), Excavata (in purple) and Amoebozoa (in red). For a detailed list of taxa and

sequences, please see Supplementary Table 1. (A) and (B) show expanded sub-clades. (A) shows the "Drp1 and 2 clade" which includes the *E. histolytica* and *E. invadens* dynamin family proteins. EhDrp1 has previously been shown to localize to the nuclear outer membrane (Jain *et al*. 2010). (B) Shows the "EhDrp3 and 4 clade" which includes *D. discoideum* DlpA, B and C previously shown to be involved in cytokinesis together with plant chloroplast division dynamin family proteins (Miyagishima *et al*. 2008).

The large-scale phylogenetic reconstruction reveals a wide diversity within the dynamin protein family and a general distribution according to function within tight systematic groups. For example, fungal Dnm1 sequences involved in mitochondrial division form a highly supported clade and do not group with other functionally different dynamin proteins from fungi, but additionally, they also do not cluster with mitochondrial dynamin related proteins from the metazoa. This is especially clear for the classical dynamins in animals involved in clathrin-mediated endocytosis, the dynamin related proteins in plants, animals and fungi (Fig. 4.9). They all form distinct systematic clades according to function. Less dynamin protein sequences were available from protist taxa and therefore, functional clades might not be as obvious as for plants, animals or fungi. A few dynamin related proteins in protists have been functionally and phylogenetically analysed previously (Fig. 4.9) (Morgan *et al*., 2004, Elde *et al*., 2005, Miyagishima *et al*., 2008, van Dooren *et al.*, 2009, Jain *et al*., 2010, Wienke *et al*., 1999). Noteworthy, is the diversification of dynamin related proteins in the excavate *Trichomonas vaginalis.* Unlike the dynamin related proteins in the ciliate *Tetrahymana thermophila*, all 8 *Trichomonas* proteins form a distinct clade (Fig. 4.9) suggesting recent local gene duplications. The resolution of the tree backbone is poor and there is low support for functional clades beyond the tight phylogenetic and functional groups. Reasons for the lack of backbone support might be a large sequence divergence within the protein family, long-branch attraction, especially in parasitic organisms and possibly the comparison of paralog with ortholog sequences due to local gene duplications and gene loss events. Therefore it is not possible to draw conclusions about large-scale dynamin evolution. An interesting exception is a strongly supported relationship between amoebozoan, plant, stramenopile and excavate proteins (termed amoebozoan/plant clade, Figs. 4.9a, 4.10, section 3.6.1.1).

4.6.1 Amoebozoan dynamin protein family

4.6.1.1 *Entamoeba* Drp1 and Drp2

Entamoeba Drp1 and Drp2 form a distinct clade that is not closely related to any other members of the dynamin protein family (Fig. 4.9 and 4.10).

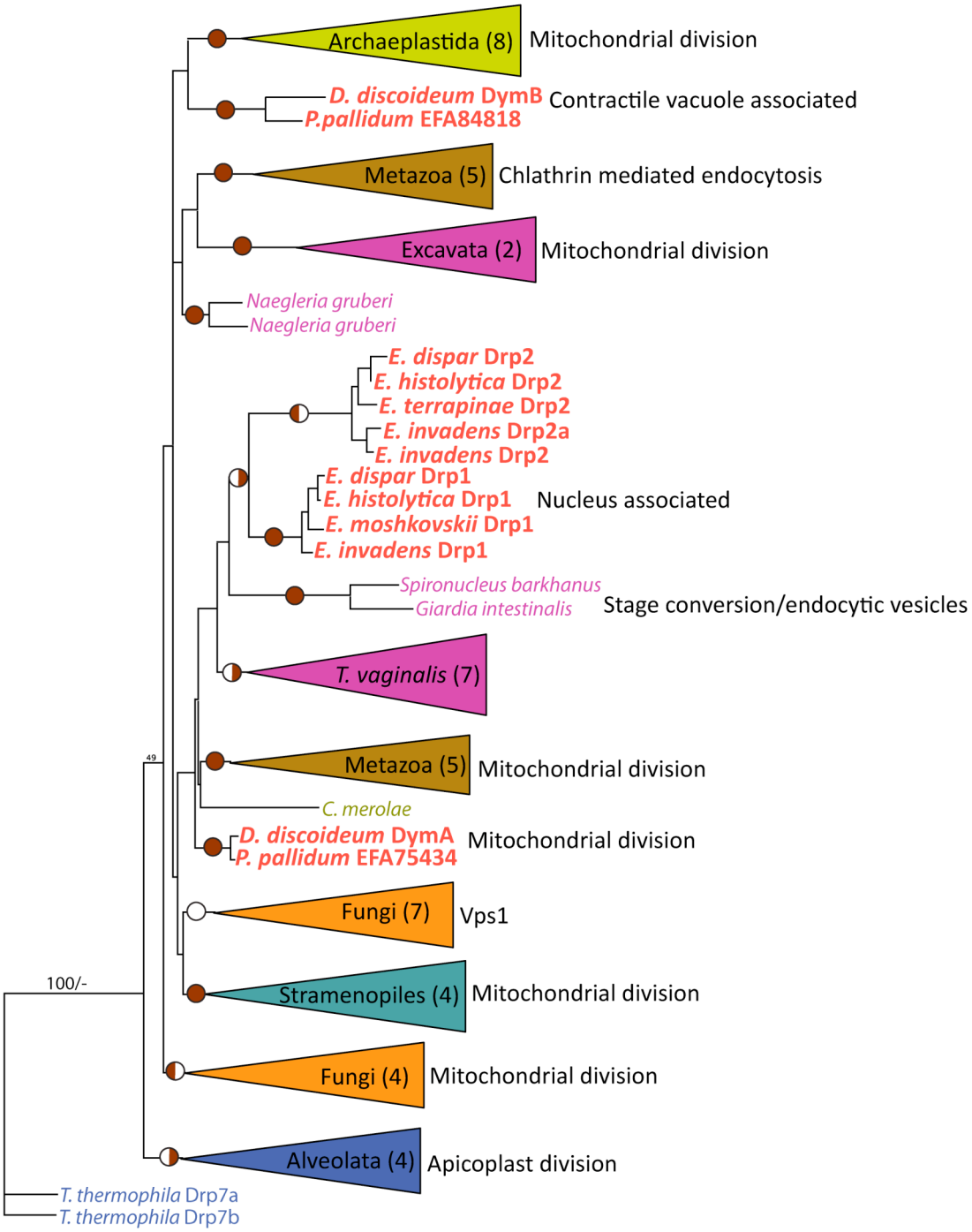

Figure 4.10 Phylogenetic reconstruction of dynamin proteins with emphasis on *Entamoeba* Drp1 and 2. Shown is a maximum likelihood topology constructed by the PhyML program.

Boostrap values were calculated using PhyML and rAXML. Circles at the nodes represent bootstrap values as determined using PhyML and rAXML (red circle: bootstrap > 70 % in both analyses; white circle: bootstrap support between 50 % and 70 % in both analyses, half circle red on the left: PhyML bootstrap > 70 % and rAXML bootstrap between 50 % and 70 %; half circle red on the right: PhyML bootstrap between 50 % and 70 % and rAXML bootstrap above 70 %. Absence of circles indicates support below 50 % in both analyses. The dataset contained 67 sequences with 233 aligned residues out of 244 sites from all supergroups. To gain more informative sites, several dynamin family protein groups were excluded. A complete list of taxa and accession numbers can be found in Supplementary Table 2.

This observation differs from a previous study by Jain *et al*. (2009) who found *E. histolytica* Drp1 nested within dynamin related proteins involved in mitochondrial division (*C. elegans*), vesicular trafficking (*P. falciparum*), vacuolar sorting (*S. cerevisae*) and clathrin coated endocytosis (*H. sapiens*) with high support. However, the present study included a larger amount of different eukaryotic taxa, which likely resulted in a different tree topology. Drp1 and Drp2 were not found to be closely related to amoebozoan proteins from the non-parasitic *D. discoideum* and *P. pallidum* (Fig. 4.9 and 4.10). *D. discoideum* DymA and *P. pallidum* EFA75434 are sister to each other. So are *D. discoideum* DymB and *P. pallidum* EFA84816. However, both clades are not closely related. The two *P. pallidum* sequences were manually annotated based on sequence comparison with *D. discoideum* Dym A and DymB. Within the *Entamoeba* cluster, Drp1 and Drp2 form two distinct clades that are sister to each other (Fig. 4.9 and 4.10), *E. histolytica* Drp1 groups with *E. dispar* (XP001734031) and *E. invadens* (EIN051430). Sequences for *E. moshkovskii* were gained by BLAST searches using *Entamoeba* Drp1 and Drp2 sequences against the genome available on the Sanger genome database. However, as there is limited genome information for *E. moshkovskii*, it was not possible to gain full-length sequences. *E. moshkovskii* Drp's were manually annotated and pieced together based on sequence similarity to the other *Entamoeba* Drp's. Two partial sequences were recovered but only one was used in the phylogeny because it was of sufficient length. The analysis shows that the *E. moshkovskii* protein sequence is most closely related to *Entamoeba* Drp1 (Fig. 4.10). The amoebozoan *Acanthamoeba castellani* was not

included into the phylogenetic reconstructions because only one gene sequence could be recovered from the genome that was long enough for the inclusion into the datasets. This sequence was very different and caused a long branch in the analyses.

4.6.1.2 Amoebozoan/Plant clade (= chloroplast division/cytokinesis clade)

The amoebozoan taxa *D. discoideum*, *P. pallidum* and *Entamoeba* spp. form a strongly supported relationship to the plant cell and chloroplast division proteins DRP5A and DRP5B and stramenopile and excavate proteins (Fig. 4.9, Fig. 4.11). *Entamoeba* Drp3, Drp4 and the non-parasitic *D. discoideum* DlpC and *P. pallidum* (EFA76188) form a well-supported clade with *Entamoeba* Drp4 being the sister to both. A Drp4 homologue in *E. moshkovskii* was not found. Surprising is the grouping of excavate *N. gruberi* with *D. discoideum* DlpC. Similar to amoebozoan species, the excavate *Naegleria* is well known for its amoeboid life style. However, no additional excavate taxon was found to cluster with *N. gruberi*. Basal to the amoebozoan Drp3/Drp4 and DlpC clade are the plant DRP5A proteins involved in cytokinesis (Miyagishima *et al*. 2008). This relationship is only weakly supported. *D. discoideum* DlpA and DlpB involved in cell division form a strongly supported clade with *P. pallidum* (EFA84098 and EFA76312). They are sister to chloroplast division proteins DRP5B. Interesting is the grouping of the basal red alga *Cyanidioschyzon merolae* with the phaeophycete taxa *Thalassiosira pseudonana*, *Phaeodactylum tricornutum* and *Ectocarpus siliculosus*, whose secondary plastid originates from a red algal endosymbiont {Archibald, 2002 #1471}. This indicates that chloroplast containing stramenopiles acquired DRP5B through the secondary plastid endosymbiosis event. The phylogenetic reconstruction supports previous analyses from Miyagishima *et al*. (2008) and van Dooren *et al*. (2009) who both discovered a well-supported relationship between *Dictyostelium* DlpA-C involved in cell division and Archaeplastida dynamin like proteins involved in chloroplast division. Furthermore, they discovered that Dnm2 from the non-pathogenic free-living excavate *Naegleria gruberi* nests within this clade. Analyses in this project contribute to the published data by including the free-living amoebozoan *P. pallidum* and the parasitic non-free

living *Entamoeba histolytica*, *E. invadens, E. moshkovskii* and *E. dispar*. The well-supported grouping of the dynamin related proteins from free-living and parasitic amoebozoans indicates that their involvement in cytokinesis might be a conserved function across the amoebozoa.

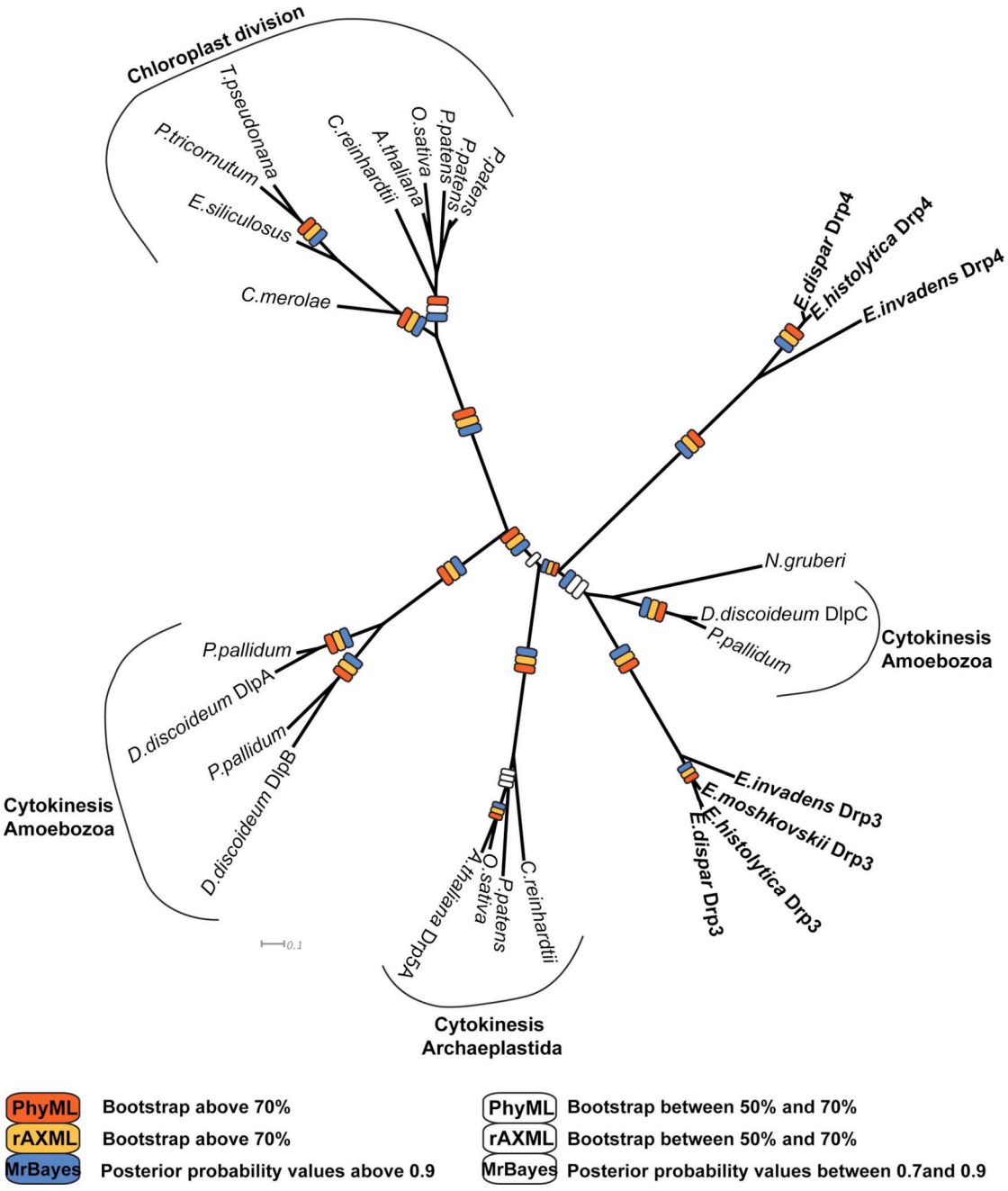

Figure 4.11 Phylogenetic reconstruction of the Plant/Amoebozoan chloroplast division/ cytokinesis clade. Shown is a protein maximum likelihood topology constructed by the PhyML program. Bootstrap values and posterior probability values were calculated using PhyML, rAXML and MrBayes. The dataset contained 28 sequences with 485 distinct aligned

residues (out of 492 sites) from Archaeplastida, Amoebozoa and Stramenopiles. A complete list of taxa and accession numbers can be found in Supplementary Table 3.

In summary, the dynamin protein family are large GTPases involved in various membrane altering processes such as organelle fission and fusion, clathrin mediated endocytosis and vesicle trafficking. Two types of dynamin related proteins where found in *Entamoeba*. Drp1, Drp2 and Drp2a exhibit the classical minimal domain structure including the large GTPase domain, the middle and GTPase effector domain. Drp3 and Drp4 only exhibit a large GTPase domain, whereas the other domains are not detectable by sequence comparison. Drp1, Drp2 and Drp2a have the dynamin signature sequence, which is however, not universally present in all dynamin related proteins. Drp1, Drp2 and Drp2a show distinct variations in the V-segment from each other, which indicate functional differences. Unlike Drp2 and Drp2a, Drp1 is proline rich, an indication for protein-protein interaction. Drp1-Drp4 do not have recognizable targeting signals. Phylogenetic analyses show that *Entamoeba* Drp1 and Drp2 form an independent distinct clade without a supported relationship to other eukaryotic proteins including the free living amoebozoan *D. discoideum* DymA and DymB. Drp3 and Drp4 are closely related to *D. discoideum* DlpA-C, which are involved in cytokinesis and plant DRP5A and DRP5B involved in cytokinesis and chloroplast division. This indicates that cytokinesis might be a conserved function throughout the Amoebozoa.

5 Localization and kinetic characterization of *Entamoeba histolytica* Drp2

Entamoeba histolytica contains four dynamin related proteins. Two of them, Drp1 and Drp2, exhibit the classical domain structure comparable to DymA and DymB from the free-living relative *Dictyostelium discoideum*. *D. discoideum* DymA has been well characterized and its GTPase domain has even been structurally analysed by protein crystallography (Niemann *et al.*, 2001). Both DymA and DymB have been shown to associate with mitochondria (Gilson *et al*., 2003, Rai *et al*., 2010). While DymA is responsible for mitochondrial division, DymB is only transferred to this organelle for protein maturation and subsequently transferred back into the cytoplasm, in particular to the contractile vacuole. Depletion of this protein leads to large morphological and metabolic alterations indicating broad functionality (Rai *et al*., 2010). Because both DymA and DymB are associated with *D. discoideum* mitochondria, we were interested in the localization and function of *E. histolytica* Drp1 and Drp2. Furthermore, we wanted to analyze if these dynamin related proteins are also involved in mitochondrial division, especially as there is no information on mitosomal division in *Entamoeba*. While conducting this project, Jain *et al*. (2010) reported that Drp1 is localized to the outer nuclear envelope and is therefore not mitosomal associated. Because of this, we focused our analyses on Drp2. Part of this analysis included co-localization studies using a homologous *E. histolytica* Drp2 antibody and a homologous mitosomal Hsp70 antibody (chapter 3), which were both produced in this project. While the experiments for Drp2 and Hsp70 antibody productions were conducted by Maria A. Siegesmund, the localizations were kindly carried out by Prof. Adrian Hehl (University Zürich, Switzerland). In addition, complementation experiments in *D. discoideum* DymA negative cells were performed in collaboration with Prof. Dietmar Manstein's research group (Hannover Medical School, Germany) to analyze, if Drp2 can functionally complement the mitochondrial division dynamin DymA in *D. discoideum* (chapter 6). To achieve a better understanding of Drp2 functionality and its comparability to other members of the

dynamin protein family, the enzyme was kinetically characterized using two biochemical essays.

5.1 Cloning and amplification of EhDrp2

The DNA fragment including the complete Drp2 gene sequence was amplified from *E. histolytica* genomic DNA using a combination of proofreading *Pfu* DNA Polymerase and *Taq* DNA polymerase to minimise the likelihood of mutations introduced during standard PCR and to add T-overhangs onto the PCR product for TA-cloning. The DNA fragment was inserted into the TA-cloning vector pGEM-T-Easy. The resulting construct was confirmed by DNA sequencing using the primers M13F, M13R and the gene specific primer 731F and EhDrp2middle (Table 2.4). The gene specific primers EhDrp2pET14b_F and EhDrp2pET14b_R (Table 2.4), including both the *Nco*I restriction site, were used to amplify the gene from the Drp2pGEM-T-Easy construct (Fig. 5.1).

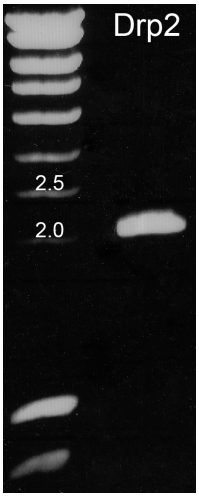

Figure 5.1 PCR amplification of *E. histolytica* Drp2. 1 % TAE agarose gel showing the amplified putative Drp2 PCR product. The 1-kb DNA marker is shown on the left and the PCR product on the right. The size of the relevant reference DNA is indicated on top of each marker band. The expected fragment size of the digested construct, including the *Nco*I restriction sites, is 2004 bp.

Following restriction digest with *Nco*I, the fragment was successfully inserted into the *Nco*I restriction site of the gene expression vector pET-14b in frame with the C-terminal His-tag. The construct was confirmed by DNA sequencing using the

sequencing primers T7 and T7 term. Two types of *E. coli* expression cells were used. First, recombinant protein was produced in the routine protein expression system *E. coli* BL21 pLysY. This system was used to raise sufficient amounts of recombinant protein for antibody production. Because Drp2p was not highly expressed and insoluble in this system, the *E. coli* Rosetta 2 (DE3) pLyS (Novagen) strain was employed, which is designed to express eukaryotic genes by providing codons rarely used by *E. coli* BL21 cells. The recombinant Drp2 protein produced in *E. coli* Rosetta 2 was soluble indeed and used for kinetic characterization experiments.

5.2 Recombinantly produced Drp2p is deposited as inclusion bodies in *E. coli* BL21 and in the soluble fraction in Rosetta 2 cells.

The recombinant Drp2 protein was produced at 37 °C and was almost exclusively deposited as insoluble aggregates called inclusion bodies. Inclusion bodies are often formed because the prokaryotic folding machinery fails to correctly fold the polypeptide chains of recombinant eukaryotic protein. To isolate the recombinant protein from the insoluble fraction the protein isolation protocol was modified by including 8 M urea as a denaturant. Protein was purified using immobilised Ni^{2+}-affinity chromatography under denaturing conditions. The purification resulted in a band of approximately 75 kDa corresponding to the expected molecular mass of recombinant Drp2p (Table 4.1, Fig. 5.2).

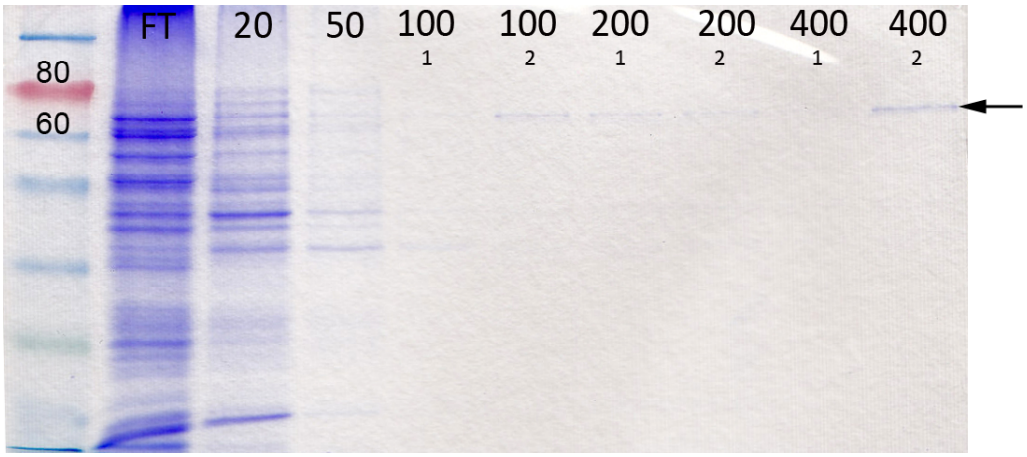

Figure 5.2 Purification of recombinant EhDrp2p from BL21 *E. coli* using affinity chromatography. 12 % SDS gel showing stepwise purification of recombinant Drp2p from the insoluble fraction. FT = Flow through of total protein incubated with Ni^{2+} - NTA; 20 , 50, 100, 200 and 400 = 20 mM- 400 mM imidazole elutions. The numbers (1) and (2) indicate representative fractions from each elution. The arrow points at the purified recombinant Drp2p. The prestained protein marker is shown on the left and the two marker bands of 60 kDa and 80 kDa, important for mass estimation of EhDrp2p, are indicated.

After Ni^{2+} purification the fractions were further purified and concentrated in centrifugation filter units with a 50 kDa filter cut off. The purity of the recombinant protein in the 400 mM Imidazole fraction was estimated to at least 95 % based on SDS PAGE (Fig. 5. 3).

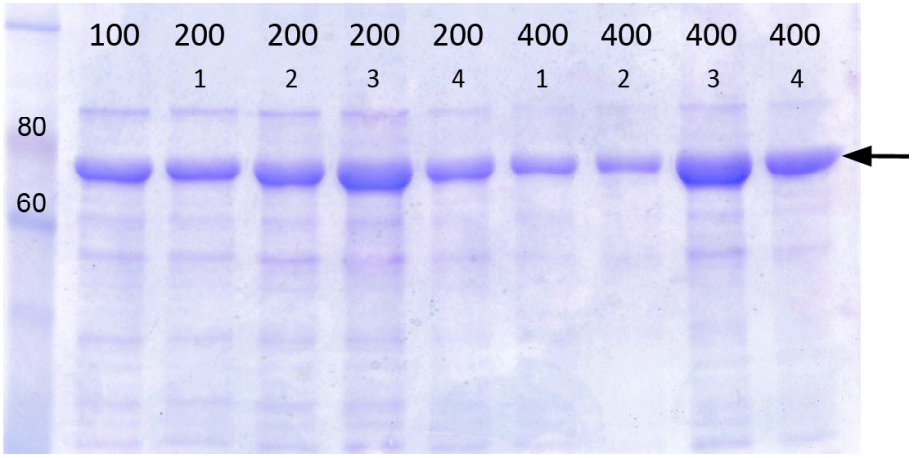

Figure 5.3 Purification and concentration of recombinant Drp2p. 12 % SDS gel showing recombinant Drp2p that was eluted from the Ni^{2+} chromatography column with 100 mM, 200 mM and 400 mM imidazole in 8 M urea. The molarity of imidazole used for elution is indicated on top of each fraction. The number below shows the fraction number. The arrow points at the purified recombinant Drp2p. The prestained protein marker is shown on the left and two marker bands of 60 kDa and 80 kDa are indicated.

The identity of the protein was verified by mass spectrometry as EhDrp2 with 61% sequence coverage (Fig. 5.4). Additionally, no contaminating peptide sequences were identified during mass spectrmetry analyses.

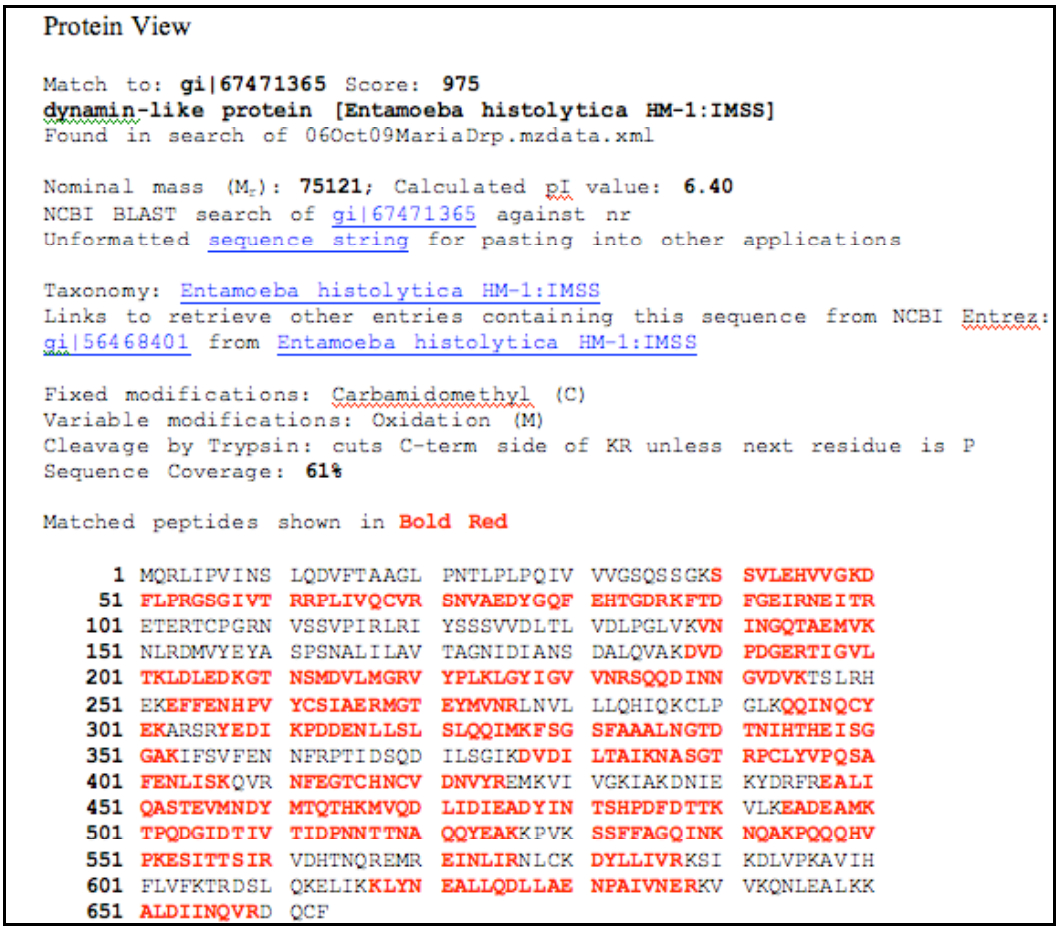

Protein View

Match to: **gi|67471365** Score: **975**
dynamin-like protein [Entamoeba histolytica HM-1:IMSS]
Found in search of 06Oct09MariaDrp.mzdata.xml

Nominal mass (M_r): **75121**; Calculated pI value: **6.40**
NCBI BLAST search of gi|67471365 against nr
Unformatted sequence string for pasting into other applications

Taxonomy: Entamoeba histolytica HM-1:IMSS
Links to retrieve other entries containing this sequence from NCBI Entrez: gi|56468401 from Entamoeba histolytica HM-1:IMSS

Fixed modifications: Carbamidomethyl (C)
Variable modifications: Oxidation (M)
Cleavage by Trypsin: cuts C-term side of KR unless next residue is P
Sequence Coverage: **61%**

Matched peptides shown in **Bold Red**

```
    1 MQRLIPVINS LQDVFTAAGL PNTLPLPQIV VVGSQSSGKS SVLEHVVGKD
   51 FLPRGSGIVT RRPLIVQCVR SNVAEDYGQF EHTGDRKFTD FGEIRNEITR
  101 ETERTCPGRN VSSVPIRLRI YSSSVVDLTL VDLPGLVKVN INGQTAEMVK
  151 NLRDMVYEYA SPSNALILAV TAGNIDIANS DALQVAKDVD PDGERTIGVL
  201 TKLDLEDKGT NSMDVLMGRV YPLKLGYIGV VNRSQQDINN GVDVKTSLRH
  251 EKEFFENHPV YCSIAERMGT EYMVNRLNVL LLQHIQKCLP GLKQQINQCY
  301 EKARSRYEDI KPDDENLLSL SLQQIMKFSG SFAAALNGTD TNIHTHEISG
  351 GAKIFSVFEN NFRPTIDSQD ILSGIKDVDI LTAIKNASGT RPCLYVPQSA
  401 FENLISKQVR NFEGTCHNCV DNVYREMKVI VGKIAKDNIE KYDRFREALI
  451 QASTEVMNDY MTQTHKMVQD LIDIEADYIN TSHPDFDTTK VLKEADEAMK
  501 TPQDGIDTIV TIDPNNTTNA QQYEAKKPVK SSFFAGQINK NQAKPQQQHV
  551 PKESITTSIR VDHTNQREMR EINLIRNLCK DYLLIVRKSI KDLVPKAVIH
  601 FLVFKTRDSL QKELIKKLYN EALLQDLLAE NPAIVNERKV VKQNLEALKK
  651 ALDIINQVRD QCF
```

Figure 5.4 Identification of recombinant EhDrp2p by mass spectrometry. Detail from the protein identification Mascot search engine using the mass spectrometry data from putative recombinant Drp2p. Matching peptides are shown in red.

To gain 100 % pure recombinant protein for antibody production, fractions were successfully electroeluted from SDS gel slices and subsequently quantified by comparing the band intensity of the electroeluted sample on 12 % SDS gel to BSA standards (Fig.5.5).

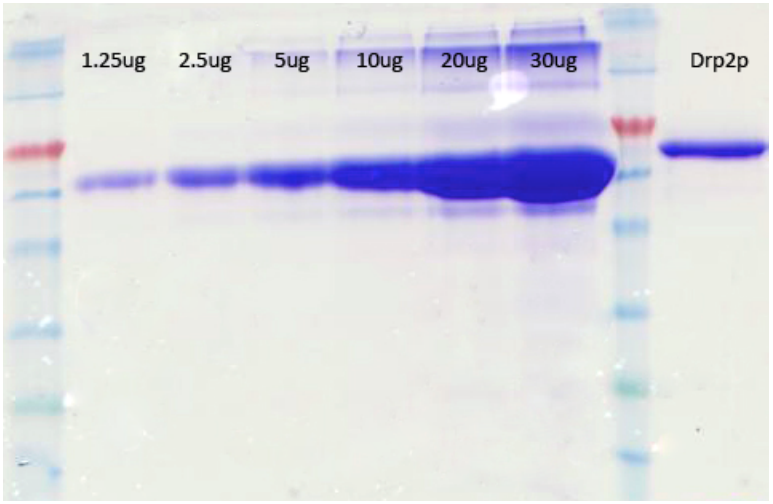

Figure 5.5 Recombinant EhDrp2p quantification. 12 % SDS gel with differing concentrations of BSA standards in comparison Drp2p. BSA standards of different quantities are shown on the left, Drp2p on the right. The Drp2 protein concentration was estimated to be approximately 7.5 μg/band.

The purified Drp2 protein was sent for antibody production in two rats (Eurogentec, Belgium). The low gene expression in *E. coli* BL21 cells is possibly due to codon bias between *E. coli* and EhDrp2 (Table 5.1). The codon bias describes the differential use of codons for amino acids in different organisms (Plotkin & Kudla, 2011). The *E. coli* Rosetta 2 commercial gene expression strain used in this study is adapted to produce eukaryotic recombinant protein, because it contains a vector with additional tRNA genes that exhibit eukaryotic amino acid codon patterns for arginine, leucine, isoleucine, proline and glycine. The *E. coli* BL21 gene expression strain does not contain this additional feature and the difference in codon usage between *E. coli* genes and the Drp2 gene might have caused a bottleneck in the expression of amino acids for recombinant Drp2 (Table 5.1). *The E. coli* BL21 strain has not been sequenced and codon usage information provided by the manufacturer Novagen are based on the *E. coli* K-12 strain (manufacturers information). The codon preference in EhDrp2 was analysed using the 'Sequence Manipulation Suite' (http://www.bioinformatics.org/SMS/index.html). The *E. coli* K-12 codon information are readily available from the 'Codon Usage Database' (http://www.kazusa.or.jp/codon).

Table 5.1 Differences in *E. histolytica* Drp2 and *E. coli* K-12 codon usage. The codon with the highest preference is emphasised in bold. Listed are only the amino acids that are provided additionally by the Ros2 *E. coli* expression strain that is specialised in expressing eukaryotic genes. Marked in red are the amino acids that are used by *E. histolytica* and potentially reduce Drp2 gene expression due to rare codon usage *in E. coli* BL21. Values in brackets show frequency of codon usage per 1000 codons.

Amino acids	*E. coli* K-12 strain codon usage	*Entamoeba histolytica* Drp2 codon usage
Arginine	**CGC** (26), CGT (21.1), CGA (4.3), CGG (4.1), AGA (1.4), AGG (1.6)	**CGA** (7.53), CGT (3.01)
Leucine	**CTG** (46.9), TTA (15.2), TTG (11.9), CTT (11.9), CTC (10.5), CTA (5.3)	**CTT** (40.66), CTA (3.01)
Isoleucine	**ATT** (30.5), ATC (18.2), ATA (3.7)	**ATT** (69.28), ATA (6.02), ATC (3.01)
Proline	**CCG** (26.7), CCT (8.4), CCA (6.6), CCC (6.4)	**CCA** (30.12), CCT (9.04)
Glycine	**GGC** (33.4), GGT (21.3), GGA (9.2), GGG (8.6)	**GGA** (28.6), GGT (18.1)

The comparison between *E. coli* K-12 and the *E. histolytica* Drp2 gene shows *that E. coli* has a lower preference for the codons used by *E. histolytica* to produce the amino acids arginine, leucine, proline and glycine. This could explain why the recombinant Drp2p is expressed poorly in *E. coli* BL21 cells. Additionally, *E. histolytica* shows a lower diversity in codon usage compared to *E. coli* K-12. Arginine for example is encoded by two codons in *E. histolytica* but 6 codons in *E. coli*. This trend is visible for all amino acids analysed except for isoleucine (table 5.1). Protein production in *E. coli* Rosetta 2 cells yielded soluble recombinant Drp2p when expressed at 18 °C overnight (Fig. 5.6), although most recombinant protein was deposited into inclusion bodies. Comparable to the recombinant protein production in the *E. coli* BL21 expression system, this can be explained by the failure of the prokaryotic folding machinery to correctly fold the recombinant Drp2 polypeptide chains. The uninduced fraction also

contains a small amount of putative recombinant Drp2p indicating basal expression without the presence of IPTG.

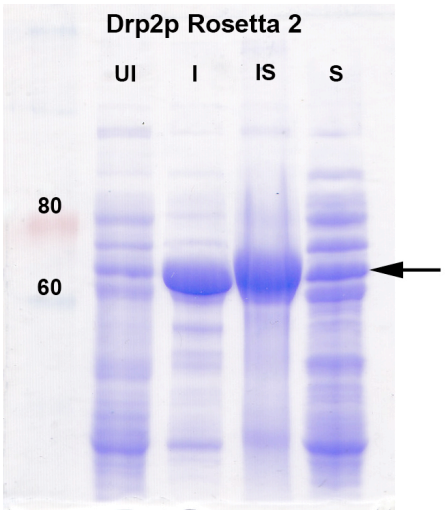

Figure 5.6 Recombinant Drp2p production in Rosetta 2 *E. coli* cells. 12 % SDS gels showing Rosetta 2 recombinant Drp2 protein produced at 18 °C. UI=total cell lysate of uninduced culture, I=total cell lysate of induced culture, IS=total protein of the insoluble fraction, S=total protein of soluble fraction. The arrow points at the putative recombinant Drp2p. The molecular weight marker is shown on the left with the two molecular weights 60 and 80 kDa indicated above the marker bands.

The recombinant EhDrp2p was purified using Ni^{2+}-affinity chromatography and subsequently concentrated and further purified in centrifugation filter units with a 50 kDa filter cut off. The final purity was estimated to be approximately 98 % (Fig. 5.7). Protein concentration was estimated by comparison to known BSA standards (Fig. 5.7) and spectrophotometrically with the Bradford assay.

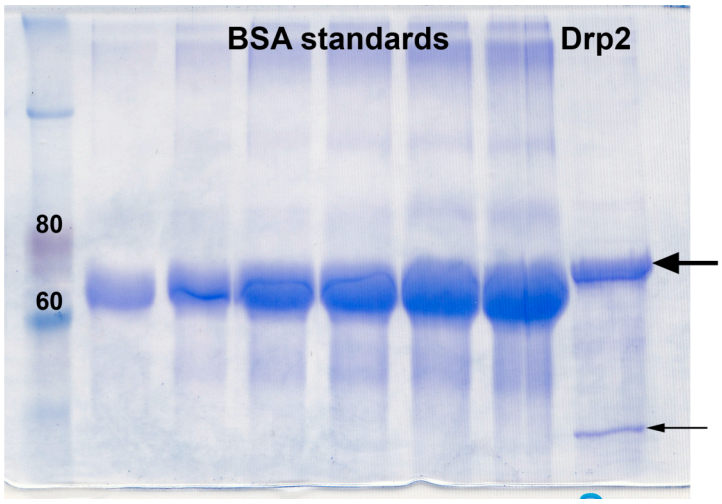

Figure 5.7 Quantification of purified recombinant soluble EhDrp2p. 12 % SDS gel showing BSA standards of different concentrations in comparison to Drp2p. The concentration of Drp2p (fat arrow) was estimated to approximately 6 µg / band. The Drp2p lane contained an additional band at approx. 45 kDa (thin arrow), which was identified by MS as Drp2p as well.

An additional 45 kDa protein band appearing on the SDS gel (Fig. 5.7) was identified by mass spectrometry as Drp2p. This is likely to be a degradation product of the protein. The soluble recombinant purified protein was used for functional GTPase assays.

5.3 Sub-cellular distribution of Drp2 using homologous antibodies

The localization of Drp2 in fixed *E. histolytica* trophozoites was monitored by confocal laser-scanning microscopy using homologous Drp2 and Hsp70 antibodies. EhDrp2 formed distinct numerous cytosolic punctate structures throughout the cell (Fig. 5.8). No localization to the outer nuclear membrane as previously described for EhDrp1 was detected (Jain *et al.*, 2010). Therefore it can be concluded that both proteins perform different tasks in the cells. Drp2 did not co-localize with mitosomal Hsp70 and is therefore probably not directly involved in mitosomal division. The distribution pattern resembles the one found for endosomes in mammalian cells (Duleh & Welch, 2011). However, co-localization studies using endosomal markers are necessary to verify this prediction.

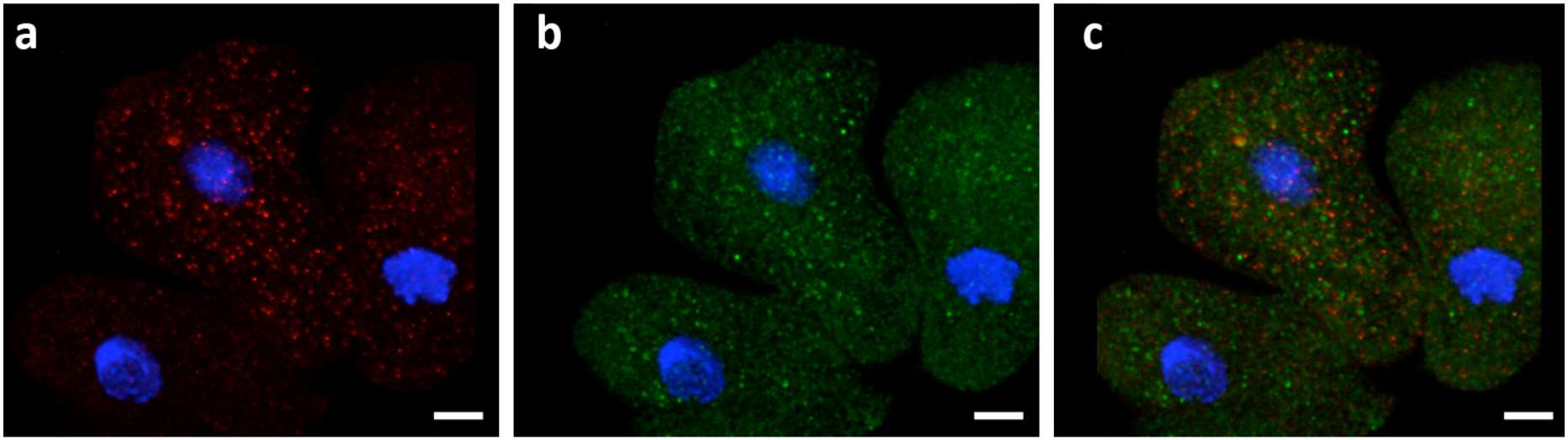

Figure 5.8 Localization of Drp2 and Hsp70 in *E. histolytica* trophozoites. (a) Drp2 stained with Texas Red (red colour), (b) Hsp70 with Alexa 488 (green colour), (c) corresponding merged localizations. The nuclear DNA was stained with DAPI (blue colour). Scale bar=3 μm.

5.4 Kinetic characterization of Drp2p

5.4.1 Refolding of denatured Drp2p into its native state

To analyse if recombinant Drp2p can be refolded from its denatured state after production in *E. coli* BL21 cells, a refolding protocol was applied by gradually removing the denaturant Urea by buffer exchange. Briefly, the isolated purified insoluble recombinant Drp2p was first concentrated in centrifugation filter units. The urea/imidazole solution, in which the recombinant protein was eluted during protein purification, was replaced with refolding buffer (10 % Glycerol, 100 mM NaCl, 100 mM Tris, pH 8) by buffer exchange in dialysis tubes. To test for protein activity two assays were applied, the malachite green assay (Quan & Robinson, 2005, Lanzetta *et al.*, 1979) and the NADH coupled GTPase assay (Ingerman & Nunnari, 2005). The malachite green assay is a sensitive colorimetric GTPase assay that measures inorganic phosphate released through enzymatic activity (Song *et al.*, 2004b, Quan & Robinson, 2005). Drp2p activity was measured by using a fixed GTP concentration and increasing amounts of Drp2p (Fig. 5.9). The protein was suspended in refolding buffer. The measurements show an increase in phosphate release with increasing amount of Drp2p and no activity was measured in the absence of GTP. A control with only GTP but no Drp2p showed a negligible inorganic phosphate release (OD=0.004). This minimal absorbance was encountered for by blanking against GTP only during the spectrophotometric measurements. The assay shows that inorganic phosphate is released in the presence of refolded Drp2p, which indicates that the enzyme is capable of releasing inorganic phosphate in the presence of GTP as might be expected from a GTPase. The amount of released inorganic phosphate resulted in a maximum OD of 0.912. This is higher than for rat dynamin-1, which was found to be between 0.4 to 0.6 OD units (Quan & Robinson, 2005).

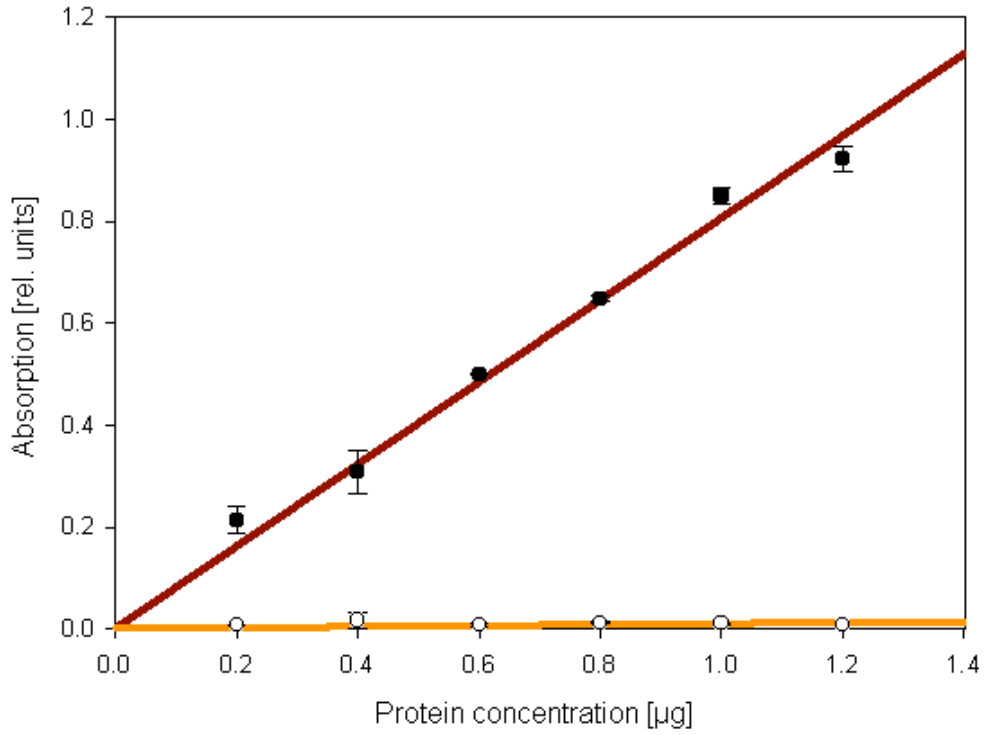

Figure 5.9 Activity measurements of refolded recombinant Drp2p. Malachite green colorimetric assay showing the comparison between the refolded Drp2p in different concentrations with (brown curve) or without (yellow curve) 0.3 mM GTP. GTP only was used to blank the spectrophotometric measurements. Error bars show standard deviation from duplicate measurements.

Although the malachite green assay is useful for measuring if an enzyme is active, its suitability for kinetic characterization is being debated because substrate limitation, especially at high levels of GTP hydrolysis, might interfere with optimal enzyme activity and therefore result in incorrect kinetic parameter estimations (Ingerman & Nunnari, 2005). The NADH coupled GTPase assay was employed for kinetic characterization because GTP is recycled in the coupled enzymatic reaction (chapter 2, section 2.5.5) and measurements are taken continuously rather than at fixed time points. In this assay, the enzyme concentration was fixed and the GTP concentration was increased. GTP auto-degrades and the activity of this process was analysed before the enzyme measurements (Fig. 5.10) and subsequently compared to the measured enzymatic activity. Approximately 10 µg of Drp2p and 100 µM to 1 mM GTP concentrations were used in each reaction. In accordance with the malachite

green assay the protein was resuspended in refolding buffer. However, when the activity measurements of refolded Drp2p were compared to the GTP auto-degradation activity, no significant difference was found (Fig. 5.10). The minimal difference between auto-degrading GTP (Fig. 5.10, black graph) and the refolded Drp2p (Fig. 5.10, grey graph) was possibly due to experimental variation because GTP on its own shows a higher "activity" than the Drp2 protein. Duplicate measurements were not taken because of the absence of activity in the first measurements.

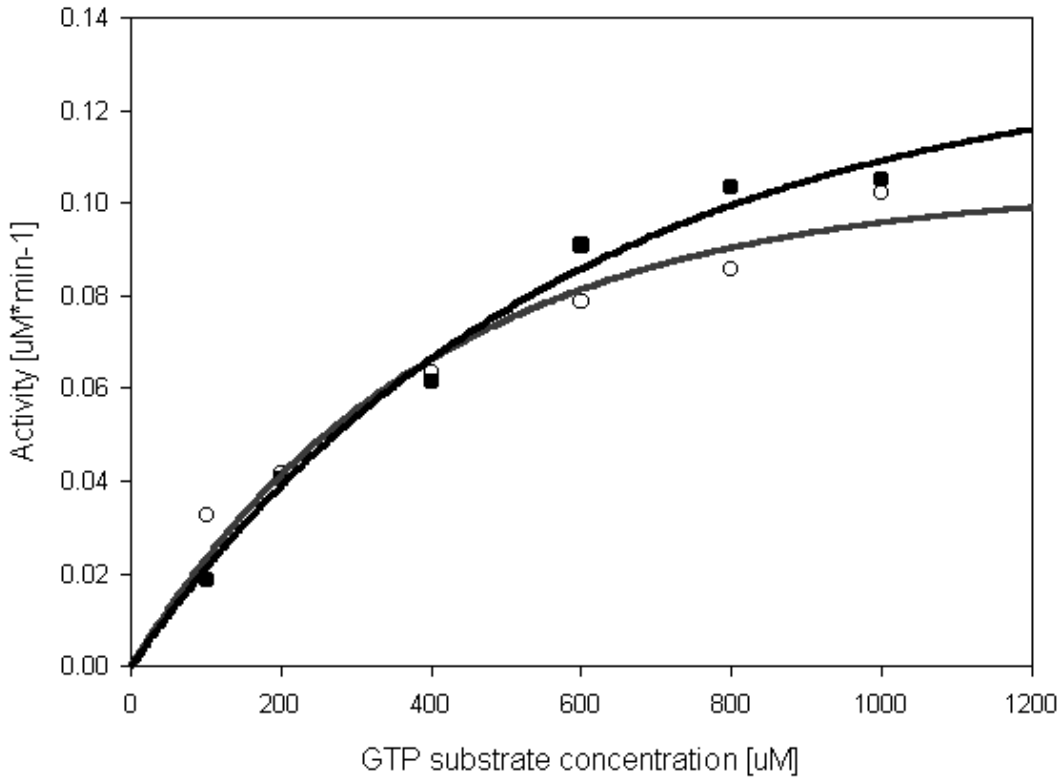

Figure 5.10 Michaelis-Menten kinetics of refolded recombinant EhDrp2p. NADH coupled assay showing the activity of the refolded EhDrp2p (grey) in comparison to the "activity" of auto-degrading GTP (black). X-axis: increasing concentrations of GTP. Y-axis: activity in μM/min. 10 μg refolded Drp2p were used in the assay.

The most obvious difference between the two assays is the buffer components (chapter 2, section 2.1.9). The reaction buffer of the NADH coupled assay might have had a negative effect on Drp2 enzyme activity. Thus the malachite green assay

suggests a successful refolding of denatured recombinant EhDrp2 protein to activity using the refolding protocol employed. However, the NADH coupled assay was not able to show enzyme activity and therefore kinetic parameters of refolded Drp2p could not be analysed.

5.5 Kinetic characterization of soluble recombinant EhDrp2p

Soluble recombinant EhDrp2p was tested for presence of activity using the malachite green assay (Fig. 5.11). It shows an increase in inorganic phosphate with increasing protein concentration, suggesting GTPase activity (Fig. 5.11). The highest measured absorbance was 0.276. This is lower than for refolded Drp2p (Fig. 5.9) and for the previously mentioned rat dynamin-1 involved in endocytosis (Quan and Robinson, 2005).

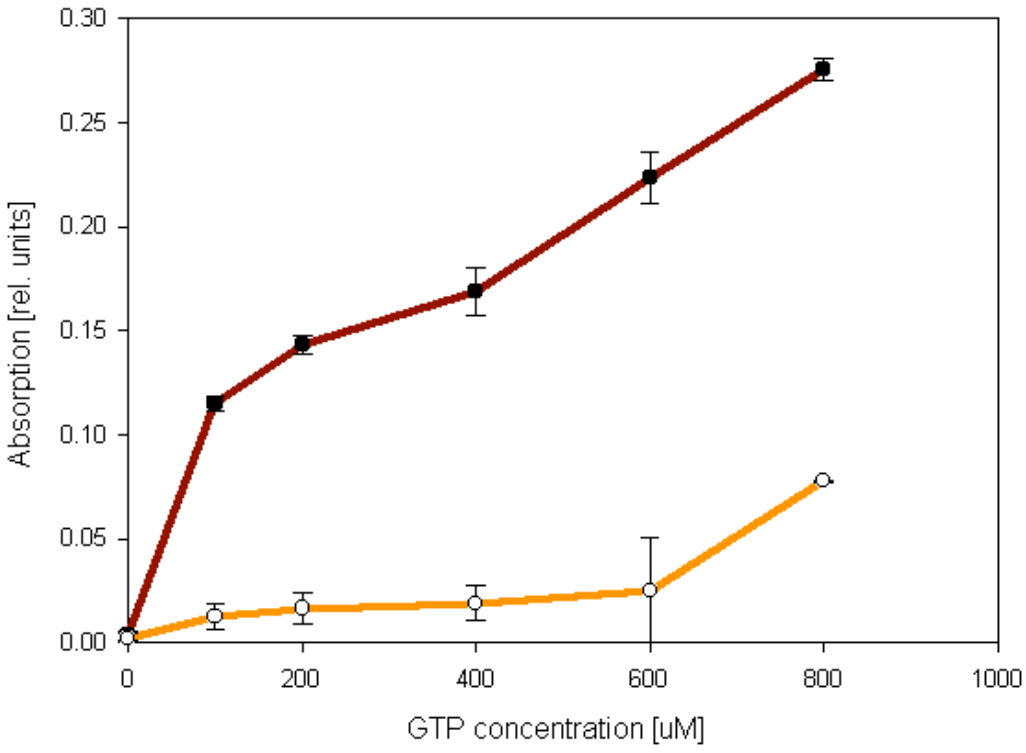

Figure 5.11 Activity measurements of soluble recombinant Drp2p. Malachite green assay showing an increase in inorganic phosphate release with increasing protein concentration in the presence of GTP. (Brown line with black circles)=Drp2p with GTP; (yellow line with white circles)=Drp2p without GTP. GTP alone was used to blank the spectrophotometric

measurements. Error bars show the standard deviated calculated from duplicate measurements.

The control measurements contained no GTP and increasing amounts of Drp2p. Inorganic phosphate was detected indicating the release of small amounts of phosphate from another source. The assay shows a much greater increase of absorption between 0 and 0.1 μg protein concentration than between 0.1 and 0.8 μg of protein concentration used. This suggests that a large amount of GTP is already turned over at low concentrations of Drp2p. To test this, the malachite green assay was repeated with smaller amounts, *i.e.* 10 μg, 20 μg, 30 μg, 40 μg and 50 μg of recombinant soluble Drp2p (Fig. 5.12). The assay shows indeed an approximately 10 times higher production of inorganic phosphate between 10 and 50 μg than between 50 and 800 μg recombinant Drp2p. This information is useful to estimate the amount of recombinant protein required to determine the kinetic parameters of EhDrp2p in the NADH coupled assay because it allows the estimation at which concentrations Drp2p shows measurable activity.

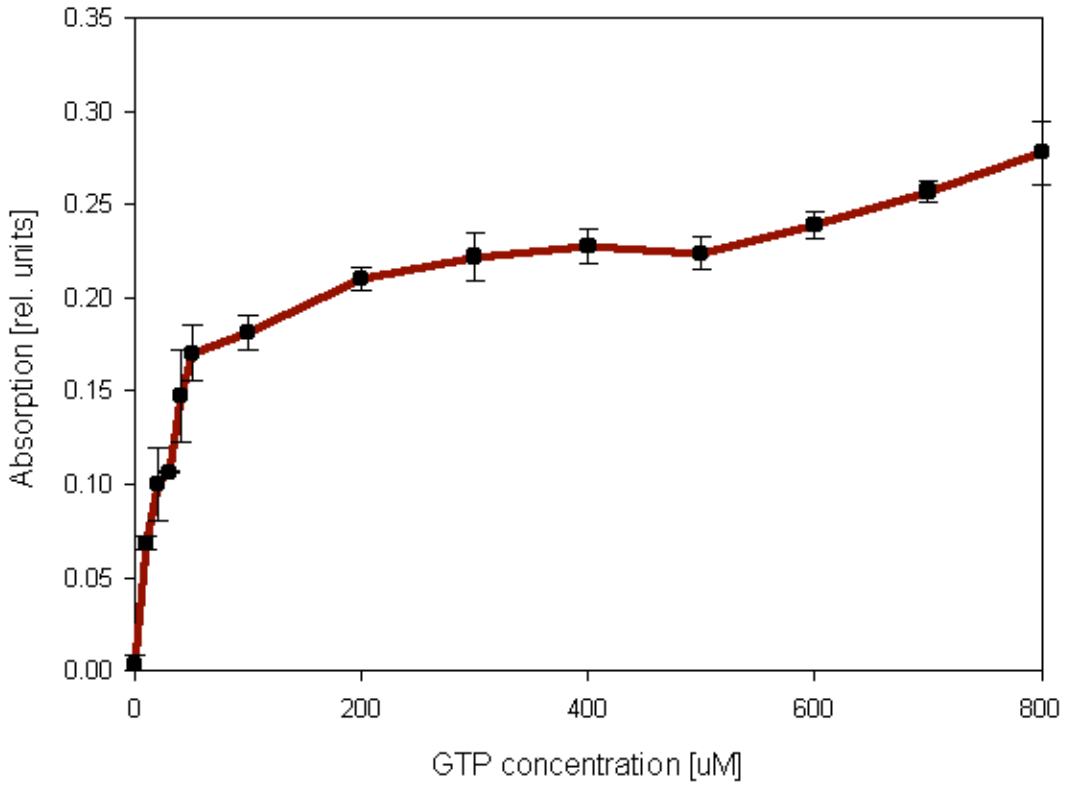

Figure 5.12 Activity measurements of soluble recombinant Drp2p. Malachite green assay showing an increase in inorganic phosphate release with increasing protein concentration in the presence of GTP. Error bars show the standard deviated calculated from duplicate measurements. OD is the optical density.

For the kinetic assay 20 μg/ml Drp2p (= 0.67 μM) and between 20 and 800 μM GTP were used. The dataset followed to the simple Michaelis-Menten equation (Fig. 5.13).

$$v_0 = v_{max} * [S] / K_m + [S]$$

Here, v_0 is the initial velocity of the enzyme, v_{max} represents the maximal velocity, [S] stand for the GTP substrate concentration used in the assay and K_m is the Michaelis-Menten constant.

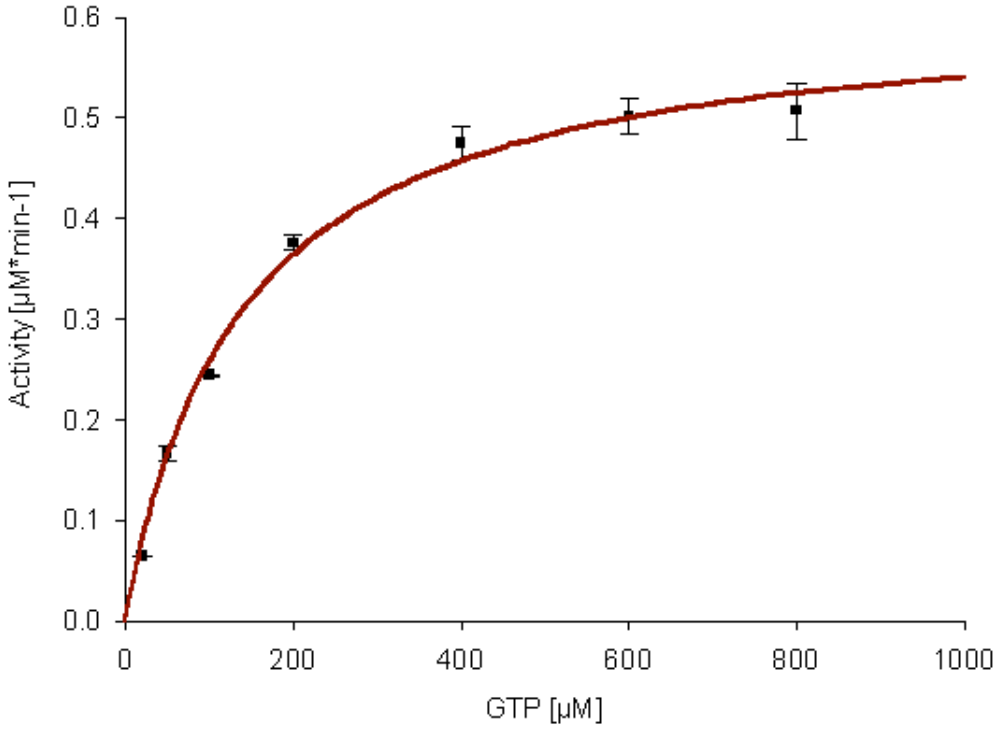

Figure 5.13 Steady state kinetics of recombinant soluble Drp2p. The assay was conducted in duplicates. X-axis=GTP substrate concentration [μM], Y-axis = activity [μM/min]. The assay was conducted in duplicates. The standard deviation was calculated based on the duplicate measurements.

The maximum velocity of recombinant EhDrp2p was calculated as 0.615 μmol/min based on the Michaelis-Menten plot using the SigmaPlot software (Fig. 5.13). The Michaelis-Menten constant resembles the substrate concentration at the point when the enzyme reaches half its maximum velocity. With a K_m of 138.25 +/- 13.62 μM the affinity for GTP is comparable to other members of the dynamin protein family such as the human dynamin-1, the Mx-protein or the yeast mitochondrial fusion dynamin like protein Mgm1 (Richter *et al*., 1995, Song *et al*., 2004a, Chappie *et al*., 2010, Meglei & McQuibban, 2009) (Table 5.2). The Michaelis-Menten constant is an important measure for the affinity of an enzyme to its substrate. The higher the K_m value the lower is the affinity of the enzyme to its substrate. It is clear that Drp2, like the other characterized members of the dynamin protein family, has a low affinity for GTP. This is in agreement with the low basal GTP turnover number (K_{cat}) of 2.3 min^{-1}, which was calculated with the formula below. The turnover number resembles the amount of substrate molecules used by the enzyme per time unit.

$$\mathbf{K_{cat} = v_{max} / [E]}$$

$$K_{cat} = 0.615\ \mu M * min^{-1} / 0.67\ \mu Mol$$

$$\mathbf{K_{cat} = 2.3\ min^{-1}}$$

Table 5.2 Kinetic parameters of different members of the dynamin protein family. Included are the K_M and K_{cat} values as well as the study in which the data were produced. Human dynamin-1 was included twice from two different studies to indicate the range of enzyme activity of the same protein.

Dynamin protein family	K_M [μM]	K_{cat} [min^{-1}]	Study
EhDrp2	138.25 +/- 13.62	2.3	This study
Human dynamin-1	102 +/- 35	2.6	Song *et al*. 2004
Human dynamin-1	65.43 +/- 1.64	1.54	Chappie *et al*. 2009
Human Mx protein	260	27	Richter *et al*. 1995
Yeast Mgm1	308 +/- 6	0.43	Meglei and McQuibban, 2009

Additionally to analyzing protein velocity and substrate affinity, the cooperative behaviour of the enzyme was analyzed by calculating the Hill coefficient. In this context, the Hill coefficient quantified the change of substrate affinity in relation to the enzyme concentration. A Hill coefficient of 1 indicates that substrate affinity is not influenced by protein concentration and that substrate binding is a non-cooperative process. A Hill coefficient less than one indicates a negative cooperative reaction, in which the affinity of the substrate decreases with increasing protein concentrations. Hill coefficients of more than 1 indicate positive cooperative enzyme behaviour, in which enzyme affinity for its substrate increases with increasing amount of enzyme. The kinetic characterization of Drp2 showed a Hill coefficient of n=1.4 +/-0.163 indicating positive cooperation with respect to GTP. Cooperative behaviour based on protein self-assembly to a higher order has been previously observed for yeast Dnm1 (Ingerman *et al*. 2005) and self-assembly to rings and spirals is a typical characteristic of the dynamin protein family (e.g. Hinshaw and Schmid 1995, Richter *et al*. 1995, Ingerman *et al*. 2005, Chappie *et al*. 2009, Gao *et al*. 2010). This is supported by the observation that recombinant Drp2p sediments during ultracentrifugation suggesting self-assembly to higher order structures (Fig. 5.14). First, Drp2p was centrifuged at 100,000 x g to pellet polymerized protein. The supernatant with the unpolymerized protein was incubated for 1 hour at room temperature and then centrifuged for 20 minutes at 100,000 x g. The pellet and the supernatant fraction were dissolved in SDS loading buffer and separated on an SDS gel. The soluble as well as the pellet fraction contained Drp2 protein. This indicates that some protein assembled to larger order structures, which sedimented during centrifugation whereas unassembled protein remained in the supernatant (Fig. 5.14).

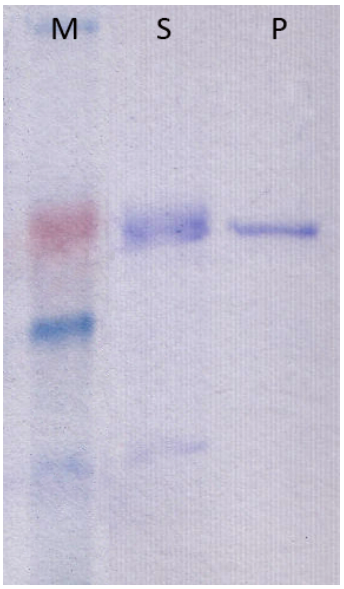

Figure 5.14 Higher order structure formation of recombinant EhDrp2p. 12% SDS gel showing EhDrp2p after a sedimentation assay. S = soluble fraction, P = pellet fraction, M = protein marker. A fraction of the protein stays in the supernatant after centrifugation at 100,000 x g for 20 min suggesting that some protein does not aggregate. Whereas a part of the Drp2p pellets during centrifugation, suggesting assembly to larger structures.

In summary, *Entamoeba histolytica* Drp2p was successfully produced in the bacterial expression systems *E. coli* BL21 and *E. coli* Rosetta 2. The expression in *E. coli* BL21 cells yielded insoluble recombinant protein whereas *E. coli* Rosetta 2 produced soluble Drp2p. Insoluble Drp2p was successfully refolded to functionality. The kinetic characteristics v_{max}, K_m and K_{cat} of the soluble recombinant Drp2p are similar to previously analysed members of the dynamin protein family and show low affinity and turnover of the GTP substrate. The Hill coefficient indicates cooperative behaviour of Drp2p with respect to GTP in accordance with other members of the dynamin protein family. Drp2 was localized into distinct punctate structures, which are evenly distributed throughout the cytosol.

6 Overexpression of EhDrp2 in *E. histolytica* and *D. discoideum* and complementation in *D. discoideum*

Members of the dynamin protein family are important in membrane alterations in eukaryotes and are involved in fundamental cell processes such as organelle dynamics, endocytosis and cytokinesis (Praefcke & McMahon, 2004). Most information about the dynamin protein family is based on model-organisms such as human, yeast and thale cress. However, in the last 15 years research extended to protist lineages including *Dictyostelium discoideum* (Niemann *et al*., 2001, Wienke *et al*., 1999, Schlosser *et al.*, 2003, Miyagishima *et al*., 2008, Rai *et al*., 2010), *Tetrahymena thermophila* (Elde *et al*., 2005, Rahaman *et al.*, 2008) and *Trypanosoma* (Morgan *et al*., 2004, Chanez *et al*., 2006). Several studies on dynamin related proteins in protists revealed novel functions and cellular localizations (Elde *et al*. 2005, Rahaman *et al*. 2008, Gaechter *et al*. 2008, Rai *et al*. 2011). *Entamoeba histolytica* possesses four dynamin related proteins of which EhDrp1 and EhDrp2 exhibit the classical domain structure, GTPase domain, middle domain and GTPase effector domain, known from members of the dynamin protein family. In order to analyse the function of EhDrp2 *in vivo*, the gene was re-introduced into *E. histolytica* using the specific constitutive expression vector pAH-DEST (Abhyankar *et al*. 2009). This vector continuously expressed extrachromosomal copies of EhDrp2. Furthermore, complementation experiments with EhDrp2 in the closely related free-living, non-parasitic amoebozoan *Dictyostelium discoideum*, which did not contain the homologous DymA, were performed. Additionally, the over-expression of EhDrp2 in *D. discoideum* wild type cells was analysed.

6.1 Cloning of EhDrp2 in the *Entamoeba histolytica* expression vector pAH-DEST

EhDrp2 was amplified using the primer set EhDrp2_FlagF and -R. PCR resulted in a fragment of approximately 2.000 bp (Fig. 6.1). The reverse primers contained the Flag-tag sequence ‘GATTATAAAGATGATGATGATAAA’ to add a C-terminal Flag-tag

(DYKDDDDK) to the EhDrp2 gene before the stop codon (Fig. 6.1, Chapter 2, section 2.1.3).

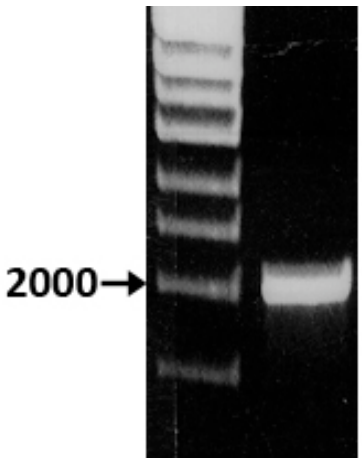

Figure 6.1 Amplification of EhDrp2 for the *Entamoeba histolytica* specific gene amplification vector pAH-DEST. The picture shows EhDrp2 with the expected fragment size of 2016 bp, which includes the 1992 bp gene and the 24 bp long Flag-tag. The 1 kb DNA marker is shown on the left of each image. The 2000 bp band of the DNA marker, which is important for the size estimation of the PCR fragments, is indicated on the left.

The pAH-DEST expression vector is a modified Gateway destination vector, which is part of the recombination Gateway cloning system (Invitrogen). It contains an *E. histolytica* ferredoxin promoter at the N-terminus of the cloning site, which results in the strong expression of the inserted target gene (Abhyankar *et al*. 2009). A detailed description of the Gateway vector pAH-DEST can be found in chapter 2, section 2.2.12. The fragment of interest was first ligated into the Gateway entry vector pCR8/GW/TOPO (Invitrogen) via TA-cloning. The TA-cloning site is flanked by recombination sites, which match equivalent sequences at the cloning site in the Gateway destination vector. The insert DNA was shuttled from the Gateway entry vector into the Gateway destination vector pAH-DEST by recombination. The construct was verified by full-length gene sequencing with the standard primers M13 F and M13 R and the gene specific primers Eh_Drp2_FlagF and Eh_Drp2_FlagR (Table 2.3). Initially, lipofection using Superfect reagent (Qiagen) was applied to chemically transfect *E. histolytica* with pAHDEST-EhDrp2. However, lipofection failed repeatedly

and subsequently electroporation was used to gain the recombinant *E. histolytica* strain. *E. histolytica* cells in logarithmic growth phase were used for transfection by electroporation with 100 μg of the pAHDEST-Drp2 construct. Expression vector pAH-DEST contains a hygromycin resistance cassette to select for transfected cells. *E. histolytica* transfected with the pAHDEST-Drp2 construct will be referred to as Ehis-Drp2 from here on. Ehis-Drp2 was grown in hygromycin containing selective TIY medium, starting with a low concentration of hygromycin and gradually increasing the dose to a final concentration of 40 μg/ml. Once stable transgenic cultures were established, cells were harvested and analyzed by fluorescent microscopy.

6.2 The *Ehis*-Drp2 strain show more nuclei than wild type strain

Dynamin and dynamin related proteins have been found to be involved in cellular modifications, e.g. cell division, organellar plasticity and cytoskeletal associations and EhDrp1 has found to be nuclear associated (Jain *et al*. 2010).

Wild-type *E. histolytica* and Ehis-Drp2 cultures were harvested by centrifugation, fixed in 3.7 % formaldehyde/PBS and stained with DAPI to visualize nuclei. The majority of wild type *E. histolytica* cells exhibited one or two nuclei (Fig. 6.2) and rarely three or more nuclei (Table 6.1). The nuclei show the typical central dot-shaped karyosome, a compact chromatin body that is characteristic for *Entamoeba* spp.. The chromatin surrounding the inside of the nuclear wall is visible as a dark layer (Fig. 6.2). The round cell shape is most likely due to turgor pressure during fixation. *In vivo* the cells are amoeboid and exhibit various cell shapes.

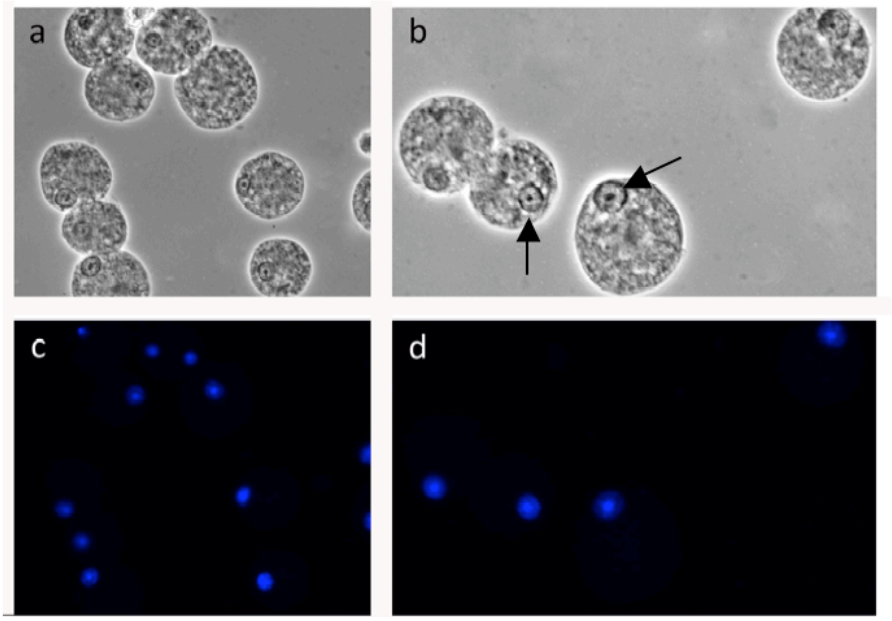

Figure 6.2 *E. histolytica* wild type cells labelled with the DNA dye DAPI. (a) and (b) bright field images showing fixed *E. histolytica* wild type cells. (c) and (d) show the corresponding DAPI stained nuclei. The arrows point at nuclei. The dense karyosome, which is characteristic for *Entamoeba* spp. is located in the middle of the nucleus and clearly visible. Images were taken under oil immersion with a 1.000 x magnification.

In contrast to the *E. histolytica* wild-type cells, Ehis-Drp2 show a significantly elevated number of nuclei (Fig. 6.3).

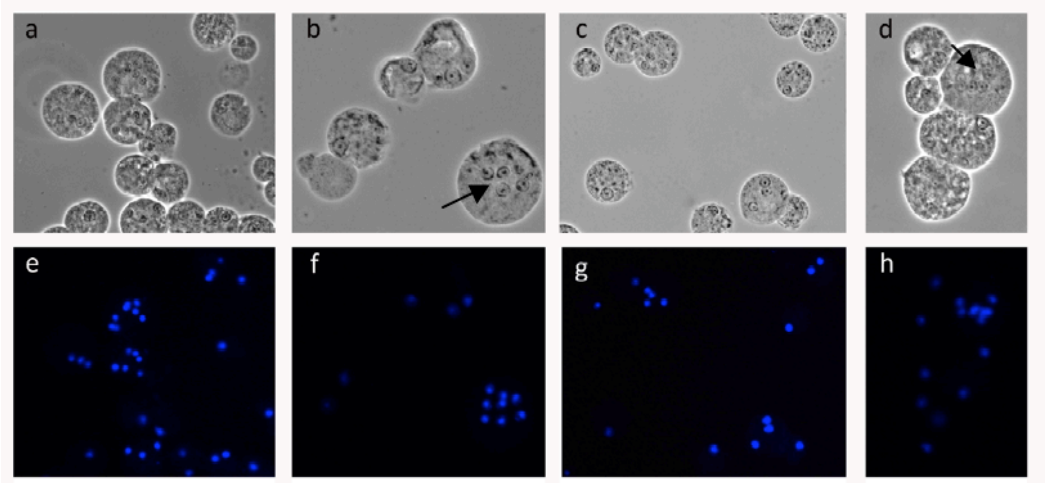

Figure 6.3 Transfected recombinant *E. histolytica* labelled with the DNA dye DAPI. (a)-(d) Bright field images of fixed cells. (e)-(h) DAPI stained cells of the same fields as in panels a-d. The dark spots within the nuclei are the dense karyosomes. Images were taken under oil immersion with a 1,000 x magnification.

The nuclei from *E. histolytica* wild type cells and Ehis-Drp2 were counted and analysed statistically. The percentages with which uni-nucleate, bi-nucleate and multi-nucleate cells in the wild type strain occur is comparable to previous analyses (Mukherjee *et al.*, 2008, Mukherjee *et al.*, 2009). In order to analyse whether the frequency with which multiple nuclei occur depends on the cell type, the G-test of independence (log-likelihood ratio test) was applied. Two separate null hypotheses were tested. The null hypothesis assumed that there is no difference in the frequency of multiple nuclei between wild type *E. histolytica* and Ehis-Drp2.

We were able to disprove the null hypothesis and found a highly significant difference amongst both strains (G with William's adjustment = 83.29, df = 4, $P < 0.001$). The wild type strain showed significantly lower numbers of multiple nuclei compared to Ehis-Drp2 strain. Therefore the null hypothesis was rejected.

The experiment was repeated two more times approximately 12 months and 16 months after transfection and in both counts Ehis-Drp2 (12 monts: G with William's adjustment = 14.34, df = 4, $P < 0.05$; 16 months: G with William's adjustment = 18.03, df = 4, $P < 0.01$) still showed a significantly higher number of nuclei in comparison to the wild type although with a less pronounced difference (Fig. 6.4). In addition to creating Ehis-Drp2, we transfected *E. histolytica* with the empty pAHDEST vector (Ehis-pAHDEST) to construct a control strain. After 16 months of establishing the Ehis-Drp2 and Ehis-pAHDEST, we also compared the difference in the number of nuclei between the wild type strain and the control strain and found no significant difference between them (G with William's adjustment = 1.58, df = 4, $P > 0.1$). Thus we can conclude confidently that the overexpression of Drp2 in *E. histolytica* leads to an increase in the number of nuclei.

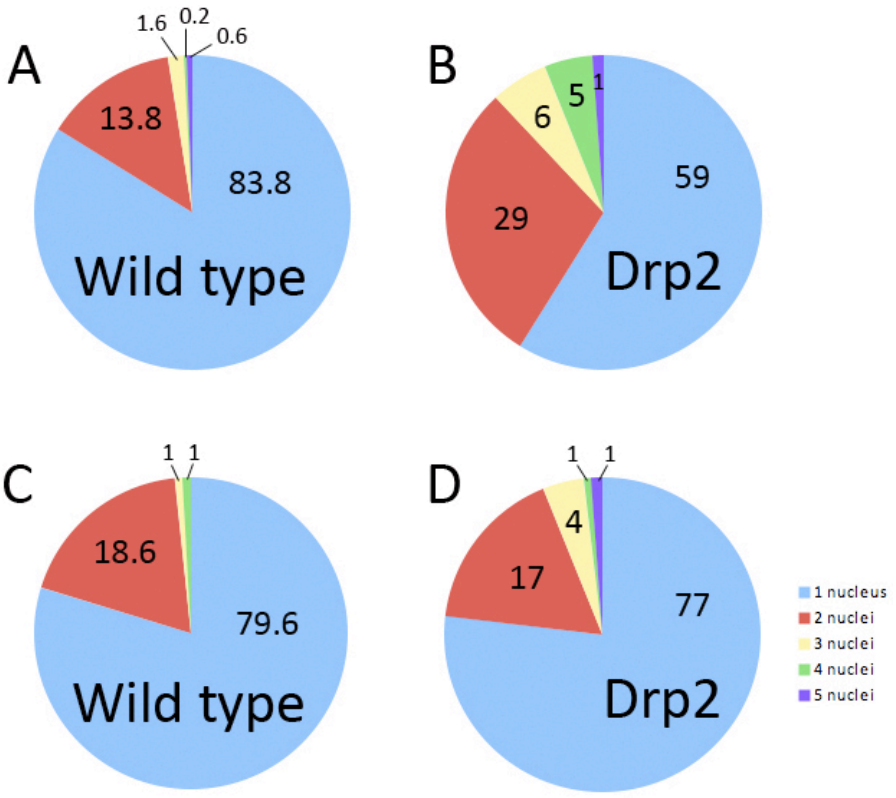

Figure 6.4. Number of nuclei per cell in *E. histolytica* wild type and Ehis-Drp2. The number of nuclei is presented in percentages in the pie. (A) Percentage of nuclei in wild type *E. histolytica*. (B) Percentage of nuclei in Ehis-Drp2. (C) and (D) result from a second nuclei count approximately one year after transfection. (C) Percentage of nuclei in wild type *E. histolytica.* (D) Percentage of nuclei in Ehis-Drp2. The number of nuclei was counted from formaldehyde-fixed and DAPI stained cells. At least 300 cells per sample were counted to determine the amount of uni-nucleated, bi-nucleated and multi-nucleated cells.

The phenomenon of multiple nuclei in *E. histolytica* has been observed in previous studies (Mukherjee *et al*. 2008, 2009). It appears to be an intrinsic property of *E. histolytica* to have cytokinesis spatially and temporally separated from the nuclear cycle (Mukherjee *et al*. 2008, 2009). The amount of multiple nuclei in the wild type of *E. histolytica* strain HM-1: IMSS in these studies was found to be approximately 1.7 %. This is in agreement with the data on wild type cells presented here.

Interesting is the decrease of number of multiple nuclei in Ehis-Drp2 over time. Adaptation of the cells to the over-expression of Drp2 may provide a possible explanation for the decrease in the number of nuclei (personal communication with Prof. Dietmar Manstein, Hannover, Germany).

6.3 Localization of Drp2 using Flag-tag antibodies against C-terminal Flag-tag

Confocal microscopy experiments using monoclonal antibodies against the C-terminal Flag-tag of Drp2 indicate localization to the margins of the cell (Fig. 6. 5).

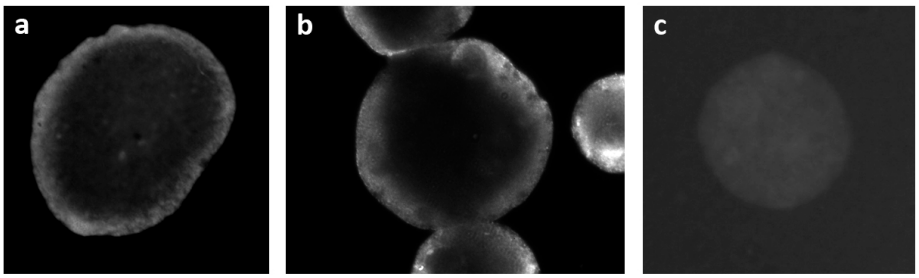

Figure 6.5 Drp2p localization in recombinant *E. histolytica*. (a) and (b) putative localization of Drp2 in the Ehis-Drp2 strain. (c) Negative control in which Ehis-Drp2 cells were not incubated with the Flag-tag antibody but were otherwise treated the same.

The localization of Drp2 suggests that the protein might play a role at the margins of the cell. However, the specificity of the monoclonal antibody was tested in Western blot analysis on total isolated protein from Ehis-Drp2. The response was high but not specific (Fig. 6.6). The expected Drp2-Flag-tag protein size was approximately 75 kDa. However, the strongest band on the Western Blot appeared at approximately 30 kDa.

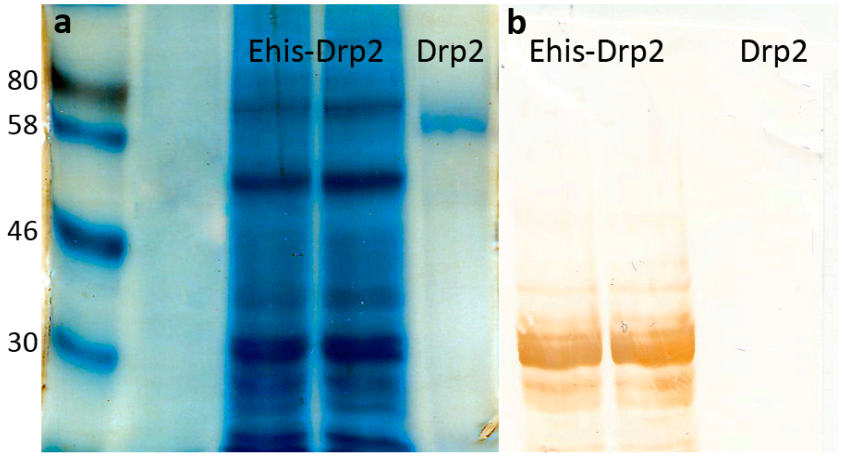

Figure 6.6 Flag-tag specificity on total protein of Drp2-*E. histolytica*. (A) 12 % SDS polyacrylamide gel showing total amounts of Drp2-*E. histolytica* cell protein (=Drp2-OE) and recombinant Drp2 protein to show expected size of cellular Drp2. (B) Corresponding western blot of Flag-tag antibody.

This indicates that the fluorescent signal measured by confocal microscopy might have been due to unspecific binding of the primary antibody rather than localization of EhDrp2. Furthermore, localization experiments conducted with monoclonal Drp2 antibody suggest a cytosolic distribution rather than an accumulation at the cell membrane (chapter 4).

6.4 Cell shape alteration in the Ehis-Drp2 strain

Ehis-Drp2 cells showed an unusual morphological feature that frequently occurred during their growth (Fig. 6.7) but was very rarely found in the wild-type strain or Ehis-pAHDEST.

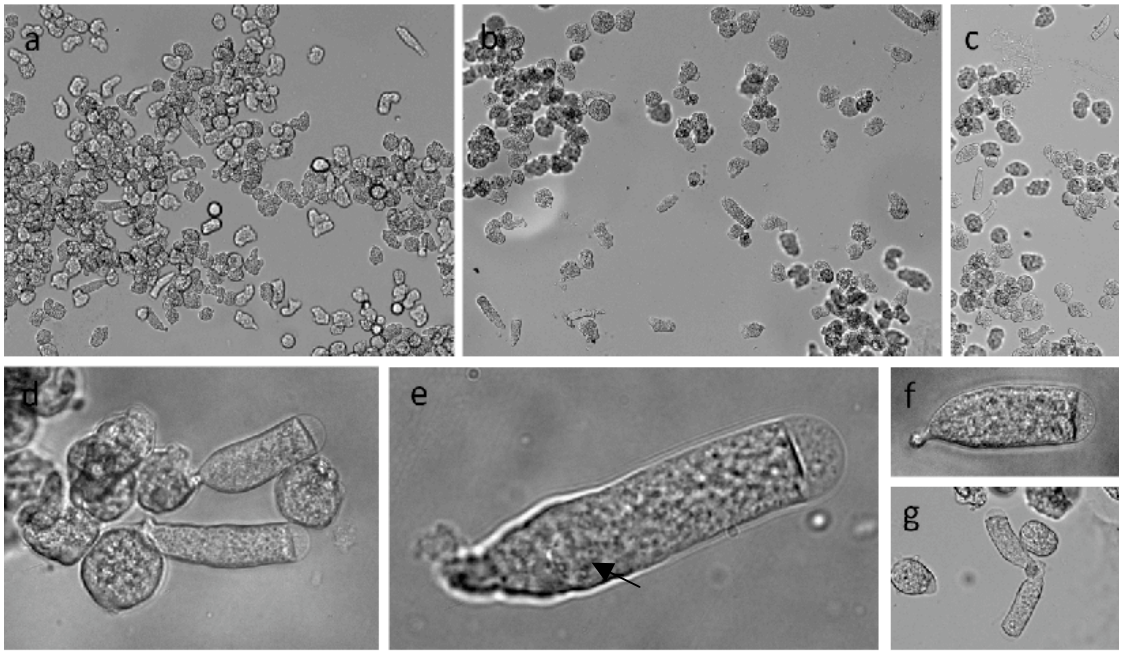

Figure 6.7 Light microscopy images from Ehis-Drp2 cells. Some cells exhibit a distinct 'bottle' shape with a clear direction, a conical disc-like attachment and a clear rounded apex. (a)-(c) overview of cell culture at 100 x magnification. (d)-(e) The 'bottle'-shaped phenotype in detail. The arrow points at the nucleus. The cells were photographed in their culture tubes to avoid oxygenation and other stresses.

The cells were 'bottle'-shaped and did not show the morphological plasticity of an amoeboid *E. histolytica* cell. They were only attached to the surface by a small disk-like protrusion (Fig. 6.7 e, f) or detached from the surface completely. The end of the cell was occupied by a clear vacuolar structure and cell plasma did not extend in this region when circulating in the cell. However, not all cells exhibited this altered phenotype (Fig. 6.7 a-c). The clear influence on cell morphology indicates a cytokinesis defect that leads to an altered cellular shape, the absence of amoeboid movement and impairment in cell to surface attachment. Dynamin related proteins have previously been found to be involved in cellular morphology in other organisms (Wienke *et al.*, 1999, Rai *et al.*, 2010, Gu *et al.*, 2010). The bottle shaped phenotype was also observed in wild type *E. histolytica* under stress conditions such as suboptimal bovine serum in the medium (Dr. Graham Clark, London School of Hygiene and Tropical Medicine, UK, personal communication). Therefore, it might be difficult to link the change in cell morphology confidently to a specific function of

Drp2 in *E. histolytica*. Nevertheless, we can conclude that the overexpression of Drp2 resulted in the strong morphological alterations described above.

6.5 Actin cytoskeleton organization differs in Ehis-Drp2

In order to understand the morphological changes in Ehis-Drp2, the cells were treated with the actin fluorescent stain rhodamine-phalloidin (Fig. 6.8). The wild type strain exhibited a homogenous distribution of actin throughout the cell and partial accumulation at the margins, which is in accordance with previous observations (Chavez-Munguia *et al.*, 2008). The bottle-shaped Ehis-Drp2 cells however reveal a strong accumulation of actin in the "attachment" disk indicating a disturbance in cytoskeletal organisation as a result to the overexpression of Drp2.

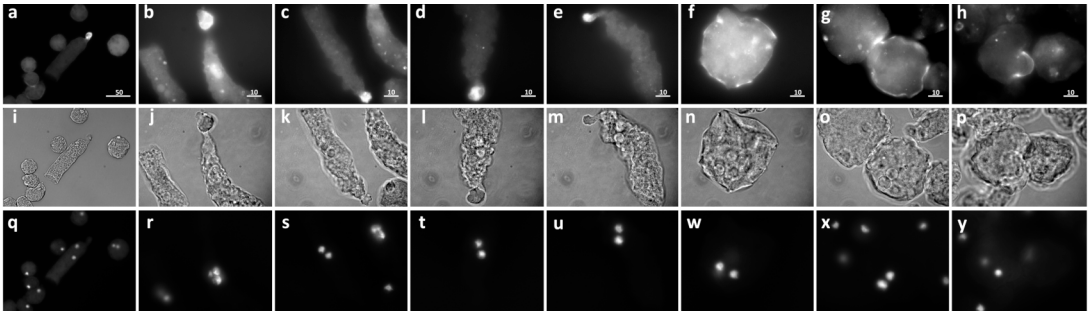

Figure 6.8Distribution of actin in Ehis-Drp2 and *E. histolytica* wild type cells. (a)-(h) show cells stained with rhodamine-phalloidin. (i)-(p) show corresponding bright field images. (q)-(y) show nuclear DNA stained with DAPI. (a)-(e), (i)-(m) and (q)-(u) display Ehis-Drp2. (f)-(h), (n)-(p) and (w)-(y) show wild-type *E. histolytica* strain. Scale bar=10 μm (except for a, i and q with a scale bar=50 μm).

Interaction between dynamin and the actin cytoskeleton and has been previously found in human cells (Gu *et al.*, 2010). Our data indicate that this association might be also be present in *Entamoeba*.

6.6 Ehis-Drp2 grows slower than *E. histolytica* wild type

The Ehis-Drp2 strain was found to grow slower than the control strain Ehis-pAHDEST (Figs. 6.9 and 6.10). The growth of all strains was monitored by counting cells with a hemocytometer every 12 h (Fig. 6.9).

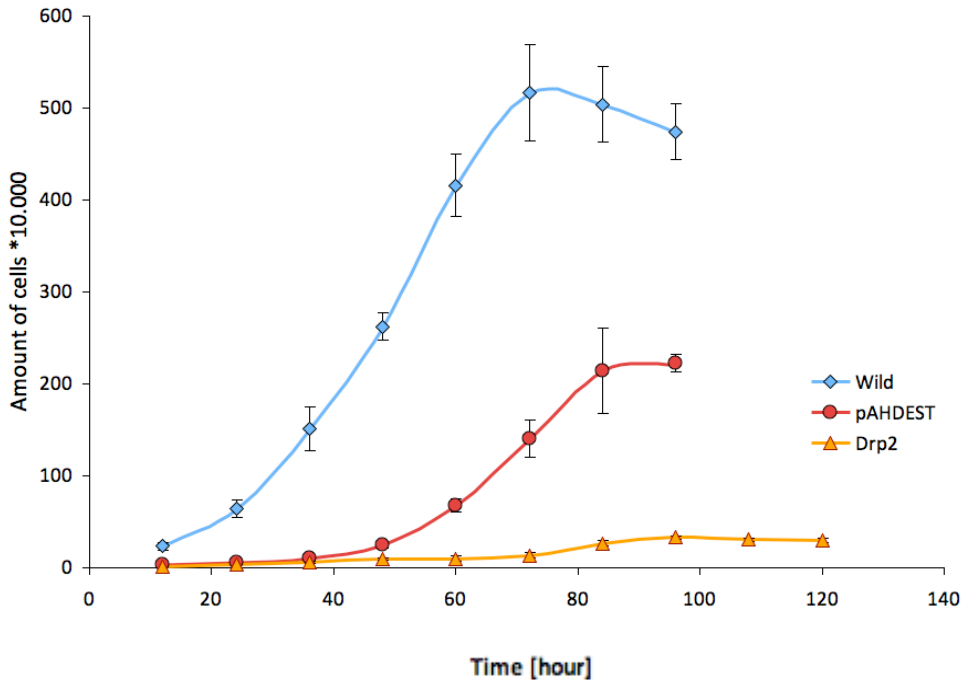

Figure 6.9 Cell counts of *E. histolytica* wild-type and recombinant strains. X-axis=time in hours, y-axis=number of cells times 10,000. The blue line represents wild-type *E. histolytica*, the red line shows the cell count results from the control strain Ehis-pAHDEST and the yellow line shows the Ehis-Drp2 growth curve. The error bars indicate the standard deviation from 12 technical counting repetitions in the hemocytometer. The error for Drp2 measurements are very small and therefore difficult to see.

Analysis of growth rates indicates that the expression of recombinant Drp2 had a negative effect on *E. histolytica* cell growth. Slow growth might be due to the presence of the antibiotic hygromycin that was used to select for Drp2-pAHDEST positive cells during culturing. However, there was also a difference between the control strain Ehis-pAHDEST and Ehis-Drp2, which suggests that an additional factor influences cell growth. Using flow cytometry for Ehis-pAHDEST and Ehis-Drp2 a similar growth pattern was observed (Fig. 6.10).

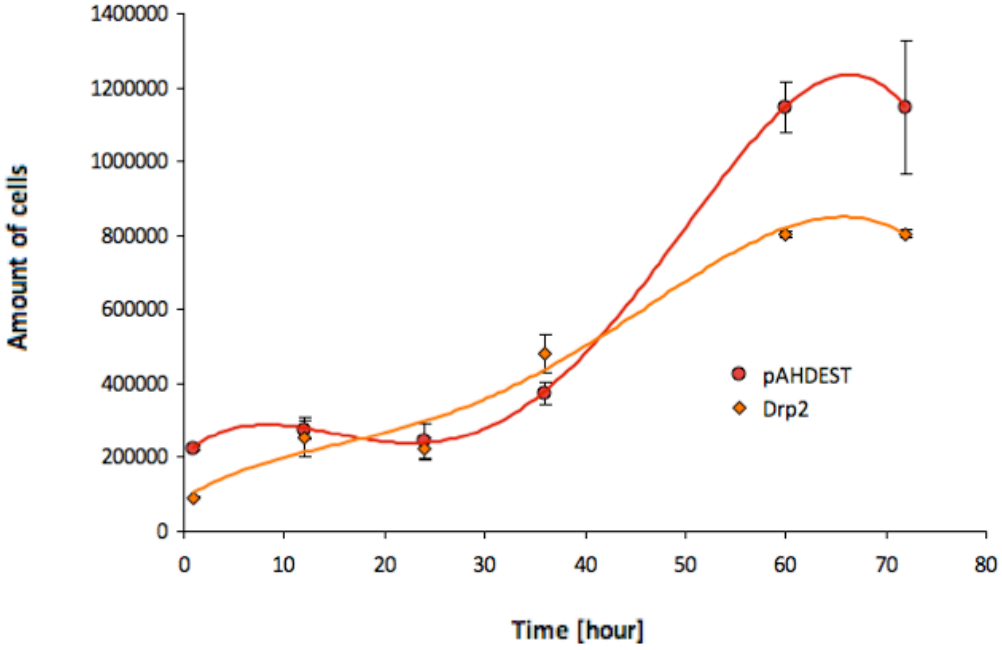

Figure 6.10 Cell counts for recombinant *E. histolytica* strains using flow cytometry. X-axis = time in hours, y-axis = number of cells counted by flow cytometry. The red line shows the pAHDEST control strain growth curve, the yellow line shows the Ehis-Drp2 growth curve. The error bars indicate the standard deviation based on counts of duplicate cultures.

6.7 Drp2 protein levels in wild type *E. histolytica* and Ehis-Drp2 do not differ

Western Blot analysis on total protein from wild-type *E. histolytica* and Drp2-*E. histolytica* using specific polyclonal EhDrp2 antibody does not show an elevation in Drp2 protein levels in the recombinant strain (Fig. 6.11).

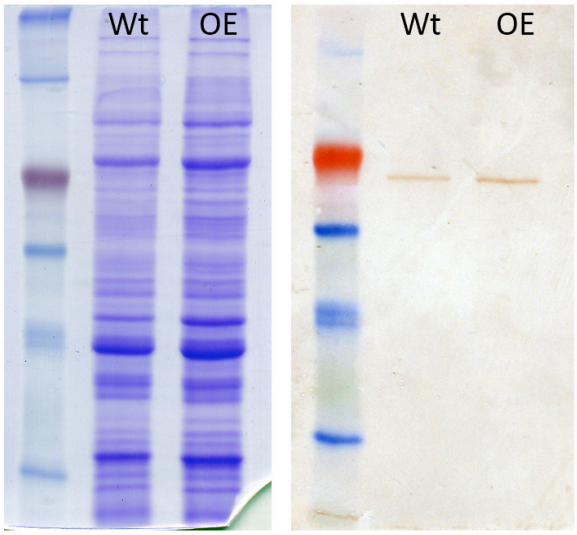

Figure 6.11 Analysis of EhDrp2 over-expression in *E. histolytica*. The image on the left side shows a 12 % SDS polyacrylamide gel with total cell protein of wild type *E. histolytica* cells (=Wt) and total cell protein from Drp2-*E. histolytica* cells (OE=over-expression). The image on the right displays the corresponding Western blot. Anti-Drp2 antibody was used to detect cellular and recombinant Drp2 in both strains.

This indicates that recombinant Drp2 protein was either not expressed or expressed at low levels. The second assumption is favoured because differences between the control strain Ehis-pAHDEST and Ehis-Drp2 were observed.

6.8 Dym A$^-$ complementation and Drp2 overexpression in *Dictyostelium discoideum*

This work was conducted in collaboration with Dr. Amrita Rai in Prof. Dietmar Manstein's research group from the Medical School Hannover, Germany. PCR, fragment digestion and vector digestion as well as cloning was conducted by myself, while the transfection, imaging and culturing of *D. discoideum* was carried out by Dr. Amrita Rai.

D. discoideum is a free living amoebozoan and closely related to *E. histolytica*. It contains five dynamin related proteins of which two, DymA and DymB, are similar in protein domain structure to EhDrp1 and EhDrp2. To investigate the function of

EhDrp2 *in vivo*, a DymA negative *D. discoideum* mutant (Wienke *et al*. 1999) was transfected with the Drp2-pDXA-3H construct to analyse if the phenotype, caused by the absence of DymA in the cell, could be complemented by recombinant extrachromosomal EhDrp2. The DymA null cells differ morphologically from the wild-type strain Ax2. The DymA null cells grow approximately twice as slow, show multiple nuclei and alterations of mitochondrial, nuclear and endosomal morphology (Wienke *et al*. 1999). The absence also causes defects in cellular division. Additional to the complementation experiment, wild-type Ax2 cells were transfected with the Drp2-pDXA-3H vector to investigate the effects overexpression of Drp2 might have on the cell.

6.8.1 Construction of the EhDrp2-pDXA-3H vector

For the construction of the EhDrp2-complementation vector, the EhDrp2 gene was amplified by PCR and subcloned into the cloning vector pGEM-T-Easy first. The DNA insert was excised from the TA-cloning construct with the restriction enzyme *Kpn*I (Fig. 6.12) and cloned into the multiple cloning site of the pDXA-3H expression vector (Manstein *et al*., 1995)(Fig. 6.13), which has a constitutive *Dictyostelium discoideum* actin promoter and a C-terminal His-tag.

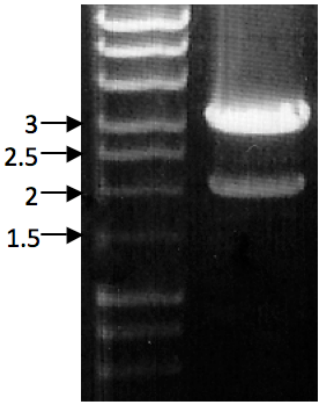

Figure 6.12 Drp2 for pDXA-3H in pGEM-T-Easy. 1 % TAE gel showing the restriction digest of Drp2 out of pGEM-T-Easy with the restriction enzyme *Kpn*I. On the left hand side of the gel is the DNA marker with the molecular weight bands of interest indicated by an arrow and the corresponding sizes in kb. On the right hand side is the digested vector product (pGEM-T-Easy) at approximately 3.1 kb and Drp2 for pDXA-3H below at approximately 1.9 kb.

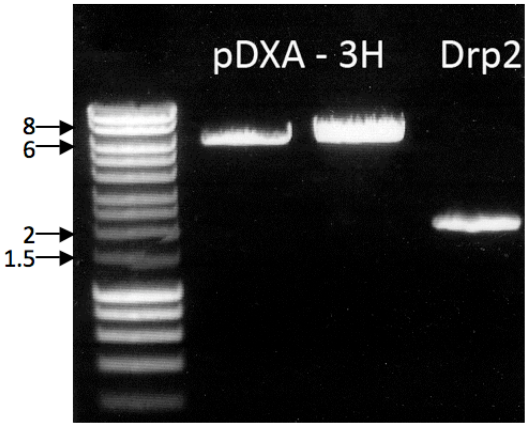

Figure 6.13 EhDrp2 fragment and *D. discoideum* vector pDXA-3H. 1 % TAE agarose gel showing the digested vector and digested Drp2 fragment. The expected fragment sizes are 6.1 kb for the vector and 1.9 kb for Drp2.

The plasmid construct was verified by restriction digest and sequencing.

6.8.2 Drp2 does not complement DymA

DymA is involved in the division of mitochondria in *D. discoideum*. Mitochondria in the wild-type *D. discoideum* cells are round or oval shaped distinct organelles that are dispersed throughout the cell (Fig. 6.14a). The DymA null cells show strong alterations in the morphology of mitochondria and the cells are larger than the wild-type cells (Fig. 6.14b). In order to analyse whether Drp2 complements DymA, the mitochondrial morphology in *D. discoideum* was observed by using anti-mitoporin antibody. Mitochondrial porins are situated in the outer membrane of mitochondria.

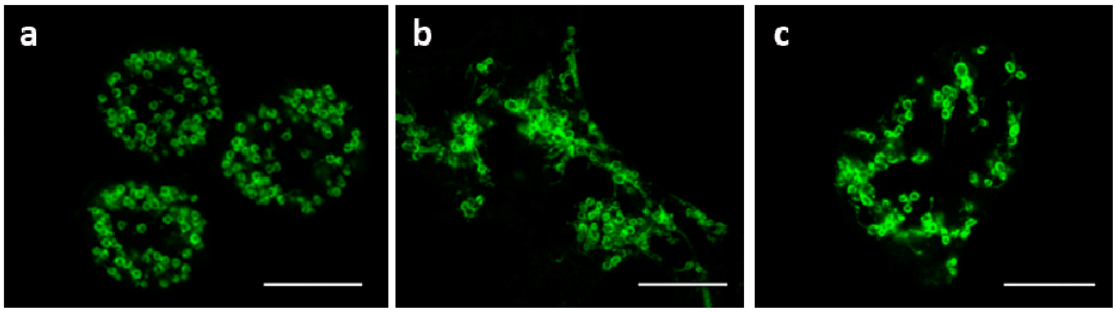

Figure 6.14 *D. discoideum* mitochondrial morphology from wild-type cells, dymA null cells and EhDrp2 complemented dymA null cells. The outer mitochondrial membranes were stained with anti-mitoporin antibody. (a) *D. discoideum* wild-type cells. (b) *D. discoideum*

DymA null cells. Visible is the altered mitochondrial morphology in comparison to the wild-type. (c) Negative complementation of DymA null cells with EhDrp2. The altered mitochondrial morphology is comparable to DymA null cells that were not transfected with the Drp2-pDXA-3H construct. Scale bar = 10 µm.

The absence of DymA in *D. discoideum* leads to mitochondrial aggregates and mitochondria show tubulation and branching because they cannot divide (Wienke *et al*. 1999). Furthermore, cytokinesis is affected and cells grow larger and exhibit multiple nuclei (Wienke *et al*. 1998).

DymA null cells transfected with the Drp2-pDXA-3H construct show similar mitochondrial morphology as untransfected DymA null cells. The mitochondria form aggregates and tubulated structures. Therefore it can be concluded that Drp2 was not able to complement DymA in DymA null cells (Fig. 6.14c).

A likely explanation for the absence of complementation could be the lack of functional similarity between DymA and EhDrp2. Alternatively, domains important for substrate-protein interaction in *D. discoideum* might not be present in EhDrp2. The overall amino acid sequence similarity is high (66 %) but they differ strongly in the variable region between the middle and the GTPase effector domain, which might be important for substrate-protein interaction (Fig. 6.15, Chapter 4) (Gao *et al*., 2010, Mears *et al*., 2010, van der Bliek & Payne, 2010). The variable region in DymA is 243 amino acids long and rich in glutamine, serine and asparagine, in EhDrp2 it contains only 63 amino acids and shows an increase in glutamine (Fig. 6.15).

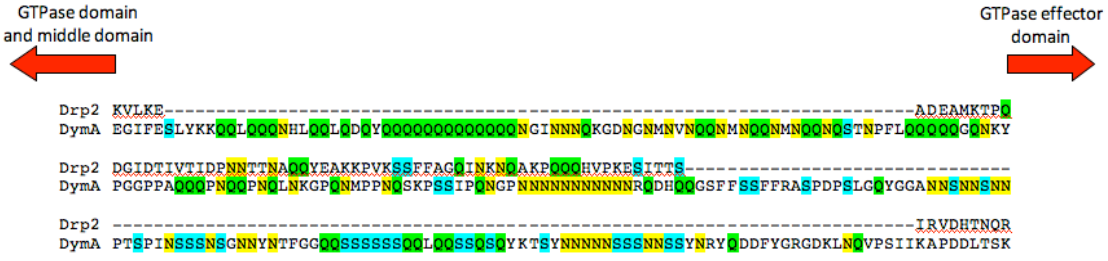

Figure 6.15 EhDrp2 and DymA variable region between the middle and the GTPase effector domain. Red arrows indicate the adjacent domains to the N- and the C-terminus. The colours emphasise repetitive amino acids in DymA and are highlighted accordingly in EhDrp2. Green=glutamine, yellow=asparagine, blue=serine.

Even if both proteins had similar functions, the lack of appropriate sequence similarity, especially in the variable region, might hinder EhDrp2 to complement the absence of DymA.

6.8.3 Overexpression of EhDrp2 in *D. discoideum* affects cell morphology

In addition, to complementation experiments in DymA null cells, EhDrp2 was over-expressed in the *D. discoideum* Ax2 wild-type cells. To test effects of EhDrp2 over-expression on cell morphology, cells were stained with anti-α tubulin antibody and DAPI nuclear stain as well as anti-mitoporin antibody (Figs. 6.16 and 6.17). In EhDrp2 over-expressing *D. discoideum* cells the mitochondrial morphology is altered to a branched and tubular network resembling the phenotype found in DymA null cells (Fig. 6.16). Whereas the wild-type cells show the typical spherical mitochondria, DymA null cells and EhDrp2 over-expressing cells show aggregated and tubulated mitochondrial morphology. EhDrp2 over-expressing cells seem to show an even stronger disruption of mitochondrial organelle integrity than DymA null cells (Fig. 6.16). The wild-type cells display the typical α-tubulin pattern found in *D. discoideum* during interphase (Fig. 6.17). The microtubule organization centre (MTOC) is visible as a dense structure from which the microtubules emanate into the cell (white arrow Fig. 6.17). The MTOC sits at the nucleus, which is visible as a dark spherical space in the cell (yellow arrow, Fig. 6.17). During interphase, *D. discoideum* exhibits one MTOC. Over-expression of EhDrp2 in *D. discoideum* leads to large cells with multiple MTOC's and nuclei (Fig. 6.17).

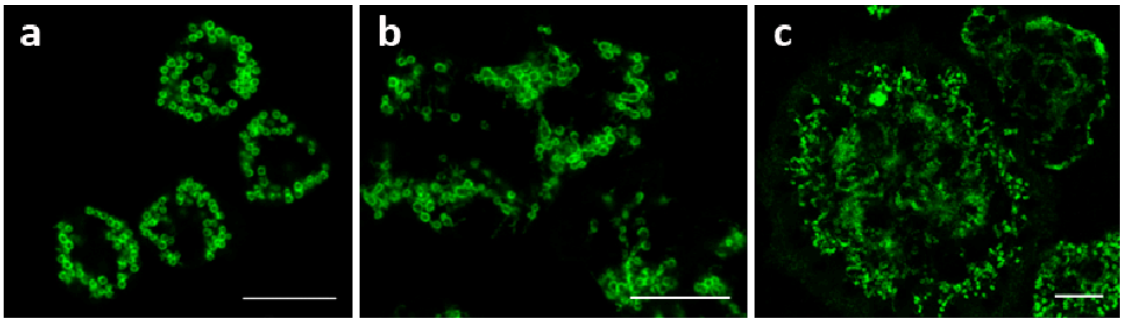

Figure 6.16 Mitochondria in wild-type, DymA null and EhDrp2 over-expressing *D. discoideum* cells. (a) Mitochondria in the wild type strain. (b) Mitochondria in the DymA null strain. (c) Mitochondria in the EhDrp2 over-expressing strain. Mitochondria were stained with anti-mitoporin antibody. Scale bar = 10 μm.

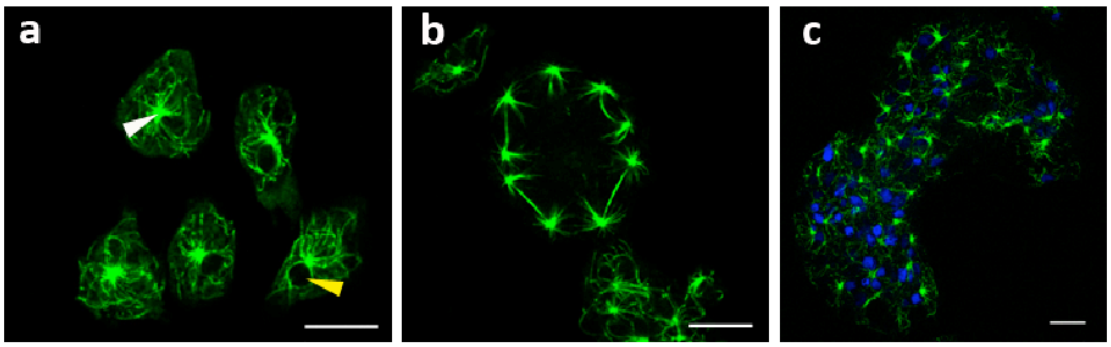

Figure 6.17 *D. discoideum* Ax2 wild-type cells and EhDrp2 over-expressing cells with alpha tubulin morphology. (a) *D. discoideum* wild-type cells. (b) and (c) *D. discoideum* Ax2 cells overexpressing EhDrp2. (b) shows cell in anaphase during mitosis, in which the chromosomes are separated by microtubule spindles. (c) *D. discoideum* Drp2 over-expressing cells with additional DAPI nuclear staining. The wild-type cells show the typical microtubule distribution with the MTOC (white arrowhead) at the nucleus and the microtubule cables stretching into the cell. The yellow arrowhead points at the nucleus. Overexpressing cells show several MTOC's and nuclei per cell. Scale bar=10 μm.

EhDrp2-*D. discoideum* shows functional mitosis by exhibiting normal appearance of bipolar spindles during anaphase (Fig. 6.17b) (Trivinos-Lagos *et al.*, 1993, Gräf, 2009). The presence of multiple nuclei and the increase in cell size indicate a defect during cytokinesis. This morphology has been observed previously in *D. discoideum* cells affected by cytokinesis defects (Wienke *et al.*, 1999, Graf *et al.*, 2000, Muller-Taubenberger *et al.*, 2009, Ishikawa-Ankerhold *et al.*, 2010).

Interestingly, *D. discoideum* cells that overexpress EhDrp2 resemble in their morphology DymA null cells. Thus, the altered cell morphology in *D. discoideum*/EhDrp2 cells could be alternatively caused by the removal of DymA through the presence of EhDrp2 and the inability of EhDrp2 to complement the DymA function. Dynamins and dynamin related proteins oligomerize to higher structures of spirals and rings, with which they bind around membranes during fission events. Responsible for oligomerization are the middle and the GTPase effector domains, which are both very similar in DymA and EhDrp2 (60 % protein

sequence similarity). It is possible that DymA and EhDrp2 oligomerize to higher order in the overexpressing cells. However, there are large differences in the variable region between middle and GTPase effector domain. In a heterogenic assembly of EhDrp2 and DymA, substrate-protein interaction could be impaired resulting in non-functional DymA-EhDrp2 assemblies and a continuous removal of DymA from the cytosol.

In summary, the overexpression of EhDrp2 in *E. histolytica* results in a significant increase in the number of nuclei per cell and a decrease in cell growth. The overexpressing strain exhibits distinct cell shape alterations and shows a strong accumulation of actin at the disk-like protrusion. The cells shape alterations result in the impairment of amoeboid movement and cell-to-surface attachment. All together, this suggests that the overexpression of EhDrp2 causes a cytokinesis defect in *E. histolytica*. The phenotypic changes are comparable to *Dictyostelium discoideum* cells that overexpress *E. histolytica* Drp2. Here, the phenotypic alterations also include the increase in the number of nuclei, changes in cell morphology and a major impact on the ability to perform cytokinesis. Finally, EhDrp2 was not able to complement DymA in *D. discoideum* null cells, indicating that both proteins do not share a common functionality in mitochondrial division.

7 Dynamin related proteins during stage conversion in *E. invadens*

Entamoeba histolytica infects approximately 1 % of the world population with high prevalence in areas with poor socioeconomic and sanitary conditions such as Central America and Southeast Asia (WHO/PAHO/UNESCO-report, 1997). The infectious form of *Entamoeba* spp. is the cyst, while the vegetative cell (trophozoites) causes disease. *E. histolytica* forms cysts in the intestines of humans, and these cysts are released into the environment with faeces. The infection cycle is completed when a new human host ingests the cysts, usually via contaminated water or food. *E. histolytica* ranks third in protist parasite-associated mortality worldwide only preceded by malaria and schistosomiasis (Walsh, 1986, Li & Stanley, 1996). Therefore, it is important to understand the factors that are involved in cyst development.

Studies on *E. histolytica* cysts are difficult because there is no laboratory system to trigger cyst formation present to date. The reptilian parasite *E. invadens* is generally used as a model for *Entamoeba* cyst formation because encystation can be easily induced under axenic conditions *in vitro. E. invadens* is closely related to *E. histolytica*, has the same parasitic life style and infectious behaviour. Therefore, it is reasonable to assume that data gathered about *E. invadens* cyst formation can be applied to *E. histolytica*. Dynamins and dynamin related proteins are involved in various fundamental cellular processes such as membrane remodelling, organelle division, cytokinesis, vesicle scission, and cytoskeleton organization (Mravec *et al.*, 2011, Mears *et al*., 2010, van Dooren *et al*., 2009, Miyagishima *et al*., 2008, Ingerman *et al*., 2005, Rai *et al*., 2010). Cyst formation involves major reorganization of cellular structures (Samuelson & Robbins, 2011, Makioka *et al.*, 2011b, Eichinger, 2001) and a previous study on *Giardia intestinalis* has shown the involvement of its only dynamin related protein in the cyst formation process (Gaechter *et al*., 2008). To analyse if the dynamin related proteins in *E. invadens* play a role during cyst formation, semi-quantitative RT-PCR and real time, quantitative PCR analyses were conducted.

7.1 Dynamin related proteins are expressed differentially in *E. histolytica* and *E. invadens* trophozoites

In order to analyse and compare the expression levels of dynamin related proteins in *E. histolytica* and *E. invadens,* semi-quantitative RT-PCR analyses were conducted. The experimental procedure is described in chapter 2, section 2.2.4. Briefly, trophozoites were harvested by centrifugation and washed in PBS. RNA was extracted using Tripure Isolation Reagent (Roche Applied Science) and treated with DNAse. The removal of DNA was monitored by conducting PCR reactions on the DNAse treated RNA. Where necessary, RNA samples were treated several times with DNAse to remove all traces of DNA. The concentration of RNA was measured spectrophotometrically and 2 μg of RNA were used to create cDNA with random primers. Prior to the RT-PCR experiments the optimal annealing temperature for the Drp specific primers and the actin primer pair of *E. histolytica* and *E. invadens,* respectively, were determined in gradient PCR ranging from 49 °C-59 °C (Figs. 7.1 and 7.2). Additionally, cDNA was used in different concentrations to test for DNA template concentration dependent PCR reactions. Based on the gradient PCR results, an annealing temperature of 53 °C was applied to all primers and undiluted cDNA was used as a template for RT-PCR analyses (Fig. 7.1 and 7.2). The gradient PCR data already reveal the dynamin related protein mRNA expression pattern in *E. histolytica*. Drp1, Drp3 and Drp4 appear to be weakly expressed in trophozoites, while Drp2 shows higher mRNA levels. Especially Drp3 shows almost no expression in the trophozoite life stage (Figs. 7.1, 7.3). Actin expression levels were high in trophozoites and used for comparison to the Drp expression levels.

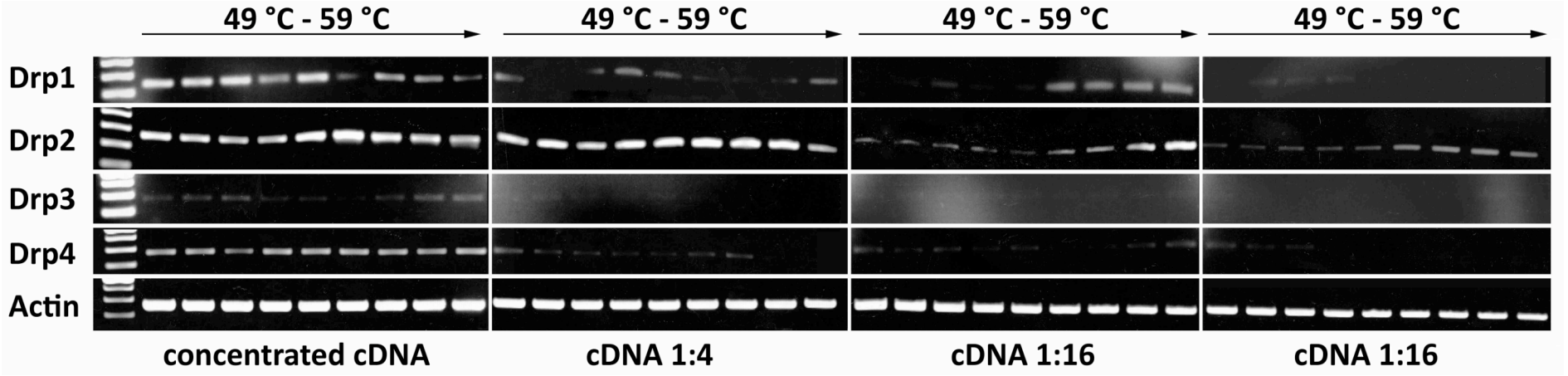

Figure 7.1 Gradient PCR on *E. histolytica* cDNA. Primers for all Drp's and actin were tested at temperatures between 49 °C and 60 °C. Additionally, different cDNA concentrations were used to estimate the importance of template concentration for the PCR.

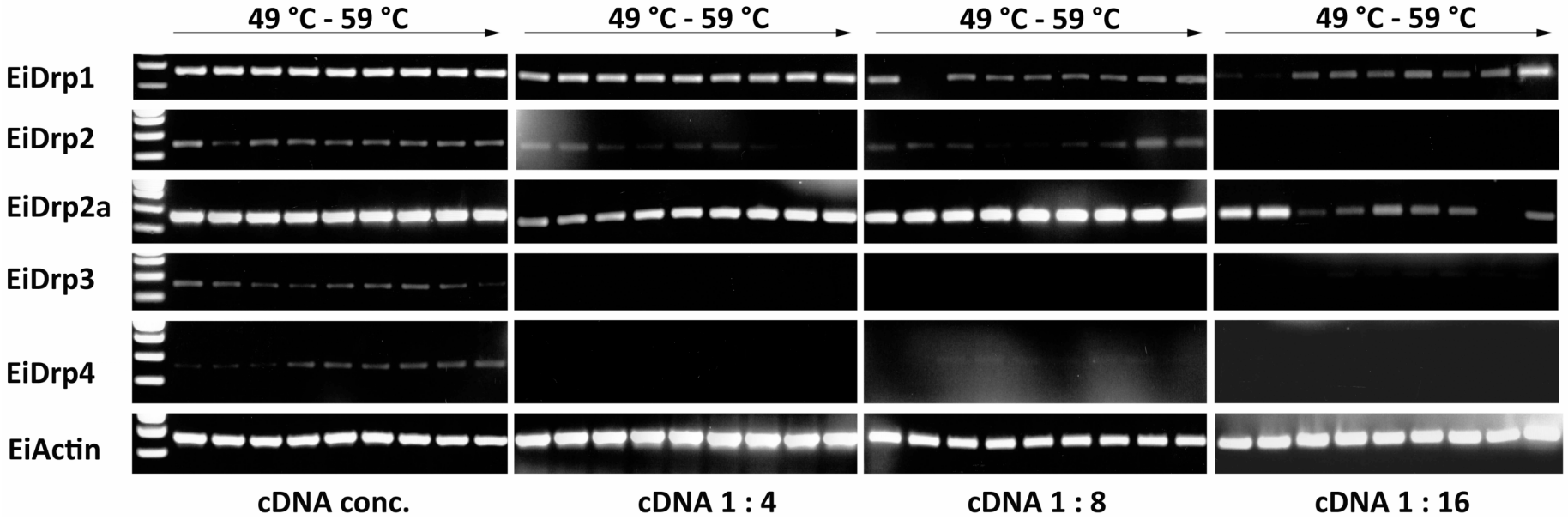

Figure 7.2 Gradient PCR on *E. invadens* trophozoite cDNA. Primers for all Drp's and actin were tested at temperatures between 49 °C and 59 °C. Additionally, different cDNA concentrations were used to estimate the importance of template concentration for the PCR.

E. invadens exhibits five dynamin related proteins (chapter 4), termed EiDrp1, EiDrp2, EiDrp2a, EiDrp3 and EiDrp4. EiDrp2 and EiDrp2a are very similar in sequence composition and sister to each other in phylogenetic reconstructions suggesting one of them appeared by recent local gene duplication in the *E. invadens* genome (Chapter 4). The mRNA expression levels for Drp1 to Drp4 differed slightly in each species. *E. invadens* exhibits a high expression of EiDrp2a, followed by EiDrp1, EiDrp2, EiDrp3 and EiDrp4 (Figs. 7.2 and 7.3). *E. histolytica* shows the highest expression in EhDrp2, followed by EhDrp1, EhDrp4 and EhDrp3 (Figs. 7.1 and 7.3).

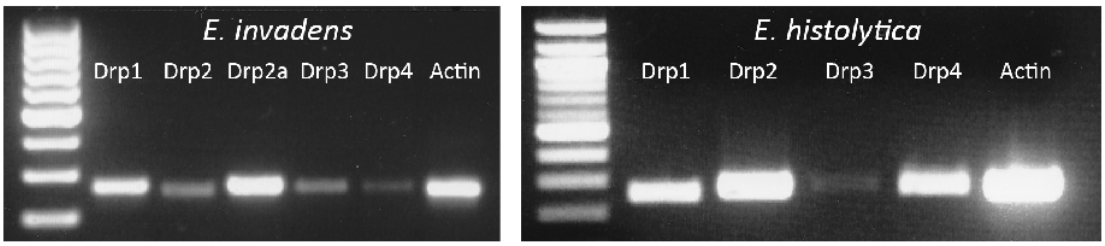

Figure 7.3 Dynamin related protein gene expression in *E. invadens* and *E. histolytica* trophozoites. Semi-quantitative RT-PCR showing the comparison between *E. invadens* Drp1, Drp2, Drp2a, Drp3 and Drp4 and E. *histolytica* Drp1, Drp2, Drp3 and Drp4 expression levels in trophozoites.

Both species show low expression of Drp3 in the trophozoites stage, which raises the question about its mRNA expression levels and potential role during cyst formation. However, all *Entamoeba* dynamin related proteins could be involved in cyst related processes and their expression levels are therefore focus of this study.

7.2 Cyst formation in *E. invadens*

Cyst formation in *E. invadens* was triggered by glucose starvation using 50 % LY-G medium (Sánchez *et al.*, 1994). Trophozoites in logarithmic growth phase were transferred from their growth medium LIY into the encystation medium and the gradual cyst formation was monitored microscopically. The process is characteristically accompanied by the development of the robust chitin containing robust cyst wall (Arroyo-Begovich *et al.*, 1980, Das *et al.*, 2006, Van Dellen *et al.*,

2006, Chatterjee *et al*., 2009). Therefore, cells were stained with Calcofluor to monitor chitin formation. RNA was extracted to analyse expression levels of the dynamin related proteins during cyst formation. *E. invadens* trophozoites and cultures that were induced to encyst were harvested at 24, 28, 32, 36, 40, 44 and 72 h after induction. Within 24 h after cyst induction, trophozoites formed aggregates (Fig. 7.4).

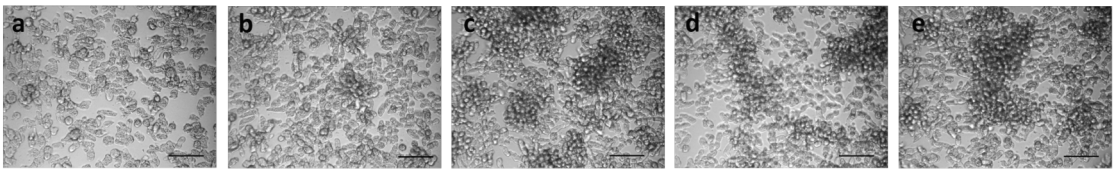

Figure 7.4 Aggregation of trophozoites after cyst induction. (a) uninduced trophozoites. (b) 16 h after cyst induction. Few cells have aggregated. (c) 22 h after cyst induction. (d) 24 h after cyst induction. Cells form aggregates and start to encyst. (e) 27 h after cyst induction. Cell aggregation is evident. Size bar = 100 μm. Images were taken from cells in culture flasks.

Cysts started forming after 24h and the majority of cells exhibited closed cyst walls after 36 h during the mid cyst stage (Fig. 7.5). Cysts usually appear round or oval shaped with a rigid chitin wall and between 10 and 15 μm wide, which is smaller than the trophozoites (Fig. 7.5). Unlike trophozoites the inside of cysts appears smooth. Typical during cyst development in *Entamoeba* is the appearance of chromatoid bodies, which are crystallized ribosomes that disappear again when the cysts are mature (Fig. 7.5, arrowhead) (Barker, 1963, Morgan *et al*., 1968, Lake & Slayter, 1972). The Calcofluor staining of samples from the different time points during cyst formation showed a successive increase in the number of cysts.

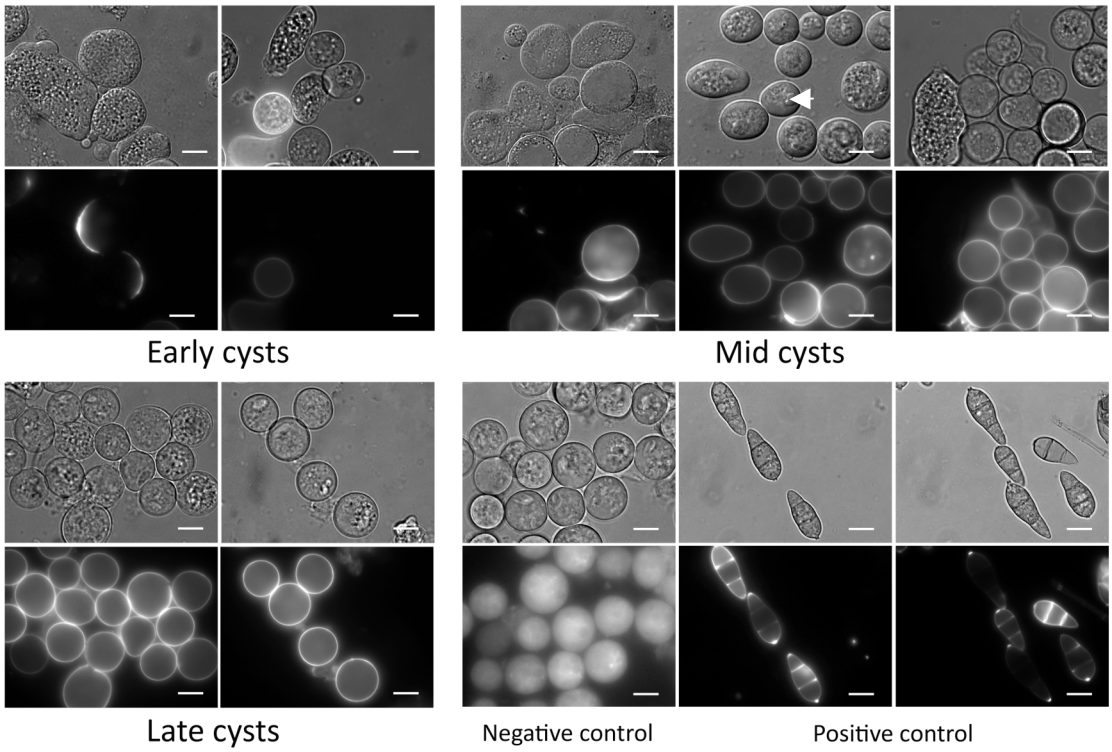

Figure 7.5. Cyst formation of *E. invadens*. Cyst walls were stained with the chitin dye Calcofluor. Early cysts=24 and 28 hour old cysts, Mid cysts=32, 36 and 40 hour old cysts, Late cysts=44 and 72 hour old cysts. Negative control=72 hour old cysts that were not stained with Calcofluor. Positive control=spores of the ascomycete fungus *Magnaporthe grisea*. The scale bar is 10 μm wide. The arrowhead at the mid cyst formation picture points at a putative chromatoid body, which typically occurs during mid cyst development.

Additionally to monitoring cyst formation by Calcofluor staining, expression levels of chitinases were analysed. Chitinases are secretory enzymes, which are essential during cyst formation (Villagomez-Castro *et al.*, 1992). *E. invadens* exhibits four chitinases called EiChit1-EiChit4, which have shown to be upregulated during cyst formation (Makioka *et al.*, 2011a). Makioka *et al*. took four time points for measuring expression levels of the chitinases: trophozoites stage, early cyst stage (= 44 % cyst formation), mid cyst stage (= 70 % cyst formation) and final stage (= 100 % cyst formation). They find no chitinases gene expression in trophozoites and a strong upregulation of all chitinases in the early cyst stage. Expression levels decreased during mid and late cyst formation. Our analyses included 8 time points: trophozoites, 24 h, 32 h, 36 h, 40 h, 44 h and 72 h after cyst induction. Our RT-PCR

analyses using the chitinase primers published in Makioka *et al*. (2011) showed a similar expression pattern to the previous findings. Chitinases were not expressed during the trophozoites stage. With the formation of cysts after 24 h, the levels of expression increased and peaked at 32 h after cyst induction.

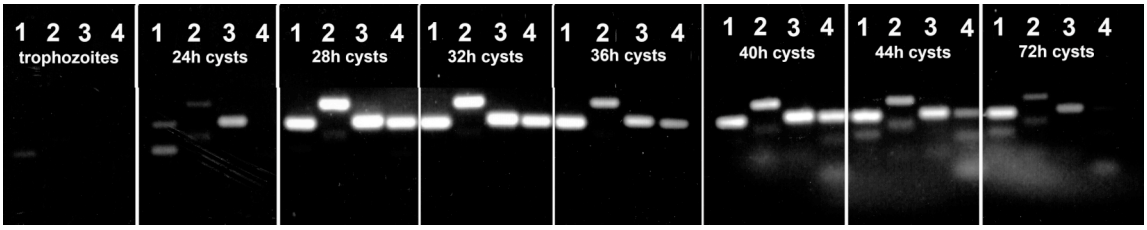

Figure 7.6 RT-PCR of the *E. invadens* chitinases 1-4 from trophozoites, 24h, 28h, 32h, 36h, 40h, 44h and 72h old cysts. cDNA was produced by RT-PCR with random primers. 1=EiChit1, 2=EiChit2, 3=EiChit3, 4=EiChit4.

While EiChit1 was still upregulated at 36 h after cyst induction, the expression levels of EiChit2-4 decreased. During mid cyst formation (36 h and 40 h after cyst induction) chitinases expression levels were lower than during early cyst formation and decreased even further during the late phase (44 h and 72 h after induction). EiChit1 was expressed strongest in comparison to EiChit2-4 during mid and late cyst stage. This is also in agreement with Makioka *et al*. (2011). Our study found low levels of EiChit4 expression during late cyst formation. This finding differs to Makioka *et al*. who measure a higher expression of EiChit4 than of EiChit2 and 3. Overall, the expression patterns of EiChit1-EiChit4 in combination with the Calcofluor staining of the developing cysts confirm correct encystation of *E. invadens.*

7.3 Expression patterns of EiDrp1-EiDrp4

7.3.1 Relative changes in Drp gene expression in *E. invadens* during cyst formation

E. invadens Drp mRNAs are expressed differentially. Trophozoites show a stronger expression in EiDrp2a in comparison to the other Drp's, which appear to be expressed in low quantities. Especially EiDrp3 and EiDrp4 are almost absent. During cyst formation all Drp's experience upregulation, indicating that they play a role in cyst formation processes. The Drp's differ to each other in the levels of mRNA expression and the time points at which they start to increase (Fig. 7.7).

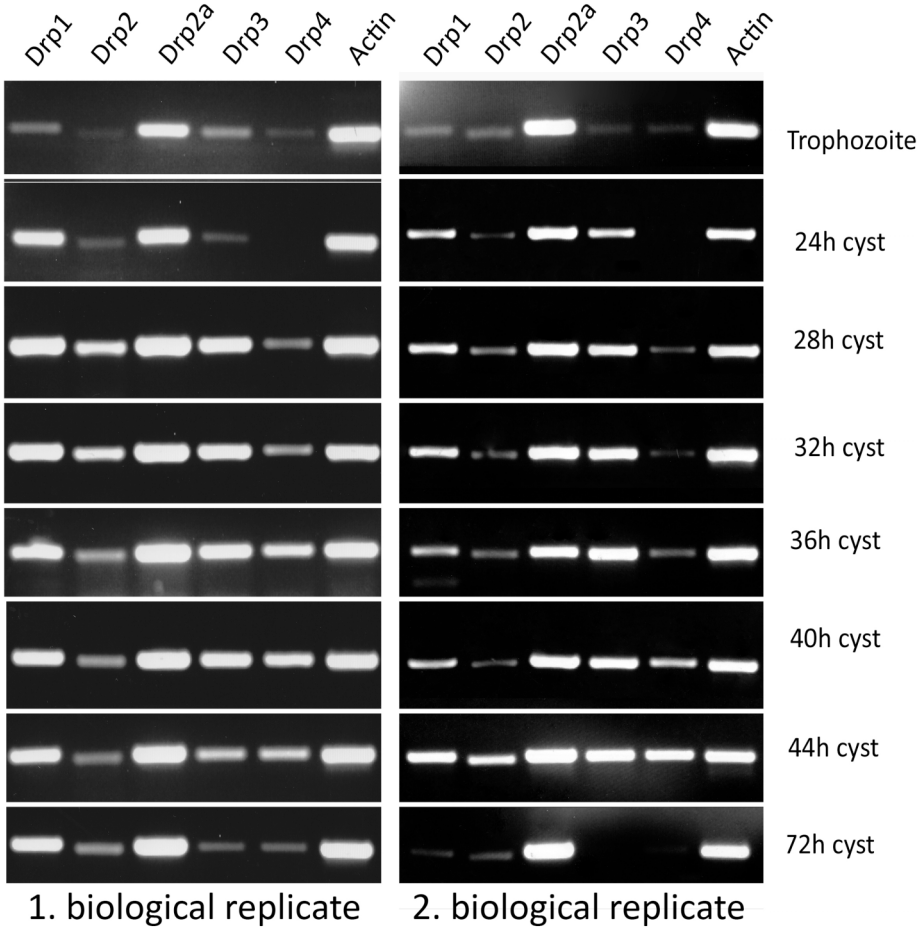

Figure 7.7 mRNA expression pattern of *E. invadens* dynamin related proteins. Each gel shows one time point. From left to right: Drp1, Drp2, Drp2a, Drp3, Drp4 and Actin. Actin was used as a loading control. Left column shows the first biological replicate. Right column shows the second biological replicate.

EiDrp1

EiDrp1 was expressed at low levels in the trophozoite stage. 24 h after cyst induction mRNA levels started to increase and showed stable high expression until late cyst stage, in which it decreased (44 h and 72 h). The first biological replicate shows elevated expression levels of Drp1 72 h after cyst induction but the second biological replicate does not. This might be explained with variation in the biological samples. *E. histolytica* Drp1 has been found to be nuclear associated (Jain *et al*. 2010). The increase in EiDrp1 mRNA expression co-insides with the increase in the number of nuclei from one to four in the developing cyst. However, it can only be speculated if Drp1 is involved in a nuclear division related process.

EiDrp2

Like EiDrp1, EiDrp2 was expressed at low levels in trophozoites. Elevation of mRNA expression was detectable 28 h after cyst induction (Fig. 7.7) and continued to be upregulated until 40 and 44 h after cyst induction. The first biological replicate shows a stronger upregulation 28h to 40 h after induction. The second biological replicate shows a lower level of Drp2 expression compared to the first biological replicate throughout the experiment. An increase in expression was detected 28 h and 44 h after cyst induction.

EiDrp2a

EiDrp2a shows high expression levels in the trophozoite stage as well as all cyst stages. The first biological replicate shows less mRNA expression in trophozoites and an increase during cyst formation. The second biological replicate however, exhibits high and stable expression of this gene throughout all stages. Even in the last cyst stage 72 h after induction, mRNA expression levels are high and comparable to the high expression levels of actin. The strong and stable expression of EiDrp2a indicates an important role in the overall metabolism in all stages of the parasitic life cycle.

EiDrp3

EiDrp3 was lowly expressed in the trophozoite stage. Expression increased during early cyst formation (24 h, 2nd biological replicate), peaked at the mid cyst stage and decreased again in late cyst formation. The first and second biological replicates differ slightly in the start of Drp3 expression. While the Drp3 expression level in the first biological replicate starts to elevate 32 h after cyst induction, the second biological replicate already shows increase 24 h after cyst induction. Both however exhibit a similar overall expression pattern in that they reveal a clear increase in expression levels during mid cyst formation. The strong increase in Drp3 expression levels indicates that Drp3 plays mainly a role during the cyst development process rather than in the trophozoite stage.

EiDrp4

EiDrp4 expression is virtually absent in trophozoites and expressed at a low level in early cysts and up to 40 h after cyst induction. Expression levels increased 40 h after cyst formation and decreased again in the final cyst stage 72 h after induction. This expression pattern was exhibited by both biological replicates and indicates that EiDrp4 plays mainly a role during the late cyst formation process but not in trophozoites and early cysts.

7.3.2 Analysis of relative Drp3 and Drp4 gene expression using real-time quantitative PCR

Real-time quantitative PCR (qPCR) provides an alternative to semi-quantitative RT-PCR. The differences include the use of the more sensitive DNA stain Sybr Green and the detection of PCR product formation during the PCR cycling (real-time). Sybr Green is approximately 25 times more sensitive in staining DNA than ethidium bromide (Singer *et al.*, 1999). Furthermore, PCR reactions can plateau at different levels due to the limitation of one of the PCR reagents, even if the same amounts of template DNA were used (Applied Biosystems support tutorial: Real-Time PCR Vs. Traditional PCR). Therefore, comparing band intensities on an agarose gel as in semi-quantitative RT-PCR analyses can be potentially misleading. Measuring mRNA concentrations using qPCR circumvents these methodological difficulties. Quantitative gene expression analysis typically requires the use of a reference gene, which should be expressed constitutively during the life stages that are analysed, and functions as an internal normalizer to account for varying cDNA template concentrations (Vandesompele *et al.*, 2002, Livak & Schmittgen, 2001). The requirement for a reference gene is the most crucial drawback in qPCR analyses because the stability of the reference gene expression defines the resolution of the assay (Huggett *et al.*, 2005). So far, no gene is known in *E. invadens*, which has been shown to exhibit stable mRNA expression during stage conversion using qPCR analysis. However, (Ehrenkaufer *et al*., 2007) demonstrated by semi-quantitative RT-PCR analysis that the SKI interacting protein SKIP (accession number: AANW01003268) showed no difference of mRNA expression levels in *E. invadens* trophozoites and 48 h old cysts. Therefore, SKIP was used as a reference gene during qPCR experiments. Additionally to SKIP, EiActin-1 (Accession number: AB522086) was employed to normalize for variations of cDNA template concentrations. The 18S ribosomal RNA gene was applied in the same way to follow EiDrp3 gene expression levels during stage conversion. Reliable and unique primers are very important for qPCR analyses and were therefore designed according to the manufacturers

recommendations (Eurogentec qPCR guide) and analysed prior qPCR experimentation by conducting a melt curve for each primer pair (chapter 7.4.1.2).

7.3.3 Standard curves and primer specificity for Drp3, Drp4, Actin, SKIP and 18S rDNA

To determine the PCR replication efficiency and the quality and specificity of primer sets, a standard curve and a melt curve for each primer pair using serial dilutions of template cDNA were determined.

7.3.3.1 Standard curves show optimal PCR efficiencies

The slope of the standard curve is important for the calculation of PCR efficiency (Fig. 7.9). It is calculated based on the PCR cycle threshold (C_t) values against the log concentration of initial cDNA template used for the PCR reaction. The C_t value or cross point indicates the amount of PCR cycles necessary for creating fluorescently detectable PCR product (Fig. 7.8). C_t values are inversely proportional to the amount of target cDNA in the sample. When the C_t value is low, the detection of PCR product started early during PCR. This indicates that the specific template cDNA was present in higher abundance than compared to samples with a high C_t value. The example in Fig.7.8 shows the qPCR amplification data that were used for constructing the actin standard curve. Each PCR reaction was conducted on differently diluted cDNA templates. The more diluted the cDNA template, the higher the C_t value.

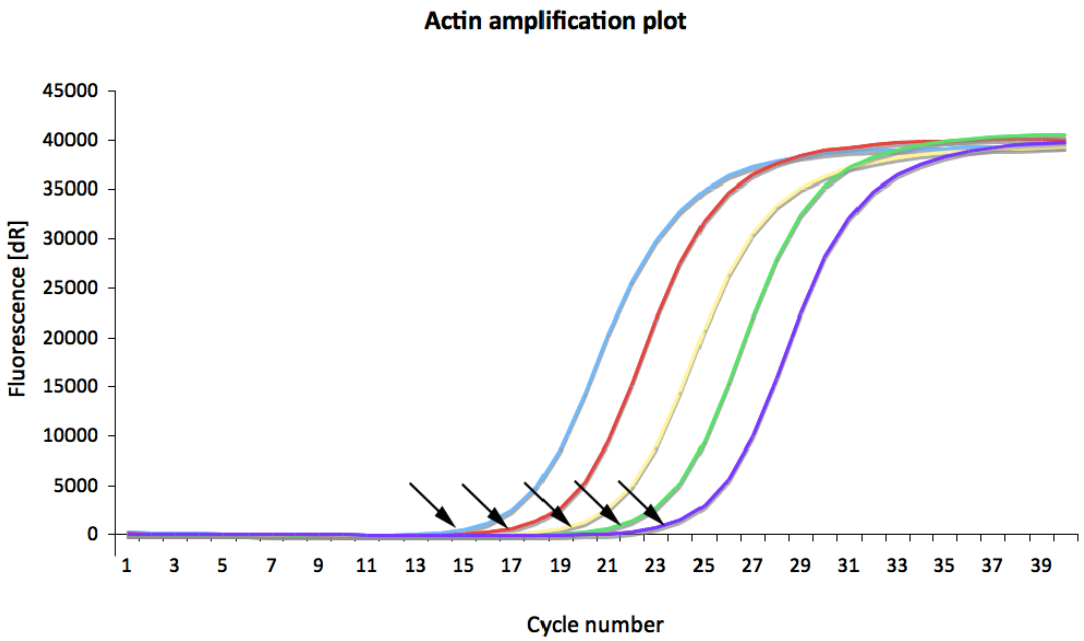

Figure 7.8 Amplification plots from different cDNA dilutions using actin primers to demonstrate the meaning of C_t values in qPCR. X-axis: cycle number. y-axis: delta fluorescence, *i.e*. Sybr Green net fluorescence excluding background fluorescence. Arrows point at C_t values for each PCR reaction. Light blue curve=concentrated cDNA template, red curve=cDNA template diluted 1:8, yellow curve=cDNA template diluted 1:16, green curve=cDNA template diluted 1:64, blue=cDNA template diluted 1:256.

To calculate PCR efficiency the C_t values are plotted against the Log cDNA concentration values. PCR efficiencies between 90 % and 110 % are acceptable for qPCR analyses (Fig. 7.9) (Eurogentec qPCR guide). They are calculated using the following equations.

Exponential amplification = $10^{(-1/slope)}$

Efficiency = $(10^{(-1/slope)}-1)*100$ %

Example calculation using data for actin:

Exponential amplification = $10^{(-1/-3.23)}$ = 2.05

Efficiency = 2.05 – 1 = 1.05*100 %= 105 %

The PCR efficiency values of Drp3, Drp4, SKIP, Actin and 18S rDNA were within the acceptable range (Fig. 7.9). Another factor important for the estimation of PCR assay quality is the R squared parameter. R^2 evaluates how linear the PCR assay proceeded or in other words how the experimental data fit the regression line. If the amplification efficiency is similar for each cDNA template dilution, linearity will be high. However, if linearity is low, it indicated variability during amplification, which could be caused by pipetting inaccuracies or inhibition during the PCR reaction. R^2 values higher than 0.985 are acceptable. The R^2 values in this study were within the acceptable range and indicate high linearity (Fig. 7.9).

*The legend for the following figure was exceptionally placed before the figure due to space limitations on the horizontally outlined page.

Figure 7.9 cDNA standard curves for qPCR primers based on 5 cDNA template dilutions. X-axis: Log values of cDNA template concentrations used in this assay: concentrated cDNA, 1:4 diluted cDNA, 1:16 diluted cDNA, 1:64 diluted cDNA and 1:256 diluted cDNA. Y-axis: Crossing point or C_t value, the value at which the measured fluorescence becomes positive in comparison to background fluorescence. This indicates amplification. Value below the graph indicates the slope of the standard curve, important for PCR efficiency calculation. The table on the right shows the PCR efficiencies and the R^2 values for each primer pair and qPCR reaction, Drp3, Drp4, SKIP, Actin and 18S rDNA. The standard curves are based on duplicate measurements.

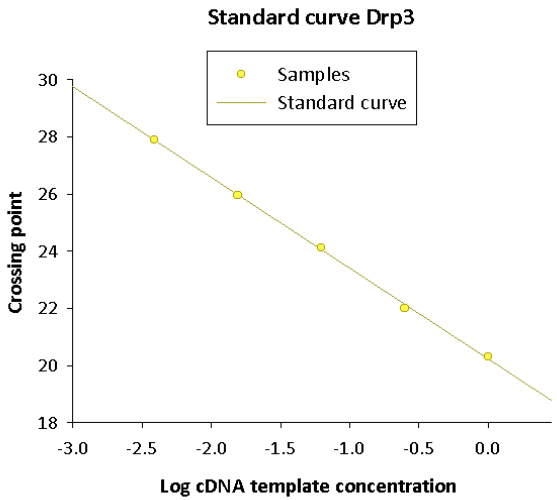

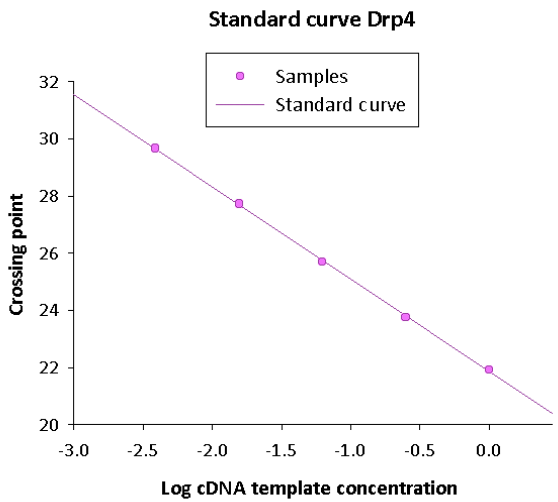

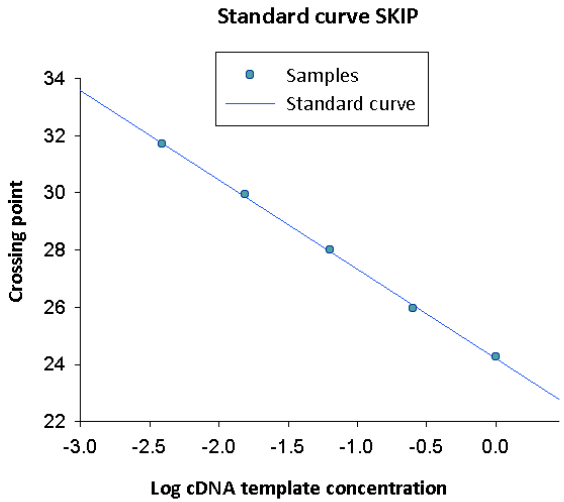

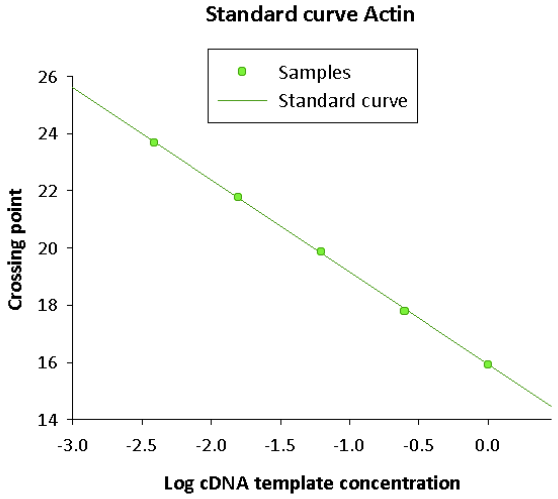

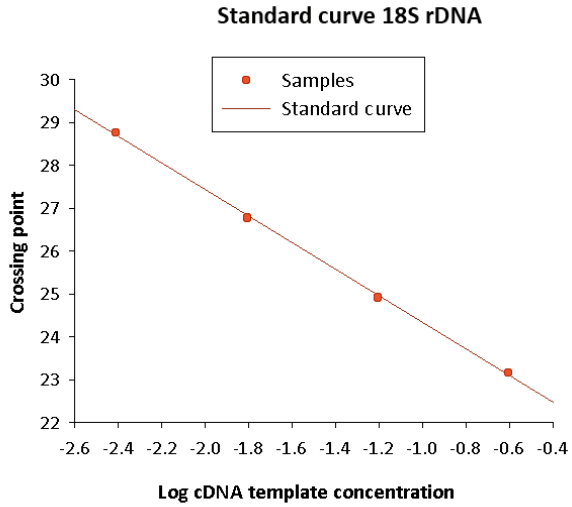

Samples	PCR efficiency [%]	R^2
Drp3	106	0.999
Drp4	104	1.000
SKIP	109	0.999
Actin	105	1.000
18S rDNA	110	0.999

7.3.3.2 Meltcurves show primers to be gene specific

To test if primers were gene specific and free from creating secondary structures and primer dimers, a melt curve for each primer set was created by increasing temperatures at the end of the PCR reaction from 55 to 94 °C, while monitoring the fluorescence. At the amplicon specific melting temperature the dsDNA separates to single stranded DNA, the fluorescent dye Sybr Green detaches and the fluorescence drops. When a single PCR product is amplified only one melt curve is present. Several products will create several melt curves depending on the melting temperature of each double stranded fragment. The same accounts for the presence of primer dimers. The melt curves in this study show single dissociation peaks (Fig. 7.10), which verifies the presence of only one amplicon per primer pair. This confirms optimal primer specificity and the absence of primer dimers or secondary structure formation.

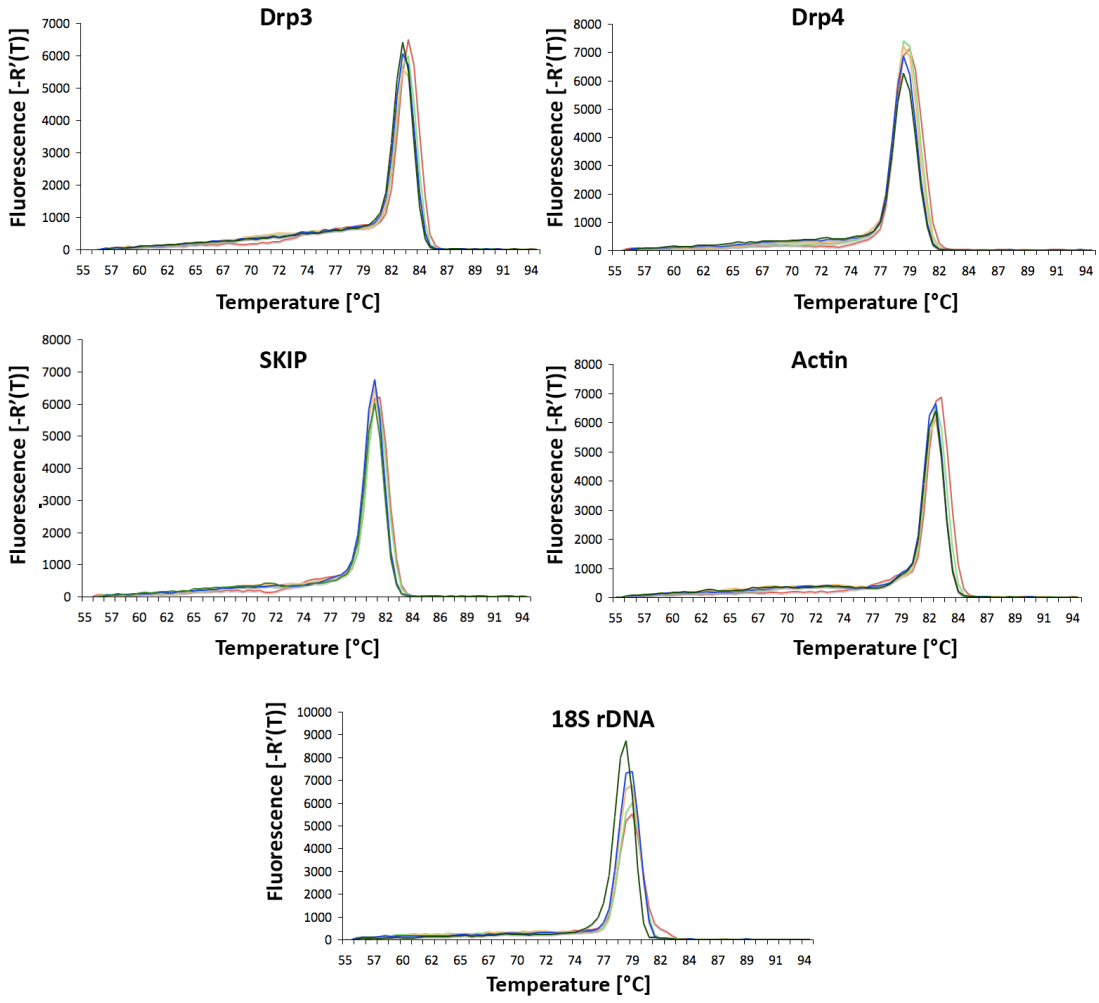

Figure 7.10 Clean meltcurves of qPCR products from each primer pair used in this study. The primers used on cDNA are indicated above each graph. The curves are based on the different cDNA dilutions used in the analysis: concentrated cDNA, cDNA diluted 1:8, cDNA diluted 1:16, cDNA diluted 1:64, cDNA diluted 1:256. Therefore, the amount of fluorescence might differ.

7.3.4 QPCR data confirm semi-quantitative PCR results

The mRNA levels of Drp3 and Drp4 were compared at different developmental stages of *E.invadens* by real-time PCR. The analyses revealed an up-regulation of Drp3 and Drp4 during cyst formation (Fig. 7.11). Drp3 showed a strong increase between 24 h (1st biological replicate) and 28 h (2nd biological replicate) after cyst induction in comparison to trophozoites. The maximum mRNA expression was reached in 32 h

(2nd biological replicate) to 36 h (1st biological replicate) old cysts, *i.e.* during the mid cyst stage.

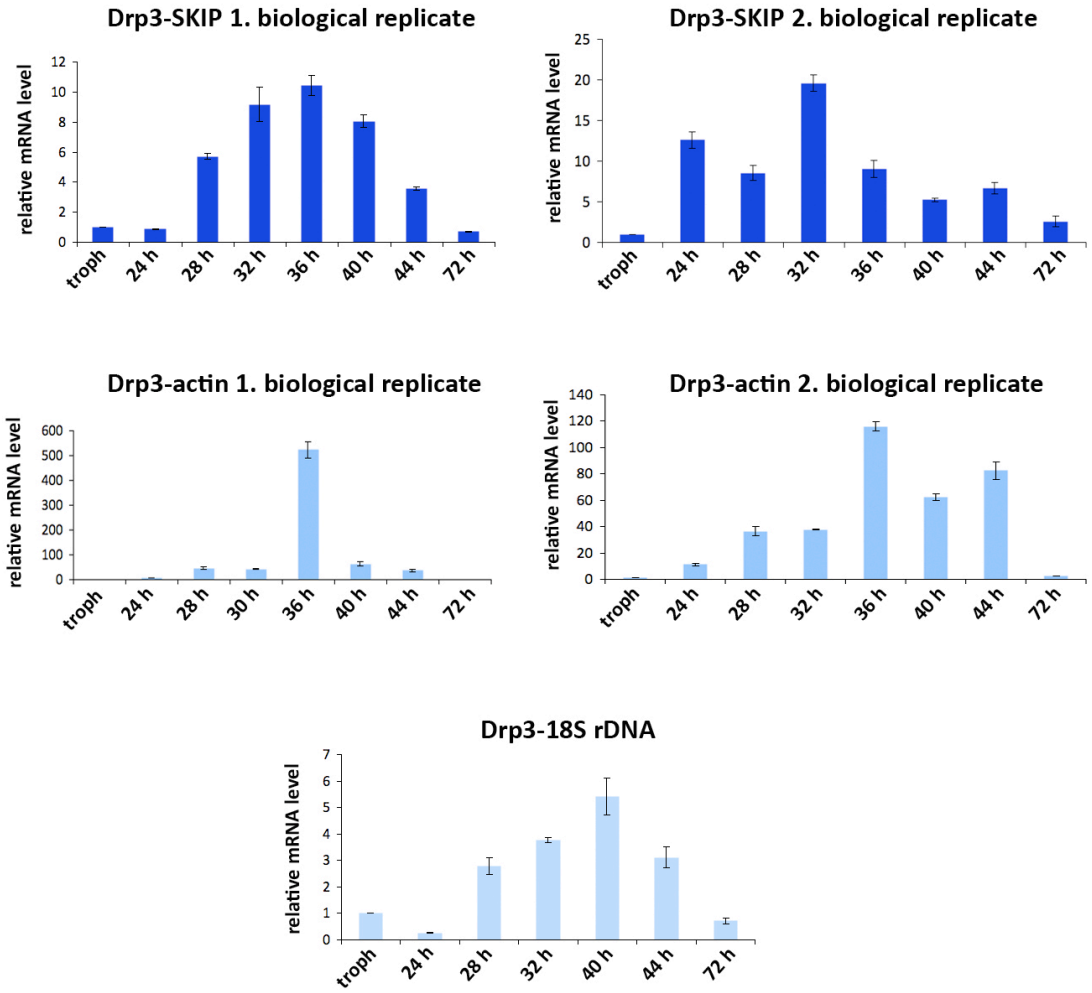

Figure 7.11 Change in the expression of EiDrp3 in trophozoites and during cyst formation using SKIP (=Drp3-SKIP), actin (=Drp3-actin) and 18S rDNA (Drp3-18S rDNA) as reference genes. The mRNA levels of Drp3 were measured using real-time RT-PCR. Two biological replicates were analysed in this study. X-axis=time points at which RNA for cDNA transcription was isolated; trophozoites and 24h, 28h, 32h, 36h, 40h, 44h and 72h after cyst induction. Y-axis=relative mRNA levels in comparison to the respective reference gene. Drp3 mRNA expression measurements normalized to ssU were conducted only once on cDNA from the second biological replicate and excludes time point 36h due to measurement difficulties. Standard deviations are based on technical triplicates.

The comparison of Drp3 expression to the different reference genes SKIP, Actin and 18S rDNA show the same overall pattern. The level of expression was low in trophozoites, increased during early cyst formation, reached the maximum during mid cyst formation and a decreased again in final cysts.

Expression levels of Drp4 in the various cyst stages differ to Drp3.

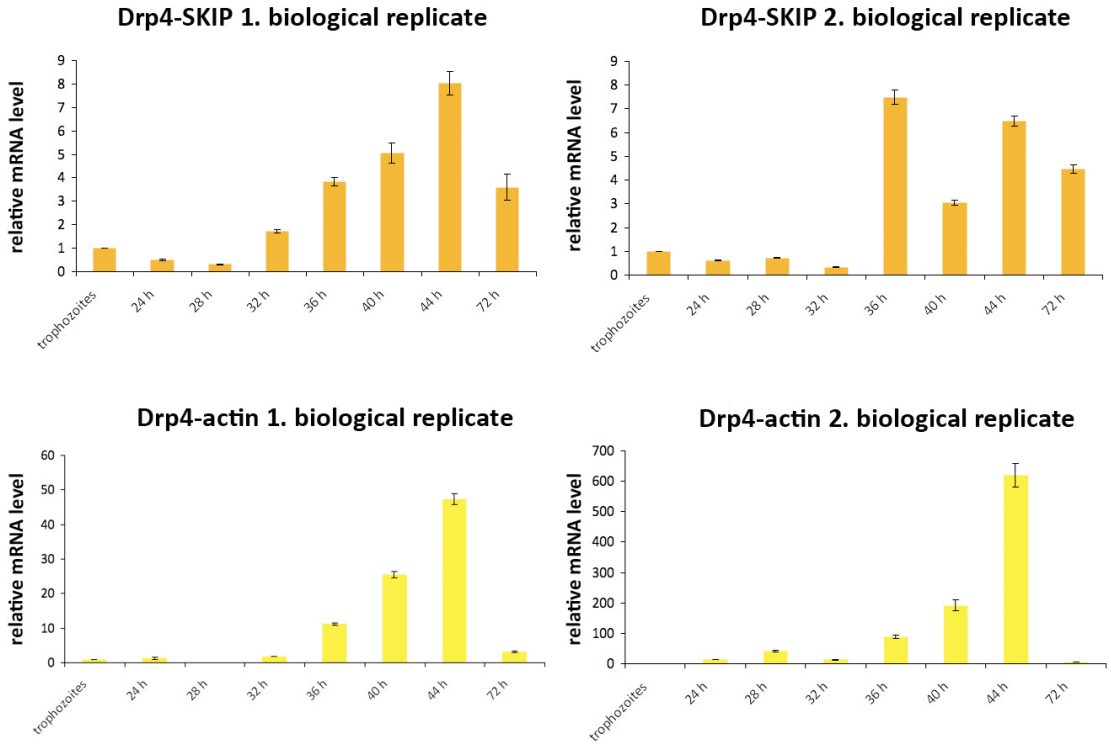

Figure 7.12 Change in the expression of EiDrp4 in trophozoites and during cyst formation using SKIP (=Drp4-SKIP) and actin (=Drp4-actin) as reference genes. The mRNA levels of Drp4 were analysed using real-time RT-PCR. Two biological replicates were analysed in this study. X-axis=time points at which RNA for cDNA transcription was isolated; trophozoites and 24h, 28h, 32h, 36h, 40h, 44h and 72h after cyst induction. Y-axis=relative mRNA levels of Drp4 in comparison to the respective reference gene. Standard deviations are based on technical triplicates.

Drp4 showed increase in mRNA expression during mid and late cyst formation (Fig. 7.12), while trophozoites and early cysts show low Drp4 expression levels. An increase in expression was measured during mid cyst formation in 36 h old cysts. The maximum expression level was reached 44 h after cyst induction during the late cyst stage, and dropped again in final cysts. The biological replicates and the comparison

to the different reference genes show the same overall expression pattern. However, the expression profile of Drp4 in comparison to SKIP in the second biological replicate differs somewhat from the other Drp4 expression patterns (Fig. 7.12). Here the expression peak is shown to be highest 36 h after cyst induction, decreases slightly in 40 h old cysts and increases again during late cyst formation. It is worth noting that Drp4 mRNA expression normalized to SKIP shows an elevated expression level in final cysts (72 h) in comparison to trophozoites and early cysts. This was not the case when using actin as a reference gene (Fig. 7.12). Here the mRNA levels appear similar in trophozoites, early to mid cysts and final cysts. Due to qPCR machine failure experiments were not repeated for the 18S rDNA reference gene.

The strong increase in expression levels of Drp3 and Drp4 during *E. invadens* cyst formation indicates a functional role for both proteins in cyst development but not in the trophozoite stage. The expression patterns are distinct from each other. While Drp3 mRNA levels were shown to be highest during mid cyst formation, Drp4 exhibited highest expression in late cysts. The qPCR data confirm the semi-quantitative RT-PCR results (section 7.3) independently. Although the overall mRNA expression patterns are in agreement with the semi-quantitative RT-PCR data, variation was detected depending on the reference gene used. Quantitative real-time PCR depends on the careful selection of the internal control genes. In general, a reference gene should exhibit stable expression throughout the analysed cellular life stages, because variations might artificially enhance or decrease the measurements for the gene expression profiles of interest. Thus it is possible that the variation within the qPCR data reflect variation in reference gene mRNA levels.

7.4 Expression patterns of Drp1-Drp4 during excystation using semi-quantitative RT-PCR

In order to understand the *E. invadens* dynamin expression pattern at each life cycle stage, we conducted semi-quantitative RT-PCR analyses during excystation (Fig. 7.14). Excystation was induced following the protocol of (Mitra *et al*., 2010). Briefly, mature cysts were washed in PBS and incubated for 1 h in 0.05 % Sarkosyl to remove remaining trophozoites. This step was monitored microscopically to ensure a

homogenous cyst sample. Cysts were then transferred into 50 % TIY medium supplemented with glucose, bile salts and sodium bicarbonate ($CHNaO_3$). Samples were taken every 12 hours and RNA isolation for cDNA synthesis. Additionally, excystation was monitored microscopically (Figs. 7.13 and 7.14). The process of excystation involves the partial resolution of the rigid chitin wall. Upon the opening of the wall, the amoeboid trophozoite emerges singly leaving the cyst wall behind (Fig. 7.13).

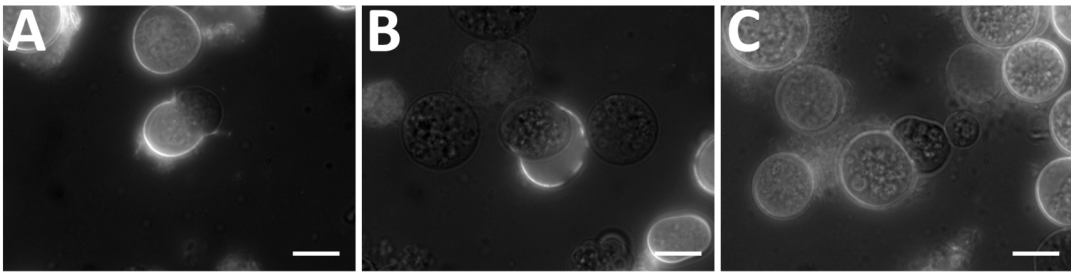

Figure 7.13 Excysting *E. invadens* trophozoites. Cells were stained with Calcofluor to show the difference between chitin containing cysts and cyst wall residues and the emerging trophozoites. (A-C) show cysts and trophozoites that are in the process of leaving their cyst wall. Scale bar=10 μm.

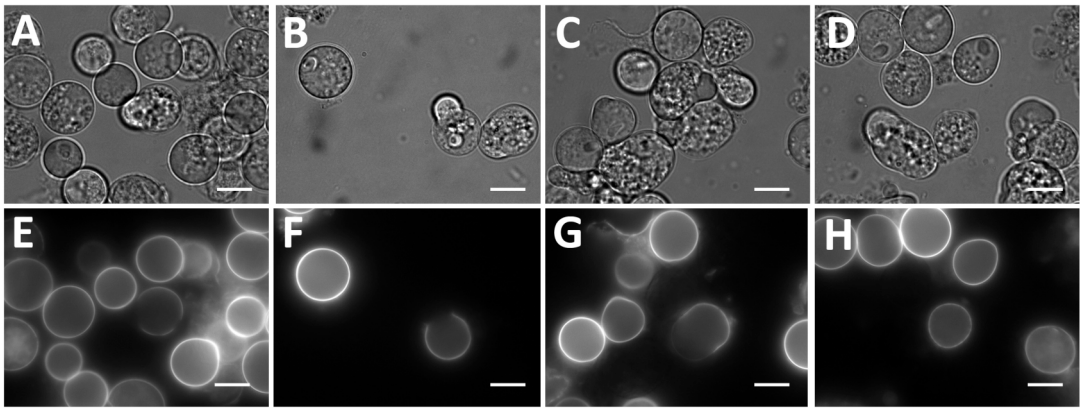

Figure 7.14 Excysting *E. invadens* cells at different time points stained with Calcofluor. A-D show cells after 12h (A), 24 h (B), 36 h (C) and 60 h of excystation. E-H are the corresponding fluorescence images. Scale bar=10 μm.

In contrast to Mitra *et al*. (2010), who report an excystation rate of greater than 80 % after 24 h in excystation medium, our trophozoite recovery rate was low. Even 72 h after incubation in excystation medium, the majority of cysts did not show

progression to trophozoites. Nevertheless, it was possible to gain viable cultures from cysts.

Semi-quantitative RT-PCR analysis reveals a dynamin protein expression pattern comparable to mature cysts and trophozoites (Fig. 7.15).

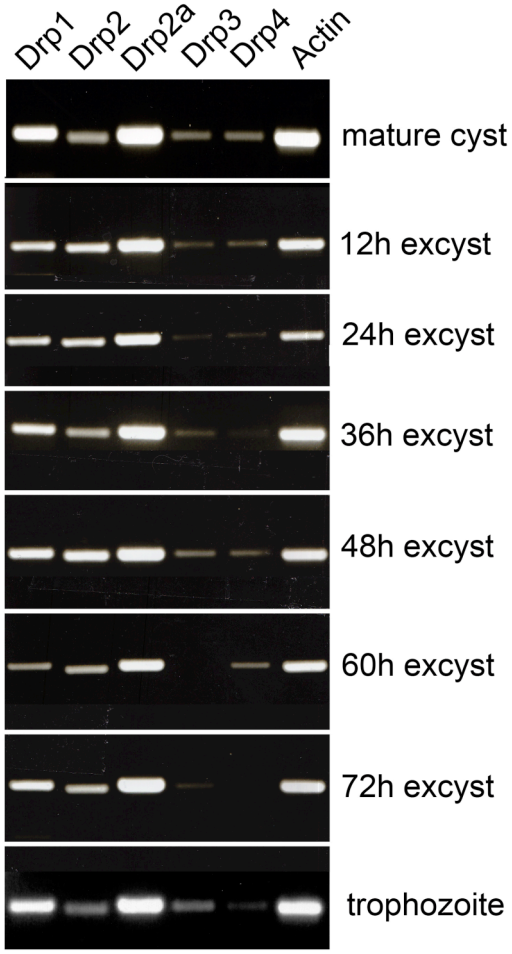

Figure 7.15 mRNA expression pattern of *E. invadens* dynamin related proteins during excystation. Each gel shows one time point. From left to right: Drp1, Drp2, Drp2a, Drp3, Drp4 and Actin. Actin was used as a loading control.

Drp2a exhibits the strongest mRNA expression throughout the time course, followed by Drp1 and Drp2. In contrast, Drp3 and Drp4 show low to absent mRNA levels indicating that both proteins do not play a significant role in the excystation process.

In summary, all dynamin related proteins are expressed in *E. histolytica* and *E. invadens* trophozoites in varying amounts. In both *Entamoeba* species, Drp3 appears to be expressed the least, while Drp2 in *E. histolytica* and Drp2a in *E. invadens* exhibit

the highest expression levels. During cyst formation all dynamin related proteins show an increase in mRNA expression levels. Drp2a appears to be expressed strongly throughout suggesting an important function in both life stages. Drp3 and Drp4 were expressed in low amounts in trophozoites but showed a significant rise in expression levels during encystation. Drp3 expression levels were highest during mid cyst formation, while Drp4 was expressed strongly during the late phase. The differential rise in Drp3 and Drp4 expression levels indicate specific functional roles of both proteins during cyst formation. In contrast, dynamin expression levels during excystation showed no significant variation to trophozoites or final cysts. Drp3 and Drp4 are both absent from human cells and might therefore provide potentially interesting drug targets assuming that their expression is essential for cyst development.

8 Discussion

8.1 Key findings in this study

1. Mitosomes are abundant in *Entamoeba histolytica* and *Entamoeba invadens* suggesting the presence of mitosomes in all *Entamoeba* spp..
2. *Entamoeba invadens* cysts contain mitosomes in high abundance.
3. *Entamoeba* mitosomal Hsp70 groups within the amoebozoan members of this protein family and is of mitochondrial origin as shown by *in silico* characterization and localization experiments using the homologous Hsp70 antibody.
4. *Entamoeba* spp. contain 'classical' as well as derived members of the dynamin protein family. The 'classical' *Entamoeba* dynamins do not group with any functionally characterized dynamins, while the derived dynamins are closely related to amoebozoan and archaeplastidan proteins involved in cytokinesis and chloroplast division.
5. The kinetic characteristics of the *E. histolytica* Drp2 GTPase protein are comparable to other members of the eukaryotic dynamin protein family by exhibiting low substrate specificity, the ability to oligomerize to higher structures and a substrate dependent cooperative enzyme activity.
6. Drp2 localizes to numerous punctate structures in the cytosol but not together with mitosomes. In addition, Drp2 was not able to complement *D. discoideum* DymA. Both findings suggest that Drp2 is not directly involved in mitosomal division.
7. All *Entamoeba* dynamins are expressed differentially in trophozoites with Drp2 and EiDrp2a appearing to be most abundant and Drp3 and Drp4 expressed at a low level. During stage conversion to cysts all dynamin related proteins are upregulated. Drp3 and Drp4 are highly expressed in the mid and final cyst stages, suggesting an important functional role for both proteins during stage conversion to cysts.

8.2 Discussion

Entamoeba histolytica is an important human parasite that causes severe intestinal illness and organ destruction, especially of the colon and the liver, leading to ten thousands of deaths each year (WHO/PAHO/UNESCO-report, 1997). From a medical anthropocentric perspective it is important to study this organism and its relatives in detail in order to understand its life cycle and cellular organisation and to identify unique characteristics that might provide potential drug targets. From an evolutionary perspective, *E. histolytica* is interesting because it is one of the few organisms that contain highly reduced mitochondria called mitosomes and whose free-living non-parasitic mitochondria-containing relative *Dictyostelium discoideum* is well studied and provides a useful comparison. The discovery that *E. histolytica* had a mitochondrial ancestry (Clark & Roger, 1995) and the subsequent finding of relic mitochondria (Tovar *et al*., 1999) had a large impact on the understanding of eukaryotic evolution. Prior to the discovery of mitosomes in *E. histolytica*, evidence suggested the presence of basal eukaryotic taxa that arose before the acquisition of mitochondria. They were named the Archezoa in accordance with their supposedly primitive nature and included the parasitic Metamonadea (exemplified by *Giardia)*, Microsporidia, Parabasalia (such as *Trichomonas),* and the Archamoebae, such as *Entamoeba* (Cavalier-Smith, 1983). The now defunct Archezoa harboured taxa that seemed to lack a complex endomembrane system, mitochondria and peroxisomes and often grouped basal to eukaryotes in small subunit rDNA phylogenetic analyses (Sogin *et al.*, 1989, Sogin, 1989, Vossbrinck *et al.*, 1987, Viscogliosi *et al.*, 1993, Kamaishi *et al.*, 1996). This view was challenged by the identification of mitochondrial genes and relic mitochondria in all archezoan species as well as the discovery of the mitochondrial origin of hydrogenosomes (Williams *et al*., 2002, Tovar *et al*., 2003, Vavra, 2005, Gill *et al*., 2007, Riordan *et al.*, 1999, Riordan et al., 2003, Hampl *et al.*, 2008, Bui *et al.*, 1996, Germot *et al*., 1996, Roger *et al.*, 1996).

8.2.1 Mitosomes and mitochondrial division

Since the discovery of the first mitosome, research has progressed in understanding why these organelles are retained. The common function for mitosomes appears to be iron-sulphur maturation (van der Giezen, 2009). The exception seemed to be *E.*

histolytica, whose iron-sulphur co-factor maturation pathway was found to be cytosolic and acquired through lateral gene transfer from ε-proteobacteria (Ali *et al.*, 2004, van der Giezen *et al.*, 2004). However, this view has recently been challenged by (Maralikova *et al.*, 2010), who found that the bacterial-type Fe-S cluster assembly proteins NifS and NifU are indeed recruited to function within the mitosomes (although partially so). Little is known about the actual mode of mitosome replication, division and inheritance.

Mitochondrial division in all studied organisms relies on members of the dynamin protein family for the process of membrane scission. The amoebozoan *D. discoideum* and relative of *Entamoeba* encodes two classical dynamin related proteins DymA and DymB, which are associated with the mitochondrion. DymA is responsible for mitochondrial division, while DymB is processed in the mitochondrial matrix for protein maturation. It was therefore our aim to identify and characterize the *Entamoeba* dynamin related proteins and to analyze which cellular processes they are involved in. The cyst phase is important in the *Entamoeba* life cycle as it represent the infectious stage of this parasite. Because it is currently not possible to induce cyst formation in *E. histolytica in vitro*, we used its proxy *E. invadens* for which cyst production in the laboratory is reproducible. Mitosomes have thus far only been shown in *E. histolytica* trophozoites.

8.2.2 Mitosomes in *Entamoeba invadens* cysts

We discovered in our localization experiments that mitosomes are also present in high abundance in *E. invadens*. Because *invadens* and *histolytica* are distant *Entamoeba* species, this observation suggests that mitosomes are characteristic for all *Entamoeba* spp. and perhaps part of their adaptation to a parasitic life style. Mitosomal presence has never been shown in cysts before, for any mitosomal species. In this study, we clearly demonstrate that mitosomes are present in this life cycle stage as well. Their high abundance furthermore indicates that they might play an important role during stage conversion too.

Our analyses also showed that we could not observe mitosome organization centres (MOC) comparable to *Giardia intestinalis*, in which mitosomes are divided (Regoes *et al*. 2005). The high abundance of mitosomes in trophozoites as well as

cysts leads us to the conclusion that mitosomes are inherited stochastically and are not centrally proliferated in MOC's. Thus, two unrelated mitosome containing lineages (*i.e. Giardia* and *Entamoeba*) appear to have evolved different ways of mitosomal inheritance. There seems to be large variation in the number of mitosomes in the different species. While microsporidian taxa may contain < 10 organelles per cell (Vavra, 2005), *Giardia* harbours in the range of 10-100 mitosomes (Regoes *et al*. 2005) and *E. histolytica* 100-1,000 of mitosomes (León-Avila & Tovar, 2004). Our study suggests that the number of mitosomes in *Entamoeba invadens* is comparable to *E. histolytica.* This indicates that high numbers of several hundreds of mitosomes are common among *Entamoeba* spp. in trophozoites as well as cysts.

8.2.3 Characterization of *Entamoeba* spp. mitosomal Hsp70

In addition to analyzing mitosomal presence and abundance, this study allowed us to revisit the characterization of the mitosomal markers Hsp60 (also named Cpn60 in many relevant studies) and Hsp70. Hsp60 has been previously shown to be mitosomal and closely related to other mitochondrial Hsp60 proteins (Clark & Roger, 1995, Tovar *et al*., 1999). Hsp70 however, has not been analysed previousy using a homologous Hsp70 antibody. Previous studies have shown, that *E. histolytica* mitosomal Hsp70 is indeed of mitochondrial ancestry (Bakatselou *et al*., 2000, Bakatselou & Clark, 2000, Tovar *et al*., 2007), but its position within the eukaryotic phylogeny was not resolved. Our analyses clearly show that mitosomal *Entamoeba* Hsp70 is indeed sister to the free-living Amoebozoa and nests within the α-proteobacterial derived eukaryotic Hsp70 sequences. Furthermore, we could include additional amoebozoan sequences from *Hartmannella vermiformis*, *Polysphondylium pallidum*, *Entamoeba invadens* and *E. moshkovskii* that have not been analyzed previously. The *Entamoeba* clade exhibits a very long branch in our phylogenetic reconstruction. This is probably due to their fast evolving nature of gene sequences in the *Entamoeba* genome in comparison to Hsp70 sequences from free-living Amoebozoa. Thus, the lack of closely related sequences may have resulted in a long-branch leading to the *Entamoebae*. With the availability of more amoebozoan Hsp70 sequences this divergence gap could probably be closed.

8.2.4 *In silico* characterization of the dynamin related proteins in *Entamoeba* spp.

In order to study the involvement of dynamins in mitosomal division we searched the *Entamoeba histolytica* genome for all available gene sequences. We identified four putative dynamin sequences, which we named Drp1 (XP649650), Drp2 (XP651634), Drp3 (XP653348) and Drp4 (XP651307) and analyzed their domain structures, sequence compositions and phylogenetic positions in the eukaryotic tree of life in order to understand their potential function. We discovered two types of dynamin related proteins in *Entamoeba histolytica*. Drp1 and Drp2 exhibit the conserved domain structure found in most member of the dynamin protein family including the large GTPase domain and the middle and GTPase effector domain. Both sequences differ in amino acid composition especially in V-segment between middle and GTPase effector domain, which suggests functional differences. Unlike Drp2, Drp1 is proline rich in this segment, an amino acid motif that is often associated with protein-protein interaction (Kay *et al*., 2000). In contrast, Drp3 and Drp4 only exhibit the large dynamin GTPase domain, whereas the other domains are not detectable by sequence comparison. None of the *Entamoeba histolytica* dynamins have recognizable targeting signals suggesting that they function in the cytosolic fraction of the cell. However, as observed for mitosomal Hsp60 and Hsp70 proteins, the available localization prediction tools do not recognize *Entamoeba* targeting signals. During this work a study by Jain *et al*. (2010) discovered that Drp1 was indeed cytosolic and localized additionally to the outer nuclear envelope. Our localization experiments for Drp2 using our homologous antibody clearly show a cytosolic distribution. Thus, both findings verify the *in silico* localization predictions for Drp1 and Drp2 and demonstrated that in *Entamoeba* these two proteins are not associated with mitosomal function.

Phylogenetic reconstructions show that *Entamoeba* Drp1 and Drp2 form an independent distinct clade without a supported relationship to other eukaryotic dynamin proteins including the DymA and DymB sequences of the free-living amoebozoan *D. discoideum*. Because Drp1 was not found to be involved in mitosomal division (Jain *et al*. 2008), we concentrated our analyses on Drp2.

8.2.5 *In vivo* and *in vitro* characterization of the *Entamoeba* dynamin protein family

The kinetic characterisation shows that the recombinant Drp2 protein behaves similar to previously analysed members of the dynamin protein family in exhibiting a low affinity and turnover of the GTP substrate as well as showing cooperative behaviour with respect to GTP. We could show that Drp2 is actively expressed in *E. histolytica* and *E. invadens* trophozoites as well as in different stages of *E. invadens* cyst formation.

E. invadens contains a local gene duplication of Drp2, which we called EiDrp2 and EiDrp2a. EiDrp2a is highly expressed in all life stages, while EiDrp2 shows lower expression levels. Thus, both proteins appear to be functional in the cell but it is not possible to know at this point which of the two proteins functionally resemble Drp2 in *E. histolytica*. Our localization studies using the homologous Drp2 and Hsp70 antibodies show that Drp2 is highly abundant in the cell and localizes to punctate structures dispersed throughout the cytosol. It does, however, not co-localize with mitosomes suggesting that Drp2 is not directly involved in the division of these organelles. This is further supported by the inability of Drp2 to complement DymA in *D. discoideum* null mutants, indicating that both proteins do not share a common functionality in mitochondrial division. This is in agreement with Gaechter *et al*. (2008) who discovered that the single dynamin present in the metamonad *Giardia* plays a role during stage conversion and endocytic transport and not in mitosomal division. The distribution of Drp2 in the cystosol also suggests an involvement with the endocytic pathway because it strongly resembles endosomal distribution patterns found in metazoan cells (Duleh & Welch, 2011). This is however purely speculative and cellular markers are required for further co-localization studies in order to understand the function of Drp2 in the *Entamoeba* cell.

EhDrp2 was overexpressed in *E. histolytica* trophozoites and *D. discoideum* cells. The over-expression in *E. histolytica* cells resulted in a statistically significant increase in the number of nuclei per cell. The Drp2 over-expression resulted in the decrease of cell growth and produced distinct cell shape alterations, which resulted in the absence of amoeboid movement and prevented the attachment of the cells to

surfaces. The effect of Drp2 overexpression, the slower growth, cell shape alterations and the subsequent impairment of cell motility in transfected *E. histolytica* cells indicate an effect on cytoskeletal organisation. Dynamins involved in cytoskeletal organisations have been observed previously in human cells (Gu *et al*., 2010) and for DymB in *D. discoideum* (Rai *et al*. 2010). In human cells, dynamin has been shown to assemble around actin and stimulate short actin filament assembly to actin bundles. In *D. discoideum* the absence of DymB affects cell motility, cell-to-cell and surface adhesion. Thus, the over-expression of Drp2 in *E. histolytica* in comparison to *D. discoideum* DymB negative cells could be interpreted as a dominant negative effect. However, it is difficult to understand the actual process in the cell and draw conclusions about the specific function of Drp2 yet. Over-expression of *E. histolytica* Drp2 in *D. discoideum* cells lead to a decoupling of cytokinesis from nuclear division resulting in numerous nuclei and increased cell size. The EhDrp2/*D. discoideum* phenotype resembled *D. discoideum* DymA null cells, in which DymA is absent. Like for Drp2/*E. histolytica* the actual process in the cell is difficult to interpret. Over-expression appears to strongly influence cytoskeletal organisation and cell division in accordance with Drp2/*E. histolytica.* An alternative scenario resulting in the Drp2/*D. discoideum* phenotype could be the formation of mixed assemblies of DymA and/or DymB with recombinant Drp2 leading to insufficient functionality of the *D. discoideum* dynamins in the cell and thus a dominant negative effect comparable to DymA null cells.

Drp3 and Drp4 are closely related to *D. discoideum* DlpA, DlpB and DlpC, which are involved in cytokinesis, and plant DRP5A and DRP5B involved in cytokinesis and chloroplast division (Miyagishima *et al*., 2008). Our phylogenetic analyses indicate that cytokinesis involving dynamin related proteins might be a conserved characteristic throughout the Amoebozoa. However, our data also show that Drp3 is only weakly expressed in trophozoites and thus might not play a major role during cell division. Using *E. invadens* as proxy for stage conversion experiments, we were able to show that Drp3 experiences a strong up-regulation during encystation. Thus it appears that this protein has acquired new as yet unknown functions in the *Entamoebae*.

For Drp4 the results are not as clear. In *E. histolytica* trophozoites, Drp4 shows higher expression levels than Drp3, which suggests a functional role in this life cycle stage. In *E. invadens* however, Drp4 levels are as low as for Drp3, which was supported by semi-quantitative RT-PCR and qPCR analyses. In *E. invadens,* Drp4 is upregulated only during late cyst formation suggesting that it acts predominantly in this life cycle stage. It is reasonable to assume that both Drp3 and Drp4 play a major, yet unknown role during cyst formation in *Entamoeba* spp. that does not involve cytokinesis. Whether Drp4 acts as a component during *Entamoeba* cytokinesis has to be analysed in future. Both dynamin proteins are especially interesting because they are not present in metazoan cells and might therefore be promising candidates for drug development.

8.3 Future work

In order to understand the process of mitosomal division in *Entamoeba*, a series of electron microscopy experiments including *E. histolytica* and *E. invadens* could be carried out. I would recommend concentrating on dividing cells and different stages of cyst formation to search for mitosomal division stages. In order to gain a high number of dividing cells, a 2-day culture with cells in exponential growth phase should be used. Although growth synchronization of *Entamoeba histolytica* cells by serum starvation is possible (Gangopadhyay *et al.*, 1997), our attempts this far were unsuccessful (data not shown). Further experiments in gaining synchronous cultures to increase the amount of dividing cells would possibly be beneficial for microscopy experiments. The advantage of electron microscopy over fluorescent microscopy lies in the higher magnification and resolution and the possibility to observe single mitosomes and their exact position during cell division. Vavra, (2005) found single mitosomes positioned at the nuclear spindles in microsporidia indicating that organelle and cell division are coordinated. If this was the case in *Entamoeba* we would expect a differentiation between mitosomes that are responsible for division and mitosomes that are stochastically separated into the daughter cells in accordance with the mitosomal inheritance in *Giardia* (Regoes *et al*., 2005). Cryo-electron microscopy in particular might be a promising tool because cells can be

analyzed without fixation or staining, processes that potentially harm or displace cellular structures. This method also allows the observation of microtubules and could highlight if they are involved in the mitosomal division process.

In order to understand the role of Drp2 in the cells, co-localization studies could be carried out by using additional cellular markers such as the binding immunoglobulin protein (BiP=ERHsp70), an endoplasmic reticulum marker, and Transferrin, an endosomal marker in combination with our homologous Drp2 antibody. In addition, cellular Drp2 could be functionally inhibited by introducing a truncated Drp2 peptide with the *Entamoeba* specific pAH-DEST vector into the cell. As direct mutagenesis studies are currently impossible in *Entamoeba*, this would be a gentle approach to produce functional mutants as this would result in an assembly of the introduced Drp2 peptide with cellular Drp2 and thus functionally inactive the protein polymers.

To further understand Drp2 protein functionality, inhibition and stimulation experiments could be conducted on recombinant soluble Drp2 protein using the NADH coupled GTPase enzyme assay. Furthermore, temperature dependency in substrate turnover could be analysed. Our experiments were conducted at 20 °C. *E. histolytica* is a human parasite and is adapted to grow and function at 37 °C. Thus, is would be interesting to analyse if temperature changes result in different kinetic behaviours.

In future studies, I would especially concentrate on analyzing the Drp3 protein. This is a promising protein because it would likely enhance our understanding of dynamin protein evolution and functionality. Furthermore, it might provide a promising drug target due to its role in cyst formation and its absence in human cells. I would produce recombinant protein in order to conduct crystallization studies to understand the three dimensional structure of the protein and would like to perform kinetic enzyme studies to understand its functional behaviour in comparison to classical dynamins. Additionally, I would produce homologous antibodies for both Drp3 and Drp4, in order to localize both proteins in trophozoites and cyst stages.

To enhance our understanding of cyst production in *Entamoeba*, transcriptomic studies on different cyst formation stages could be carried out. This

would involve the isolation of total RNA from different cyst formation stages followed by mRNA isolation and cDNA production and subsequent sequencing using next generation technology such as the department's Illumina HiSeq 2000 sequencer.

Finally, I would aim to understand the broad range diversity of dynamins by focusing on dynamin distribution in bacteria and archaea. There are only a few studies on bacterial dynamins and none for archaeal homologous. As dynamins are essential in fundamental membrane alteration processes, it is likely that they are ubiquitously present across the tree of life. Initial sequence search experiments using BLAST suggest the presence of dynamin homologous in Archaea (data not shown). Furthermore, several archaeal sequences were annotated as dynamin proteins in genome projects. Studying the diversity of this protein family will likely help in understanding the evolution of the dynamin protein family and its function and importance for the evolution of membrane alteration processes.

Bibliography

Abhyankar, M. M., A. E. Hochreiter, S. K. Connell, C. A. Gilchrist, B. J. Mann & W. A. Petri, Jr., (2009) Development of the Gateway system for cloning and expressing genes in *Entamoeba histolytica*. *Parasitology International* **58**: 95-97.

Alexander, C., M. Votruba, U. E. Pesch, D. L. Thiselton, S. Mayer, A. Moore, M. Rodriguez, U. Kellner, B. Leo-Kottler, G. Auburger, S. S. Bhattacharya & B. Wissinger, (2000) OPA1, encoding a dynamin-related GTPase, is mutated in autosomal dominant optic atrophy linked to chromosome 3q28. *Nature Genetics* **26**: 211-215.

Ali, V., Y. Shigeta, U. Tokumoto, Y. Takahashi & T. Nozaki, (2004) An intestinal parasitic protist, *Entamoeba histolytica*, possesses a non-redundant nitrogen fixation-like system for iron-sulfur cluster assembly under anaerobic conditions. *The Journal of Biological Chemistry* **279**: 16863-16874.

Altschul, S. F., W. Gish, W. Miller, E. W. Myers & D. J. Lipman, (1990) Basic local alignment search tool. *Journal of Molecular Biology* **215**: 403-410.

Arimura, S.-i. & N. Tsutsumi, (2002) A dynamin-like protein (ADL2b), rather than FtsZ, is involved in *Arabidopsis* mitochondrial division. *PNAS* **99**: 5727-5731.

Arisue, N., L. B. Sánchez, L. M. Weiss, M. Müller & T. Hashimoto, (2002) Mitochondrial-type hsp70 genes of the amitochondriate protists, *Giardia intestinalis*, *Entamoeba histolytica* and two microsporidians. *Parasitology International* **51**: 9-16.

Arroyo-Begovich, A., A. Carabez-Trejo & J. Ruiz-Herrera, (1980) Identification of the structural component in the cyst wall of *Entamoeba invadens*. *The Journal of Parasitology* **66**: 735-741.

Bakatselou, C., D. Beste, A. O. Kadri, S. Somanath & C. G. Clark, (2003) Analysis of genes of mitochondrial origin in the genus *Entamoeba*. *Journal of Eukaryotic Microbiology* **50**: 210-214.

Bakatselou, C. & C. G. Clark, (2000) A Mitochondrial-Type Hsp70 Gene of *Entamoeba histolytica*. *Archives of Medical Research* **31**: S176-S177.

Bakatselou, C., C. Kidgell & C. G. Clark, (2000) A mitochondrial-type hsp70 gene of *Entamoeba histolytica*. *Molecular Biochemistry and Parasitology* **110**: 177-182.

Ballard, T. E., X. Wang, I. Olekhnovich, T. Koerner, C. Seymour, P. S. Hoffman & T. L. Macdonald, (2010) Biological activity of modified and exchanged 2-amino-5-nitrothiazole amide analogues of nitazoxanide. *Bioorganic & Medicinal Chemistry Letters* **20**: 3537-3539.

Bapteste, E., H. Brinkmann, J. A. Lee, D. V. Moore, C. W. Sensen, P. Gordon, L. Durufle, T. Gaasterland, P. Lopez, M. Muller & H. Philippe, (2002) The analysis of 100 genes supports the grouping of three highly divergent amoebae: *Dictyostelium*, *Entamoeba*, and *Mastigamoeba*. *Proceedings of the National Academy of Sciences of the United States of America* **99**: 1414-1419.

Barker, D. C., (1963) Ribosome Structures Revealed by Negative Staining Subcellular Fractions from a Crystalline Ribonucleoprotein Body. *Experimental Cell Research* **32**: 272-279.

Bashkirov, P. V., S. A. Akimov, A. I. Evseev, S. L. Schmid, J. Zimmerberg & V. A. Frolov, (2008) GTPase cycle of dynamin is coupled to membrane squeeze and release, leading to spontaneous fission. *Cell* **135**: 1276-1286.

Beech, P. L., T. Nheu, T. Schultz, S. Herbert, T. Lithgow, P. R. Gilson & G. I. McFadden, (2000) Mitochondrial FtsZ in a chromophyte alga. *Science (New York, N.Y* **287**: 1276-1279.

Benchimol, M., P. J. Johson & W. De Souza, (1996) Morphogenesis of the hydrogenosomes: An ultrastructural study. *Biological Cell* **87**: 197-205.

Bleazard, W., J. M. McCaffery, E. J. King, S. Bale, A. Mozdy, Q. Tieu, J. Nunnari & J. M. Shaw, (1999) The dynamin-related GTPase Dnm1 regulates mitochondrial fission in yeast. *Nature Cell Biology* **1**: 298-304.

Bourne, H. R., D. A. Sanders & F. McCormick, (1991) The GTPase superfamily: conserved structure and molecular mechanism. *Nature* **349**: 117-127.

Boxma, B., R. M. de Graaf, G. W. van der Staay, T. A. van Alen, G. Ricard, T. Gabaldon, A. H. van Hoek, S. Y. Moon-van der Staay, W. J. Koopman, J. J. van Hellemond, A. G. Tielens, T. Friedrich, M. Veenhuis, M. A. Huynen & J. H. Hackstein, (2005) An anaerobic mitochondrion that produces hydrogen. *Nature* **434**: 74-79.

Bradford, J. F., (1976) A rapid and sensitive method for the quantitation of microgram quantities of protein utilizing the principle of protein-dye binding. *Analytical.Biochemistry* **72**: 248-254.

Brameier, M., A. Krings & R. M. MacCallum, (2007) NucPred--predicting nuclear localization of proteins. *Bioinformatics (Oxford, England)* **23**: 1159-1160.

Bui, E. T. N., P. J. Bradley & P. J. Johnson, (1996) A common evolutionary origin for mitochondria and hydrogenosomes. *PNAS USA* **93**: 9651-9656.

Burri, L., B. A. Williams, D. Bursac, T. Lithgow & P. J. Keeling, (2006) Microsporidian mitosomes retain elements of the general mitochondrial targeting system. *PNAS USA* **103**: 15916-15920.

Carlton, J. M., R. P. Hirt, J. C. Silva, A. L. Delcher, M. Schatz, Q. Zhao, J. R. Wortman, S. L. Bidwell, U. C. Alsmark, S. Besteiro, T. Sicheritz-Ponten, C. J. Noel, J. B. Dacks, P. G. Foster, C. Simillion, Y. Van de Peer, D. Miranda-Saavedra, G. J. Barton, G. D. Westrop, S. Muller, D. Dessi, P. L. Fiori, Q. Ren, I. Paulsen, H. Zhang, F. D. Bastida-Corcuera, A. Simoes-Barbosa, M. T. Brown, R. D. Hayes, M. Mukherjee, C. Y. Okumura, R. Schneider, A. J. Smith, S. Vanacova, M. Villalvazo, B. J. Haas, M. Pertea, T. V. Feldblyum, T. R. Utterback, C. L. Shu, K. Osoegawa, P. J. de Jong, I. Hrdy, L. Horvathova, Z. Zubacova, P. Dolezal, S. B. Malik, J. M. Logsdon, Jr., K. Henze, A. Gupta, C. C. Wang, R. L. Dunne, J. A. Upcroft, P. Upcroft, O. White, S. L. Salzberg, P. Tang, C. H. Chiu, Y. S. Lee, T. M. Embley, G. H. Coombs, J. C. Mottram, J. Tachezy, C. M. Fraser-Liggett & P. J. Johnson, (2007) Draft genome sequence of the sexually transmitted pathogen *Trichomonas vaginalis*. *Science (New York, N.Y* **315**: 207-212.

Cavalier-Smith, T., (1983) A 6 kingdom classification and a unified phylogeny. In: Endocytobiology II. W. Schwemmler & H. E. A. Schenk (eds). Berlin: De Gruyter, pp. 1027-1034.

Chadee, K. & E. Meerovitch, (1984) The pathogenesis of experimentally induced amebic liver abscess in the gerbil (*Meriones unguiculatus*). *The American journal of pathology* **117**: 71-80.

Chan, K. W., D. J. Slotboom, S. Cox, T. M. Embley, O. Fabre, M. van der Giezen, M. Harding, D. S. Horner, E. R. Kunji, G. Leon-Avila & J. Tovar, (2005) A novel ADP/ATP transporter in the mitosome of the microaerophilic human parasite *Entamoeba histolytica*. *Current Biology* **15**: 737-742.

Chanez, A. L., A. B. Hehl, M. Engstler & A. Schneider, (2006) Ablation of the single dynamin of *T. brucei* blocks mitochondrial fission and endocytosis and leads to a precise cytokinesis arrest. *Journal of Cell Science* **119**: 2968-2974.

Chappie, J. S., S. Acharya, M. Leonard, S. L. Schmid & F. Dyda, (2010) G domain dimerization controls dynamin's assembly-stimulated GTPase activity. *Nature* **465**: 435-440.

Chatterjee, A., S. K. Ghosh, K. Jang, E. Bullitt, L. Moore, P. W. Robbins & J. Samuelson, (2009) Evidence for a "wattle and daub" model of the cyst wall of *Entamoeba*. *PLoS Pathogens* **5**: e1000498.

Chavez-Munguia, B., M. Espinosa-Cantellano, G. Castanon & A. Martinez-Palomo, (2000) Ultrastructural evidence of smooth endoplasmic reticulum and golgi-like elements in *Entamoeba histolytica* and *Entamoeba dispar*. *Archives of Medical Research* **31**: S165-167.

Chavez-Munguia, B., P. Talamas-Rohana, A. Rios, M. Gonzalez-Lazaro & A. Martinez-Palomo, (2008) Entamoeba histolytica: fibrilar aggregates in dividing trophozoites. *Experimental Parasitology* **118**: 280-284.

Clark, C. G., (2000) The evolution of *Entamoeba*, a cautionary tale. *Research in Microbiology* **151**: 599-603.

Clark, C. G. & L. S. Diamond, (1997a) Intraspecific variation and phylogenetic relationships in the genus *Entamoeba* as revealed by riboprinting. *The Journal of Eukaryotic Microbiology* **44**: 142-154.

Clark, C. G. & L. S. Diamond, (1997b) Molecular phylogeny of the genus *Entamoeba* as revealed by riboprinting. *Archives of medical research* **28 Spec No**: 69-70.

Clark, C. G., F. Kaffashian, B. Tawari, J. J. Windsor, A. Twigg-Flesner, M. C. Davies-Morel, J. Blessmann, F. Ebert, B. Peschel, A. Le Van, C. J. Jackson, L. Macfarlane & E. Tannich, (2006) New insights into the phylogeny of *Entamoeba* species provided by analysis of four new small-subunit rRNA genes. *International Journal of Systematic and Evolutionary Microbiology* **56**: 2235-2239.

Clark, C. G. & A. J. Roger, (1995) Direct evidence for secondary loss of mitochondria in *Entamoeba histolytica*. *PNAS USA* **92**: 6518-6521.

Claros, M. G. & P. Vincens, (1996) Computational method to predict mitochondrially imported proteins and their targeting sequences. *European Journal of Biochemistry* **241**: 779-786.

Conner, S. D. & S. L. Schmid, (2003) Regulated portals of entry into the cell. *Nature* **422**: 37-44.

Danino, D. & J. E. Hinshaw, (2001) Dynamin family of mechanoenzymes. *Current Opinion in Cell Biology* **13**: 454-460.

Danino, D., K. H. Moon & J. E. Hinshaw, (2004) Rapid constriction of lipid bilayers by the mechanochemical enzyme dynamin. *Journal of structural biology* **147**: 259-267.

Das, S., K. Van Dellen, D. Bulik, P. Magnelli, J. Cui, J. Head, P. W. Robbins & J. Samuelson, (2006) The cyst wall of *Entamoeba invadens* contains chitosan (deacetylated chitin). *Molecular and Biochemical Parasitology* **148**: 86-92.

David, C., P. S. McPherson, O. Mundigl & P. de Camilli, (1996) A role of amphiphysin in synaptic vesicle endocytosis suggested by its binding to dynamin in nerve terminals. *PNAS USA* **93**: 331-335.

Di, A., D. J. Nelson, V. Bindokas, M. E. Brown, F. Libunao & H. C. Palfrey, (2003) Dynamin regulates focal exocytosis in phagocytosing macrophages. *Molecular Biology of the Cell* **14**: 2016-2028.

Dobell, C., (1919) The Amoebae living in Man.

Doherty, G. J. & H. T. McMahon, (2009) Mechanisms of endocytosis. *Annual Review of Biochemistry* **78**: 857-902.

Dolezal, P., M. J. Dagley, M. Kono, P. Wolynec, V. A. Likic, J. H. Foo, M. Sedinova, J. Tachezy, A. Bachmann, I. Bruchhaus & T. Lithgow, (2010) The essentials of protein import in the degenerate mitochondrion of *Entamoeba histolytica*. *PLoS Pathogens* **6**: e1000812.

Duleh, S. N. & M. D. Welch, (2011) WASH and the Arp2/3 complex regulate endosome shape and trafficking. *Cytoskeleton (Hoboken, N.J* **67**: 193-206.

Ehrenkaufer, G. M., R. Haque, J. A. Hackney, D. J. Eichinger & U. Singh, (2007) Identification of developmentally regulated genes in *Entamoeba histolytica*: insights into mechanisms of stage conversion in a protozoan parasite. *Cellular Microbiology* **9**: 1426-1444.

Eichinger, D., (2001) Encystation in parasitic protozoa. *Current Opinion in Microbiology* **4**: 421-426.

Elde, N. C., G. Morgan, M. Winey, L. Sperling & A. P. Turkewitz, (2005) Elucidation of clathrin-mediated endocytosis in tetrahymena reveals an evolutionarily convergent recruitment of dynamin. *PLoS Genetics* **1**: e52.

Emanuelsson, O., S. Brunak, G. von Heijne & H. Nielsen, (2007) Locating proteins in the cell using TargetP, SignalP and related tools. *Nature Protocols* **2**: 953-971.

Embley, T. M. & W. Martin, (2006) Eukaryotic evolution, changes and challenges. *Nature* **440**: 623-630.

Embley, T. M., M. van der Giezen, D. S. Horner, P. L. Dyal, S. Bell & P. Foster, (2003) Hydrogenosomes, mitochondria and early eukaryotic evolution. *IUBMB Life* **55**: 387-395.

Ferguson, K. M., M. A. Lemmon, J. Schlessinger & P. B. Sigler, (1994) Crystal structure at 2.2 A resolution of the pleckstrin homology domain from human dynamin. *Cell* **79**: 199-209.

Finn, R. D., J. Mistry, J. Tate, P. Coggill, A. Heger, J. E. Pollington, O. L. Gavin, P. Gunasekaran, G. Ceric, K. Forslund, L. Holm, E. L. Sonnhammer, S. R. Eddy & A. Bateman, (2010) The Pfam protein families database. *Nucleic Acids Research* **38**: D211-222.

Gaechter, V., E. Schraner, P. Wild & A. B. Hehl, (2008) The single dynamin family protein in the primitive protozoan *Giardia lamblia* is essential for stage conversion and endocytic transport. *Traffic (Copenhagen, Denmark)* **9**: 57-71.

Gangopadhyay, S. S., S. S. Ray, K. Kennady, G. Pande & A. Lohia, (1997) Heterogeneity of DNA content and expression of cell cycle genes in axenically growing *Entamoeba histolytica* HM1:IMSS clone A. *Molecular and biochemical parasitology* **90**: 9-20.

Gao, S., A. von der Malsburg, S. Paeschke, J. Behlke, O. Haller, G. Kochs & O. Daumke, (2010) Structural basis of oligomerization in the stalk region of dynamin-like MxA. *Nature* **465**: 502-506.

Gasper, R., S. Meyer, K. Gotthardt, M. Sirajuddin & A. Wittinghofer, (2009) It takes two to tango: regulation of G proteins by dimerization. *Nature reviews* **10**: 423-429.

Gathiram, V. & T. F. Jackson, (1987) A longitudinal study of asymptomatic carriers of pathogenic zymodemes of Entamoeba histolytica. *South African medical journal = Suid-Afrikaanse tydskrif vir geneeskunde* **72**: 669-672.

Germot, A., H. Philippe & H. Le Guyader, (1996) Presence of a mitochondrial-type 70-kDa heat shock protein in *Trichomonas vaginalis* suggests a very early mitochondrial endosymbiosis in eukaryotes. *PNAS USA* **93**: 14614-14617.

Ghosh, A., G. J. Praefcke, L. Renault, A. Wittinghofer & C. Herrmann, (2006) How guanylate-binding proteins achieve assembly-stimulated processive cleavage of GTP to GMP. *Nature* **440**: 101-104.

Gill, E. E., S. Diaz-Triviño, M. J. Barberà, J. D. Silberman, A. Stechmann, D. Gaston, I. Tamas & A. J. Roger, (2007) Novel mitochondrion-related organelles in the anaerobic amoeba *Mastigamoeba balamuthi*. *Molecular Microbiology* **66**: 1306-1320.

Gilson, P. R., X. C. Yu, D. Hereld, C. Barth, A. Savage, B. R. Kiefel, S. Lay, P. R. Fisher, W. Margolin & P. L. Beech, (2003) Two *Dictyostelium* orthologs of the prokaryotic cell division protein FtsZ localize to mitochondria and are required for the maintenance of normal mitochondrial morphology. *Eukaryotic Cell* **2**: 1315-1326.

Goldberg, A. V., S. Molik, A. D. Tsaousis, K. Neumann, G. Kuhnke, F. Delbac, C. P. Vivares, R. P. Hirt, R. Lill & T. M. Embley, (2008) Localization and functionality of microsporidian iron-sulphur cluster assembly proteins. *Nature* **452**: 624-628.

Gouy, M., S. Guindon & O. Gascuel, (2010) SeaView version 4: A multiplatform graphical user interface for sequence alignment and phylogenetic tree building. *Molecular Biology and Evolution* **27**: 221-224.

Gräf, R., (2009) Microtubule Organization in *Dictyostelium*. *John Wiley & Sons, Ltd*.

Graf, R., C. Daunderer & M. Schliwa, (2000) *Dictyostelium* DdCP224 is a microtubule-associated protein and a permanent centrosomal resident involved in centrosome duplication. *Journal of Cell Science* **113 (Pt 10)**: 1747-1758.

Gray, M. W., G. Burger & B. F. Lang, (1999) Mitochondrial evolution. *Science (New York, N.Y* **283**: 1476-1481.

Grote, A., K. Hiller, M. Scheer, R. Münch, B. Nörtemann, D. C. Hempel & D. Jahn, (2005) JCat: a novel tool to adapt codon usage of a target gene to its potential expression host. *Nucleic Acids Research* **33**: W526-W531.

Gu, C., S. Yaddanapudi, A. Weins, T. Osborn, J. Reiser, M. Pollak, J. Hartwig & S. Sever, (2010) Direct dynamin-actin interactions regulate the actin cytoskeleton. *The EMBO Journal* **29**: 3593-3606.

Guan, K., L. Farh, T. K. Marshall & R. J. Deschenes, (1993) Normal mitochondrial structure and genome maintenance in yeast requires the dynamin-like product of the MGM1 gene. *Current Genetics* **24**: 141-148.

Guindon, S., J. F. Dufayard, V. Lefort, M. Anisimova, W. Hordijk & O. Gascuel, (2010) New algorithms and methods to estimate maximum-likelihood phylogenies: assessing the performance of PhyML 3.0. *Systematic Biology* **59**: 307-321.

Gupta, S. S., O. Singh, S. Shukla & M. K. Raj, (2009) Acute fulminant necrotizing amoebic colitis: a rare and fatal complication of amoebiasis: a case report. *Cases Journal* **2**: 6557.

Gupta, Y. K., M. Gupta, S. Aneja & K. Kohli, (2004) Current drug therapy of protozoal diarrhoea. *Indian Journal of Pediatrics* **71**: 55-58.

Hampl, V., J. D. Silberman, A. Stechmann, S. Diaz-Trivino, P. J. Johnson & A. J. Roger, (2008) Genetic evidence for a mitochondriate ancestry in the 'amitochondriate' flagellate *Trimastix pyriformis*. *PloS One* **3**: e1383.

Haque, R., C. D. Huston, M. Hughes, E. Houpt & W. A. Petri, Jr., (2003) Amebiasis. *The New England Journal of Medicine* **348**: 1565-1573.

Haque, R., D. Mondal, P. Duggal, M. Kabir, S. Roy, B. M. Farr, R. B. Sack & W. A. Petri, Jr., (2006) *Entamoeba histolytica* infection in children and protection from subsequent amebiasis. *Infection and Immunity* **74**: 904-909.

Hawkins, J., L. Davis & M. Boden, (2007) Predicting nuclear localization. *Journal of Proteome Research* **6**: 1402-1409.

Henley, J. R., E. W. Krueger, B. J. Oswald & M. A. McNiven, (1998) Dynamin-mediated internalization of caveolae. *The Journal of Cell Biology* **141**: 85-99.

Heymann, J. A. & J. E. Hinshaw, (2009) Dynamins at a glance. *Journal of Cell Science* **122**: 3427-3431.

Hinshaw, J. E. & S. L. Schmid, (1995) Dynamin self-assembles into rings suggesting a mechanism for coated vesicle budding. *Nature* **374**: 190-192.

Hoepfner, D., M. van den Berg, P. Philippsen, H. F. Tabak & E. H. Hettema, (2001) A role for Vps1p, actin, and the Myo2p motor in peroxisome abundance and inheritance in *Saccharomyces cerevisiae*. *The Journal of Cell Biology* **155**: 979-990.

Hoffman, P. S., G. Sisson, M. A. Croxen, K. Welch, W. D. Harman, N. Cremades & M. G. Morash, (2007) Antiparasitic drug nitazoxanide inhibits the pyruvate oxidoreductases of *Helicobacter pylori*, selected anaerobic bacteria and parasites, and Campylobacter jejuni. *Antimicrobial Agents and Chemotherapy* **51**: 868-876.

Hoppins, S., L. Lackner & J. Nunnari, (2007) The machines that divide and fuse mitochondria. *Annual review of biochemistry* **76**: 751-780.

Hoppins, S. & J. Nunnari, (2009) The molecular mechanism of mitochondrial fusion. *Biochimica et Biophysica Acta* **1793**: 20-26.

Horton, P., K. J. Park, T. Obayashi, N. Fujita, H. Harada, C. J. Adams-Collier & K. Nakai, (2007) WoLF PSORT: protein localization predictor. *Nucleic Acids Research* **35**: W585-587.

Huggett, J., K. Dheda, S. Bustin & A. Zumla, (2005) Real-time RT-PCR normalisation; strategies and considerations. *Genes and Immunity* **6**: 279-284.

Ingerman, E. & J. Nunnari, (2005) A continuous, regenerative coupled GTPase assay for dynamin-related proteins. *Methods in Enzymology* **404**: 611-619.

Ingerman, E., E. M. Perkins, M. Marino, J. A. Mears, J. M. McCaffery, J. E. Hinshaw & J. Nunnari, (2005) Dnm1 forms spirals that are structurally tailored to fit mitochondria. *The Journal of Cell Biology* **170**: 1021-1027.

Ishikawa-Ankerhold, H. C., G. Gerisch & A. Muller-Taubenberger, (2010) Genetic evidence for concerted control of actin dynamics in cytokinesis, endocytic traffic, and cell motility by coronin and Aip1. *Cytoskeleton (Hoboken, N.J* **67**: 442-455.

Jain, R., S. Shrimal, S. Bhattacharya & A. Bhattacharya, (2010) Identification and partial characterization of a dynamin-like protein, EhDLP1, from the protist parasite *Entamoeba histolytica*. *Eukaryotic Cell* **9**: 215-223.

Jin, J. B., Y. A. Kim, S. J. Kim, S. H. Lee, D. H. Kim, G. W. Cheong & I. Hwang, (2001) A new dynamin-like protein, ADL6, is involved in trafficking from the trans-Golgi network to the central vacuole in *Arabidopsis*. *The Plant Cell* **13**: 1511-1526.

Kamaishi, T., T. Hashimoto, Y. Nakamura, F. Nakamura, S. Murata, N. Okada, K. Okamoto, M. Shimizu & M. Hasegawa, (1996) Protein phylogeny of translation elongation factor EF-1 alpha suggests microsporidians are extremely ancient eukaryotes. *Journal of Molecular Evolution* **42**: 257-263.

Karlin, S. & L. Brocchieri, (1998) Heat shock protein 70 family: multiple sequence comparisons, function, and evolution. *Journal of Molecular Evolution* **47**: 565-577.

Kay, B. K., M. P. Williamson & M. Sudol, (2000) The importance of being proline: the interaction of proline-rich motifs in signaling proteins with their cognate domains. *FASEB Journal* **14**: 10.

Keane, T., C. Creevey, M. Pentony, T. Naughton & J. McLnerney, (2006) Assessment of methods for amino acid matrix selection and their use on empirical data shows that ad hoc assumptions for choice of matrix are not justified. *BMC Evolutionary Biology* **6**: 29.

Keeling, P. J., (1998) A kingdom's progress: Archezoa and the origin of eukaryotes. *BioEssays* **20**: 87-95.

Kiefel, B. R., P. R. Gilson & P. L. Beech, (2004) Diverse eukaryotes have retained mitochondrial homologues of the bacterial division protein FtsZ. *Protist* **155**: 105-115.

Kjaeldgaard, P., E. Gutschik, B. Finnerup & K. Steven, (1985) Urinary tract infection with Entamoeba histolytica after ileocaecal bladder replacement. *Lancet* **1**: 1051.

Kobayashi, S., J. Suzuki & T. Takeuchi, (2009) Establishment of a continuous culture system for *Entamoeba muris* and analysis of the small subunit rRNA gene. *Parasite (Paris, France)* **16**: 135-139.

Koch, C. A., D. Anderson, M. F. Moran, C. Ellis & T. Pawson, (1991) SH2 and SH3 domains: elements that control interactions of cytoplasmic signaling proteins. *Science (New York, N.Y* **252**: 668-674.

Kuroiwa, T., (2010) Mechanisms of organelle division and inheritance and their implications regarding the origin of eukaryotic cells. *Proceedings of the Japan Academy* **86**: 455-471.

Laemmli, U. K., (1970) Cleavage of structural proteins during the assembly of the head of bacteriophage T4. *Nature* **227**: 680-685.

Lake, J. A. & H. S. Slayter, (1970) Three dimensional structure of the chromatoid body of Entamoeba invadens. *Nature* **227**: 1032-1037.

Lake, J. A. & H. S. Slayter, (1972) Three-dimensional structure of the chromatoid body helix of *Entamoeba invadens*. *Journal of Molecular Biology* **66**: 271-282.

Lane, N., (2011) Energetics and genetics across the prokaryote-eukaryote divide. *Biology direct* **6**: 35.

Lanzetta, P. A., L. J. Alvarez, P. S. Reinach & O. A. Candia, (1979) An improved assay for nanomole amounts of inorganic phosphate. *Analytical Biochemistry* **100**: 95-97.

Lawford, R. & T. C. Sorrell, (1994) Amebic abscess of the spleen complicated by metronidazole-induced neurotoxicity: case report. *Clinical Infectious Diseases* **19**: 346-348.

Le, S. Q. & O. Gascuel, (2008) An improved general amino acid replacement matrix. *Molecular Biology and Evolution* **25**: 1307-1320.

Lee, S. H., J. B. Jin, J. Song, M. K. Min, D. S. Park, Y. W. Kim & I. Hwang, (2002) The intermolecular interaction between the PH domain and the C-terminal domain of Arabidopsis dynamin-like 6 determines lipid binding specificity. *The Journal of Biological Chemistry* **277**: 31842-31849.

León-Avila, G. & J. Tovar, (2004) Mitosomes of *Entamoeba histolytica* are abundant mitochondrion-related remnant organelles that lack a detectable organellar genome. *Microbiology* **150**: 1245-1250.

Levecke, B., L. Dreesen, P. Dorny, J. J. Verweij, F. Vercammen, S. Casaert, J. Vercruysse & P. Geldhof, Molecular identification of *Entamoeba* spp. in captive nonhuman primates. *Journal of Clinical Microbiology* **48**: 2988-2990.

Li, E. & S. L. Stanley, Jr., (1996) Protozoa. Amebiasis. *Gastroenterology clinics of North America* **25**: 471-492.

Liu, Y. W., S. Neumann, R. Ramachandran, S. M. Ferguson, T. J. Pucadyil & S. L. Schmid, Differential curvature sensing and generating activities of dynamin isoforms provide opportunities for tissue-specific regulation. *Proceedings of the National Academy of Sciences of the United States of America* **108**: E234-242.

Livak, K. J. & T. D. Schmittgen, (2001) Analysis of relative gene expression data using real-time quantitative PCR and the 2(-Delta Delta C(T)) Method. *Methods (San Diego, Calif* **25**: 402-408.

Loftus, B., I. Anderson, R. Davies, U. C. Alsmark, J. Samuelson, P. Amedeo, P. Roncaglia, M. Berriman, R. P. Hirt, B. J. Mann, T. Nozaki, B. Suh, M. Pop, M. Duchene, J. Ackers, E. Tannich, M. Leippe, M. Hofer, I. Bruchhaus, U. Willhoeft, A. Bhattacharya, T. Chillingworth, C. Churcher, Z. Hance, B. Harris, D. Harris, K. Jagels, S. Moule, K. Mungall, D. Ormond, R. Squares, S. Whitehead, M. A. Quail, E. Rabbinowitsch, H. Norbertczak, C. Price, Z. Wang, N. Guillen, C. Gilchrist, S. E. Stroup, S. Bhattacharya, A. Lohia, P. G. Foster, T. Sicheritz-Ponten, C. Weber, U. Singh, C. Mukherjee, N. M. El-Sayed, W. A. Petri, C. G. Clark, T. M. Embley, B. Barrell, C. M. Fraser & N. Hall, (2005) The genome of the protist parasite *Entamoeba histolytica*. *Nature* **433**: 865-868.

Low, H. H. & J. Löwe, (2006) A bacterial dynamin-like protein. *Nature* **444**: 766-769.

Low, H. H. & J. Löwe, (2010) Dynamin architecture--from monomer to polymer. *Current Opinion in Structural Biology* **20**: 791-798.

Low, H. H., C. Sachse, L. A. Amos & J. Löwe, (2009) Structure of a bacterial dynamin-like protein lipid tube provides a mechanism for assembly and membrane curving. *Cell* **139**: 1342-1352.

Lupas, A., M. Van Dyke & J. Stock, (1991) Predicting coiled coils from protein sequences. *Science (New York, N.Y* **252**: 1162-1164.

Maeda, K., T. Nakata, Y. Noda, R. Sato-Yoshitake & N. Hirokawa, (1992) Interaction of dynamin with microtubules: its structure and GTPase activity investigated by using highly purified dynamin. *Molecular Biology of the Cell* **3**: 1181-1194.

Magalhaes, A. C., J. A. Silva, K. S. Lee, V. R. Martins, V. F. Prado, S. S. Ferguson, M. V. Gomez, R. R. Brentani & M. A. Prado, (2002) Endocytic intermediates involved with the intracellular trafficking of a fluorescent cellular prion protein. *The Journal of Biological Chemistry* **277**: 33311-33318.

Mai, Z., S. Ghosh, M. Frisardi, B. Rosenthal, R. Rogers & J. Samuelson, (1999) Hsp60 is targeted to a cryptic mitochondrion-derived organelle ("crypton") in the microaerophilic protozoan parasite *Entamoeba histolytica*. *Molecular Cellular Biology* **19**: 2198-2205.

Makioka, A., M. Kumagai, K. Hiranuka, S. Kobayashi & T. Takeuchi, (2011a) Different structure and mRNA expression of *Entamoeba invadens* chitinases in the encystation and excystation. *Parasitology Research* **109**: 417-423.

Makioka, A., M. Kumagai, K. Hiranuka, S. Kobayashi & T. Takeuchi, (2011b) Entamoeba invadens: identification of ADF/cofilin and their expression analysis in relation to encystation and excystation. *Experimental Parasitology* **127**: 195-201.

Manstein, D. J., H. P. Schuster, P. Morandini & D. M. Hunt, (1995) Cloning vectors for the production of proteins in *Dictyostelium discoideum*. *Gene* **162**: 129-134.

Maralikova, B., V. Ali, K. Nakada-Tsukui, T. Nozaki, M. van der Giezen, K. Henze & J. Tovar, (2010) Iron-sulphur protein mediated oxygen detoxification in amoebal mitosomes. *Cellular Microbiology* **12**: 331-342.

Martin, W. & M. Müller, (1998) The hydrogen hypothesis for the first eukaryote. *Nature* **392**: 37-41.

Mason, J. M. & K. M. Arndt, (2004) Coiled coil domains: stability, specificity, and biological implications. *Chembiochem* **5**: 170-176.

Mayer, B. J. & M. J. Eck, (1995) SH3 domains. Minding your p's and q's. *Current Biology* **5**: 364-367.

Mears, J. A., L. L. Lackner, S. Fang, E. Ingerman, J. Nunnari & J. E. Hinshaw, (2010) Conformational changes in Dnm1 support a contractile mechanism for mitochondrial fission. *Nature Structural & Molecular Biology* **18**: 20-26.

Meeusen, S., R. DeVay, J. Block, A. Cassidy-Stone, S. Wayson, J. M. McCaffery & J. Nunnari, (2006) Mitochondrial inner-membrane fusion and crista maintenance requires the dynamin-related GTPase Mgm1. *Cell* **127**: 383-395.

Meglei, G. & G. A. McQuibban, (2009) The dynamin-related protein Mgm1p assembles into oligomers and hydrolyzes GTP to function in mitochondrial membrane fusion. *Biochemistry* **48**: 1774-1784.

Merrifield, C. J., M. E. Feldman, L. Wan & W. Almers, (2002) Imaging actin and dynamin recruitment during invagination of single clathrin-coated pits. *Nature Cell Biology* **4**: 691-698.

Mettlen, M., T. Pucadyil, R. Ramachandran & S. L. Schmid, (2009) Dissecting dynamin's role in clathrin-mediated endocytosis. *Biochemical Society transactions* **37**: 1022-1026.

Mi-ichi, F., M. Abu Yousuf, K. Nakada-Tsukui & T. Nozaki, (2009) Mitosomes in *Entamoeba histolytica* contain a sulfate activation pathway. *Proceedings of the National Academy of Sciences of the United States of America* **106**: 21731-21736.

Misaka, T., T. Miyashita & Y. Kubo, (2002) Primary structure of a dynamin-related mouse mitochondrial GTPase and its distribution in brain, subcellular localization, and effect on mitochondrial morphology. *The Journal of Biological Chemistry* **277**: 15834-15842.

Mitra, B. N., G. Pradel, U. Frevert & D. Eichinger, (2010) Compounds of the upper gastrointestinal tract induce rapid and efficient excystation of *Entamoeba invadens*. *International Journal for Parasitology* **40**: 9.

Miyagishima, S. Y., H. Kuwayama, H. Urushihara & H. Nakanishi, (2008) Evolutionary linkage between eukaryotic cytokinesis and chloroplast division by dynamin proteins. *Proceedings of the National Academy of Sciences of the United States of America* **105**: 15202-15207.

Morgan, G. W., D. Goulding & M. C. Field, (2004) The single dynamin-like protein of Trypanosoma brucei regulates mitochondrial division and is not required for endocytosis. *The Journal of Biological Chemistry* **279**: 10692-10701.

Morgan, R. S., H. S. Slayter & D. L. Weller, (1968) Isolation of ribosomes from cysts of *entamoeba invadens*. *The Journal of Cell Biology* **36**: 45-51.

Morrison, H. G., A. G. McArthur, F. D. Gillin, S. B. Aley, R. D. Adam, G. J. Olsen, A. A. Best, W. Z. Cande, F. Chen, M. J. Cipriano, B. J. Davids, S. C. Dawson, H. G. Elmendorf, A. B. Hehl, M. E. Holder, S. M. Huse, U. U. Kim, E. Lasek-Nesselquist, G. Manning, A. Nigam, J. E. Nixon, D. Palm, N. E. Passamaneck, A. Prabhu, C. I. Reich, D. S. Reiner, J. Samuelson, S. G. Svard & M. L. Sogin, (2007) Genomic minimalism in the early diverging intestinal parasite *Giardia lamblia*. *Science (New York, N.Y* **317**: 1921-1926.

Mravec, J., J. Petrasek, N. Li, S. Boeren, R. Karlova, S. Kitakura, M. Parezova, S. Naramoto, T. Nodzynski, P. Dhonukshe, S. Y. Bednarek, E. Zazimalova, S. de Vries & J. Friml, (2011) Cell Plate Restricted Association of DRP1A and PIN Proteins Is Required for Cell Polarity Establishment in *Arabidopsis*. *Current Biology* **21**: 1055-1060.

Muhlberg, A. B., D. E. Warnock & S. L. Schmid, (1997) Domain structure and intramolecular regulation of dynamin GTPase. *The EMBO journal* **16**: 6676-6683.

Mukherjee, C., C. G. Clark & A. Lohia, (2008) Entamoeba shows reversible variation in ploidy under different growth conditions and between life cycle phases. *PLoS Neglected Tropical Diseases* **2**: e281.

Mukherjee, C., S. Majumder & A. Lohia, (2009) Inter-cellular variation in DNA content of Entamoeba histolytica originates from temporal and spatial uncoupling of cytokinesis from the nuclear cycle. *PLoS Neglected Tropical Diseases* **3**: e409.

Muller-Taubenberger, A., H. C. Ishikawa-Ankerhold, P. M. Kastner, E. Burghardt & G. Gerisch, (2009) The STE group kinase SepA controls cleavage furrow formation in Dictyostelium. *Cell Motility and the Cytoskeleton* **66**: 929-939.

Nakayama, M., K. Yazaki, A. Kusano, K. Nagata, N. Hanai & A. Ishihama, (1993) Structure of mouse Mx1 protein. Molecular assembly and GTP-dependent conformational change. *The Journal of Biological Chemistry* **268**: 15033-15038.

Nannapaneni, S., D. Wang, S. Jain, B. Schroeder, C. Highfill, L. Reustle, D. Pittsley, A. Maysent, S. Moulder, R. McDowell & K. Kim, (2010) The yeast dynamin-like protein Vps1:vps1 mutations perturb the internalization and the motility of endocytic vesicles and endosomes via disorganization of the actin cytoskeleton. *European Journal of Cell Biology* **89**: 499-508.

Niemann, H. H., M. L. Knetsch, A. Scherer, D. J. Manstein & F. J. Kull, (2001) Crystal structure of a dynamin GTPase domain in both nucleotide-free and GDP-bound forms. *The EMBO Journal* **20**: 5813-5821.

Nishida, K., M. Takahara, S. Y. Miyagishima, H. Kuroiwa, M. Matsuzaki & T. Kuroiwa, (2003) Dynamic recruitment of dynamin for final mitochondrial severance in a primitive red alga. *PNAS USA* **100**: 2146-2151.

Nothwehr, S. F., N. J. Bryant & T. H. Stevens, (1996) The newly identified yeast GRD genes are required for retention of late-Golgi membrane proteins. *Molecular and Cellular Biology* **16**: 2700-2707.

Obar, R. A., C. A. Collins, J. A. Hammarback, H. S. Shpetner & R. B. Vallee, (1990) Molecular cloning of the microtubule-associated mechanochemical enzyme dynamin reveals homology with a new family of GTP-binding proteins. *Nature* **347**: 256-261.

Oh, P., D. P. McIntosh & J. E. Schnitzer, (1998) Dynamin at the neck of caveolae mediates their budding to form transport vesicles by GTP-driven fission from the plasma membrane of endothelium. *The Journal of Cell Biology* **141**: 101-114.

Ohnishi, K., M. Murata, H. Kojima, N. Takemura, T. Tsuchida & H. Tachibana, (1994) Brain abscess due to infection with Entamoeba histolytica. *The American journal of tropical medicine and hygiene* **51**: 180-182.

Okamoto, P. M., B. Tripet, J. Litowski, R. S. Hodges & R. B. Vallee, (1999) Multiple distinct coiled-coils are involved in dynamin self-assembly. *The Journal of Biological Chemistry* **274**: 10277-10286.

Osteryoung, K. W., (2001) Organelle fission in eukaryotes. *Current Opinion in Microbiology* **4**: 639-646.

Osteryoung, K. W. & J. Nunnari, (2003) The division of endosymbiotic organelles. *Science (New York, N.Y* **302**: 1698-1704.

Pai, E. F., U. Krengel, G. A. Petsko, R. S. Goody, W. Kabsch & A. Wittinghofer, (1990) Refined crystal structure of the triphosphate conformation of H-ras p21 at 1.35 A resolution: implications for the mechanism of GTP hydrolysis. *The EMBO Journal* **9**: 2351-2359.

Pawlowski, J. & F. Burki, (2009) Untangling the phylogeny of amoeboid protists. *The Journal of Eukaryotic Microbiology* **56**: 16-25.

Pelloquin, L., P. Belenguer, Y. Menon, N. Gas & B. Ducommun, (1999) Fission yeast Msp1 is a mitochondrial dynamin-related protein. *Journal of Cell Science* **112 (Pt 22)**: 4151-4161.

Peters, C., T. L. Baars, S. Buhler & A. Mayer, (2004) Mutual control of membrane fission and fusion proteins. *Cell* **119**: 667-678.

Petri, W. A., Jr., D. Mondal, K. M. Peterson, P. Duggal & R. Haque, (2009) Association of malnutrition with amebiasis. *Nutrition Reviews* **67 Suppl 2**: S207-215.

Pitts, K. R., M. A. McNiven & Y. Yoon, (2004) Mitochondria-specific function of the dynamin family protein DLP1 is mediated by its C-terminal domains. *The Journal of Biological Chemistry* **279**: 50286-50294.

Plotkin, J. B. & G. Kudla, (2011) Synonymous but not the same: the causes and consequences of codon bias. *Nat Rev Genet* **12**: 32-42.

Ponce Gordo, F., R. A. Martinez Diaz & S. Herrera, (2004) *Entamoeba struthionis* n.sp. (Sarcomastigophora: Endamoebidae) from ostriches (*Struthio camelus*). *Veterinary Parasitology* **119**: 327-335.

Praefcke, G. J. & H. T. McMahon, (2004) The dynamin superfamily: universal membrane tubulation and fission molecules? *Nat. Rev. Mol. Cell. Biol.* **5**: 133-147.

Prakash, B., G. J. Praefcke, L. Renault, A. Wittinghofer & C. Herrmann, (2000) Structure of human guanylate-binding protein 1 representing a unique class of GTP-binding proteins. *Nature* **403**: 567-571.

Pritt, B. S. & C. G. Clark, (2008) Amebiasis. *Mayo Clinic proceedings* **83**: 1154-1159; quiz 1159-1160.

Pucadyil, T. J. & S. L. Schmid, (2008) Real-time visualization of dynamin-catalyzed membrane fission and vesicle release. *Cell* **135**: 1263-1275.

Quan, A. & P. J. Robinson, (2005) Rapid purification of native dynamin I and colorimetric GTPase assay. *Methods in Enzymology* **404**: 556-569.

Rahaman, A., N. C. Elde & A. P. Turkewitz, (2008) A dynamin-related protein required for nuclear remodeling in *Tetrahymena*. *Current Biology* **18**: 1227-1233.

Rai, A., H. Nothe, N. Tzvetkov, E. Korenbaum & D. J. Manstein, (2010) *Dictyostelium* dynamin B modulates cytoskeletal structures and membranous organelles. *Cellular and Molecular Life Sciences*

Ramachandran, R., (2011) Vesicle scission: dynamin. *Seminars in Cell & Developmental Biology* **22**: 10-17.

Reeves, R. E., (1968) A new enzyme with the glycolytic function of pyruvate kinase. *The Journal of Biological Chemistry* **243**: 3202-3204.

Reeves, R. E., R. A. Menzies & D. S. Hsu, (1968) The pyruvate-phosphate dikinase reaction. The fate of phosphate and the equilibrium. *The Journal of Biological Chemistry* **243**: 5486-5491.

Reeves, R. E., D. J. South, H. J. Blytt & L. G. Warren, (1974) Pyrophosphate:D-fructose 6-phosphate 1-phosphotransferase. A new enzyme with the glycolytic function of 6-phosphofructokinase. *The Journal of Biological Chemistry* **249**: 7737-7741.

Regoes, A., D. Zourmpanou, G. León-Avila, M. van der Giezen, J. Tovar & A. B. Hehl, (2005) Protein import, replication, and inheritance of a vestigial mitochondrion. *The Journal of Biological Chemistry* **280**: 30557-30563.

Reubold, T. F., S. Eschenburg, A. Becker, M. Leonard, S. L. Schmid, R. B. Vallee, F. J. Kull & D. J. Manstein, (2005) Crystal structure of the GTPase domain of rat dynamin 1. *PNAS USA* **102**: 13093-13098.

Richter, M. F., M. Schwemmle, C. Herrmann, A. Wittinghofer & P. Staeheli, (1995) Interferon-induced MxA protein. GTP binding and GTP hydrolysis properties. *The Journal of Biological Chemistry* **270**: 13512-13517.

Riordan, C. E., J. Ault, S. G. Langreth & J. S. Keithly, (2003) *Cryptosporidium parvum* Cpn60 targets a relict organelle. *Current Genetics* **44**: 138-147.

Riordan, C. E., S. G. Langreth, L. B. Sánchez, O. Kayser & J. S. Keithly, (1999) Preliminary evidence for a mitochondrion in *Cryptosporidium parvum*: phylogenetic and therapeutic implications. *Journal of Eukaryotic Microbiology* **46**: 52S-55S.

Roger, A. J., C. G. Clark & W. F. Doolittle, (1996) A possible mitochondrial gene in the early-branching amitochondriate protist *Trichomonas vaginalis*. *PNAS USA* **93**: 14618-14622.

Ronquist, F. & J. P. Huelsenbeck, (2003) MrBayes 3: Bayesian phylogenetic inference under mixed models. *Bioinformatics (Oxford, England)* **19**: 1572-1574.

Rossignol, J. F., S. M. Kabil, Y. El-Gohary & A. M. Younis, (2007) Nitazoxanide in the treatment of amoebiasis. *Transactions of the Royal Society of Tropical Medicine and Hygiene* **101**: 1025-1031.

Roux, A., G. Koster, M. Lenz, B. Sorre, J. B. Manneville, P. Nassoy & P. Bassereau, (2010) Membrane curvature controls dynamin polymerization. *PNAS USA* **107**: 4141-4146.

Roux, A., K. Uyhazi, A. Frost & P. De Camilli, (2006) GTP-dependent twisting of dynamin implicates constriction and tension in membrane fission. *Nature* **441**: 528-531.

Saavedra, E., R. Encalada, E. Pineda, R. Jasso-Chavez & R. Moreno-Sanchez, (2005) Glycolysis in Entamoeba histolytica. Biochemical characterization of recombinant glycolytic enzymes and flux control analysis. *The FEBS Journal* **272**: 1767-1783.

Samuelson, J. & P. Robbins, (2011) A simple fibril and lectin model for cyst walls of Entamoeba and perhaps Giardia. *Trends in Parasitology* **27**: 17-22.

Sánchez, L., V. Enea & D. Eichinger, (1994) Identification of a developmentally regulated transcript expressed during encystation of *Entamoeba invadens*. *Molecular and Biochemical Parasitology* **67**: 125-135.

Sandvig, K., S. Pust, T. Skotland & B. van Deurs, (2011) Clathrin-independent endocytosis: mechanisms and function. *Current Opinion in Cell Biology*.

Schlosser, A., B. Klockow, D. J. Manstein & W. D. Lehmann, (2003) Analysis of post-translational modification and characterization of the domain structure of dynamin A from Dictyostelium discoideum. *Journal Mass Spectrometry* **38**: 277-282.

Schmid, S. L. & V. A. Frolov, (2011) Dynamin: Functional Design of a Membrane Fission Catalyst. *Annual Review of Cell and Developmental Biology*.

Schmidt, H. A., K. Strimmer, M. Vingron & A. von Haeseler, (2002) TREE-PUZZLE: maximum likelihood phylogenetic analysis using quartets and parallel computing. *Bioinformatics (Oxford, England)* **18**: 502-504.

Schultz, J., R. R. Copley, T. Doerks, C. P. Ponting & P. Bork, (2000) SMART: a web-based tool for the study of genetically mobile domains. *Nucleic Acids Research* **28**: 231-234.

Shamsuzzaman, S. M. & Y. Hashiguchi, (2002) Thoracic amebiasis. *Clinics in Chest Medicine* **23**: 479-492.

Shaw, J. M. & J. Nunnari, (2002) Mitochondrial dynamics and division in budding yeast. *Trends in Cell Biology* **12**: 178-184.

Shimada, S., T. Mizumoto, R. Nishioka, K. Fukami, M. Kuramoto, K. Nomura, N. Aoki & M. Ogawa, (2002) Acute fulminant necrotizing colitis caused by amebiasis: report of a case. *Surgery today* **32**: 738-741.

Shpetner, H. S. & R. B. Vallee, (1992) Dynamin is a GTPase stimulated to high levels of activity by microtubules. *Nature* **355**: 733-735.

Shupliakov, O., P. Low, D. Grabs, H. Gad, H. Chen, C. David, K. Takei, P. De Camilli & L. Brodin, (1997) Synaptic vesicle endocytosis impaired by disruption of dynamin-SH3 domain interactions. *Science (New York, N.Y* **276**: 259-263.

Silberman, J. D., C. G. Clark, L. S. Diamond & M. L. Sogin, (1999) Phylogeny of the genera Entamoeba and Endolimax as deduced from small-subunit ribosomal RNA sequences. *Molecular Biology and Evolution* **16**: 1740-1751.

Singer, V. L., T. E. Lawlor & S. Yue, (1999) Comparison of SYBR Green I nucleic acid gel stain mutagenicity and ethidium bromide mutagenicity in the Salmonella/mammalian microsome reverse mutation assay (Ames test). *Mutation Research* **439**: 37-47.

Slapeta, J. & J. S. Keithly, (2004) *Cryptosporidium parvum* mitochondrial-type HSP70 targets homologous and heterologous mitochondria. *Eukaryotic cell* **3**: 483-494.

Smaczynska-de, R., II, E. G. Allwood, S. Aghamohammadzadeh, E. H. Hettema, M. W. Goldberg & K. R. Ayscough, (2010) A role for the dynamin-like protein Vps1 during endocytosis in yeast. *Journal of Cell Science* **123**: 3496-3506.

Smirnova, E., D. L. Shurland, S. N. Ryazantsev & A. M. van der Bliek, (1998) A human dynamin-related protein controls the distribution of mitochondria. *The Journal of Cell Biology* **143**: 351-358.

Sogin, M. L., (1989) Evolution of eukaryotic microorganisms and their small subunit ribosomal RNAs. *American Zoology* **29**: 487-499.

Sogin, M. L., J. H. Gunderson, H. J. Elwood, R. A. Alonso & D. A. Peattie, (1989) Phylogenetic meaning of the kingdom concept: an unusual ribosomal RNA from *Giardia lamblia*. *Science (New York, N.Y* **243**: 75-77.

Sogin, M. L. & J. D. Silberman, (1998) Evolution of the protists and protistan parasites from the perspective of molecular systematics. *International Journal for Parasitology* **28**: 11-20.

Song, B. D., M. Leonard & S. L. Schmid, (2004a) Dynamin GTPase domain mutants that differentially affect GTP binding, GTP hydrolysis, and clathrin-mediated endocytosis. *The Journal of Biological Chemistry* **279**: 40431-40436.

Song, B. D., D. Yarar & S. L. Schmid, (2004b) An assembly-incompetent mutant establishes a requirement for dynamin self-assembly in clathrin-mediated endocytosis in vivo. *Molecular Biology of the Cell* **15**: 2243-2252.

Stabler, R. C., T.-T., (1936) Observations on an Endamoeba parasitizing opalinid Ciliates. *Biological Bulletin* **70**: 5.

Stamatakis, A., P. Hoover & J. Rougemont, (2008) A Rapid Bootstrap Algorithm for the RAxML Web Servers. *Systematic Biology* **57**: 758-771.

Stanley, S. L., (2003) Amoebiasis. *Lancet* **361**: 1025-1034.

Stechmann, A., K. Hamblin, V. Pérez-Brocal, D. Gaston, G. S. Richmond, M. van der Giezen, C. G. Clark & A. J. Roger, (2008) Organelles in *Blastocystis* that blur the distinction between mitochondria and hydrogenosomes. *Curr Biol* **18**: 580-585.

Stensvold, C. R., M. Lebbad & C. G. Clark, (2010) Genetic characterisation of uninucleated cyst-producing Entamoeba spp. from ruminants. *International Journal for Parasitology* **40**: 775-778.

Stensvold, C. R., M. Lebbad, E. L. Victory, J. J. Verweij, E. Tannich, M. Alfellani, P. Legarraga & C. G. Clark, (2011) Increased sampling reveals novel lineages of *Entamoeba*: consequences of genetic diversity and host specificity for taxonomy and molecular detection. *Protist* **162**: 525-541.

Stowell, M. H., B. Marks, P. Wigge & H. T. McMahon, (1999) Nucleotide-dependent conformational changes in dynamin: evidence for a mechanochemical molecular spring. *Nature Cell Biology* **1**: 27-32.

Sweitzer, S. M. & J. E. Hinshaw, (1998) Dynamin undergoes a GTP-dependent conformational change causing vesiculation. *Cell* **93**: 1021-1029.

Takahara, M., H. Takahashi, S. Matsunaga, S. Miyagishima, H. Takano, A. Sakai, S. Kawano & T. Kuroiwa, (2000) A putative mitochondrial ftsZ gene is present in the unicellular primitive red alga Cyanidioschyzon merolae. *Molecular Genetics and Genomics* **264**: 452-460.

Teixeira, J. E. & C. D. Huston, (2008) Evidence of a continuous endoplasmic reticulum in the protozoan parasite Entamoeba histolytica. *Eukaryotic Cell* **7**: 1222-1226.

Thrash, J. C., A. Boyd, M. J. Huggett, J. Grote, P. Carini, R. J. Yoder, B. Robbertse, J. W. Spatafora, M. S. Rappe & S. J. Giovannoni, (2011) Phylogenomic evidence for a common ancestor of mitochondria and the SAR11 clade. *Nature Scientific Reports* **1**: 9.

Tovar, J., S. S. E. Cox & M. van der Giezen, (2007) A mitosome purification protocol based on Percoll density gradients and its use in validating the mitosomal nature of *Entamoeba histolytica* mitochondrial Hsp70. *Methods in Molecular Biology* **390**: 167-177.

Tovar, J., A. Fischer & C. G. Clark, (1999) The mitosome, a novel organelle related to mitochondria in the amitochondrial parasite *Entamoeba histolytica*. *Molecular Microbiology* **32**: 1013-1021.

Tovar, J., G. León-Avila, L. Sánchez, R. Sutak, J. Tachezy, M. van der Giezen, M. Hernández, M. Müller & J. M. Lucocq, (2003) Mitochondrial remnant organelles of *Giardia* function in iron-sulphur protein maturation. *Nature* **426**: 172-176.

Trivinos-Lagos, L., T. Ohmachi, C. Albrightson, R. G. Burns, H. L. Ennis & R. L. Chisholm, (1993) The highly divergent alpha- and beta-tubulins from Dictyostelium discoideum are encoded by single genes. *Journal of Cell Science* **105 (Pt 4)**: 903-911.

Vaithilingam, A., J. E. Teixeira & C. D. Huston, (2008) Endoplasmic reticulum continuity in the protozoan parasite Entamoeba histolytica: Evolutionary implications and a cautionary note. *Communicative & Integrative Biology* **1**: 172-174.

Van Dellen, K. L., D. A. Bulik, C. A. Specht, P. W. Robbins & J. C. Samuelson, (2006) Heterologous expression of an Entamoeba histolytica chitin synthase in Saccharomyces cerevisiae. *Eukaryotic Cell* **5**: 203-206.

van der Bliek, A. M., (1999) Functional diversity in the dynamin family. *Trends in cell biology* **9**: 96-102.

van der Bliek, A. M. & E. M. Meyerowitz, (1991) Dynamin-like protein encoded by the Drosophila shibire gene associated with vesicular traffic. *Nature* **351**: 411-414.

van der Bliek, A. M. & G. S. Payne, (2010) Dynamin subunit interactions revealed. *Developmental Cell* **18**: 687-688.

van der Bliek, A. M., T. E. Redelmeier, H. Damke, E. J. Tisdale, E. M. Meyerowitz & S. L. Schmid, (1993) Mutations in human dynamin block an intermediate stage in coated vesicle formation. *The Journal of Cell Biology* **122**: 553-563.

van der Giezen, M., (2009) Eukaryotic life without mitochondria? *Comp Biochem Physiol A Mol Integr Phys* **153A**: S165-S166.

van der Giezen, M., (2011) Mitochondria and the rise of eukaryotes. *BioSci* **61**: 594-601.

van der Giezen, M., S. Cox & J. Tovar, (2004) The iron-sulfur cluster assembly genes iscS and iscU of *Entamoeba histolytica* were acquired by horizontal gene transfer. *BMC Evolutionary Biology* **4**: 7.

van der Giezen, M., G. Leon-Avila & J. Tovar, (2005) Characterization of chaperonin 10 (Cpn10) from the intestinal human pathogen *Entamoeba histolytica*. *Microbiology* **151**: 3107-3115.

van der Giezen, M. & J. Tovar, (2005) Degenerate mitochondria. *EMBO Rep* **6**: 525-530.

van Dooren, G. G., S. B. Reiff, C. Tomova, M. Meissner, B. M. Humbel & B. Striepen, (2009) A novel dynamin-related protein has been recruited for apicoplast fission in Toxoplasma gondii. *Current Biology* **19**: 267-276.

Vandesompele, J., K. De Preter, F. Pattyn, B. Poppe, N. Van Roy, A. De Paepe & F. Speleman, (2002) Accurate normalization of real-time quantitative RT-PCR data by geometric averaging of multiple internal control genes. *Genome Biology* **3**: RESEARCH0034.

Vater, C. A., C. K. Raymond, K. Ekena, I. Howald-Stevenson & T. H. Stevens, (1992) The VPS1 protein, a homolog of dynamin required for vacuolar protein sorting in Saccharomyces cerevisiae, is a GTPase with two functionally separable domains. *The Journal of Cell Biology* **119**: 773-786.

Vavra, J., (2005) "Polar vesicles" of microsporidia are mitochondrial remnants ("mitosomes")? *Folia Parasitol (Praha)* **52**: 193-195.

Verweij, J. J., A. M. Polderman & C. G. Clark, (2001) Genetic Variation among Human Isolates of Uninucleated Cyst-Producing Entamoeba Species. *Journal of Clinical Microbiology* **39**: 1644-1646.

Villagomez-Castro, J. C., C. Calvo-Mendez & E. Lopez-Romero, (1992) Chitinase activity in encysting Entamoeba invadens and its inhibition by allosamidin. *Molecular and Biochemical Parasitology* **52**: 53-62.

Viriyavejakul, P. & M. Riganti, (2009) Undiagnosed amebic brain abscess. *The Southeast Asian Journal of Tropical Medicine and Public Health* **40**: 1183-1187.

Viscogliosi, E., H. Philippe, A. Baroin, R. Perasso & G. Brugerolle, (1993) Phylogeny of trichomonads based on partial sequences of large subunit rRNA and on cladistic analysis of morphological data. *The Journal of Eukaryotic Microbiology* **40**: 411-421.

Vopel, T., A. Syguda, N. Britzen-Laurent, S. Kunzelmann, M. B. Ludemann, C. Dovengerds, M. Sturzl & C. Herrmann, (2010) Mechanism of GTPase-activity-induced self-assembly of human guanylate binding protein 1. *Journal of Molecular Biology* **400**: 63-70.

Vossbrinck, C. R., T. J. Maddox, S. Friedman, B. A. Debrunner-Vossbrinck & C. R. Woese, (1987) Ribosomal RNA sequence suggests microsporidia are extremely ancient eukaryotes. *Nature* **326**: 411-414.

Walsh, J. A., (1986) Problems in recognition and diagnosis of amebiasis: estimation of the global magnitude of morbidity and mortality. *Reviews of infectious diseases* **8**: 228-238.

Ward, J. J., L. J. McGuffin, K. Bryson, B. F. Buxton & D. T. Jones, (2004) The DISOPRED server for the prediction of protein disorder. *Bioinformatics (Oxford, England)* **20**: 2138-2139.

WHO, (1997) WHO News and activities.

WHO/PAHO/UNESCO-report, (1997) A consultation with experts on amoebiasis.

Mexico City, Mexico. *Epidemiology Bulletin* **18**: 2.

Wiejak, J., L. Surmacz & E. Wyroba, (2003) Dynamin involvement in Paramecium phagocytosis. *European Journal of Protistology* **39**: 6.

Wienke, D. C., M. L. W. Knetsch, E. M. Neuhaus, M. C. Reedy & D. J. Manstein, (1999) Disruption of a dynamin homologue affects endocytosis, organelle morphology, and cytokinesis in *Dictyostelium discoideum*. *Molecular Biology of the Cell* **10**: 225-243.

Williams, B. A. P., R. P. Hirt, J. M. Lucocq & T. M. Embley, (2002) A mitochondrial remnant in the microsporidian *Trachipleistophora hominis*. *Nature* **418**: 865-869.

Wong, E. D., J. A. Wagner, S. W. Gorsich, J. M. McCaffery, J. M. Shaw & J. Nunnari, (2000) The dynamin-related GTPase, Mgm1p, is an intermembrane space protein required for maintenance of fusion competent mitochondria. *The Journal of Cell Biology* **151**: 341-352.

Wong, E. D., J. A. Wagner, S. V. Scott, V. Okreglak, T. J. Holewinske, A. Cassidy-Stone & J. Nunnari, (2003) The intramitochondrial dynamin-related GTPase, Mgm1p, is a component of a protein complex that mediates mitochondrial fusion. *The Journal of Cell Biology* **160**: 303-311.

Ximenez, C., R. Cerritos, L. Rojas, S. Dolabella, P. Moran, M. Shibayama, E. Gonzalez, A. Valadez, E. Hernandez, O. Valenzuela, A. Limon, O. Partida & E. F. Silva, Human amebiasis: breaking the paradigm? *International Journal of Environmental Research and Public Health* **7**: 1105-1120.

Yoon, Y. & M. A. McNiven, (2001) Mitochondrial division: New partners in membrane pinching. *Current Biology* **11**: R67-70.

Zheng, J., S. M. Cahill, M. A. Lemmon, D. Fushman, J. Schlessinger & D. Cowburn, (1996) Identification of the binding site for acidic phospholipids on the pH domain of dynamin: implications for stimulation of GTPase activity. *Journal of Molecular Biology* **255**: 14-21.

Appendix

Supplementary table 1. Taxa used in large-scale dynamin protein phylogeny including accession numbers, putative functions and the supergroups.

Taxon	Accession number	Assigned function	Supergroup
Arabidopsis thaliana	NP176252	Mx-protein	Archaeplastida
Arabidopsis thaliana	NP851120	Cell plate formation	Archaeplastida
Arabidopsis thaliana	NP172936	Cell plate formation	Archaeplastida
Arabidopsis thaliana	NP567094	Disease resistance	Archaeplastida
Arabidopsis thaliana	NP565363	Mitochondrial division	Archaeplastida
Arabidopsis thaliana	NP850615	Chloroplast division	Archaeplastida
Arabidopsis thaliana	NP175722	Cytokinesis	Archaeplastida
Batrachochytrium dendrobatidis	jgi|Batde5|89027	Unknown function	Opisthokonta
Batrachochytrium dendrobatidis	jgi|Batde5|10517	Mitochondrial fusion inner membrane	Opisthokonta
Batrachochytrium dendrobatidis	jgi|Batde5|35777	Vacuolar sorting	Opisthokonta
Batrachochytrium dendrobatidis	jgi|Batde5|34336	Mitochondrial fusion inner membrane	Opisthokonta
Chlamydomonas reinhardtii	XP001700931	Cell plate formation	Archaeplastida
Chlamydomonas reinhardtii	XP001697229	Mitochondrial division	Archaeplastida
Chlamydomonas reinhardtii	XP001702662	Chloroplast division	Archaeplastida
Chlamydomonas reinhardtii	XP001696853	Cytokinesis	Archaeplastida
Ciona intestinalis	XP002130018	Clathrin mediated endocytosis	Opisthokonta
Ciona intestinalis	XP002129	Mitochondrial and peroxisomal division	Opisthokonta
Ciona intestinalis	XP002131	Mitochondrial fusion outer membrane	Opisthokonta
Cryptococcus neoformans	XP569803	Mitochondrial fusion inner membrane	Opisthokonta
Cryptococcus neoformans	XP566870	Vacuolar sorting	Opisthokonta
Cryptococcus neoformans	XP569513	Mitochondrial division	Opisthokonta
Cryptococcus neoformans	XP569513	Mitochondrial division	Opisthokonta
Cryptococcus neoformans	XP571622	Mitochondrial fusion inner membrane	Opisthokonta
Cryptosporidium parvum	XP627103	Apicoplast division clade	Alveolata
Cryptosporidium parvum	XP001388141	Secretory pathway clade	Alveolata
Cryptosporidium parvum	XP001388234	Unknown function	Alveolata
Cyanidioschyzon merolae	AAO23012	Mitochondrial division	Archaeplastida
Cyanidioschyzon merolae	BAC55068	Chloroplast division	Archaeplastida
Dictyostelium discoideum	DDB0215390	Cytoskeleton	Amoebozoa
Dictyostelium discoideum	DDB0216177	Mitochondrial division	Amoebozoa
Dictyostelium discoideum	DDB0229901	Cytokinesis	Amoebozoa

Dictyostelium discoideum	DDB0302371	Cytokinesis	Amoebozoa
Dictyostelium discoideum	DDB0302372	Cytokinesis	Amoebozoa
Drosophila melanogaster	NP732840	Mitochondrial fusion inner membrane	Opisthokonta
Drosophila melanogaster	NP001162768	Clathrin mediated endocytosis	Opisthokonta
Drosophila melanogaster	AAN71025	Mitochondrial and peroxisomal division	Opisthokonta
Drosophila melanogaster	NP610941	Mitochondrial fusion outer membrane	Opisthokonta
Emiliania huxleyi	Ehux451602	Unknown	Stramenopiles
Emiliania huxleyi	Ehux461229	No assigned function	Stramenopiles
Emiliania huxleyi	Ehux96578	Chloroplast division	Stramenopiles
Encephalitozoon cuniculi	NP586287	Unknown function	Opisthokonta
Encephalitozoon cuniculi	XP965959	Unknown function	Opisthokonta
Entamoeba histolytica	XP651634	Unknown function	Amoebozoa
Entamoeba histolytica	XP649650	Nuclear associated	Amoebozoa
Entamoeba histolytica	XP653348	Cytokinesis clade	Amoebozoa
Entamoeba histolytica	XP651307	Cytokinesis clade	Amoebozoa
Entamoeba invadens	EIN070060	Unknown function	Amoebozoa
Entamoeba invadens	EIN254810	Unknown function	Amoebozoa
Entamoeba invadens	EIN051430	Unknown function	Amoebozoa
Entamoeba invadens	EIN050690	Cytokinesis clade	Amoebozoa
Entamoeba invadens	EIN222460	Cytokinesis clade	Amoebozoa
Gallus gallus	XP417640	Mitochondrial fusion inner membrane	Opisthokonta
Gallus gallus	BAC06346	Mx-protein	Opisthokonta
Gallus gallus	XP415501	Clathrin mediated endocytosis	Opisthokonta
Gallus gallus	NP001073190	Mitochondrial and peroxisomal division	Opisthokonta
Gallus gallus	NP001034398	Mitochondrial fusion outer membrane	Opisthokonta
Giardia intestinalis	XP00170496	Encystation specific vesicles	Excavata
Homo sapiens	NP0055681	Mitochondrial fusion inner membrane	Opisthokonta
Homo sapiens	NP002454	Mx-protein	Opisthokonta
Homo sapiens	NP001005336	Clathrin mediated endocytosis	Opisthokonta
Homo sapiens	NP005681	Mitochondrial and peroxisomal division	Opisthokonta
Homo sapiens	NP056375	Mitochondrial fusion outer membrane	Opisthokonta
Leishmania major	XP847885	Mitochondrial division	Excavata
Monosiga brevicollis	XP001750100	Unknown function	Opisthokonta
Monosiga brevicollis	XP001749319	Clathrin mediated endocytosis	Opisthokonta

Monosiga brevicollis	XP001750431	Mitochondrial and peroxisomal division	Opisthokonta
Monosiga brevicollis	XP001746637	Mitochondrial fusion outer membrane	Opisthokonta
Naegleria gruberi	XP002670416	Unknown function	Excavata
Naegleria gruberi	XP002683124	Unknown function	Excavata
Naegleria gruberi	XP002681690	Unknown function	Excavata
Naegleria gruberi	XP002683545	Cytokinesis clade	Excavata
Oryza sativa	NP001049617	Mx-protein	Archaeplastida
Oryza sativa	CAE02378	Mx-protein	Archaeplastida
Oryza sativa	NP001064002	Cell plate formation	Archaeplastida
Oryza sativa	NP001064002	Cell plate formation	Archaeplastida
Oryza sativa	AC090882	Cell plate formation	Archaeplastida
Oryza sativa	NP001065436	Cell plate formation	Archaeplastida
Oryza sativa	NP001052600	Mitochondrial division	Archaeplastida
Oryza sativa	NP001045220	Mitochondrial division	Archaeplastida
Oryza sativa	EEE52865	Chloroplast division	Archaeplastida
Oryza sativa	BAD86966	Cytokinesis	Archaeplastida
Phycomyces blakesleeanus	Phybl1_62295	Mitochondrial fusion inner membrane	Opisthokonta
Phycomyces blakesleeanus	Phybl1_41775	Mitochondrial fusion inner membrane	Opisthokonta
Phycomyces blakesleeanus	Phybl1_30271	Mitochondrial fusion inner membrane	Opisthokonta
Phycomyces blakesleeanus	Phybl1_37829	Vacuolar sorting	Opisthokonta
Phycomyces blakesleeanus	Phybl1_57948	Vacuolar sorting	Opisthokonta
Phycomyces blakesleeanus	Phybl1_32212	Mitochondrial division	Opisthokonta
Phycomyces blakesleeanus	Phybl1_20253	Mitochondrial division	Opisthokonta
Phycomyces blakesleeanus	Phybl1_10554	Mitochondrial fusion inner membrane	Opisthokonta
Physcomitrella patens	XP001773410	Cell plate formation	Archaeplastida
Physcomitrella patens	XP001766173	Mitochondrial division	Archaeplastida
Physcomitrella patens	XP001758540	Mitochondrial division	Archaeplastida
Physcomitrella patens	XP001779783	Chloroplast division	Archaeplastida
Physcomitrella patens	XP001781521	Chloroplast division	Archaeplastida
Physcomitrella patens	XP001759610	Chloroplast division	Archaeplastida
Physcomitrella patens	XP001752691	Cytokinesis	Archaeplastida
Phythophtora ramorum	PhyRa86760	Unknown function	Alveolate
Phythophtora ramorum	PhyRa72119	Unknown function	Alveolata
Plasmodium falciparum	XP001350587	Unknown function	Alveolata
Plasmodium falciparum	XP001348132	Kinetoplast division clade	Alveolata
Plasmodium falciparum	XP001347652	Secretory pathway clade	Alveolata
Polysphondylium pallidum	EFA84816	Cytoskeleton	Amoebozoa
Polysphondylium pallidum	EFA75434	Mitochondrial division	Amoebozoa
Polysphondylium pallidum	EFA84098	Cytokinesis	Amoebozoa
Polysphondylium pallidum	EFA76312	Cytokinesis	Amoebozoa
Polysphondylium pallidum	EFA76188	Cytokinesis	Amoebozoa
Saccharomyces cerevisiae	NP014854	Mitochondrial fusion	Opisthokonta

		inner membrane	
Saccharomyces cerevisiae	NP012926	Vacuolar sorting	Opisthokonta
Saccharomyces cerevisiae	NP013100	Mitochondrial division	Opisthokonta
Saccharomyces cerevisiae	NP009738	Mitochondrial fusion inner membrane	Opisthokonta
Tetrahymena thermophila	ABB13594	Macronuclear remodelling	Alveolata
Tetrahymena thermophila	ABB13593	Macronuclear remodelling	Alveolata
Tetrahymena thermophila	XP001029982	Macronuclear remodelling	Alveolata
Tetrahymena thermophila	XP001029980	Macronuclear remodelling	Alveolata
Tetrahymena thermophila	ABB13592	Unknown function	Alveolata
Tetrahymena thermophila	ABB13595	Clathrin mediated endocytosis	Alveolata
Tetrahymena thermophila	XP001009829	Clathrin mediated endocytosis	Alveolata
Thalassiosira pseudonana	XP002296064	Mitochondrial division	Stramenopiles
Thalassiosira pseudonana	XP002290986	Chloroplast division	Stramenopiles
Theileria annulata	XP952965	Apicoplast division clade	Alveolata
Theileria annulata	XP764712	Secretory pathway clade	ALveolata
Toxoplasma gondii	EEA98594	Unknown function	Alveolata
Toxoplasma gondii	EEB01708	Apicoplast division	Alveolata
Toxoplasma gondii	EEB04563	Secretory pathway	Alveolata
Trichomonas vaginalis	XP001581	Unknown function	Excavata
Trichomonas vaginalis	XP001308	Unknown function	Excavata
Trichomonas vaginalis	XP001316	Unknown function	Excavata
Trichomonas vaginalis	XP001579	Unknown function	Excavata
Trichomonas vaginalis	XP001305	Unknown function	Excavata
Trichomonas vaginalis	XP001311	Unknown function	Excavata
Trichomonas vaginalis	XP001324	Unknown function	Excavata
Trichomonas vaginalis	XP00132	Unknown function	Excavata
Trypanosoma brucei	XP844064	Mitochondrial division	Excavata

Supplementary table 2. Taxa used in the Drp1 and Drp2 dynamin protein phylogeny including accession numbers, putative functions and the supergroups.

Taxon	Accession number	Assigned function	Supergroup
Giardia intestinalis	XP001704962	Stage conversion/endocytosis	Excavata
Spironucleus barkhanus	ABI15596	Stage conversion/endocytosis	Excavata
Trichomonas vaginalis	XP001308653	Unknown	Excavata
Trichomonas vaginalis	XP001316433	Unknown	Excavata
Trichomonas vaginalis	XP001579617	Unknown	Excavata
Trichomonas vaginalis	XP001305587	Unknown	Excavata
Trichomonas vaginalis	XP001311094	Unknown	Excavata
Trichomonas vaginalis	XP001324893	Unknown	Excavata
Trichomonas vaginalis	XP001324471	Unknown	Excavata
Plasmodium falciparum	XP001347652	Mitochondrial division	Alveolata
Leishmania major	XP847885	Mitochondrial division	Alveolata
Trypanosoma brucei	AAN05457	Mitochondrial division and endocytosis	Alveolata
Entamoeba histolytica	XP649650	Unknown function	Amoebozoa
Entamoeba histolytica	XP651634	Unknown function	Amoebozoa
Entamoeba moshkovskii	mosh054c06.p1k + mosh030g01.p1k	Unknown function	Amoebozoa
Entamoeba moshkovskii	mosh131a08.q1k + mosh054c06.p1k + mosh093a04.p1k + mosh092a03.q1k + mosh092a03.q1k	Unknown function	Amoebozoa
Entamoeba invadens	EIN_051430	Unknown function	Amoebozoa
Entamoeba invadens	EIN_070060	Unknown function	Amoebozoa
Entamoeba invadens	EIN_254810	Unknown function	Amoebozoa
Entamoeba terrapinae	terra244d12.q1k	Unknown function	Amoebozoa
Entamoeba dispar	XP001734031	Unknown function	Amoebozoa
Entamoeba dispar	XP001735320	Unknown function	Amoebozoa
Tetrahymena thermophila	ABB13595	Clathrin mediated endoyctosis	Alveolata
Tetrahymena thermophila	XP001009829	Clathrin mediated endoyctosis	Alveolata
Chlamydomonas reinhardtii	XP001697229	Mitochondrial division	Archaeplastida
Monosiga brevicollis	XP001749319	Clathrin mediated endocytosis	Opisthokonta
Drosophila melanogaster	NP001162768	Clathrin mediated endocytosis	Opisthokonta
Ciona intestinalis	XP002130319	Clathrin mediated endocytosis	Opisthokonta
Homo sapiens	NP001005336	Clathrin mediated	Opisthokonta

		endocytosis	
Gallus gallus	XP415501	Clathrin mediated endocytosis	Opisthokonta
Cryptosporidium parvum	XP001388234	Unknown function	Opisthokonta
Polysphondylium pallidum	EFA84816	Cytoskeleton	Amoebozoa
Dictyostelium discoideum	XP642447	Cytoskeleton	Amoebozoa
Encephalitozoon cuniculi	NP586287	Vacuolar sorting clade	Opisthokonta
Neurospora crassa	XP002995380	Vacuolar sorting clade	Opisthokonta
Monosiga brevicollis	XP001750431	Mitochondrial and peroxisomal division	Opisthokonta
Cyanidioschyzon merolae	AAO23012	Mitochondrial division	Archaeplastida
Oryza sativa	NP001052600	Mitochondrial division	Archaeplastida
Physcomitrella patens	XP001766173	Mitochondrial division	Archaeplastida
Physcomitrella patens	XP001777446	Mitochondrial division	Archaeplastida
Physcomitrella patens	XP001775158	Mitochondrial division	Archaeplastida
Physcomitrella patens	XP001761534	Mitochondrial division	Archaeplastida
Arabidopsis thaliana	NP565363	Mitochondrial division	Archaeplastida
Oryza sativa	NP001045220	Mitochondrial division	Archaeplastida
Theileria annulata	XP764712	Secretory pathway	Alveolata
Toxoplasma gondii	EEE27889	Secretory pathway	Alveolata
Saccharomyces cerevisiae	NP012926	Vacuolar sorting	Opisthokonta
Cryptococcus neoformans	XP566870	Vacuolar sorting	Opisthokonta
Batrachochytrium dendrobatidis	jgi|Bate5|35777	Vacuolar sorting	Opisthokonta
Phycomyces blakesleeanus	Phybl1_37829	Vacuolar sorting	Opisthokonta
Phycomyces blakesleeanus	Phybl1_57948	Vacuolar sorting	Opisthokonta
Saccharomyces cerevisae	NP013100	Mitochondrial division	Opisthokonta
Cryptococcus neoformans	XP569513	Mitochondrial division	Opisthonta
Phycomyces blakesleeanus	Phybl1_32212	Mitochondrial division	Opisthokonta
Phycomyces blakesleeanus	Phybl1_20253	Mitochondrial division	Opisthokonta
Ciona intestinalis	XP002130018	Clathrin mediated endocytosis	Opisthokonta
Drosophila melanogaster	AAN71025	Mitochondrial and peroxisomal division	Opisthokonta
Gallus gallus	NP001073190	Mitochondrial and peroxisomal division	Opisthokonta
Homo sapiens	NP005681	Mitochondrial and	Opisthokonta

		peroxisomal division	
Pinnularia infestans	XP002908808	Mitochondrial division	Stramenopiles
Naegleria gruberi	XP002683124	Unknown function	Excavata
Naegleria gruberi	XP002681690	Unknown function	Excavata
Polysphondylium pallidum	EFA75434	Mitochondrial division	Amoebozoa
Dictyostelium discoideum	DDB_G0277849	Mitochondrial division	Amoebozoa
Thalassiosira pseudonana	XP002296064	Mitochondrial division	Stramenopiles
Phytophthora ramorum	XP002908808	Mitochondrial division	Stramenopiles
Phaeodactylum tricornutum	XP002181636	Mitochondrial division	Stramenopiles